REGULATION OF SODIUM CHANNEL DENSITIES IN A6 RENAL EPITHELIAL CELLS BY HORMONALLY-DEPENDENT MECHANISMS.

Michael Bruce Butterworth

Thesis presented for the Degree of

DOCTOR OF PHILOSOPHY

in the Department of Anatomy and Cell Biology

Faculty of Health Sciences

UNIVERSITY OF CAPE TOWN

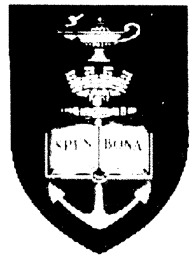

September 2001

University of Cape Town

The copyright of this thesis vests in the author. No quotation from it or information derived from it is to be published without full acknowledgement of the source. The thesis is to be used for private study or non-commercial research purposes only.

Published by the University of Cape Town (UCT) in terms of the non-exclusive license granted to UCT by the author.

University of Cape Town

TABLE OF CONTENTS

SECTION		PAGE
ABSTRACT		vi
ACKNOWLEDGEMENTS		vii
CHAPTER 1	ION TRANSPORT AND SODIUM CHANNELS: INTRODUCTION, LITERATURE REVIEW AND STUDY AIMS	
1.1. Introduction		1
1.1.1. Homeostasis		
1.1.2. The Kidney		
1.1.3. Epithelial Barriers		
1.1.4. Responsive Epithelia		
1.2. Membrane Transporters		8
1.2.1. Crossing an Epithelium		
1.2.2. Channel Proteins		
1.3. Epithelial Sodium Channel (ENaC)		12
1.3.1. Cloning		
1.3.2. Expression		
1.3.3. Properties		
1.3.4. Composition and Structure		
1.3.5. PY Motif		
1.3.6. Extracellular Loop		
1.3.7. Carboxy-terminus		
1.3.8. Liddle's Syndrome		
1.4. Regulation of ENaC		21
1.4.1. Proteases		
1.4.2. Regulation by Intracellular and Extracellular Sodium Ion Levels		
1.4.3. Hormonal Regulation (Aldosterone and Insulin)		

1.5. The Action of Vasopressin 25
1.5.1. The V Receptors
1.5.2. PKA Response
1.5.3. Direct Channel Phosphorylation
1.5.4. Evidence for Channel Insertion

1.6. Aims 32

CHAPTER 2 **COMMON METHODOLOGIES USED IN ALL INVESTIGATIONS**

2.1. General Materials and Methods 35

2.2. A6 Cell Culture 35
2.2.1. The A6 Clone
2.2.2. Culture Medium
2.2.3. Cells on Filter Supports
2.2.4. Progress to Mature Cultures

2.3. Electrophysiological Procedures 39
2.3.1. Electrode Preparation
2.3.2. Ussing Chamber Assembly
2.3.3. Tissue Short-Circuiting

2.4. Fluorescence Microscopy 42
2.4.1. Fluorescence
2.4.2. Resolution

2.5. Confocal Microscopy 47
2.5.1. General Comments
2.5.2. Confocal Lateral Resolution
2.5.3. Confocal Axial Resolution
2.5.4. Implications for this Study

CHAPTER 3 **A6 CELLS AND ADENYLATE CYCLASE**

3.1. Introduction 55

3.2. Materials and Methods 57
3.2.1. Cell culture
3.2.2. Cytochemical Localisation
3.2.3. Electron Microscopy
3.2.4. Measurement of AC Activity

3.3. Results 62
3.3.1. A6 Cell Culture Morphology
3.3.2. Adenylate Cyclase Localisation
3.3.3. Adenylate Cyclase Activity

3.4. Discussion 69
3.4.1. Electrically Maturing Cells
3.4.2. Morphology and AC Localisation
3.4.3. Signalling Cascades

CHAPTER 4 CURRENT FLUCTUATION ANALYSIS

4.1. Introduction 72
4.1.1. Membranes Modelled as Electrical Circuits
4.1.2. Electrical Recordings
4.1.3. Patch Clamp
4.1.4. Current Fluctuation
4.1.5. Theoretical Background (Fluctuation Analysis)
4.1.6. Blocker Introduction
4.1.7. Models for Blocker Interactions
4.1.8. Pulse Inhibition Protocol
4.1.9. Considerations for the Pulse-Protocol
4.1.10. Advantages and Disadvantages of Current Fluctuation Analysis

4.2. Materials and Methods 88
4.2.1. Cell Culture
4.2.2. Ussing Chamber Preparation and Tissue Mounting
4.2.3. Short-Circuit Current Measurements
4.2.4. Current Fluctuation Analysis

4.3. Results 93
4.3.1. Short-Circuit Current
4.3.2. Current Fluctuation Analysis

4.4. Discussion 101
4.4.1. Forskolin Effects on Sodium Transport
4.4.2. Blocker Interactions

CHAPTER 5 FLUID-PHASE MARKER UPTAKE

5.1. Introduction 104

5.2. Materials and Methods 106
5.2.1. Cell Culture
5.2.2. Fluid-Phase Marker Uptake
i) HRP Detection
ii) FITC Measurement
5.2.3. Time course of Uptake
5.2.4. Resistance Measurements
5.2.5. Cell Suspensions

5.3. Results 112
5.3.1. Marker Uptake
5.3.2. Time Course of Marker Uptake
5.3.3. Background Contamination

5.4. Discussion 117
5.4.1. Background Marker Contamination
5.4.2. Cell Suspensions

CHAPTER 6 **ENDOCYTOSIS VIEWED BY CONFOCAL MICROSCOPY**

6.1. Introduction 121
6.1.1. Aims

6.2. Materials and Methods 123
6.2.1. Cell Culture
6.2.2. Membrane Labelling
6.2.3. Confocal Chamber Assembly
6.2.4. Confocal Imaging
6.2.5. Time Course of Vesicle Uptake and Depth Analysis
6.2.6. Vesicle Counts
6.2.7. ENaC Labelling and Imaging
6.2.8. Autofluorescent Imaging
6.2.9. Differential Interference Contrast (DIC) Microscopy

6.3. Results 129
6.3.1. Autofluorescence
6.3.2. Cell Heights
6.3.3. Monolayer Imaging
6.3.4. Effect of Forskolin on Endocytosis
6.3.5. Time Course of Vesicle Uptake
6.3.6. Vesicle Counts
6.3.7. Channel Number Decline and Vesicle Accumulation
6.3.8. Depth Analysis
6.3.9. ENaC and Vesicles

6.4. Discussion 145
6.4.1. Troubleshooting
6.4.2. Vesicle Endocytosis
6.4.3. Membrane Capacitance
6.4.4. Is ENaC Involved?
6.4.5. Vesicle Destinations
6.4.6. Two Pools of Channels

CHAPTER 7 GFP-ENaC

7.1. Introduction **155**
7.1.1. GFP
7.1.2. GFP Properties and Structure
7.1.3. GFP as a Reporter Molecule
7.1.4. GFP Detection
7.1.5. EGFP Filtering

7.2. Materials and Methods **161**
7.2.1. Cell Culture
7.2.2. Green Fluorescent Protein Expression Vector Construction
7.2.3. A6 Cell Transfection
7.2.4. Transfection Controls (Null Vectors)
7.2.5. Electrophysiology
7.2.6. Confocal Microscopy
7.2.7. WGA-Rhodamine Labelling

7.3. Results **169**
7.3.1. Electrophysiology
7.3.2. EGFP Expression
7.3.3. EGFP-ENaC Imaging

7.4. Discussion **183**
7.4.1. GFP Clone Characterisation
7.4.2. Hormonal Response
7.4.3. Direct Channel Activation?
7.4.4. EGFP Localisation
7.4.5. Conclusions

CHAPTER 8 DISCUSSION AND SUMMARY

8.1. General Discussion **188**
8.1.1. The Use of A6 Cells
8.1.2. Hypotheses for ENaC Regulation
8.1.3. Cytoskeleton Involvement

8.2. Summary **194**
8.2.1. Adenylate Cyclase in A6 Cells
8.2.2. Electrophysiology
8.2.3. Marker Uptake Studies
8.2.4. Confocal Studies
8.2.5. GFP-ENaC

8.3. Conclusions **204**

8.4. Future Work **207**

CHAPTER 9 REFERENCES **209**

ABSTRACT

Regulation of sodium channel densities in A6 renal epithelial cells by hormonally-dependent mechanisms.

By Michael Bruce Butterworth

September 2001

Epithelial sodium channels (ENaC) located in the apical membranes of transporting epithelia, such as cells of the renal distal nephron, constitute the rate limiting step in the transcellular transport of sodium. The regulation of sodium ion reabsorption in the kidney, which is essential for salt and water homeostasis, is therefore governed by the cellular control of ENaC activity.

It is well established that the neurohypophysial hormone vasopressin (antidiuretic hormone) is responsible for both water and sodium regulation and, in renal cells, increases sodium permeability by regulating ENaCs at their apical membranes. The mechanisms involved in acute ENaC regulation have however not been demonstrated unequivocally. Evidence exists to suggest that sodium ion transport rates could be increased either by direct activation of membrane-resident ENaCs, or recruitment of channels from cytoplasmic storage pools. In order to address the issue, this study aimed to investigate the hypothesis that vasopressin regulation of ENaC occurred by targeted exocytic delivery of channels to the apical membrane from sub-apical pools.

All investigations were carried out on the sodium transporting A6 cultured cell line derived from *Xenopus laevis* kidney. The secondary messenger pathway of vasopressin stimulation had not been extensively characterised in these cells and this was the first study undertaken. Once it was established that an adenosine-3',5'-cyclic monophosphate (cAMP) secondary messenger pathway was in operation, attention was shifted to ENaC regulation in response to a raised intracellular cAMP level.

The electrophysiological technique of current-fluctuation analysis was employed to characterise the single channel response to cAMP production. These studies demonstrated that the main factor responsible for increased sodium transport was a dramatic increase in the number of channels at the apical surface despite declines in both single channel conductance and channel open probability. Investigating intracellular membrane traffic by marker-uptake and confocal microscopic techniques demonstrated that cAMP pre-stimulation significantly altered the rates of membrane endocytosis from the apical surface implicating regulated recruitment and retrieval mechanisms for ENaC regulation.

These methods provided indirect evidence for the shuttling hypothesis and established that the vesicle trafficking machinery was responsive to cAMP, but did not associate ENaC directly with the process. In order to demonstrate the movement of ENaC in conjunction with membrane trafficking mechanisms, a green fluorescent protein (GFP) tagged-ENaC was employed. By using live cell confocal microscopic techniques, the dynamic movement of GFP-ENaC in response to cAMP was demonstrated. Shuttling of ENaC to the apical surface was observed on cAMP stimulation with endocytic retrieval on removal of stimulus.

For the first time in live cells these data directly demonstrate the dynamic regulation of ENaC by shuttling mechanisms.

ACKNOWLEDGEMENTS

My thanks go first and foremost to my supervisor, Prof. Callie Els. His patience and guidance put me into a scientific mind-frame very early on in my time in his laboratory. Without his support I would not have achieved as much as I have to date. I also thank Prof. Lutz Thilo whose sweeping scientific (and political) discussions always kept me thinking.

I would like to acknowledge the generous financial assistance from the following sources during the course of my studies:

Champion Bursary for undergraduate studies
Foundation for Research Development (South Africa) Doctoral Scholarship
University of Cape Town Doctoral Travel Bursary
Stella & Paul Loewenstein Trust Medical Research Scholarship
National Research Foundation (South Africa) Doctoral Scholarship
Research Associateship (University of Cape Town)

Thanks to Prof. Van Driessche at the KU Leuven, Belgium, Drs Blazer-Yost and Rhodes at the Indiana University, University of Perdue, Indianapolis, USA for the generous donations of cell lines used in these studies.

I would like to thank a number of people for their technical assistance during this study which helped to facilitate my work. Dr Ian Harper who was brave enough to allow me loose on his confocal microscope, to tinker with chambers of dubious construction, never fearing the worst and always encouraging more. Anne Grobler, continued in that collaboration, allowing me unprecedented access to the confocal facility at the Tygerberg branch of the Medical Research Council of South Africa. The Department of Cardio-thoracic Surgery, UCT Medical School for free use of their confocal facility. Tommy Haylett for assisting me in getting started with marker-uptake studies and Ed Merrifield for his useful comments and suggestions. Thanks goes to Kieron Baldwin who introduced me to tissue culture techniques and the subtleties of noise-analysis.

On a more personal note I thank my wife Cassandra for her support, patience and loving assistance, especially when this thesis was in the final stages of preparation.

To my family and especially my parents my biggest thanks goes to you. Your encouragement, belief in me and my goals and unquestioning love and support allowed me to express my ambition and realise so many of my aspirations. I hope I have "made it count!"

CHAPTER 1

ION TRANSPORT AND SODIUM CHANNELS : INTRODUCTION, LITERATURE REVIEW AND STUDY AIMS

1.1. INTRODUCTION

1.1.1. Homeostasis

All eukaryotic cells in vertebrate organisms can only survive within very controlled environments. The availability of nutrients, ions and oxygen is balanced with the essential removal of waste and toxins from this regulated environment. It is most likely that ancestral vertebrates lived in a marine environment where the most important factor in the regulation of this internal cellular environment was the removal of nitrogenous wastes (Pough *et al.*, 1989). Water and ion regulation would not have been as essential.

As soon as vertebrates emerged on land, greater demands were placed on systems involved in homeostatic regulation. In order for any animal to survive out of water it was essential that the harsh variable external environment could be separated from the relatively stable internal environment (Cereijido *et al.*, 1993). In addition to the early requirements of waste removal, water and ion regulation became essential along with other homeostatic functions of temperature regulation, pH balance, energy use and the development of new reproductive strategies. Most important of these new demands was the regulation and conservation of water and ions (Ganong, 1991), which were no longer readily available from the surrounding environment.

The early sea-dwelling vertebrates would have evolved a primitive excretory organ, a precursor to the kidney responsible for waste regulation. In land-dwelling vertebrates this precursor is seen to increase in complexity of design with more complex vertebrate groups. Descriptive names following phylogenetic classification of holonephros, opisthonephros and metanephros have been used to describe this increase in complexity (Natochin, 1996; Pough *et al.*, 1989).

1.1.2. The kidney

One of the pioneers in furthering an understanding of extracellular fluid homeostasis, Homer Smith, commented that, "The history of renal physiology has erred, more often than not, by attempts at oversimplification. The problems of water and salt excretion appear to be extremely complex, and especially liable to this danger." (Smith, 1937). Even though the mammalian kidney appears complex in its ability to regulate so many homeostatic functions, it is composed of millions of nephrons each of which can be viewed as the basic microanatomical unit of all vertebrate kidneys. Of the numerous functions performed by vertebrate kidneys probably the most important and essential to life on land is the conservation of water and internal ionic regulation (Ganong, 1991). In this regard distal segments of the nephrons in particular have become specialised to respond to changes in the internal osmotic environment to regulate the water/ion levels reabsorbed in the kidney.

Of interest in this study was the reabsorption of sodium ions which occurs across the entire length of the nephron. Figure 1.1 schematically depicts the uptake of sodium ions (Na^+) along the nephron with the relative percentages reabsorbed in different regions illustrated. Although the majority of the Na^+ is taken back in the proximal section of the nephron, this occurs mainly by bulk reabsorption and is relatively unregulated. It is at the distal end where much of the regulated transport occurs and the region where most of the discussion will

focus. Although most of the attention will be paid to Na^+ regulation in the cortical collecting ducts (CCD) or collecting tubules it should be kept in mind that equally complex mechanisms are implicated in the uptake and secretion of a variety of different ions both in terms of transporters involved and controls employed.

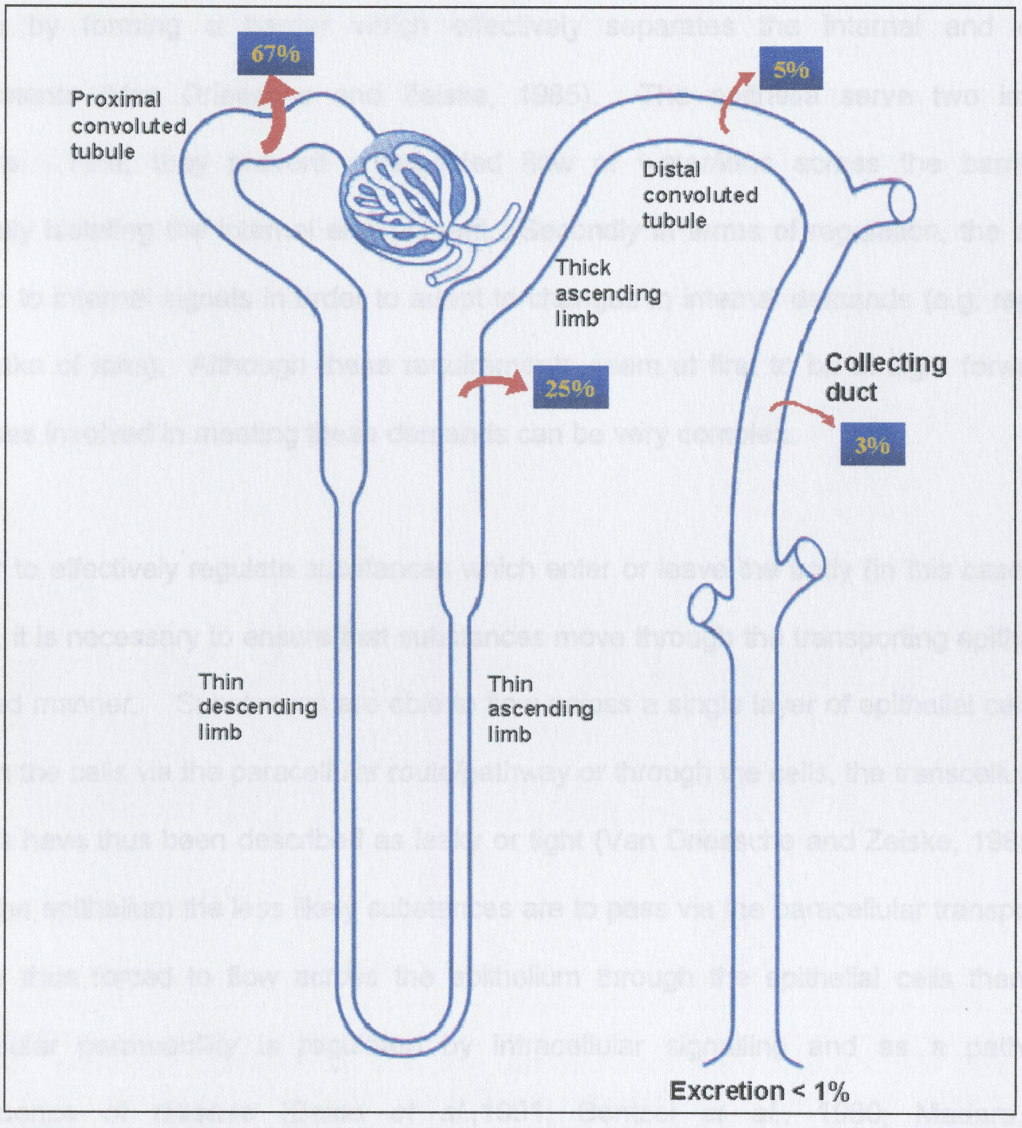

Fig.1.1. Schematic representation of a single nephron in the mammalian kidney. The relative percentage of Na^+ reabsorbed along the length of the nephron is indicated in the blue boxes. Notice that the collecting duct is only responsible for approximately 3% of the regulated Na^+ reabsorption, but that it is at this point where most of the control of internal Na^+ levels is affected. Less than 1% of total filtered Na^+ is excreted. (based on Navar and Hamm, 1999).

1.1.3. Epithelial barriers

Essential to all transporting processes both in the kidney and elsewhere is a specialised transporting epithelium. The epithelial cells are responsible for maintaining homeostatic balance by forming a barrier which effectively separates the internal and external environments (Van Driessche and Zeiske, 1985). The epithelia serve two important functions. First, they prevent unregulated flow of water/ions across the barrier thus effectively isolating the internal environment. Secondly in terms of regulation, the epithelia respond to internal signals in order to adapt to changes in internal demands (e.g. regulating the uptake of ions). Although these requirements seem at first to be straight forward, the processes involved in meeting these demands can be very complex.

In order to effectively regulate substances which enter or leave the body (in this case via the kidney), it is necessary to ensure that substances move through the transporting epithelia in a regulated manner. Substances are able to flow across a single layer of epithelial cells either between the cells via the paracellular route/pathway or through the cells, the transcellular path. Epithelia have thus been described as leaky or tight (Van Driessche and Zeiske, 1985). The tighter the epithelium the less likely substances are to pass via the paracellular transport route and are thus forced to flow across the epithelium through the epithelial cells themselves. Paracellular permeability is regulated by intracellular signalling and as a pathological consequence of disease (Balda *et al.*,1991; Bentzel *et al.*, 1980; Madara, 1988; Schneeberger and Lynch, 1992). The interest in this study however was the regulation of epithelial sodium channels, which represent the rate limiting step in the transepithelial movement of sodium ions through the epithelial cells and focus will thus be directed at transepithelial transport only. By forcing substance to pass through the cells, regulation can be exercised by the cells themselves. A schematic diagram of a tight epithelial layer is illustrated in figure 1.2.

In order to achieve a tight layer cells employ a variety of junctional proteins to ensure adjacent cells adhere tightly to one another. In so doing cells effectively block the paracellular pathway and prevent substances from leaking through the epithelium in an unregulated manner. There are a number of proteinaceous junctional complexes found in a variety of epithelial cells. Most common are the zonula adherens; macula adherens (desmosomes); nexus (gap junctions) and zonula occludens or tight junctions (Anderson and Van Itallie, 1995; Denker and Nigam, 1998). Gap junctions facilitate cell-to-cell communication, desmosomes serve to attach cells together at specific points in a rivet-like fashion and provide anchorage points for intermediate filaments (Denker and Nigam, 1998).

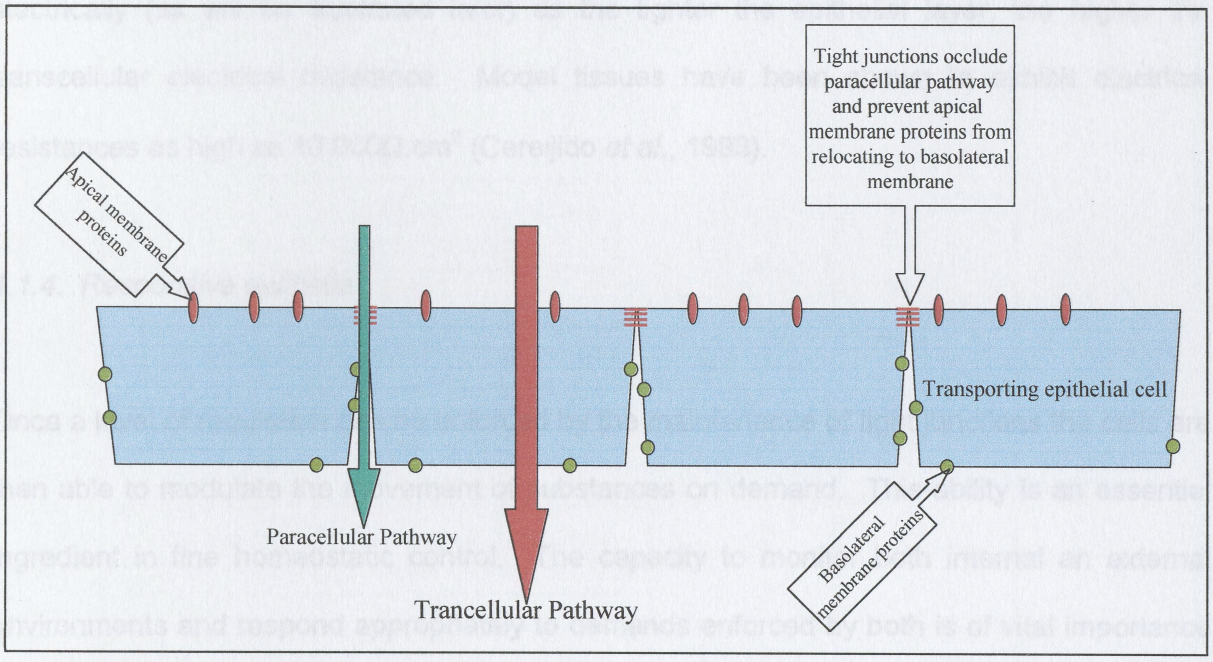

Fig.1.2. Schematic representation of a tight epithelial monolayer. Adjacent cells (blue boxes) adhere to one another by tight junctions (red strands indicated) forcing substances to move through the cells via a transcellular pathway (red arrow). In this way an apical and basolateral domain can be established with distinct protein populations in each membrane.

It is the last group, the tight junctions (TJ), which are responsible mainly for the establishment of a tight epithelium. This protein is usually located towards the apical membrane and in epithelial cells forms an occluding band around the edge of cells effectively stitching adjacent cells together whilst occluding the paracellular pathway. In so doing it acts as the fence for the paracellular pathway (Denker and Nigam, 1998) and effectively isolates

the apical plasma membrane from the basolateral membrane. Many proteins like zonula occludens (ZO)-1, ZO-2, ZO-3, 7H6 antigen, symplekin, cinulin and occludin have been associated with the formation of tight junctions (Anderson and Stevenson, 1992; Drubin and Nelson, 1996; Gumbiner *et al.*, 1991; Itoh *et al.*, 1993; Jesaitis and Goodenough, 1994; Mitic and Anderson, 1998; Stevenson *et al.*, 1986, 1996; Van Itallie and Anderson, 1997). However the exact nature of the strands comprising the TJ is still not clear.

The transporting epithelia in the distal kidney are characterised by particularly abundant TJ's which in turn result in a tight epithelial cell layer. This fact can be readily demonstrated electrically (as will be illustrated later) as the tighter the epithelial layer, the higher the transcellular electrical resistance. Model tissues have been shown to exhibit electrical resistances as high as 10 000$\Omega.cm^2$ (Cereijido *et al.*, 1993).

1.1.4. Responsive epithelia

Once a level of regulation can be enforced by the maintenance of tight junctions the cells are then able to modulate the movement of substances on demand. This ability is an essential ingredient in fine homeostatic control. The capacity to monitor both internal an external environments and respond appropriately to demands enforced by both is of vital importance to ensuring the continued survival of the organism. To maintain a constant internal environment an epithelium is usually required to keep regulation within narrowly defined parameters. In addition it is essential to have a continuous monitoring system in order to adapt responses should the environment change. This is most commonly achieved in almost all homeostatic systems by a negative feedback mechanism. Very rarely is a positive feedback loop, which elicits an ever-increasing response utilised. In order to illustrate the mechanism of a negative feedback loop, a generalised description of the hormonal response to decreased blood osmolarity is depicted in figure 1.3.

The blood osmolarity in humans is kept fairly constant at approximately 290mOsm/l (Navar, 1984). An increase in blood plasma osmolarity initiates a feedback loop implicating the hormonal messenger antidiuretic hormone (ADH)/vasopressin. The effect of vasopressin is to increase water reabsorption to reset osmolarity levels. Once the osmolarity goes up, the release of hormone stops and the negative feedback loop is complete.

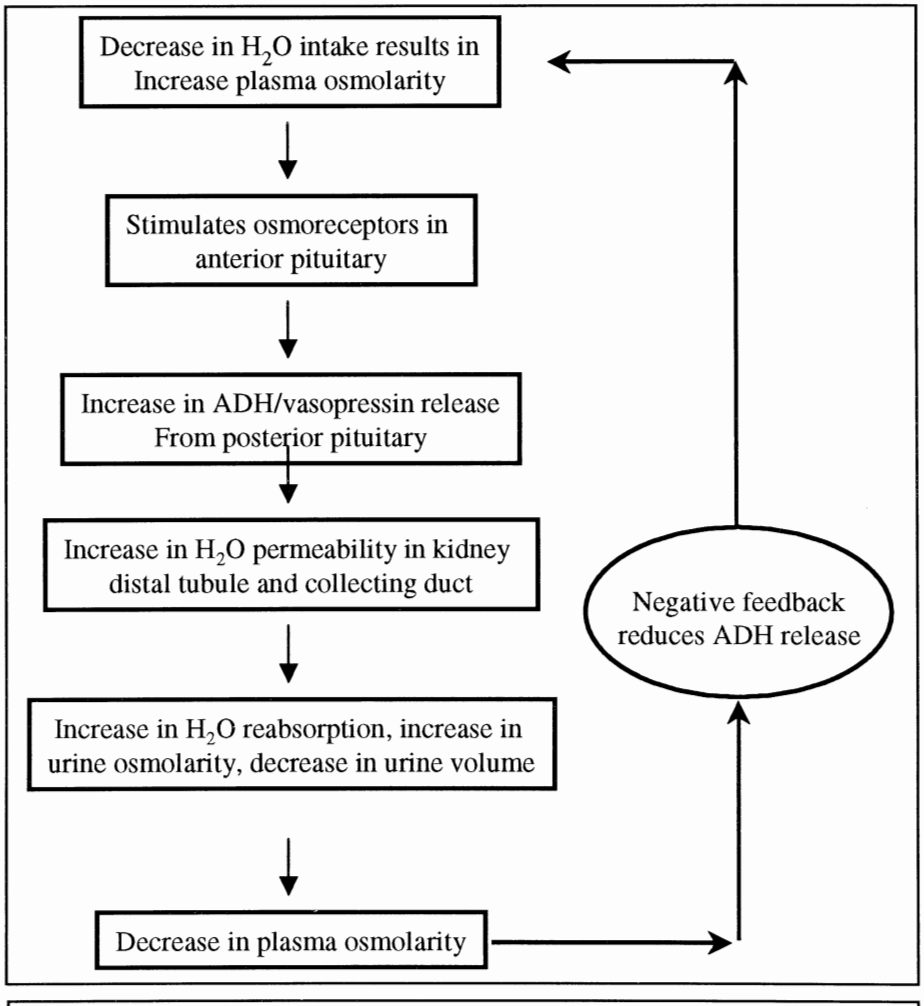

Fig.1.3. Descriptive example of a negative feedback loop.

In addition to increasing water reabsorption in the kidney, vasopressin also influences sodium ion (Na^+) regulation. The reabsortion of Na^+ is probably the most important function of the kidney as Na^+ is responsible for the maintenance of the extracellular fluid (ECF) volume (Navar and Hamm, 1999).

1.2. MEMBRANE TRANSPORTERS

1.2.1. Crossing an epithelium

Due to their charged nature, ions are mostly driven passively across epithelia by an electrochemical gradient. In order to move ions against this gradient requires energy, and due to the differences between extracellular and intracellular ionic environments, at least one step in the movement of ions across an epithelial barrier requires energy (Van Driessche and Zeike, 1985). The lipid membrane of epithelial cells is virtually impermeable to all non-polar substances (Alberts *et al.*, 1989). Only very small or polar substances are able to cross the membrane by simple diffusion. The charged nature of ions therefore makes them relatively impermeable to the hydrophobic environment of cell membranes and in order to cross a tight epithelial lipid bilayer a number of transport proteins are required (Starr and Taggart, 1998).

Transporters have been categorised by their specific transport characteristics and can basically be placed in one of three categories, namely; pumps, transporters and channels (Stryer, 1988). Pumps are the only transport proteins that require energy and are therefore mainly involved in transporting substances against a concentration gradient and help in the maintenance of such gradients. The other two all transport substances down their respective electrochemical gradients (Starr and Taggart, 1998).

Regardless of classification, some general characteristics (Stryer, 1988; Voet and Voet, 1990) have been described for all transporters namely:

i) Transport is far more rapid than would be the case in simple diffusion or movement across an epithelium without the transporter. Transport of ions in particular are accelerated thousands of fold in some cases.

ii) The transport is saturable. Even if the transport follows a simple linear kinetic rate, a maximal transport rate can be demonstrated when the transporter becomes saturated and a kinetic curve will be seen to plateaux at this point. The saturation of the transporter can be expressed by the following equation: $J = \frac{J_{MAX}[S]}{K_M + [S]}$ where : J = Transport Rate, J_{MAX}=maximal transport rate, [S]= concentration of transported substance (solute) and K_M = Michaelis constant (Voet and Voet, 1990).

iii) Transporters generally exhibit chemical specificity. This important characteristic ensures that only the solute of interest can cross the membrane, excluding any others. Where this not the case, all substances would enter or leave the cells down their specific electrochemical gradients negating any barrier effect of the epithelium.

iv) Transporters can be competitively inhibited. A molecule that is similar to that being transported can often compete for binding sites on the transporter and be shuttled through the membrane in preference to that molecule intended to be transported. This fact is often exploited in drug design to inhibit transport of specific substances by "blocking" or inhibiting the transporter by competitive inhibition.

v) Some transporters can also be non-competatively inhibited. In such situations, the inhibitor does not compete for the binding site on or in the transporter, but binding inhibits transport nevertheless. This is most commonly associated with pumps.

1.2.2. Channel proteins

The proteins in this group form highly selective water-filled pores across membranes. Almost all channels in animal cells are concerned with ion transport and are commonly referred to as ion channels. The flow of ions is down an electrochemical gradient and can reach rates of a millions of ions per second in some cases. This is more than 100 times greater than rates achieved by carrier proteins (Alberts *et al.*, 1989). Channel proteins are either open all the time allowing ions to flow through membranes in a constitutive manner or most often channels can be switched on or off according to requirements. This ability to open or close channels is referred to as "gating". Gating has evolved in many forms and a number of different channels have been described which have different types of gates (Ganong, 1991).

Common gating strategies include:

i) Voltage-gated channels: The opening of channels in response to change in potential difference/voltage across the membrane. These channels are commonly involved in the transmission of nervous signals, in the form of action potentials, in the acquisition and transmission of sensory information.

ii) Mechanically-gated channel: Mechanical stimulation or stretching of the membrane in which these channels reside cause them to open and transport ions.

iii) Ligand-gated channels: The binding of a signalling molecule results in the opening of these channels. The signalling molecule can be an extracellular or intracellular mediator. A good example of an extracellular mediator comes once again from the nervous system. Extracellular mediators are in the form of

neurotransmitters that are responsible for transmitting the electrical signal, generated by voltage gated channels, from one cell to the adjacent cells via a synapse. In this case the ligand-gated channel is sometimes referred to as a transmitter-gated channel. There are numerous examples of intracellular mediators such as ions (ion-gated channels), nucleotides (nucleotide-gated channels) and GTP-binding proteins (G-gated-channels).

From these basic classifications almost all of the transport proteins can be described. The focus of the discussion will shift to describe the channel whose regulation this thesis specifically addresses, namely the epithelial sodium channel (ENaC). This is a channel protein and therefore transports in a passive manner. This channel is a specific sodium ion transporter and has been well described in a number of different tissues.

1.3. EPITHELIAL SODIUM CHANNEL (ENaC)

The amiloride-sensitive sodium channels are the rate limiting proteins in the two-step entry of Na^+ across an epithelium. ENaCs have been placed in a class of proteins called the ENaC-Deg ion channel family (Alvarez de la Rosa *et al.*, 2000). The Deg refers to a group of genes encoding this channel in *Caenorhabtidis elegans* (Chalfie and Wollinsky, 1990; Driscoll and Chalfie, 1991; Mingxia and Chalfie, 1994). Early evidence of channel protein extracted from bovine renal papillae and A6 cells was presented suggesting that the sodium channel was composed of five nonidentical polypeptide subunits with molecular masses of 315 000, 149 000, 95 000, 71 000 and 55 000 (Benos *et al.*, 1987).

1.3.1. Cloning

Since ENaC was cloned from rat colon (Canessa *et al.*, 1994a; Lingueglia *et al.*, 1993) a large amount of information has emerged about the channel structure and composition. From the cloned channel, Canessa *et al.* (1994a) demonstrated that the channel was instead composed of three homologous subunits, α- β– and γ-ENaC. Following the first reported cloning, ENaC has been cloned in other species including human (McDonald *et al.*, 1995), bovine (Fuller *et al.*, 1995), chicken (Goldstein *et al.*, 1997), frog (Puoti *et al.*, 1995) and mouse (Ahn *et al.*, 1999).

1.3.2. Expression

The channels are expressed in a number of tissues and have been localised in many mammalian and non-mammalian organisms. Sodium transport was described early on in amphibian skin (Koefoed-Johnsen and Ussing, 1958) with this tissue used as a model to

describe sodium transport across an epithelial layer (Ussing and Zerhan, 1951). Since then ENaC has been described in a number of toad tissues namely, skin, urinary bladder, lung and collecting tubules (Fischer and Clauss, 1990; Hunter *et al.*, 1987; Nagel and Cabbé, 1980; Palmer *et al.*, 1982). In birds, ENaC is localised in the coprodeum, an excretory organ (Bindslev *et al.*, 1982; Clauss *et al.*, 1987). In mammalian tissue (of different species), ENaC is predominantly associated with the kidney and bladder, surface cells of the distal colon, airway and alveolar epithelium of the lung and ducts of exocrine glands. In the kidney, ENaC is situated predominantly along the distal end of the nephron, *inter alia* the distal convoluted tubule, connecting tubule, cortical collecting tubule, inner and outer medullary collecting tubule and the bladder (Almeida and Burg, 1982; Duc *et al.*, 1994; Frindt and Windhager, 1990; Garty and Benos; 1988; Koeppen, 1986; Lewis and Diamond, 1976; Loffing *et al.*, 2000; Rossier *et al.*, 1994; Shareghi and Stoner, 1978; Stanton, 1989). In the rat intestine ENaC was identified in the illial and colonic segments (Will *et al.*, 1985a, 1985b). From studies in human and rabbit tissue it was found that in the lung tracheal, bronchiolar and alveolar tissue contained ENaC (Boucher and Gatzy, 1983; Knowles *et al.*, 1984; O'Brodovich, 1995; Saumon and Basset, 1993) as well as sweat and salivary glands (Knauf, 1972; Quinton, 1981).

In addition to these more common sites of ENaC expression, several other reports have identified ENaC expression in other cell types, for example the sensory cells of the tongue (Heck *et al.*, 1984; Lindemann, 1995) where it appears to be involved in taste perception (Lindemann, 1996, Schiffman *et al.*, 1983). Amiloride-sensitive channels have been reported in brain microvessels (Vigne *et al.*, 1989), the thyroid gland (Verrier *et al.*, 1989) and lymphocyte cells (Bradford *et al.*, 1995; Bubien and Warnock, 1993) where the role of the channel is however unclear.

1.3.3. Properties

The three ENaC subunits are structurally similar sharing a 32-37% homology with one another at the amino acid level (Canessa *et al.*,1993). Each subunit contains two predicted transmembrane spanning domains (M1 and M2 depicted in figure 1.4) intra-cytoplasmic amino- and carboxy- termini and a cysteine-rich extracellular domain (Canessa *et al.*, 1994b; Renard *et al.*, 1994; Snyder *et al.*, 1994). There are numerous sites on the extracellular domain for N-linked glycosylation (Prince and Welsh, 1998, 1999).

The most commonly expressed channel is a highly selective low conductance channel. In these ENaCs selectivity for Na^+ over K^+ is greater than 20:1 (McNicholas and Canessa, 1997) with some earlier reports estimating the selectivity to be even higher at between 100:1 to 1000:1 (Benos *et al.*, 1980; Palmer, 1982). The ENaCs exhibit slow gating kinetics with long opening times, from milliseconds to several seconds (Ling *et al.*, 1991; Marunaka and Eaton, 1991; Palmer and Frindt, 1986) and relatively low conductances (in comparison to voltage gated channels) most commonly between 4-6 pS (Schild *et al.*, 1997). Slight variations in these channel conductances have been reported depending on the tissue or model system being studied, with ranges from 4 pS in alveolar cells (Voilley *et al.*, 1995) to 12 pS in rabbit proximal tubules (Gogelein and Greger,1986) . Channels are highly sensitive to the diuretic amiloride (Benos, 1992; Palmer, 1984) which is able to block the channel in the sub-micromolar range (Hamilton and Eaton, 1986). Sensitivity to amiloride and its analogues produces the pharmacological sensitivity profile of benzamil>amiloride>ethlisopropyl amiloride (EIPA) in contrast to the Na^+/H^+ transporter which has a profile EIPA>amiloride>benzamil (Canessa *et al.*, 1995; Kleyman and Cragoe, 1988).

Another group of amiloride-sensitive channels have been characterised which are less selective for Na^+ and typically higher conducting channels. Some of the differences in properties of these channels may be as a result of expression in non-native systems. The features of many of the different channels are discussed in the extensive review by Garty and Palmer (1997) and will not be listed in detail here. It would be suffice to add however that expression systems have enabled the role of ENaC subunits in Na^+ transport to be better explored. Expression of the α subunit alone in *Xenopus sp.* oocytes is able to produce amiloride sensitive sodium conductances, while β and γ subunit expression alone or together does not support sodium transport (Alvares de la Rosa *et al.*, 2000; Fyfe and Canessa, 1998). Expression of the β and γ subunits together with α greatly enhances the sodium conductance observed by α alone.

1.3.4. Composition and structure

The composition, number and stochiometry of the subunits that form a functional channel is still not clear. The channel is described as a heterooligmeric protein made up of the three homologous subunits (Puoti *et al.*, 1997). Earlier investigations reported putative assemblages containing eight or nine subunits, 3α, 3β and 3γ (Eskandari *et al.*, 1999; Snyder *et al.*, 1998), however additional evidence has suggested that four or six subunits are required (Firsov *et al.*, 1998; Kosari *et al.*, 1998), 2α, 1β and 1γ or 2α, 2β and 2γ with the 2:1:1 configuration most favoured at present.

A schematic diagram (fig.1.4) illustrates the main features of an ENaC subunit based on evidence to date. Features illustrated include the 2 membrane spanning domains, M1 and M2, the intracellular amino- and carboxy- termini, the cysteine rich regions (CDR1 & 2). Two proline rich regions (P1 & 2) have been described on the intracellular carboxyl end (Staub *et*

al., 1996) with the second region, P2 containing a conserved proline-tyrosine (PY) motif which has the configuration XPPXY, where X varies with different subunits.

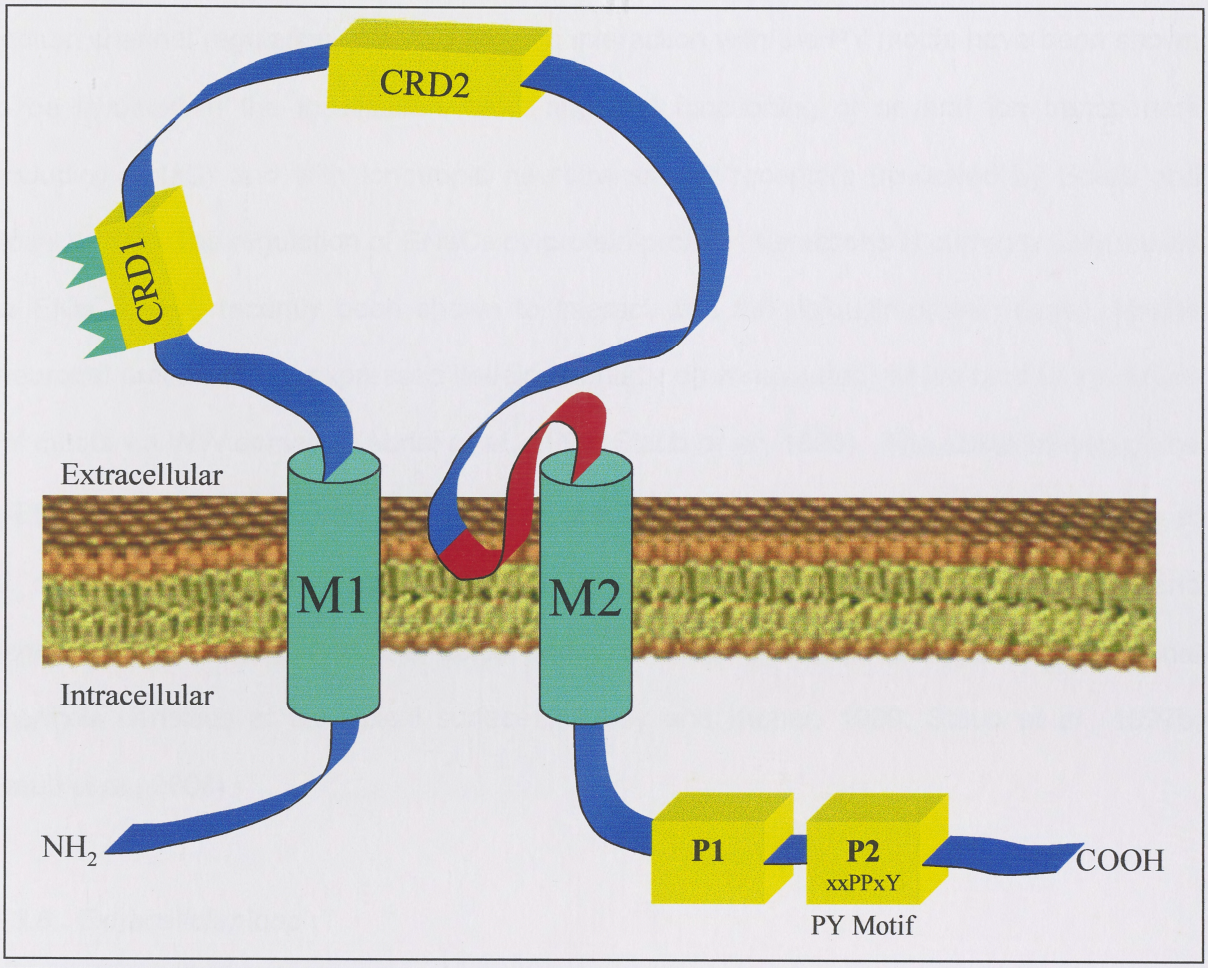

Fig.1.4. Schematic illustration of the characteristic features of an ENaC subunit based on evidence to date. Notice the membrane spanning domains (M1 & M2) the intracellular tails and the PY motif at the carboxy-terminus. There are also two cystine rich domains (CRD) on the extracellular loop.

1.3.5. PY motif

The PY motif has been found in a number of protein-protein interactions to bind to two conserved tryprophans (W), referred to as a WW domain (Sudol, 1996). The WW domain

typically consists of 35-40 amino acids. These interactions were first described for tyrosine kinases (Irusta and DiMaio, 1998), but have recently been shown in a wide number of protein interactions and have enabled researchers to document novel WW proteins involved in signaling and other cellular processes (Chen *et al.*, 1997; Pirozzi *et al.*, 1997). Of interest in sodium channel regulation, the WW domain interaction with the PY motifs have been shown to be involved in the localization, clustering and functioning of several ion transporters (including ENaC) and with ionotropic neurotransmitter receptors (reviewed by Staub and Rotin, 1997). The regulation of ENaCs by protein-protein interactions is currently very topical as ENaCs have recently been shown to interact with the ubiquitin-protein ligase, Nedd4 (neuronal precursor cell expressed developmentally downregulated) which bind to the ENaC PY motifs via WW domains (Abriel *et al.*, 1999; Staub *et al.*, 1996). The ubiquitination of the α-ENaC, but not the β-ENaC subunit has been shown to be functionally important (Staub *et al.*, 1997a). It has been suggested that Nedd4 binding acts as a signal for the retrieval and degradation of channels in the apical membrane as a means of regulating functional channels densities at the apical surface (Harvey and Kumar, 1999; Staub *et al.*, 1997b; Staub *et al.*, 2000).

1.3.6. Extracellular loop

The large hydrophilic extracellular loop represents about 70% of the amino acids (Firsov *et al.*, 1999), is approximately 50kDa and lies between the hydrophobic membrane spanning regions (Canessa *et al.*, 1994a). Preceding the second membrane-spanning domain (M2) is a conserved pre-M2 section (illustrated in red) that may be important in ion permeation and amiloride blocking (Schild *et al.*, 1997). As all the extracellular cysteines are conserved in the CRD, this region obviously plays an important role in functional channel formation. In fact a mutation in the CRD of human α-ENaC has been implicated in the disease

pseudohypoaldosteronism type 1 (PHA-1) characterised by severe salt wasting and studies have suggested that the region is essential for channel routing to the plasma membrane (Firsov *et al.*, 1999).

1.3.7. Carboxy-terminus

In humans the gene encoding the nonvoltage-gated sodium channel was mapped to chromosome 12 (Hansson *et al.*, 1995, Voilley *et al.*, 1994). Mutations in the β and γ subunits result in the human in clinically abnormal pseudohyperaldosteronism-like condition known as Liddle's syndrome. Diseases such as Liddle's syndrome often provide insights into the functional regulation of proteins by illustrating how defective regulation effects physiology. Consequently the PY motif and areas toward the carboxy-terminus of the β-ENaC subunit have been implicated in ENaC regulation as mutations in these regions result in Liddle's syndrome. Due to the information which such mutations provide, a brief description of the syndrome follows below.

1.3.8. Liddle's syndrome

Liddle's syndrome is an autosomal dominant form of hypertension characterized by early onset of hypertension associated with hypokalemia, suppressed plasma renin levels and suppressed secretion of the mineralocorticoid hormone, aldosterone. The syndrome was described by Liddle *et al.* (1963) as hypertension associated with hypokalemic alkalosis not due to hyperaldosteronism but rather a renal tubular "peculiarity". Three generations in the same family were effected, with no known male-to-male transmission at that time. A follow-up study confirmed the original description by Liddle which demonstrated that amiloride and

triamterene were effective treatments for hypertensive and hypokalemic symptoms in patients as long as dietary sodium intake was restricted (Nakada *et al.*, 1987; Rodrigues *et al.*, 1981; Wang *et al.* 1981). Complete linkage of the disorder to the gene encoding the β subunit of the ENaC was demonstrated (Shimkets *et al.*, 1994). Following the cloning of the ENaC analysis of the gene for the beta subunit in patients with Liddle's disease revealed either a premature stop codon or frameshift mutation that truncated the carboxyl terminus of the β subunit (Snyder *et al.*, 1995). The result was a constitutively active and longer lived functional channel in the apical membrane of cells expressing the mutated ENaCs with the subsequent chronic increase in transport of sodium across the apical membrane. This effect was also demonstrated in a mutation of the gamma subunit (Hansson *et al.*, 1995). Mutations to a conserved motif in the C-terminus of either of the subunits reproduced the affect of Liddle's syndrome (Snyder *et al.*, 1995). Mutated subunits produce channels which are longer lived in the apical membrane with a consequential increase in the number of active channels at the membrane surface.

A number of mutation variants have been described and the mutations which result in the subunit modifications are listed briefly below:

i) ARG567TER: C-to-T mutation at the first nucleotide of codon 564 in the β subunit produces a stop codon which results in the deletion of the last 75 amino acids from the protein (Shimkets *et al.*, 1994).

ii) PRO616LEU: Substitution of one of the highly conserved proline to a leucine in codon 616 at the c-terminus of β or γ subunits. Results in the final 45 or 76 amino acids to be deleted in the β and γ subunit respectively (Hansson *et al.*, 1995).

iii) GLY37SER: A glycine (position 37) to serine substitution in the β subunit. Reported in a small group of people with Arab kindred living in Israel (Chang *et al.*, 1996).

iv) TYR618HIS: tyrosine to histadine mutation at 618 position. Mutation produces functional expression indistinguishable from (i), when studied in oocytes (Tamura *et al.*, 1996).

v) 1-BP INS, 592C: In this case an insertion of a cytosine residue at position 592 which causes the coded protein to undergo a frameshift, resulting in premature termination of the protein at codon 605 (Findling *et al.*, 1997).

vi) 32-BP DEL: The deletion of 32bp introduced a stop codon at position 582 (Jeunemaitre *et al.*, 1997).

vii) PRO615SER: A misense mutation of proline to serine at position 615 in the conserved PY motif producing symptoms clinically diagnosed as Liddle's syndrome (Inoue *et al.*, 1998).

The fact that expression of ENaC at the surface of cells is affected in the various forms of Liddle's disease gives some insight into the possible mechanism of ENaC regulation and the idea that translocation of ENaC to and regulated removal from the apical membrane is of importance. However, although Liddle's syndrome is able to provide some insight, it does not describe a normal physiological state.

1.4. REGULATION OF ENAC

Sodium ion regulation by ENaC has been extensively studied in a variety of model systems, from native epithelia to artificial membranes. From these studies a number of different modes of ENaC regulation have been identified.

1.4.1. Proteases

Studies on the effects of extracellular proteases demonstrated that proteolysis of ENaC can lead to sodium transport modulation. Studies demonstrated a reduction in sodium transport when apical cell surfaces were treated with trypsin (Garty and Edelman, 1983). This study was supported by experiments performed in rabbit urinary bladders when three different proteases, namely kallikeirn, urokinase and plasmin all induced a decrease in sodium transport (Lewis and Alles, 1986; Lewis and Clausen, 1991). More recent studies have however found that proteases were able to activate ENaC expressed in *Xenopus sp.* oocytes (Chraïbi *et al.*, 1998) and a new channel activating protease (CAP-1), related to trypsin, has been identified which also activates ENaC (Vallet *et al.*, 1998). Although channels appear to be influenced by proteases, the mode of regulation still appears to be unclear.

1.4.2. Regulation by intracellular and extracellular sodium ion levels

Regulation of ENaC has been shown to be modulated by levels of both extracellular and intracellular sodium ions (Na^+). Research has provided evidence for the inhibition of sodium transport with increased extracellular Na^+ levels (Fuchs *et al.*, 1977; Kroll *et al.*, 1991; Palmer *et al.*, 1998; Smets *et al.*, 1998). This regulation of ENaC by the ion it transports has been classified into two categories, namely self-inhibition and feedback inhibition (Lindemann, 1984).

Feedback inhibition of the channels is defined as a downregulation due to the transport of Na^+ across the apical membrane, that is when sodium enters the cell. Self-inhibition is defined as a regulation of the channel activity by the apical sodium concentration, here extracellular sodium levels do not need to be transported into the cells to effect ENaC regulation (Palmer *et al.*, 1998).

Evidence for feedback inhibition has been found by electrophysiological analysis of ENaC in frog skin (Abramcheck *et al.*, 1985; Helman & Baxendale, 1990), epithelial A6 cells (Ling & Eaton, 1989) and rat cortical collecting tubule (Breyer, 1991; Frindt *et al.*, 1993, 1996; Silver *et al.*, 1993). Mediating factors of voltage (Frindt *et al.* 1993), intracellular Ca^{2+} and Ca^{2+}-dependent protein kinase activity (Breyer, 1991; Frindt *et al.* 1996; Ling & Eaton, 1989; Silver *et al.* 1993), and cellular metabolism (Frindt *et al.* 1995) have been suggested. Feedback inhibition typically exhibits a longer time course than self-inhibition and is thought to involve a second messenger cascade (see cascades described below), probably implicating protein kinase C (Abramcheck *et al.*, 1985; Els and Chou, 1993; Els and Helman, 1991; Frindt *et al.*, 1993, 1996; Ling and Eaton, 1989; Rokaw *et al.*, 1996a; Silver *et al.*, 1993).

Self-inhibition on the other hand was been demonstrated some time ago in frog skin (Fuchs *et al.*, 1977). More recent investigations using patch clamp on rat cortical collecting tubules produced a similar result (Palmer *et al.*, 1998).

Regulation of ENaC by intracellular Na^+ levels has also been demonstrated. Studies using *Xenopus sp.* oocytes established ENaC inhibition by increased intracellular Na^+ concentrations (Abriel and Horisberger, 1999; Kellenberger *et al.*, 1998). Awada (1999) further reported two inhibitory responses, separated temporally when effects of intracellular Na^+ were investigated in the same model system. Investigations on the mouse salivary duct cells confirmed results

demonstrated in oocytes (Komwatana *et al.*, 1996). The inhibition of ENaC in this study was independent of cytosolic pH, Ca^{2+} and Cl^-, but suggested a role for the guanine nucleotide-binding regulatory (G) protein (see secondary messenger cascades below). In a subsequent study making use of the same cell type, the authors demonstrated the involvement of Nedd4 (see discussion above) in the inhibition of ENaC by increased cytosolic Na^+ levels (Dinudom *et al.*, 1998).

1.4.3. Hormonal regulation (aldosterone and insulin)

Extensive studies on have been carried out on hormonal regulation of ENaC in a variety of model systems. As the mineralocorticoid aldosterone is the major regulator of salt and water balance in the kidney its actions have been intensively investigated (Garty and Palmer, 1997). Its main effect is to bring about an increase in Na^+ absorption through ENaC, but it has been show to influence a number of other transporters and exchangers (reviews by: Bastl and Hayslett, 1992; Garty, 1986, 1992; Schafer and Hawk, 1992; Verrey, 1995). The slow acting, long term effects of aldosterone seem to indicate either *de novo* synthesis of ENaC (Asher *et al.*, 1992,1996; Renard *et al.*, 1995) or an alteration in channel open probability (a measure of channel open time) to account for increases in sodium transport (Kemendy *et al.*, 1992). As the regulation of ENaC by aldosterone is not being investigated here, a debate on mode of regulation is not warranted. However with so much work done on the actions of aldosterone it is clear that ENaC is involved and that regulation of Na^+ is thus affected (extensively reviewed: Bastl and Hayslett, 1992; Clauss and Skadhauger, 1988; Garty, 1986, 1992; Garty and Palmer, 1997; Horisberger and Rossier, 1992; Palmer, 1992; Palmer and Frindt, 1992; Rossier and Palmer, 1992; Schafer and Hawk, 1992; Verrey, 1995; Wang *et al.*, 1992). In addition to direct effects in terms of synthesis or alterations in transport properties of ENaC a number of additional proteins have been demonstrated to be expressed by long-term exposure of cells to

aldosterone (Benjamin and Singer, 1974; Kirsten *et al.*, 1968, 1970; Minuth *et al.*, 1989; Rachamim *et al.*, 1995; Scott *et al.*, 1978; Truscello *et al.*, 1986). The role these aldosterone-induced proteins (AIP) play in Na^+ regulation is yet to be fully determined. Some of the proteins have been implicated in energy production (to provide for increases in the Na^+/K^+ ATPase expression) but in other cases, the proteins are often closely associated with ENaC subunits suggesting that they are involved directly in regulation (Geheb *et al.*, 1981a, 1981b, 1983; Szerlip and Cox, 1989; Szerlip *et al.*, 1988, 1989, 1991)

It has also been demonstrated that insulin evokes an increase in sodium absorption by modulation of ENaCs at the apical membrane (Blazer-Yost and Cox, 1988; Blazer-Yost *et al.*, 1989; Civan *et al.*, 1988, 1989; Erlij *et al.*, 1994; Marunaka *et al.*, 1992; Rodriguez-Commes *et al.*, 1994; Schoen and Erlij, 1987). Just as in the case of vasopressin response (see comments in the next section) the regulatory mechanisms for insulin action are still under debate. Two scenarios have been suggested, namely an insertion of ENaC into the apical membranes of cells by exocytosis to increase sodium transport, or direct activation of membrane resident channels (Erlij *et al.*, 1994; Marunaka *et al.*, 1992). These scenarios will be discussed in detail in the regulation of ENaC by vasopressin (see below).

The action of vasopressin (anti diuretic hormone) on ENaC and its role in ENaC regulation are to be investigated in this study and will thus be dealt with in a bit more detail below.

1.5. THE ACTION OF VASOPRESSIN

Arginine vasopressin is synthesised in the hypothalamus and transported to the posterior pituitary (neurohypophysis) where it is secreted as a nona-peptide hormone (Stryer, 1988) whose amino-acid structure is illustrated in figure 1.5 below.

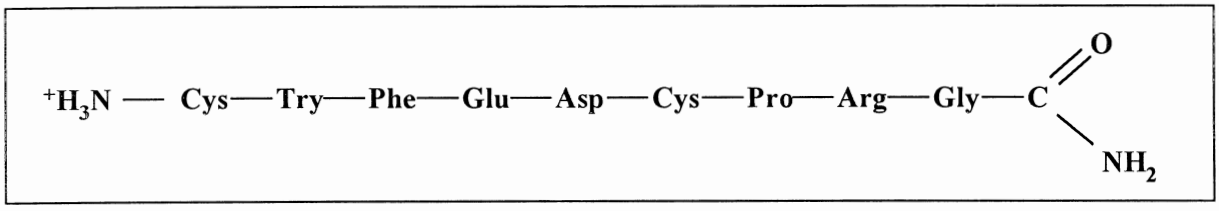

Fig. 1.6. The 9 amino acid structure of vasopressin

Vasopressin has been demonstrated to bind three different types of receptor, termed V_{1a}, V_{1b} and V_2.

1.5.1. The V receptors

The V_2 receptor is thought to be important in the vasopressin response in ion and water regulation and will be the main focus of discussion, but as will be mentioned, evidence of the involvement of the V_1 receptor has also recently emerged (see Chapter 3). The V_2 receptor is a typical member of the guanine nucleotide regulatory (G) protein-coupled receptor (GPCR) family and has seven transmembrane spanning domains (Peter *et al.*, 1995). Common features of G proteins include a heterotrimetic structure (in the same fashion as ENaCs) with α, β and γ subunits (Ausiello, 1991). The V_2 receptor is proposed to interact with the G protein-binding domain via the α subunit. Each GPCR interacts only with specific subclasses of G proteins within cells. However the vasopressin receptors are unique in their

coupling profiles to G proteins (Liu *et al.*, 1995). The three subtypes of vasopressin receptors share a 40-50% sequence identity (de Keyzer *et al.*, 1994; Lolait *et al.*, 1992; Morel *et al.*, 1992; Sugimoto *et al.*, 1994). The V_1 receptors are selectively coupled to G proteins of the $G_{q/11}$ family which are responsible for activating distinct isoforms of phospholipase Cβ which in turn is responsible for the breakdown of phosphoinositide lipids (PI hydrolysis) setting up the inositol triphosphate secondary signaling pathway illustrated in figure 1.6 (Liu *et al.*, 1995).

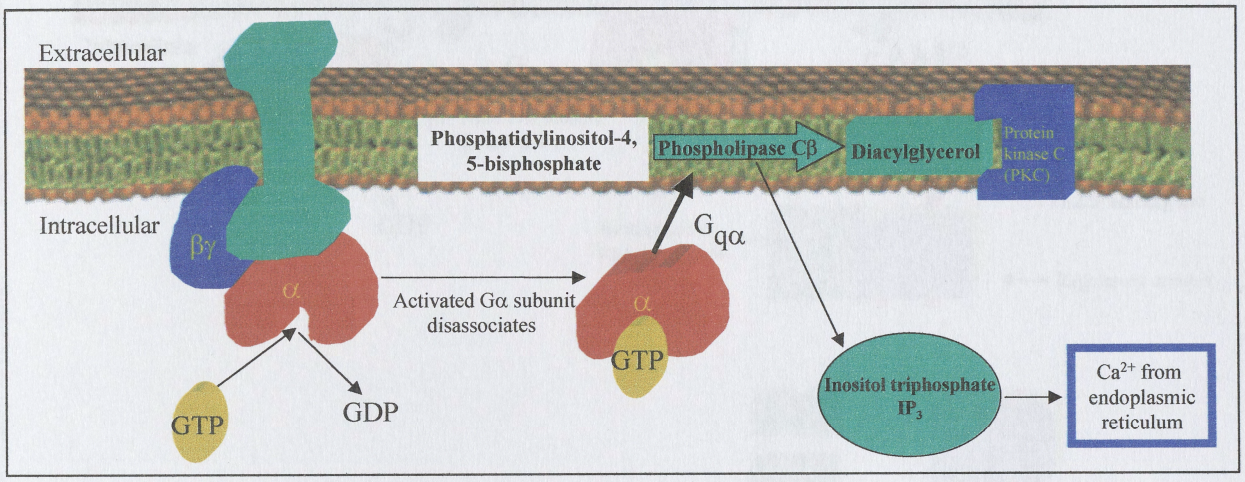

Fig. 1.6. The secondary messenger cascade set up by binding of vasopressin with a V_1 receptor results in the production of IP_3 and release of stored calcium as indicated.

On the other hand, the V_2 receptor activates the stimulatory G protein (G_s) which results in the activation of adenylate cyclase and this distinct signaling pathway is illustrated in figure 1.7. The effect of vasopressin binding with V_2 receptors is therefore the eventual production of an active catalytic protein kinase A (PKA) moiety.

Having transduced the external hormonal signal into an internal chemical message, the epithelial cells are in a position to act on the information provided by the homeostatic signal,

and will need to do so in an appropriate manner. The effect of vasopressin, acting via PKA needs to be examined in greater detail.

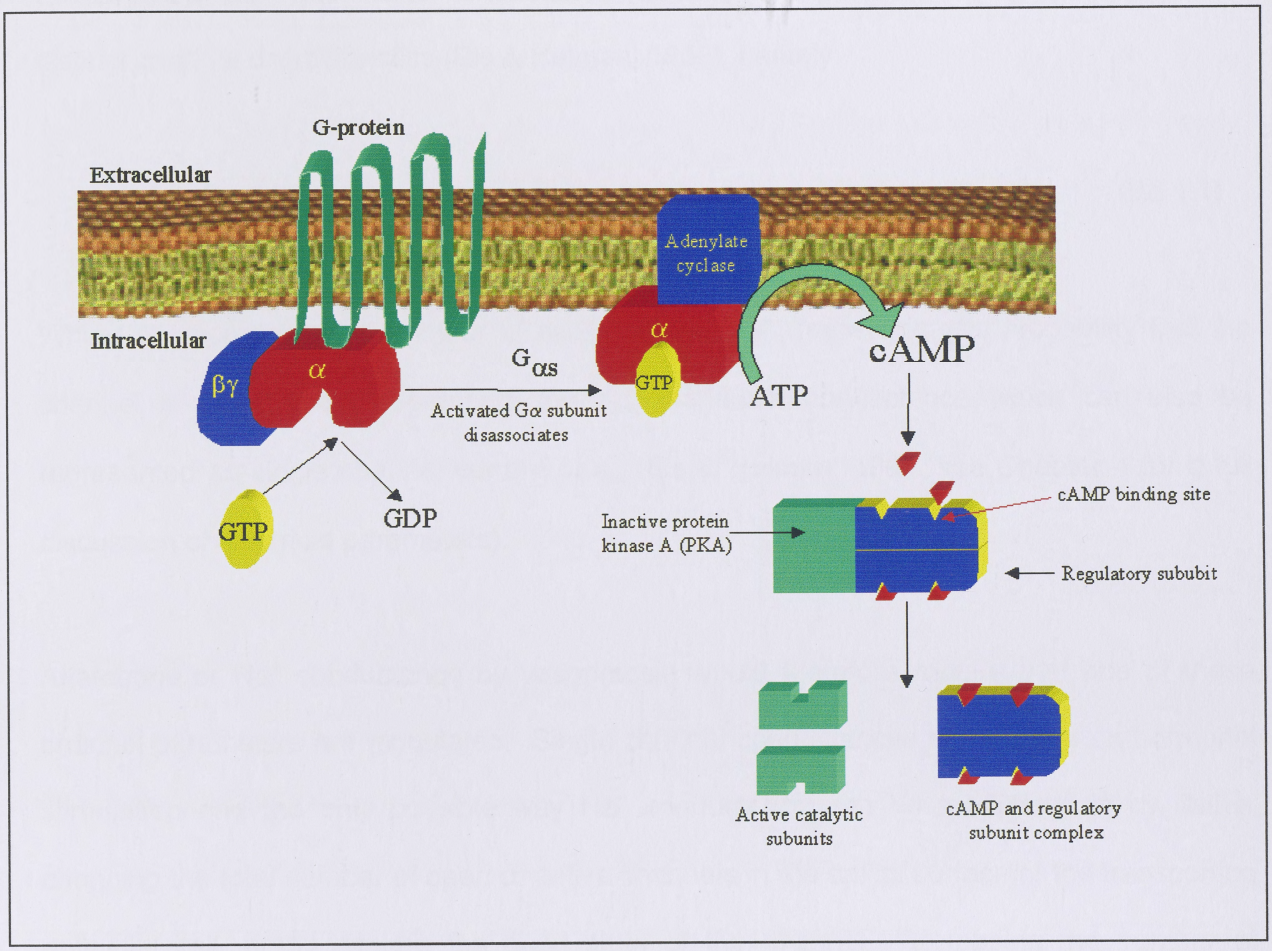

Fig. 1.6. The production of cyclic aedonsine-3'-5'-monophosphate (cAMP) by adenylete cyclase in respone to G-protein activation produces an active PKA available to transduce the hormonal signal into ENaC regulation

1.5.2. PKA response

Several investigations indicate that vasopressin, acting via the PKA secondary messenger pathway, regulates Na^+ transport and increases permeability and therefore electrical conductance of the apical membrane to Na^+ (Els & Helman, 1981; Els & Helman, 1989; Els &

Mahlangu, 1987; Helman *et al.*, 1983; MacKnight *et al.* 1980; Nagel, 1978). Sodium transport occurs through the highly selective ENaCs located in the apical membranes of tight epithelia. Modulation in Na^+ permeability can therefore only be brought about by a change in ENaC properties. Membrane conductance (G) can be expressed as the product of three distinct channel characteristics (Els & Helman, 1989), namely:

$$G=N_oP_o\gamma \qquad \text{(Eq.1.1)}$$

Where N_o represents the number of open channels, P_o represents the probability that the channel is open and γ represents the single-channel conductance which can also be represented as single channel current or i_{Na} (Els & Helman, 1989, see Chapter 4 for a full discussion of electrical parameters).

Alterations or Na^+ conductance by vasopressin would therefore require that one of these channel parameters are modulated. Single channel conductances do not alter on hormonal stimulation and the only possible way Na^+ conductance can be modulated is by, either changing the total number of open or active channels in the apical surface of the transporting epithelial cell, or by altering the open state of the channel. Increasing the number of transporting channels would obviously result in an increase in Na^+ conductance, and likewise, altering the open state of the channel (i.e. ensuring the channel spends proportionally more time in the open state) would achieve the same result. It has been found from a number of investigations (Chou & Els, 1997; Els & Helman, 1991; Li *et al.*, 1982; Marunaka & Eaton, 1991) that PKA enhances ENaC activity predominantly though increases in total channel number with little change to open probability. What is not clear however, are the mechanisms involved which bring about these changes in ENaC densities. Proposals which could account for these changes in channel densities have focused on two main

areas. One suggestion is that inactive channels resident in the apical membrane are acted on directly, most likely by direct phosphorylation, causing them to become active and therefore increase the total number of transporting channels in the apical membrane. A second hypothesis suggests that these channels are recruited from a storage pool located beneath the apical membrane. Channels would therefore be trafficked to the apical membrane on PKA stimulation to increase ENaC densities at the apical surfaces of the cells. These two conditions need not be mutually exclusive and demonstrating that one strategy may be involved may not preclude the existence of another form of regulation. In order to understand how the increase in Na^+ transport is brought about in collecting duct epithelia investigators have attempted to find confirmation for either of these hypotheses just discussed. In so doing, two bodies of evidence have emerged.

1.5.3. Direct channel phosphorylation

Evidence has been presented to support the hypothesis in a number of studies. Vasopressin-dependant phosphorylation of a peptide associated with a purified ENaC complex was demonstrated (Sariban-Sohraby *et al.*, 1988). Direct phosphorylation of channels was demonstrated in studies using ENaCs reconstituted in planar lipid bilayers (Ismailov *et al.*,1994; Oh *et al.*, 1993). Several studies using toad bladder, another CCD model tissue were also suggestive of direct activation (Levine *et al.*, 1981; Palmer and Lorenzen, 1983; Stetson *et al.*, 1982; Taylor *et al.*, 1978). In further support of the direct phosphorylation idea was the finding that the carboxy-tails of ENaC β and γ subunits could be phosphorylated directly by PKA, the downstream messenger of the AC/cAMP cascade (Shimkets *et al.* 1998). In addition, PKC, aldosterone and insulin were all shown to phosphorylate these subunits of ENaC in the same study. In a related study aimed a clarifying some of the effects of various protein kinases on ENaC activity, Volk *et al.* (2000)

demonstrated that PKC had a direct effect in regulating human ENaC kinetics which were expressed in the *Xenopus sp.* oocyte model system. A less specific PKA inhibitor however used in the Volk study seemed to have no effect on ENaC activity.

Direct activation of a 5-pS channel by PKA was reported from studies in excised toad bladder patches (Frings *et al.*, 1988). Studies on A6 epithelia membrane patches indicated channel activation by PKA (Prat *et al.*, 1993a, 1993b).

1.5.4. Evidence for channel insertion

In contrast to the idea of direct channel activation, the second hypothesis considered is recruitment of channel by exocytic insertion into the apical membrane. The idea of ENaC recruitment was first proposed from studies by Garty and Edelman (1983). Using toad bladder the authors demonstrated the emergence of new (unaltered) channels on vasopressin stimulation after membrane trypsinisation had effectively destroyed ENaC function at the apical surface. The hormonal response was not diminished significantly, suggesting that these channels had been inaccessible to the proteolytic effects of trypsin, possibly being stored beneath the apical membrane in storage pools.

Further support comes from radioiodination studies in A6 cells (Kleyman *et al.*, 1994) in which a doubling in surface labelling of specific antigens after hormone-stimulation was reported, suggesting translocation from an intracellular pool. Results from patch clamp studies performed on A6 (Marunaka and Eaton, 1991) demonstrated that the P_O of the channels was not altered by vasopressin, but rather observed an increase in the numbers of channels recorded per patch.

The recent demonstration that Nedd4 binding results in channel retrieval and degradation would also support an hypothesis of channel regulation by trafficking (see description above). The involvement of cytoskeletal proteins in this mechanism of activation will be addressed in more detail in the dicussion of results (see Chapter 8), but the role of actin in ENaC regulation was also demonstrated (Cantiello, 1995; Prat *et al.*, 1996) indicating that some type of trafficking may be implicated.

These methods however gave no direct evidence for trafficking of ENaC by hormonal stimulation and lead to the basis of this study.

1.6. AIMS

The effects of vasopressin in cells of the distal cortical collecting duct (CCD) and its model epithelia have been well documented. There is an increase in sodium ion transport through ENaC as a result of actions of vasopressin, cAMP and analogues. This increase has been demonstrated to occur by increases in ENaC transport, mainly as a result of increases in active channel densities at the apical cell surface. The mechanisms responsible for the observed increase in channel density are however less clear.

Two hypothesis have been described above which would support the observed increases in sodium ion transport. The first advocates direct activation of "electrically silent" channels resident in the membranes of the cell while the second suggest a recruitment of channels from storage pools beneath the membrane. The mechanisms involved in acute ENaC regulation may indeed be more complex than just these two scenarios, and may well implicate both hypothesis, but to date evidence for the recruitment hypothesis has come from indirect means, often not investigating ENaC at all.

In order to resolve some of the unanswered questions concerning ENaC regulation by cAMP, studies were carried out to examine the hypothesis that ENaC is recruited by trafficking mechanisms. In this regard cultured A6 cells, a model cell line for the CCD were used in all investigations. The central aim of this study was therefore to investigate the hypothesis that in A6 epithelia, ENaC is regulated by trafficking mechanisms.

As the activation of ENaC by a cAMP secondary messenger pathway was to be investigated, and because no information about localisation and activity of adenylate cyclase (the enzyme responsible for cAMP production) was available for these A6 cells, the first aim was to

characterise the production of cAMP within maturing cell cultures and determine both the level and location of cAMP production.

Once this information was established, regulation of ENaC by cAMP was investigated directly. Questions that needed to be addressed were:

1) The electrical effect of elevated cAMP production as it pertained to sodium transport and more specifically single channel, ENaC parameters.
2) Whether cAMP altered trafficking, in terms of endocytosis from or exocytosis to the membranes of these cells, and what the vesicular mechanisms involved in trafficking processes may be. The aim was therefore to establish if the A6 cells produced and employed the required vesicular machinery which may be involved in ENaC regulation.
3) Whether ENaC was involved in vesicular traffic and if this could be linked to observed changes to channel densities reported in earlier studies.

To answer these questions a variety of techniques were employed which included:

1) Current-fluctuation analysis in order to obtain single channel electrical information from ENaCs within the cell membrane.
2) Short-circuit current measurements to investigate macroscopic Na^+ regulation.
3) Fluid-phase endocytic marker uptake protocols to study vesicular trafficking.
4) Confocal microscopic techniques to examine vesicular trafficking events in living A6 cultures.
5) The use of a green-fluorescent protein (GFP) reporter system in cloned A6 cells to investigate ENaC regulation by live cell by microscopy.

Evidence gained from these investigations would not only address unresolved questions regarding the actions of cAMP, but would also serve as a model for the actions of other acute agonists in ENaC regulation. Microscopic techniques developed for use in these studies and described in the thesis can be applied to many other epithelial cell systems in the study of a variety of intracellular processes.

CHAPTER 2

COMMON METHODOLOGIES USED IN ALL INVESTIGATIONS

2.1. GENERAL MATERIALS AND METHODS

As A6 cells were used in all investigations and due to the fact that much of the cell preparation for individual experiments was so similar, a general methods description will be presented here for the common elements of the work. Specific protocols and modifications of the methods presented here will be supplied for each new section as it is relevant. Mention will be made of changes to these protocols, but should no mention be made it can be assumed that procedures outlined below were followed. In addition, general theoretical considerations about common techniques (like microscopy) outside the scope of the specific discussions of experimental results will be presented. Although the theoretical background may not be directly applicable to the results *per se*, a better understanding of the techniques involved were important to avoid potential experimental pitfalls.

2.2. A6 CELL CULTURE

2.2.1. The A6 clone

Stocks of A6 cells, derived from *Xenopus sp.* kidney, (Johnson clone) at passage 106 (a gift form Professor W. van Driessche of the K.U. Leuven, Belgium) were stored in cryovials in liquid nitrogen. Cells were subcultured from these stocks by defrosting and placing in 260 ml culture flasks (Nunclon Delta, Nunc, Napperville, USA) to obtain a seed stock. Flasks were placed in a 28^{0}C, humidified incubator with 2.5% CO_2 at a pressure of 3 kPa. The medium was changed after the first day and subsequently after every second day.

2.2.2. Culture medium

The culture medium was a powdered Delbecco's Modified Eagle Medium (DMEM) from Highveld Biological (Johannesburg, South Africa) to which 1,041 g/l of Hepes (sodium salt, Fw: 260.3 g/mol) was added as a buffer (Sigma, St. Louis, USA). The final pH was adjusted to 7.4. Medium was filtered using a 2 μm hollow fibre media filter (MediaKap -5 or Millipore) and a peristaltic pump (Masterflex pump controller Cole Parmer Instrument Co.) into 500 ml autoclaved bottles. Medium in use was supplemented with 50 ml heat inactivated (30 minutes in a 56 ^{0}C water bath) foetal calf serum (FCS) from Highveld Biological, added to 450 ml of the filtered medium. To combat infection, 5 ml of an antibiotic solution (Highveld Biological) containing penicillin (100 μg/ml) and streptomycin (100 units/ml) was added to the 500 ml medium (plus FCS). The final osmolality of the medium was approximately 250 mOsm/kg. Before use, medium was supplemented with 10 ml/l of the amino acid L-glutamine (Sigma) from a 3% stock solution.

2.2.3. Cells on filter supports

All tissue culture procedures were carried out under sterile conditions in a laminar flow hood. Cells maintained on plastic culture flasks were lifted when they had reached 80-90% confluency (about 5 days) and either subcultured or frozen down (to maintain stocks). Cells were never subcultured more than 5 times before reverting to frozen stocks. This ensured a constant passage age and similar physiological condition of all cultures. Cells to be seeded onto filter supports were lifted by washing flasks first with 15 ml phosphate-buffered saline (PBS comprised 8.5 mM NaCl; 17.5 mM $NaHCO_3$; 4 mM KCl ; 0.8 mM K_2HPO_4) followed by incubation at 28 ^{0}C with 5 ml of a 0.05% trypsin and 0.02% ethylenediaminetetraacetic acid (EDTA) PBS solution at pH 7.4. Cells typically lifted from the culture flasks within 10 minutes after which 5 ml DMEM containing FCS was added to the solution to inactivate the trypsin.

The cell suspension was then collected, placed into 10 ml centrifuge tubes and spun down at 1000 g for 2 minutes. The supernatant was discarded and the pellet of cells resuspended in 10 ml culture medium. Due to the fact that cells grown on non-porous surfaces, such as plastic, do not form polarized epithelial monolayers (Lewis and Donaldson, 1990) all electrophysiological protocols required culturing on filter supports.

The same filter supports were used in all investigations as it had been shown by previous research that different filter supports produced differences in transport characteristics of the same A6 cell line (Candia *et al.*, 1993; Helman and Liu, 1997). The nitrocellulose membrane (pore size of 0.45 μm) Millicel-HA inserts (30mm) from Millipore (Bedford, USA) were used in this case. Inserts were placed into a six-well multidish plate (Nunc) with 2 ml of the prepared DMEM in each well (basolateral surface). Sufficient time was given to allow DMEM to permeate the membranes (by sight). Filters were then seeded with the cell suspension at a density of 1×10^5 cells/cm^2. Cells were periodically counted with the aid of a Nebula counting chamber to ensure uniform seeding densities were maintained. Once the appropriate volume of cell suspension had been seeded, DMEM was added to the filter cup so that the apical medium was made up to 3 ml. The cells were then incubated until needed for experimentation. The DMEM was initially changed after one day to remove non-adherent cells and every second day thereafter.

2.2.4. Progress to mature cultures

Transepithelial voltages (V_T) and resistances (R_T) of cells growing on inserts were periodically measured, in their wells, with the aid of a Millicell-Electrical Resistance System (Millipore) and chopstick electrodes. These measurements aided in determining suitability of filters for experimental use. An increase in R_T indicated that a tight cell monolayer had been formed and

increase in V_T that vectoral transport had been established in the cultures. Cultures with a V_T greater than 20 mV and R_T above 1000 Ω/cm^2 were used in all cases. Typically cultures took from 7-10 days to reach this point and as a rule cultures younger than seven days were not used. Mature cultures maintained these characteristics even more than 28 days after seeding, but in all cases no cells over 21 days were ever used. Cells between passages 107 to 115 were used in the experiments.

2.3. ELECTROPHYSIOLOGICAL PROCEDURES

In order to perform electrical measurements on the cells cultured on filters, investigations were carried out in a modified 4-electrode Ussing chamber. Despite the eventual protocol employed, all cells and equipment were prepared in a similar manner and can thus be described here.

2.3.1. Electrode preparation

The electrodes used to measure both current and voltage were sliver/silver chloride (Ag/AgCl) made with thin silver wire. Previously used wire was scraped clean and electrocoated with chloride ions (Cl^-) by placing in a 1:50 diluted 30% hydrochloric acid (HCl) solution and passing current through the solution. The Ag wire was placed at the anode and a reference Ag wire on the cathode terminal and a small potential (2V) applied across the HCl solution for 10 minutes to coat the wire. Once coated a Ag/AgCl electrode was prepared by placing the coated wire in a small tube filled with a 5 M NaCl solution kept in the tube with a 5 M NaCl/agar bridge. The electrodes were filled with NaCl as opposed to KCl as it has been considered that possible leakage of small amounts of KCl would influence the experiment system to a far greater extent that NaCl (Van Driessche and Erlji, 1983). The bridge was prepared as 2% agar (May and Baker, U.K.) in the 5 M NaCl solution. Four identical electrodes were prepared with two serving as current and two as voltage electrodes in the chamber. The voltage electrodes however were placed closest to the cells on the filter (see chamber assembly below). Electrode offsets (inter-electrode potentials) were measured with a multimeter and electrodes with offsets greater than 1 mV were discarded. This was done to ensure that false short-circuit current values were not recorded.

2.3.2. Ussing chamber assembly

One advantage of using a cell line derived from amphibious tissue was the fact that experiments could be performed at room temperature. Thus all assembly and electrical recordings were done without the need for a heated incubator. Once selected filter inserts were ready for mounting in the Ussing chamber, they were taken from the incubator, lifted out of the culture plate and excess fluid was removed from the basal surface. At this point the inserts were no longer sterile and were therefore never kept if it was found that they could not be used to avoid risk of contaminatory infections. Each insert was glued onto a polycarbon (perspex) transfer ring (see figure 2.1), approximately 15 mm in diameter, using a cyanoacrylate tissue glue (Eurecryl, Silicone Technical Products, South Africa). A sharpened metal tissue punch with a diameter slightly larger than the transfer ring was used to cut out the insert membrane. The ring with its attached tissue was transferred to the Ussing chamber where it was held in place by two gaskets with small amount of silicone grease (Dow Coming high vacuum grease). The grease minimised edge damage (Helman and Miller, 1971) and was used to obtain a tight seal and avoid medium leakage. As soon as the tissues were mounted, the chambers were filled with medium to minimise the time tissue was exposed to air. The cells in the chamber were then continuously perfused with medium without FCS or antibiotics for the duration of the experiment. The assembly of the Ussing chamber is illustrated schematically in figure 2.1.

Each chamber was individually perfused at a rate of about 9ml/min which could be varied if needed. This arrangement allowed substances to be introduced to each side of the cell layer independently if desired. Each chamber had a volume of 600 µl with an area of 0.75 cm^2 of tissue exposed to the medium in the chamber. Once medium flow had been established cells were allowed to stabilise for at least 20 minutes before the start of any experimental protocol.

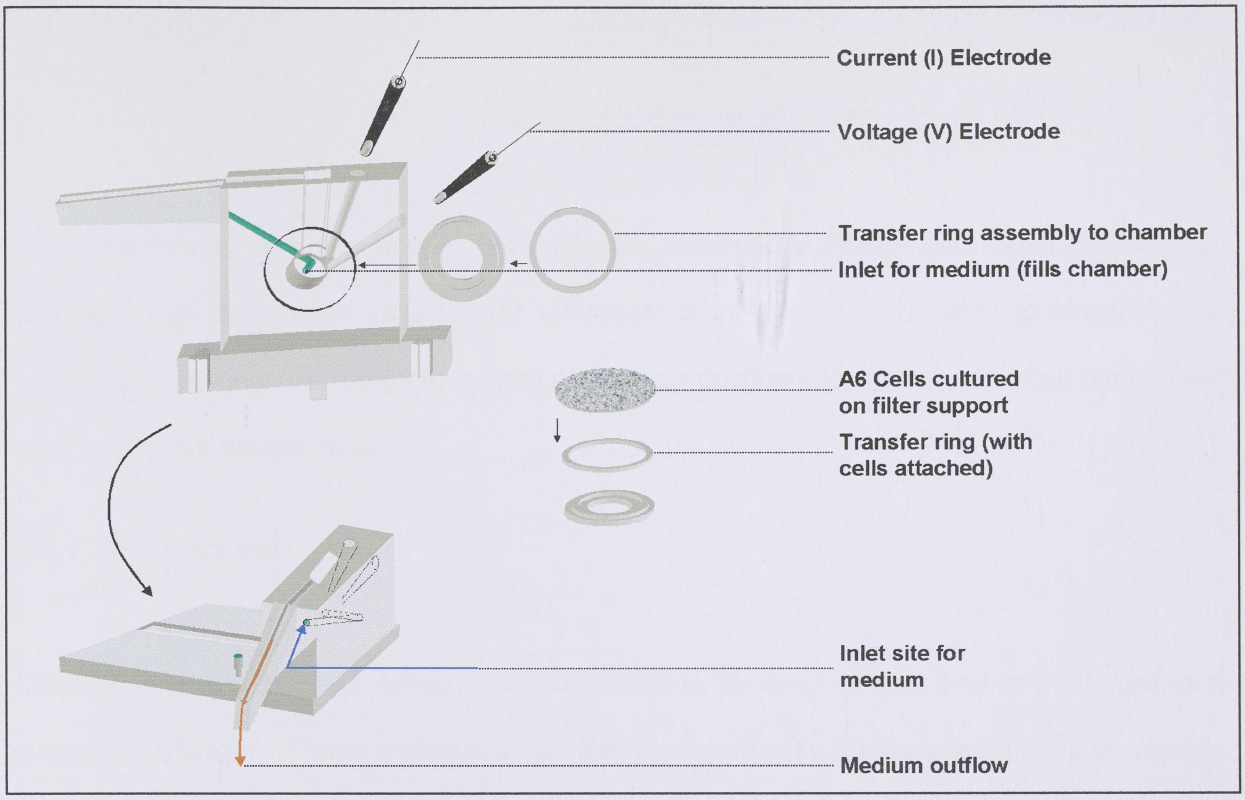

Fig. 2.1. Schematic illustration of the Ussing chamber assembly used for all electrophysiological investigations. The 4-electrode chamber had a current and voltage electrode on each side of a mounted epithelial cell layer. Medium flowed continuously into each of the sealed chambers and was collected after flowing down a spillway from the top of the chamber as indicated.

2.3.3. Tissue short-circuiting

The Ussing chamber assembly was housed in a shielded (Faraday) cage and all connections earthed. The entire rig was mounted on a marble table to minimise vibration. The clamp apparatus was powered by a 12 V direct current (DC) battery to reduce any noise input which would have occurred had an alternating current (AC) source (electrical mains) been used. Mounted epithelia were continuously short-circuited with a low noise clamp (Van Driessche and Gullentops, 1982; Van Driessche and Lindemann, 1978) which was clamped at 0 mV to eliminate movement of ions via the paracellular pathway. Records of short-circuited current were kept for all experiments and recorded on a strip-chart recorder (Liner 1200, Anatech Instruments Ltd., South Africa). To check transepithelial resistances, tissues were periodically pulsed with a small (3 mV) pulse and resistances calculated by Ohm's law by observing the change in short-circuit current.

2.4. FLUORESCENCE MICROSCOPY

The basis for confocal microscopy, which is to be employed in studies detailed in chapters six and seven of this thesis, is standard fluorescence microscopy. In order to describe the variations involved in the confocal system a brief introduction into fluorescence and fluorescent microscopy is therefore required.

2.4.1. Fluorescence

Fluorescence results when certain molecules absorb photons of light and re-emit light at a longer wavelength. These molecules, generally polyaromatic hydrocarbons or heterocycles are termed fluorophores, fluorochromes, or fluorescent dyes (Ploem, 1993). The absorption of photons of light by a population of these molecules raises their energy level to a brief excited state. As they decay from this excited state back to the ground state, they emit fluorescent light. When the fluorescent molecule falls from the excited to ground state light is often emitted at a characteristic wavelength. The energy of the emitted photon ($h\nu_{EM}$) is the difference between the energy levels of the two states which then determines the wavelength of the light emitted (Van Vliet *et al.*, 1998),

$$\lambda_{EM} = \frac{hc}{E_{EM}} \qquad \text{(Eq.2.1)}$$

where

E = the energy difference between the 2 states

h =Plank's constant

and c = the speed of light.

Fluorophores are excited maximally at a specific wavelength of light (excitation wavelength), but this peak excitation wavelength is the maximum point in a range of wavelengths above and below the peak wavelength. Thus it is more accurate to refer to an excitation spectra which is the plotted curve of light wavelength and intensity of excitation. In the same way the emission wavelengths of light also produce a spectra referred to as the emission spectra. A theoretical example of a fluorophore's excitation and emission spectra are depicted in figure 2.2. The width of the excitation spectrum reflects the fact that the fluorochrome molecule can be in any of several vibrational and rotational energy levels within the ground state and can end up in any of several vibrational and rotational energy levels within the excited state. In practice, a fluorochrome is most effectively excited by wavelengths near the apex of its excitation peak. The wavelength difference between the excitation and emission peaks is referred to as the Stokes' shift.

The relevance of this phenomenon is that it is important when deciding on the type of fluorophore to use for a particular application. The greater the Stokes' shift, the easier the excited and emitted wavelengths are to filter from one another and this makes for a less noisy detected signal. Overlapping emitted signals can be particularly problematic when multicolour (two or more fluorophores) imaging is attempted. The overlap between the trailing tail of the emission spectrum of one fluorophore or filter and the leading tail of the emission spectrum of another fluorophore or filter is often referred to as the "cross-talk" between the two fluorophores or filters.

The effective choice of fluorophores with emission wavelengths markedly separate from each other and the correct choice of specific emission filters is one of the most important considerations when attempting this multi-coloured imaging.

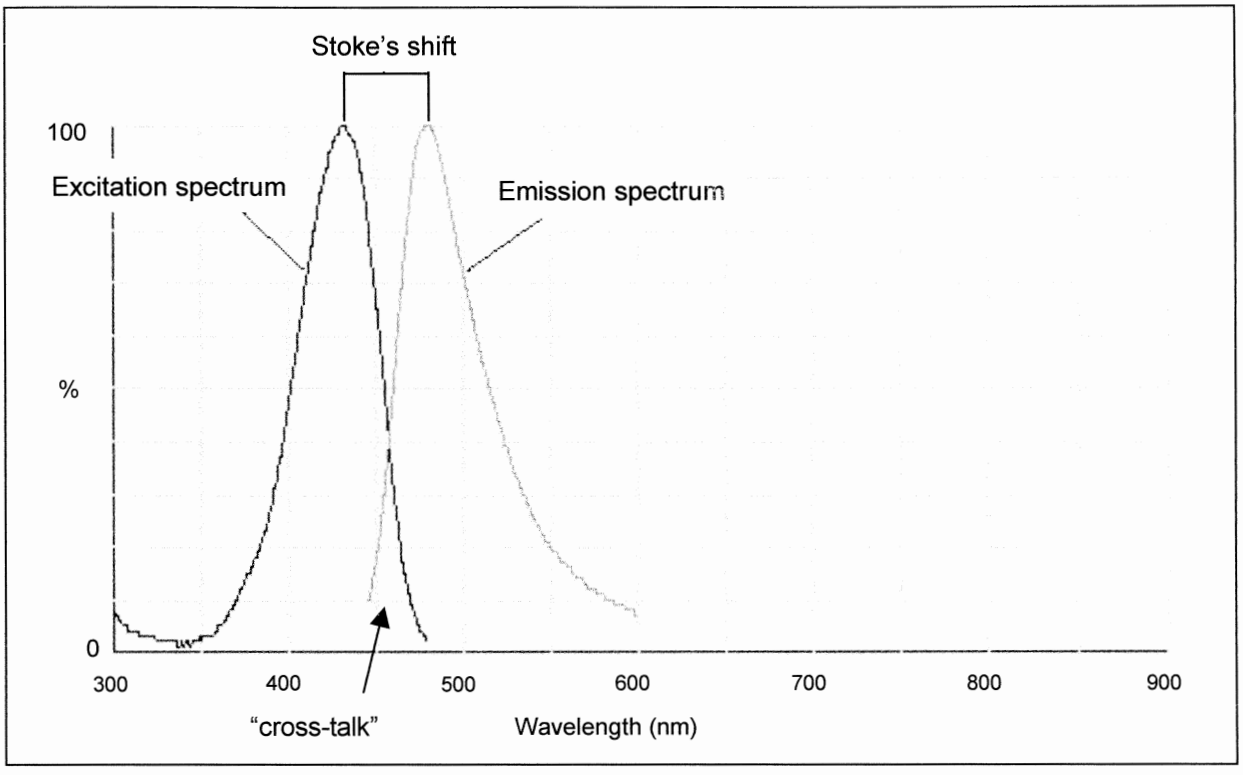

Fig.2.2. Schematic excitation and emission spectra of a theoretical fluorophore. The difference between the excitation and emission peaks is termed the Stoke's shift of the fluorophore. (Based on Ploem, 1993)

Considerations about the microscope setup, lenses selected and equipment limitations (e.g. detectors) should also be kept in mind to realise what could be realistically be expected from the equipment used. In the case of high powered imaging used in these studies it is essential to get an understanding of the maximum theoretical lateral and axial resolution obtainable.

2.4.2. Resolution

The smallest separation between two discreet points whilst still ensuring that they are resolved separately is referred to as the limit of resolution. More specifically in microscopy, these points are not distinct spots of light as the light emitted from a point spreads out in all

directions. Due to diffraction, a point of light in the focal plane of an objective is imaged as a bright disc surrounded by increasingly dimmer rings. The classical two-dimensional diffraction spectrum is known as the Airy pattern or Airy-disk (Van Vliet *et al.*, 1998) named after the British astronomer G.B. Airy. Therefore every point in the specimen is represented by an Airy diffraction pattern having a finite spread which is often referred to as a point spread function (Van Vliet *et al.*, 1998). This occurs because light waves emitted from a point source are not focused into an infinitely small point by the objective, but converge together and interfere near the intermediate image plane to produce a three-dimensional diffraction pattern (figure 2.3).

Airy pattern size changes with objective numerical aperture, the wavelength of illumination and with the magnification of the objective and additional magnification factors of the system. The particulars of Airy pattern formation are of theoretical interest and will therefore only be discussed very briefly in the consideration of lateral and axial resolution of confocal microscopy.

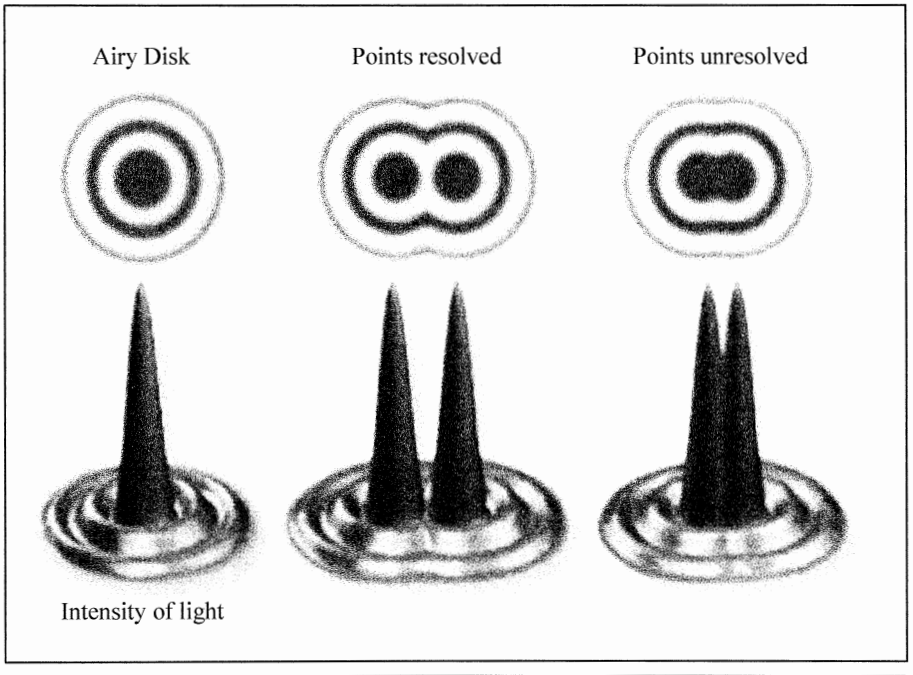

Fig 2.3. Schematic illustration of hypothetical Airy-disks. The central maximum point (0th order) is surrounded by concentric orders (1st and 2nd here) of decreasing intensity. The two points in the central image illustrate the limit of resolution with the two points on the right unresolved. (Modified from Davidson and Abramowitz, 1989)

The separation of these points in an x-y plane by the definition above, refers to the lateral resolution of the system. Axial resolution is measured along the optical axis and is, amongst other things, mainly a function of the objective used and important when considering optical slicing in confocal microscopy. For the purposes of this discussion and as the Airy-disks concept will be used of in calculations later on, one should bear in mind that the lateral resolution for an Airy diffraction pattern generated by a point light source is defined within a single plane of focus. In reality, the diffraction image of a point source extends periodically and symmetrically above and below this plane.

One of the limits of conventional fluorescence microscopy is that even though the lateral resolution is extremely good, axial resolution is plagued by interference from out of focus light emitted from above and below the specimen. One of the tasks in setting up a fluorescent microscope before imaging is to ensure even distribution of the illuminating light source over the whole field of view. Even though this ensures even illumination of the specimen to be viewed it has the unfortunate disadvantage of exposing the entire specimen to the damaging effects of intense light sources needed for high magnification fluorescent microscopy. In addition the even illumination produces out of focus fluorescence from all fluorophores in the light path. The confocal microscope eliminates many of these problems and is the instrument of choice for many imaging applications.

2.5. CONFOCAL MICROSCOPY

2.5.1. General comments

Having just mentioned a limitation of conventional fluorescent microscopy, several additional advantages can be gained by using confocal microscopy. Some of the major advantages include (White *et al*, 1987):

- Out of focus fluorescence is almost entirely eliminated and a clearer image in the plane of the objective focus can be obtained.
- This thin optical cross-section can be regulated and serial optical sections used to construct three dimensional (3-D) images.
- The x-y and z resolution is improved.
- Images can be obtained from thick and light scattering objects.
- The excitation illumination intensity of the laser confocal is adjustable to minimise the harmful effects to the entire specimen (photobleaching).
- The detector sensitivity is adjustable enabling small amounts of emitted light to be detected.
- Simultaneous multichannel (multicolour) imaging is possible.
- Magnification can be digitally enhanced and is not limited by the optics alone.
- Instant imaging is available with no need for darkroom developing techniques as in older fluorescence setups.
- Time lapse imaging can be performed automatically on living preparations to obtain 3-D data in real time.

Confocal microscopy can only be performed with point illumination and detection and therefore the light source of choice for use in a confocal setup is laser light. This fact proves to be one of the disadvantages of the confocal microscope though as cells can be damaged

by the intense illumination needed to excite a small amount of fluorophore. Illustrated in figure 2.4 is a schematic diagram of the essential design of all confocal microscopes.

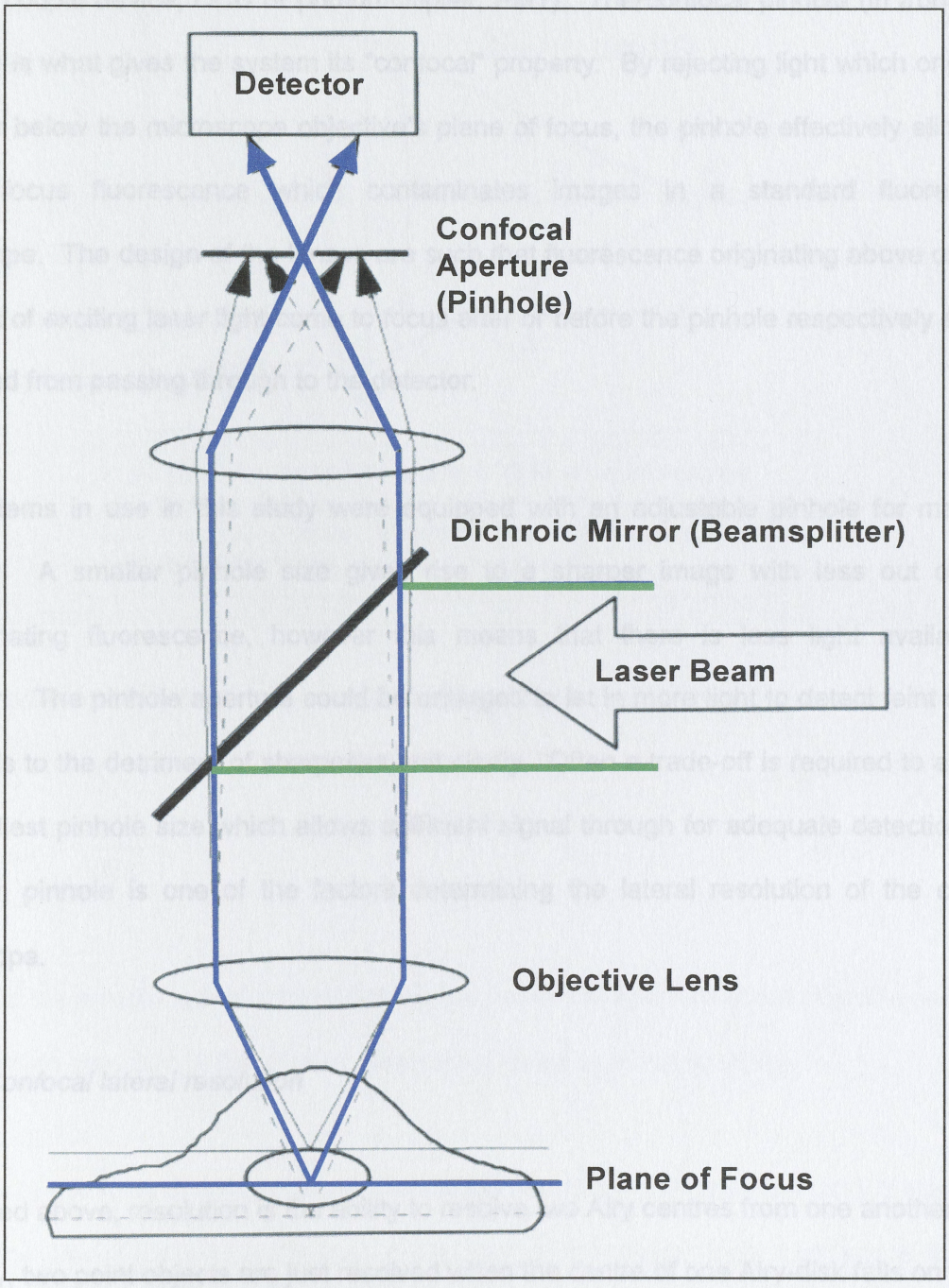

Fig.2.4. Schematic depiction of the basic configuration for confocal microscopy. Focused laser light (depicted by blue lines) is directed to a specific desired point within the object. The reflected or emitted light is passed back up the objective and through a dichroic mirror to the confocal pinhole. The lens configuration ensures that only light in the focal plane (blue) passes through the pinhole while light from above (solid black line) and below (hashed black line) the focal plane is excluded. (Based on Sheppard, 1993).

One of the most important components is the introduction of a pinhole which is typically placed in the path of the laser before hitting the specimen and more importantly a second pinhole is placed in the path of reflected/emitted light before reaching the detectors (usually a charged couple device, CCD or photomultiplier, PMT). The confocal pinhole (in front of the detector) is what gives the system its "confocal" property. By rejecting light which originates above or below the microscope objective's plane of focus, the pinhole effectively eliminates out of focus fluorescence which contaminates images in a standard fluorescence microscope. The design of the lenses are such that fluorescence originating above or below the point of exciting laser light come to focus after or before the pinhole respectively and are prevented from passing through to the detector.

The systems in use in this study were equipped with an adjustable pinhole for maximum flexibility. A smaller pinhole size gives rise to a sharper image with less out of focus contaminating fluorescence, however this means that there is less light available for detection. The pinhole aperture could be enlarged to let in more light to detect feint signals, but this is to the detriment of sharpness and clarity. Often a trade-off is required to adjust to the smallest pinhole size which allows sufficient signal through for adequate detection. The detection pinhole is one of the factors determining the lateral resolution of the confocal microscope.

2.5.2. Confocal lateral resolution

As defined above, resolution is the ability to resolve two Airy centres from one another. More precisely, two point objects are just resolved when the centre of one Airy-disk falls on the first minimum (see fig. 2.4) of another Airy-disk (Rayleigh's criterion). The radius of an Airy-disk is commonly defined as the distance from the centre to the fist minimum (first order) and this is equal to the lateral resolution of the objective lens.

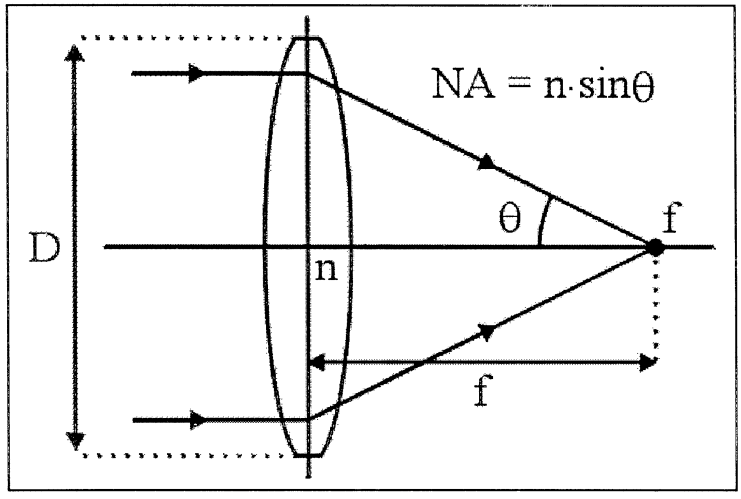

Fig.2.5. The numerical aperture (NA) of a microscope objective is calculated from the half-angle (θ) of the cone of light it is able to focus. Where f = the focal distance, n = refractive index of the lens and D = lens width.

With the schematic illustration of an objective lens presented in figure 2.5 the Airy-disk radius can be calculated as (Davidson and Abramowitz, 1989):

$$r_{AIRY} = \frac{1.22\lambda}{2NA} \qquad \text{(Eq.2.2)}$$

where λ is the wavelength of light and NA is the numerical aperture of the objective lens. The NA of an objective is therefore a measure of its light gathering ability.

The size of the pinhole determines the resolution as this determines the field of view. The smaller the field of view, as is the case in the point of light for confocal microscope the better the lateral resolution. As a general rule for confocal microscopy, lateral resolution can be approximated as:

Confocal lateral resolution = $r_{airy}/\sqrt{2}$ = 1/1.4 x 1.22λ/2NA (Eq.2.3)

The specific resolution for the system in use needs to be determined for each case as there are many factors involved which vary from system to system.

In the systems used for these investigations an approximation can be made for the objectives used to obtain a lateral resolution between 150-250 nm. It must be realised that this is an approximation which depends not only the NA, by also wavelength of light, embedding material and other factors.

2.5.3. Confocal axial resolution

Unlike physical limitation of mechanical sections taken from embedded tissue with the use of a microtome, the optical section thickness is not defined as the physical dimensions of this type of mechanical process, but by the axial resolution of the system. Axial resolution is even more ambiguous than lateral resolution, but once again is highly influenced by objective NA. The higher the NA the better the possible axial resolution. As a general approximation, axial resolution (d_z) can depend on:

$$d_z = \frac{1.77\lambda}{(\quad)^2} \qquad \text{(Eq.2.4).}$$

The theoretically thinnest optical section in the z-plane is therefore determined by the quality of the objective used, with an increase in NA resulting in a smaller optical section. A more inclusive calculation however takes into account the refractive index (n) and pinhole diameter (PH) along with magnification. For the systems in use in this study this resolution can be approximated as (manufacturers estimation, Leica Microsystems, Heidelberg, Germany):

$$d_z = \sqrt{\left(\frac{0.88\lambda}{n-\sqrt{n^2-NA^2}}\right)^2 + \left(\frac{1.4n(PH)}{NA}\right)^2} \qquad \text{(Eq.2.5).}$$

It is therefore important that the system corrects for changes in refractive indices of different immersion and mounting media as failure to do so would "distort" the final 3-D image obtained.

Once again based on the objectives used and making similar assumptions as for the lateral resolution, an approximation of the axial resolution for this study has been made of between 280-400 nm.

Although the confocal microscope has improved on aspects of conventional fluorescence microscopy there are several limitations which need to be considered when designing experiments. These include (Sheppard, 1993):

- Photobleaching. Most fluorophores are subject to degradation with excessive exposure to the excitatory laser light. This is as a result of photochemical destruction of the fluorophore.
- Phototoxicity. Often the products produced by photobleaching of fluorophores are themselves toxic to the cells under investigation. Cells can also be damaged by the intense illumination needed to excite a small amount of fluorophore. In addition to toxic agents, excessive heat, transferred by the photons themselves will destroy the cells. These first two problems can be counteracted to some extent by scanning the cells for less time (shorter dwell time) or taking fewer scans (fewer accumulations) to the impairment however of image quality.
- There is a limit to the excitation wavelengths of light due to the nature of laser illumination. Laser light does not produce a continuum of light spectra (see Fig.2.6) as is the case for many of the fluorescent bulbs. The discrete wavelengths of light produced by lasers filled

with different gasses restricts the available fluorophores based on the unique excitation requirements for each fluorophore.

- Autofluorescence of endogenous molecules in the scanned area needs to be considered.

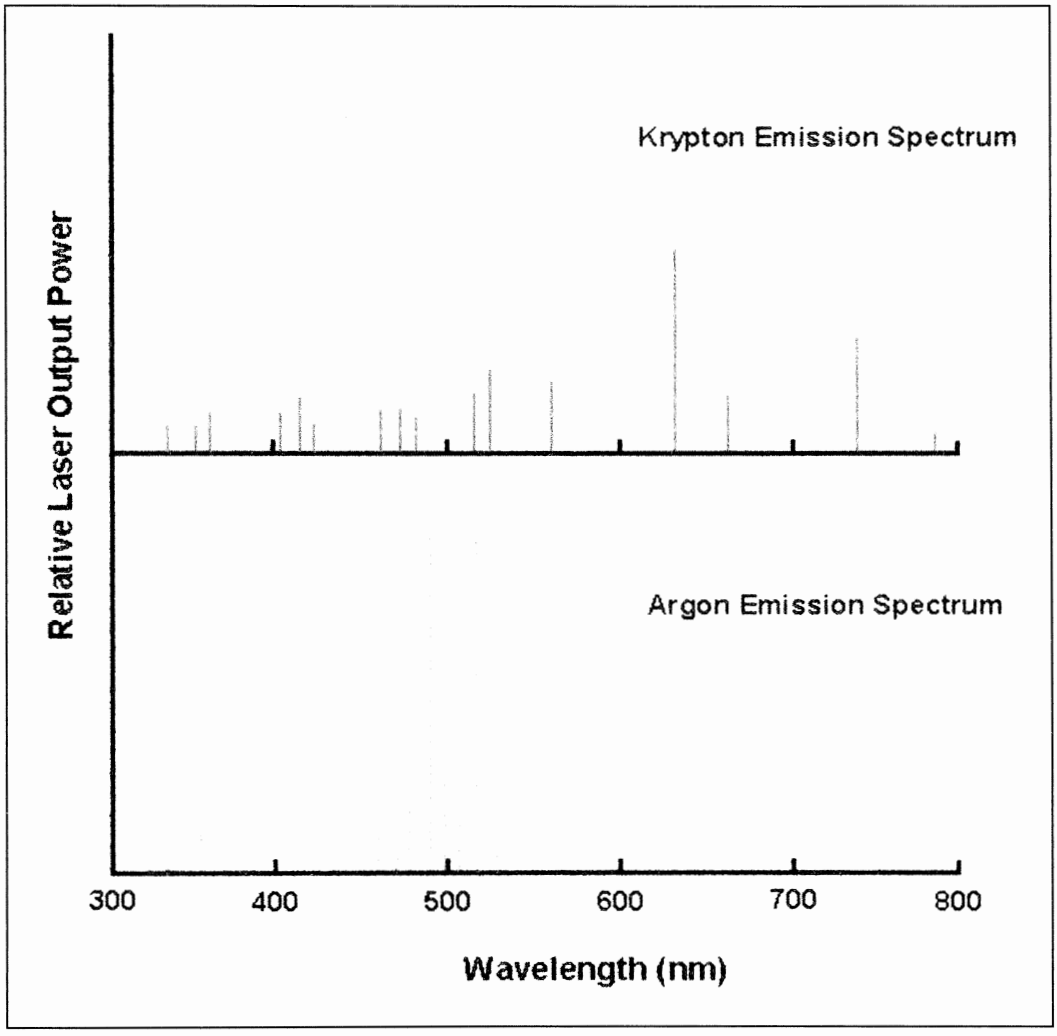

Fig.2.6. Specific excitation lines available from a Krypton/Argon laser. Note the most intense emission occurs as a few discreet lines and these are the lines most often used for exiting specific fluorophores. (Based of Sheppard, 1993)

2.5.4 Implications for this study

From the theoretical discussion of the principles of fluorescence and confocal microscopy, several key considerations were important when designing specific experimental protocols.

Firstly, the selection of fluorophores required properties that would maximise detection but minimise cross-talk, be resistant to fading and excitable by laser lines available on the confocal systems in use. Secondly, when imaging the system would require optimal (i.e. smallest practical) settings of pinhole diameter (to obtain the best resolution), reduced scan time (to minimise photobleaching and phototoxicity) and selection of a high NA objective (for optimal lateral and axial resolution).

Finally, the approximations made for axial resolution were important and needed to be kept in mind when evaluating 3-D data reconstructed from serial optical sectioning. What this value for axial resolution indicated was the fact that the smallest meaningful optical section obtainable from the system could never be thinner than about 300 nm as this is the physical limitation of the optical systems in place. In practice, this value was closer to 500 nm when all the components in the path of light were taken into account. In addition, due to limitations in lateral resolution, no meaningful comments of sub-300 nm sized structures or localisations could therefore be inferred based on images obtained. Comments on intracellular structures under this limit (see chapter six for example) should be viewed as theoretical discussions rather than actual imaged sizes. In the same way, localisations within the cell can only practically be made to about the nearest 0.5 μm.

These limitations notwithstanding, use of confocal microscopy expanded the available information obtainable from cultured A6 cells when compared to conventional fluorescent microscopic techniques used in other investigations (Morris *et al.*, 1998 for example).

CHAPTER 3

A6 CELLS AND ADNEYLATE CYCLASE

3.1. INTRODUCTION

As mentioned in the opening chapter, vasopressin is able to exert its homeostatic effect acting via external V-receptors. This interaction sets in motion a secondary messenger cascade (illustrated in Chapter 1) which results, in investigated model epithelia, in an increased Na^+ and Cl^- transport (Bindels *et al.*, 1988; Chalfant *et al.*, 1993; Lang *et al.*, 1986; Marunaka and Eaton, 1991; Yanase and Handler, 1986a). Several studies have shown that in A6 cells modulation of the channel may occur via a G-protein pathway (Cantiello *et al.*, 1989; Prat *et al.*, 1993) which is directly linked to apical Na^+ channels (Ausiello *et al.*, 1992). There has recently been some debate however as to the exact nature of the secondary messenger cascade set up by the stimulation with vasopressin in this cultured cell line. Reports suggesting that V_2 binding results in eventual release of stored intracellular Ca^{2+} (Chou *et al.*, 2000; Hayslett *et al.*, 1995) are in contrast to findings which suggest a V_2/cAMP pathway (Imbert-Teboul *et al.*, 1980). It should be noted however that brief calcium transients have been previously observed following V_2 ligand binding, even though cAMP is thought to be the main secondary messenger (Champigneulle *et al.*, 1993; Ecelbarger *et al.*, 1996; Maeda *et al.*, 1993; Star *et al.*, 1988).

As an additional impetus to re-investigate the cAMP signalling cascade, reports in mammalian kidney have demonstrated the occurrence of V-receptors on the apical surface of cortical collecting duct cells, in contrast to the long held idea that these cells were only acted on by vasopressin basolaterally (Abramow *et al.*, 1987; Ammar *et al.*, 1992; Ando and Asano, 1993; Ando *et al.*, 1991). As this localisation would be an important consideration in the design of

both electrophysiological and live-cell microscopy studies, characterisation of the adenylate cyclase/cAMP pathway in the A6 epithelial was of some significance.

In order to isolate the forskolin-associated secondary messenger pathway in operation in the cultured renal (A6) cells initial investigations focused on the location of adenylate cyclase which would result in the production of intracellular cAMP. In addition an attempt was undertaken to quantify the production of cAMP within the cells at various culture ages under control and forskolin-stimulated conditions. Findings from these investigations therefore lead to a better understanding of the electrophysiological responses to be presented in subsequent chapters and went some way towards clarifying conflicting reports from the various investigations mentioned above. The work is presented in the following categories:

1) First, the cytochemical localisation of adenylate cyclase (AC), responsible for the production of cAMP, was observed by scanning electron microscopy on ultrathin sections of A6 cells.

2) Effects of culture age on AC localisation were investigated.

3) Levels of cAMP production in the various age groups were compared.

The method of cytochemical localisation used in these investigations was described in investigations of AC in rat liver (Reik *et al.*, 1970). The protocol was subsequently modified (Howell and Whitfield, 1972) for investigations of rat pancreas. Some debate arose as to the validity of the protocol to accurately detect AC activity prompting a review on the efficiency of the procedure (Cutler, 1983). Initial difficulties however were identified to stem from the use of lead as the electron dense detection agent for the AC activity. A substitution of cerium as the capturing agent has been successfully employed to ensure a more reliable protocol (see materials and methods below) for AC detection (Cutler and Christian, 1980; Davis *et al.*, 1987). Using a further modified procedure closely followed here, Richards and Els (1993) were able to localise the site of AC activity, by observing electron dense deposits in frog skin epithelial cells.

3.2. MATERIALS AND METHODS

3.2.1. Cell culture

The general cell culture conditions have been outlined above and these procedures were followed in culturing A6 cells to be used in all investigations (See general materials and methods Chapter 2). In this study however, differences in cAMP response due to age of cultures was investigated. As described above, confluency is tracked by electrophysiological maturity as the cells begin transporting at around 10 days. Two different experimental age groups were used to determine effect of age on cAMP production. Cells in the younger group were investigated between 5-7 days from seeding, while older cells which were fully transporting were selected between 9-14 days. In addition AC activity was investigated in cultures 6, 14 and 21 days. Apart from selecting inserts at different ages cell culture was carried out routinely as described above.

3.2.2. Cytochemical localisation

The main method of AC detection was by the use of transmission electron microscopy (TEM). However, processing such as fixation and dehydration (see below) would adversely affect the physiological properties of the enzyme *in situ* since glutaraldehyde fixation affects the physiological transport rates of epithelial cells (Richards and Els, 1993). Due to this, the localisation protocol was carried out on unfixed cells, with a postfixation procedure. The drawback was the minor loss of morphological preservation of the cells' intracellular ultrastructure. After removal from the culture wells, the supports with the cells were rinsed in the reaction buffer to remove the culture medium and divided into small pieces. The small sections were incubated for 30 min at 30°C in the following reaction medium to expose adenylate cyclase. The medium contained 0.5 mM of 5'-adenylyimidoiphosphate (AMP-PNP) as the substrate for AC. AMP-PNP was the substrate of choice since it is readily hydrolyzed by

adenylate cyclase to cAMP and imidodiphosphate which in turn is not readily cleaved by hydrolyzing enzymes present within the cells (Richards and Els, 1993). The AMP-PNP was purified by running through a Dowex AG-50 (W-X4) chromatography column (Sigma, St.Louis, USA) immediately before it was added to the incubating solution. The AMP-PNP was added to a solution consisting of 5 mM $MgCl_2$, 80 mM Tris-maleate buffer (at pH 8.2) and 8% glucose. In addition, the medium contained 10 µM 3-isobutyl-1-methylxanthine (IBMX) to inhibit AMP-PNP hydrolysis, 1 mM levamisol to inhibit non-specific phosphatases, dithiothreitol to inhibit ATP-phosphotases, and 5 mM g-strophanthin (oubain) to block Na/K-ATPase activity. Finally, in order to stimulate adenylate cyclase activity and increase the deposits of reaction product, 2.5 µM forskolin (Sigma, St Louis, USA) was added to the incubation medium of certain cells. The capturing agent used in all experiments was 5 mM $CeCl_3$. Following incubation cells were washed 3 times in DMEM to remove non specific deposit. As cytochemical controls, tissues were incubated in a reaction medium without any AMP-PNP substrate. Verification of the specificity of the reaction was also obtained by results from tissues that were first heated to 70°C for 45 minutes before incubation in the standard medium.

Following the 30 minutes incubation, tissues were rinsed in Tris-maleate buffer and then postfixed by a two-step process in a 1% glutaraldehyde and paraformaldehyde for 30 minutes followed by 2% osmium tetroxide in a 0.1 M cacodylate buffer (pH 7.2) for 30 minutes. This procedure preserved the morphological features of the cells. Cells were then processed for transmission electron microscopy (TEM).

3.2.3. Electron microscopy

Cells were processed for both scanning and transmission electron microscopy. To inspect the morphology of cells cultured on filter inserts, cultures of different ages were processed for standard scanning electron microscopy (SEM). Samples prepared for SEM underwent a 4-

step process, namely; dehydration, critical point drying, mounting and sputter coating before final viewing

The dehydration step was performed for both SEM and TEM. Following fixation, samples were washed 5 times for 5 minutes in a 0.16M cacodylate buffer. Samples were then passed down an alcohol dehydration gradient by immersing in 50%, 70% and 90% alcohol for 10 minutes each. Samples were then placed 3 times in 100% alcohol for 15 minutes each. Following dehydration, samples were dried in a Balzer 020 critical point drier and mounted on aluminium stubs. In order to coat the samples prior to viewing, argon gas was leaked into a previously evacuated chamber at a pressure of 0.05 torr. They were gold coated for 4 minutes at 20mA. Prepared samples were viewed with a Joel JSM 5200 scanning electron microscope at an acceleration voltage of 20 kV.

To observe the electron dense deposit laid down as a result of AC activity samples were processed and viewed with a Hitachi H-600 TEM. The initial processing was similar to the SEM protocol as samples were passed down an alcohol dehydration series as described above. After immersion in 100% alcohol, samples were incubated twice in propylene oxide (Electron Microscopy Sciences, Fort Washington, PA, USA) for 5 minutes. A resin solution was prepared for final embedding and contained: 20% Araldite (epoxy resin), 27% Agar 100 and 53% Dodecenyl Succinic Anhydride (DDSA) (Electron Microscopy Sciences).

Samples were placed in a 50:50 mixture of prepared resin and propylene oxide for 1 hour at room temperature. Next the samples were placed in undiluted resin for at least 2 hours to allow penetration of the resin into the tissue. Finally 2.5% 2,4,6-Tri(dimethylaminomethyl) phenol (DMP-30) accelerator was added to previously mixed resin and filter pieces were incubated for 1 hour in this mixture at 40°C. At this point samples could be embedded in TEM moulds and cured for 48 hours at 60°C. In all cases tissue pieces were orientated side on to the cutting face to ensure cross-sectional thin sections were obtained.

After 48 hours, cured blocks were removed from the moulds, trimmed and mounted on a Riechert-Jung Ultrucut ultramicrotome to obtain ultrathin sections. Fresh glass knives were prepared on a LKB knifemaker and mounted onto the ultramicrotome. Silver to gold sheen sections were obtained from the most suitable blocks and collected on pre-washed 200 mesh uncoated nickel grids.

Sections on grids were counterstained with a 2% filtered urinyl acetate solution and washed in double distilled water. Once prepared samples could be viewed in the TEM at an electron acceleration voltage of 75kV.

3.2.4. Measurement of AC activity

Adenylate cyclase activity was determined indirectly by an adenine-labelling method described previously (Salomon, 1991). The method relies on the measurement of cAMP formed from radioactively labelled substrate followed by isolation and determination of the labelled product. Briefly, the culture medium in the apical compartment of cells 6, 14 and 21 days old were removed on the day of the experiment and replaced with fresh medium containing 10 mCi/ml [^{3}H]-2' adenine for 120 min at 28°C. During this period most of the adenine residues in the cell, including the ATP substrate utilised by AC, would have been radioactively labelled. After incubation, cells were washed twice with DMEM to remove excess radioactivity and replaced with DMEM containing 0.1mg/ml bovine serum albumin (BSA) and 0.1 mM IBMX.

Tissues were divided into two groups, the first received 2.5 µM forskolin in the basolateral medium while the other tissues did not receive any forskolin. The latter group was used as a control to determine baseline levels of AC activity. Cells were then incubated for 30 min at 28° C to allow sufficient time for the production of [^{3}H]-cAMP. The reaction was terminated by removing the incubation medium, placing the cells on ice and replacing the incubation medium with a 2.5% solution of perchloric acid (PCA). This solution contained 0.1 mM unlabeled cAMP

to act as a carrier. The cells remained on ice in PCA for 30 min to allow cells to disintegrate and release radioactively labelled products. The cell free extract was then collected and 4.2 N KOH solution was added to the extract at a 1/10 volume. In order to separate the [^{3}H]-cAMP from the rest of the radioactively labelled substances, extracts of 1.3 ml were passed through a Dowex AG-50W column and then directly into a neutral alumina column (Sigma, St. Louis, USA). Equal volumes of each sample was passed directly into scintillation vials for radioactive measurement as described by Johnson and Salomon (1991). The activity of AC was measured as the percentage conversion of the labelled ATP to [^{3}H]-cAMP from the total radioactive pool.

3.3. RESULTS

3.3.1. A6 cell culture morphology

The cultured A6 cells developed at variable rates to polarized monolayers on the filter supports. However the cultures are mostly electrically mature by seven to ten days. This trend is evident in the SE micrographs of cultures at various ages and therefore various stages toward a fully differentiated monolayer. Figure 3.1.1 illustrates a culture at 5 days post seeding and 3.1.2. a fully differentiated monolayer of 21 days. Note the bunching of closely packed cells in figure 3.1.1. This trend is common in the younger cultures and cells are often overlying each other. The older culture has flattened out and cells are more uniformly arranged, with the culture in a monolayer configuration. This fact is illustrated in figure 3.1.3. which is a transmission electron micrograph of an older culture, also 21 days post seeding. Here the single layer of cells attached to the filter substrate is clearly illustrated.

One characteristic observed in several renal and cardiovascular cultured cells lines is the appearance of a central cilium in well-differentiated cultures (Briffeuil *et al.*, 1994; Duffy and Suzuki, 1968; Ganote *et al.*, 1968; Koechlin *et al.*, 1991). A suggestion has been made that this structure is responsible for detecting fluid flow rates in order for cells and systems to respond appropriately to changes in both renal and blood flow rates (Dr. Mark Knepper, NIH, Bethesda, MD, USA, personal communication). It is therefore of interest to note that in the more mature, electrically active cell cultures, the majority of the cells can be seen to have such a structure. This is better illustrated in figure 3.2. where the SEM taken from a 21 day old culture has been further magnified to illustrate this phenomenon. Although the role of this structure has yet to be determined it is interesting to note that it appears in the mature A6 cultures and is absent in the immature state.

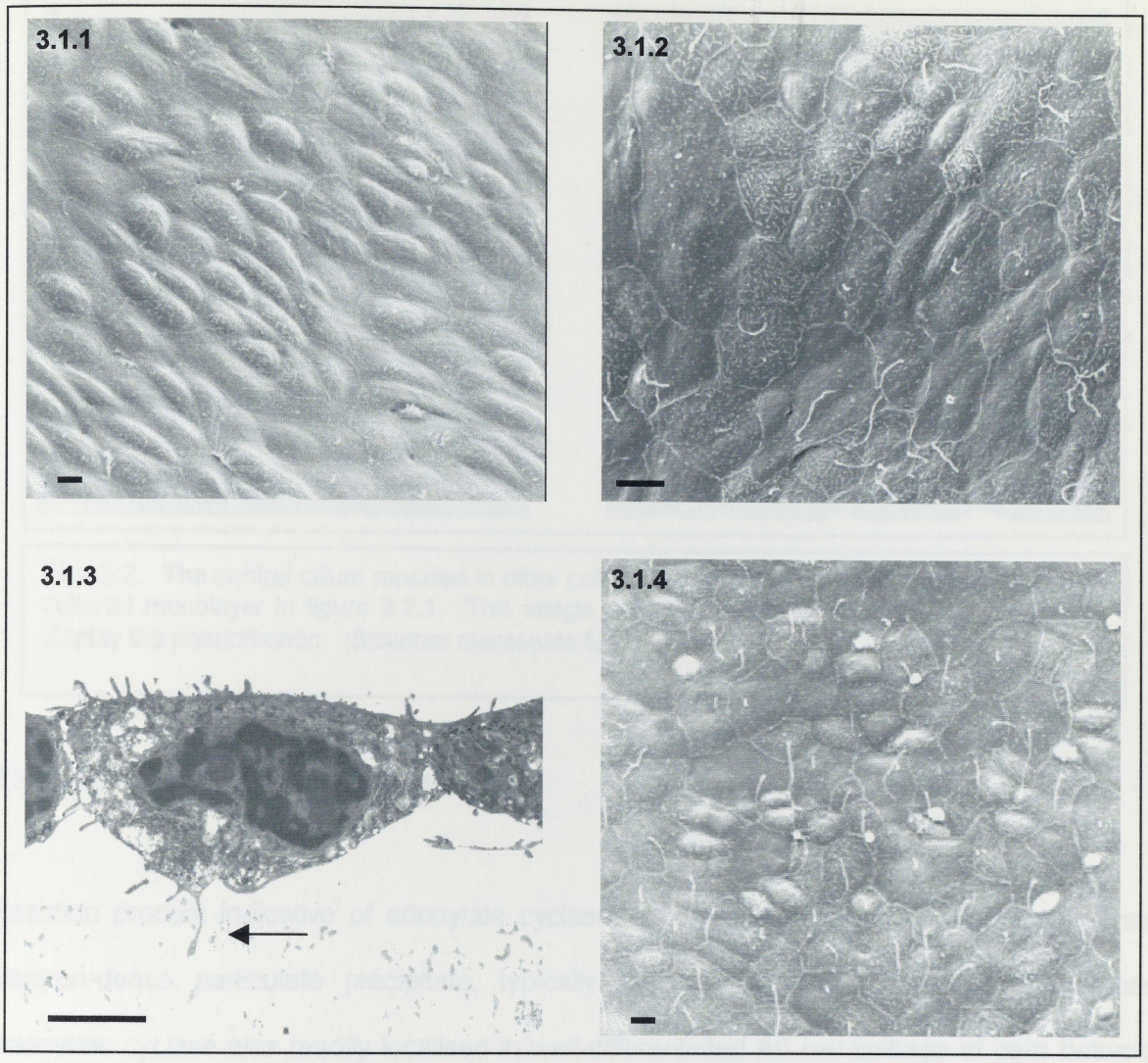

Fig. 3.1. Typical morphology of cultured renal (A6) cells grown on filter supports is illustrated in the SEMs and TEMs. Figure 3.1.1 is a young, 5 day culture where the cells are bunched and non-uniformly arranged. Note the absence of a central cilium in each cell. Figures 3.1.2-3.1.4 illustrate features of a mature, 21 day old culture. The cells are more uniformly arranged, flatter and in a monolayer configuration. Cells are attached to the filter support and often send projections into the filter matrix for better anchorage (fig.3.1.3.arrow). Note the presence of the central cilium (3.1.4) further magnified in figure 3.2. (Scalebar represents 5μm)

The trends observed in the morphological development corroborate electrophysiological measurements which suggest that cultures under 7 days old are seldom electrically competent and rarely respond to hormonal or chemical stimuli (see chapter 4).

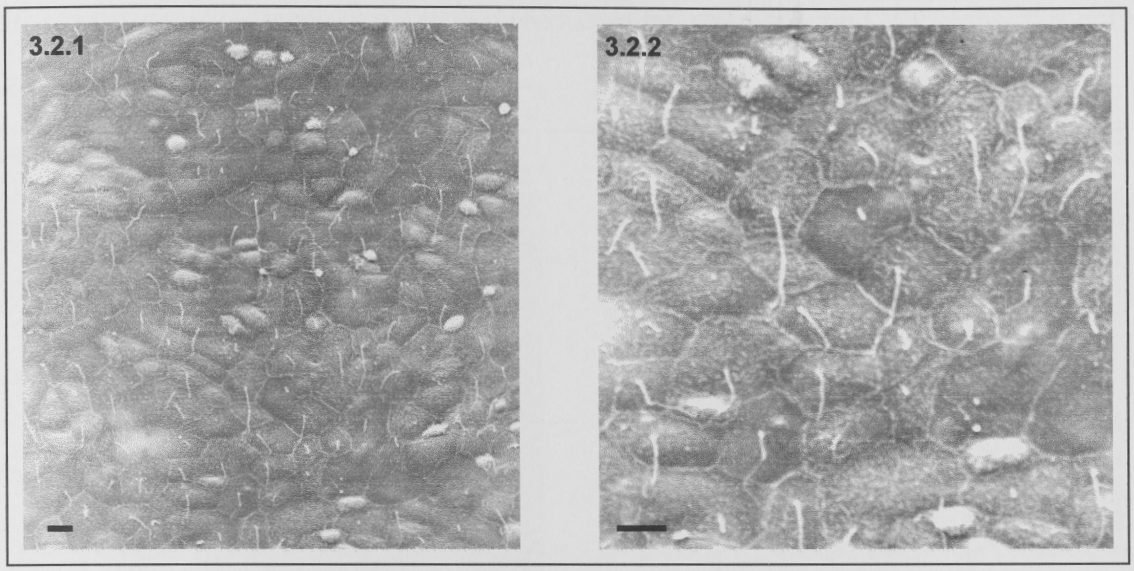

Fig. 3.2. The central cilium reported in other cultured renal cell lines is illustrated in a mature cultured monolayer in figure 3.2.1. This image is further magnified in figure 3.2.2 to better display the phenomenon. (Scalebar represents 5μm)

3.3.2. Adenylate cyclase localisation

Reaction product indicative of adenylate cyclase activity was observed in TEM as discrete, electron-dense particulate precipitate, typically restricted to the lateral cell membranes. Adenylate cyclase was readily localised in well-differentiated A6 cell cultures of cells between ages of 10 to 21 days. The characteristic localisation in mature cultures is illustrated in figure 3.3.

Despite the fact that the cells were not prefixed, morphological features of the cells were adequately preserved. It was clear that addition of forskolin to the incubating medium markedly enhanced the production of the reaction precipitate and in its absence the degree of precipitation was noticeably reduced (Fig. 3.3.3). In earlier experiments non-specific precipitate was observed within the filter support which apparently had an affinity for the cerium in the medium. This problem was reduced by the washing procedure after incubation. Thereafter the

cells were relatively free of non-specific precipitate. Control sections incubated without the substrate did not show signs of a reaction product in the cells, attesting to the specificity of the reaction (Fig. 3.3.4).

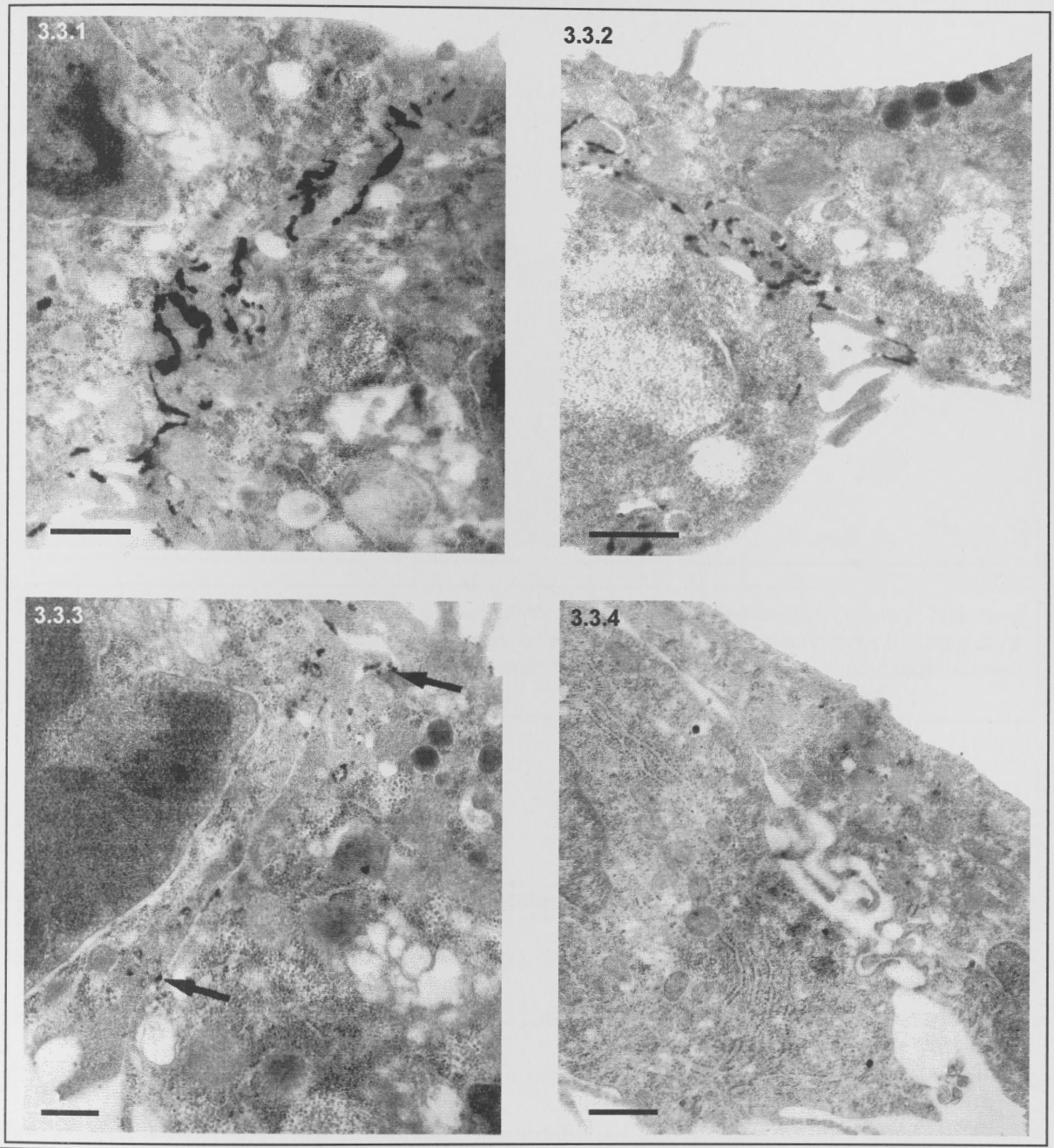

Fig. 3.3. Observed deposit at the sight of AC activity. Note the electron dense deposit in figs. 3.3.1 & 3.3.2 in 14 day cultures treated for 30 min with forskolin. The majority of AC activity is located in the lateral membranes of adjacent cells with little or no deposit on the basolateral and apical membranes. Figure 3.3.3 illustrates AC produced deposit (arrows) in an unstimulated culture of the same age as a control. Cells in the TEM of fig.3.3.4 were incubated in a substrate free medium and exhibited no detectable deposit. (Scalebar represents 2 μm)

In the older cultures the distribution of adenylate cyclase followed a characteristic pattern. This is displayed in figures 3.3.1 & 3.3.2 and further illustrated in figure 3.4.

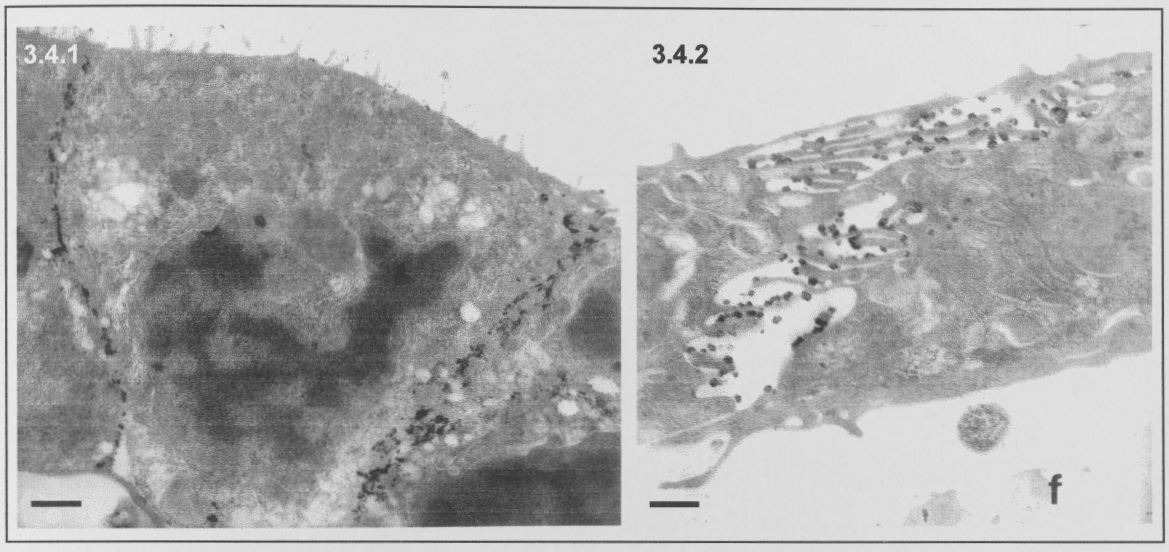

Fig. 3.4. TEM illustrating the typical distribution in older, well differentiated cultures. The cells are well adhered to the filter substrate (f) and form a continuous monolayer. Note the abundant deposit on the intracellular membrane folds with no deposit located on the apical membranes. (Scalebar represents 2.5μm)

As shown in Fig. 3.4.1 & 3.4.2, the apical membranes of the cells were free from deposits and adenylate cyclase was mainly restricted to the lateral cell membranes. Occasionally limited adenylate cyclase activity was observed in the basal membranes of the cells but then mainly in the younger cells (see Fig.3.5.). Thus far the distinctive characteristics of mature A6 cultures and the AC activity has been presented. As mentioned above, cultures of a younger age did not follow this typical morphology.

It has already been demonstrated that the cells of cultures under 7 days have not always formed a tight monolayer (figure 3.1.1) and do not possess some of the distinguishing features

of fully differentiated cells (e.g. the central cilium). Of interest therefore was to determine the AC localisation in these cultures to see how, if at all, these cultures would differ from the mature electrically competent cells. AC localisation presented in figure 3.5 illustrates a variable amount of reaction product. Figure 3.5.2 further confirms the fact that there is not a single layer of cells as a multi-layered arrangement can be observed above the filter substrate.

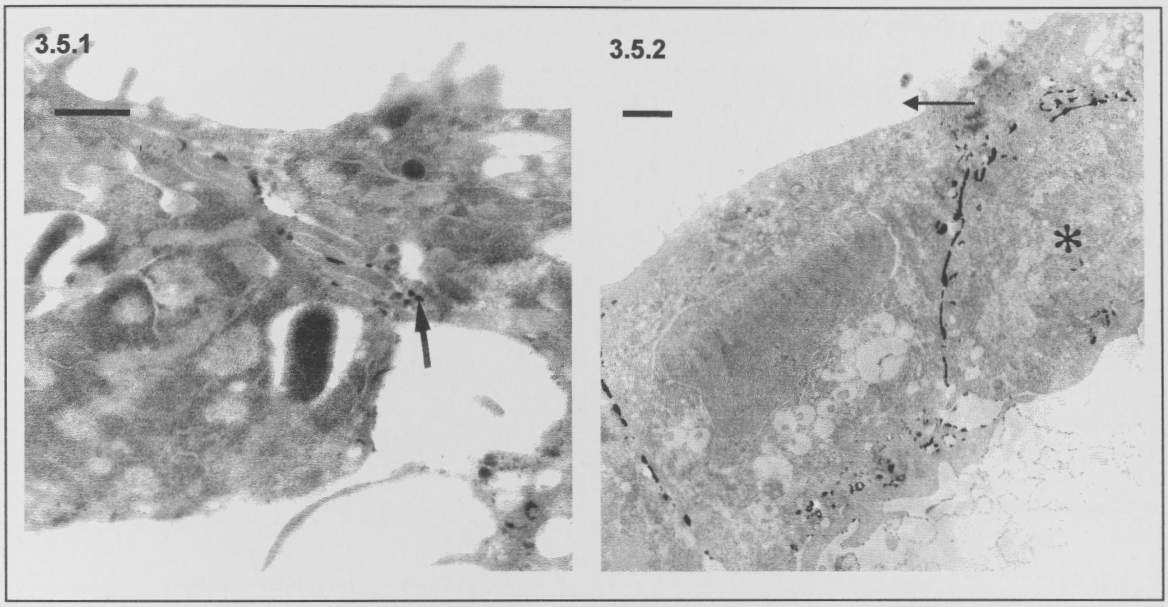

Fig. 3.5. TEM illustrating the variable distribution and amount of AC deposit in young undifferentiated cultures (5 days old). The cells in 3.4.1 exhibit very little deposit (arrow) compared to the same aged cells in 3.5.2. Note the underlying cell (*) in 3.5.2. which has AC deposit on the apical membranes. Note also the uncharacteristic basolateral deposit (arrow) not seen in mature cultures. (Scalebar represents 2.5μm)

3.3.3 Adenylate cyclase activity

In order to examine and compare the degree of adenylate cyclase activity in cells from young and older cultures the indirect method of determining the amount of [^{3}H]cAMP produced from a radioactively labelled pool was used. This was done to determine whether there was any correlation between the evolvement of Na^+ transport properties of the cells and the apparent degree of enzyme activity in the membranes. Quantitative estimates (the percentage of [^{3}H]adenine converted to [^{3}H]cAMP by AC activity) of adenylate cyclase activity in cells were determined indirectly by an adenine-labeling method in cells that were respectively cultured for 5, 14 and 21 days after seeding on filter supports. Results are presented in table 3.1.

Condition	5 Days	14 Days	21 Days
Basal (unstimulated) activity	1.68±0.27	1.06±0.13	1.01±0.49
Forskolin stimulated cells	2.88±1.05 *†	3.65±2.80 *	6.31±2.06 *†

Table 3.1. Basal and forskolin stimulated AC activity in A6 cells of different culture ages.

The mean AC activity ± standard deviation was calculated as the percentage of [^{3}H]adenine converted to [^{3}H]cAMP by AC activity. * denotes significant difference ($p<0.05$) from basal levels and † significant difference ($p<0.05$) between stimulated cultures of 5 and 21 days old. All results compared using standard student's t-test and n=6 paired cultures.

The mean basal activity amongst individual cultures was quite variable as seen by the relatively large standard deviations of the means. There was no highly significant difference ($p<0.01$) between the young and old cultures for untreaded/basal AC activity. However the method of quantitiation was sensitive enough to pick up changes in AC activity from the basal to stimulated states. In addition the level of stimulated AC activity in cultures of 5 days was significantly lower than that of older cultures of 21 days.

3.4. DISCUSSION

3.4.1. Electrically maturing cells

One important consideration when working with cultured epithelial cells is maturation time. Physiological events are often not observed until cells have developed tight junctions allowing vectoral trafficking of ions to be established across a tight cell monolayer. In A6 epithelia progress to mature monolayers can easily be monitored by recording transepithelial open circuit potential several days post filter seeding. In younger cells the transepithelial open-circuit potential difference (PD) was in the range of 0-12 mV and the transepithelial resistances measured a few hundred ohms per square centimetre , while in cells that were about seven days and older the PD was consistently higher (about 20-80 mV) with transepithelial resistances in the kΩ range.

3.4.2. Morphology and AC localisation

The morphological characterisation of the cultures as shown by scanning electron microscopy, illustrate that in the younger cultures many of the cells were rounded rather than having the usual flattened appearance (Fig. 3.1.1). Expression of AC as detected by the electron-dense reaction deposit in the transmission electron micrographs shows a variable distribution in most of the membranes of the undifferentiated epithelia (figure 3.5). These young cultures were often multilayered with cells very compressed. In addition the cells were not uniformly distributed in the cultures under 5 days and very few if any central cilia were observed (figures 3.1 & 3.2).

As the cultures matured the cells formed a much more homogenous monolayer across the filter support. The AC expression pattern became more structured in older cultures with AC activity readily detected in lateral membranes of adjacent cells. Furthermore, the level of AC

activity increased as the cultures become physiologically competent. (figures 3.3 & 3.4) Also apparent was the uniform levels of AC activity within the cells. Stimulated cells typically had higher levels of AC deposit than the basal state which was confirmed by the AC activity results (table 3.1).

The idea that the variable degrees of AVP-responsiveness found in the cultured epithelia may be related to the degree of differentiation of the cells and to the degree of adenylate cyclase activity has been suggested by Wilson and Horster (1985), and these results would confirm this. This variability may also be related to the amount of adenylate cyclase which, by visual assessment, appears to be markedly less in A6 cells than levels found in epithelia from frog skin (Richards and Els, 1993).

It should be noted that the abundance of reaction product produced by the cytochemical procedure can not be directly correlated quantitatively with AC or its reactivity, but is rather indicative of enzyme activity localised at the site of deposition.

3.4.3. Signalling cascades

Several lines of evidence have shown that in A6 cells grown to confluence, the Na^+ transport rate is sensitive to stimulation by cAMP and AVP (Bindels *et al.*, 1988; Lang *et al.*, 1986; Marunaka and Eaton, 1991) although not to the same extent as in native tissues. Due to the limited response of A6 cells compared to native tissue, Perkins and Handler (1981) suggested that A6 cells do not develop V_2 receptors necessary for the AVP response. In an attempt to address this, Preston *et al.* (1988) were unable to determine the responsiveness of the presumptive V_2 receptors in cell membranes because of the high levels of non-specific binding. However, subsequent results did demonstrate indirectly that there was a V_2-cAMP coupled regulation of Na^+ transport in A6 epithelia (Candia *et al.*, 1993; Lang *et al.*, 1986).

With regard to the cAMP secondary messenger cascade, results demonstrated that in well-differentiated cells adenylate cyclase was predominantly restricted to the abundant lateral folds of the cells and there were no signs of activity in apical membranes of postfixed cultured A6 cells. The abundance of AC in matured monolayers presented here suggests that cAMP production by AC does occur and that A6 epithelia are utilising a cAMP cascade mechanism when stimulated with forskolin. The initial lag in electrical response (see next chapter) after forskolin addition further support the idea that a signalling cascade is involved. Conceptually, some time would be needed in the production of cAMP and transduction of the signal to the apical membrane for sodium transport to be altered.

In addition, the results suggest that as long as the epithelial layer remains intact it would be necessary to evoke the acute cAMP response from the basolateral or more specifically lateral domain alone. The signalling cascade would therefore serve to couple the receptor, located on a lateral membrane, to modulations in sodium transport observed at the apical membrane. V-receptors are closely associated with the membrane-bound AC and the lack of AC activity on the apical membrane strongly refutes suggestions of apically located V-receptors in this cell line.

These results lay the foundation in understanding the basis for the electrical response observed in the A6 cells. It is clear therefore that forskolin would have a direct effect on the AC located on the lateral membranes of these cultured cells, and would thus needed to be added basolaterally to elicit a response. The nature of the A6 cell response to elevated production of cAMP and the regulation of ENaC as a result is to be investigated in the subsequent chapters.

CHAPTER 4

CURRENT FLUCTUATION ANALYSIS

4.1. INTRODUCTION

4.1.1. Membranes modelled as electrical circuits

The secondary messenger cascade which set about a hormonal response in the A6 cells, was outlined in the previous chapter. The elevated levels of cAMP that result from vasopressin V_2 receptor binding or direct forskolin stimulation of AC produces an increase in Na^+ transport across the A6 epithelial cell layer. The facilitated movement of ions across the cell monolayer has been discussed, but essentially in the A6 cells it is the movement of Na^+ across the apical membranes which establishes an electrical current. The measurement of this current therefore provides physiological information about the transport processes taking place. Much of the early experimental and theoretical work on the Na^+ electrophysiological process was described by Hans Ussing (see Koefoed-Johnsen and Ussing, 1958; Ussing, 1949; Ussing and Zerahn, 1951) and was reviewed by Ussing *et al.* in 1974. Essentially stated the movement of ions across the membrane epithelial layer can be described by a simplified electrical circuit. This electrical model was further expanded by Helman and Fisher (1977) to describe a Thévenin equivalent electrical circuit depicted in figure 4.1.

The two-step process of Na^+ entry into the body across the renal epithelium is achieved by the establishment of an electrochemical gradient set up by the selective barrier of the apical membrane and the transport of sodium out of the cells via the basolateral membrane Na^+/K^+

ATPase. In this scenario there is no driving force resulting from the apical membrane and therefore in the circuit diagram depicted in fig.4.1 the Thévenin electromotive force (EMF) of E_a could be considered to be zero.

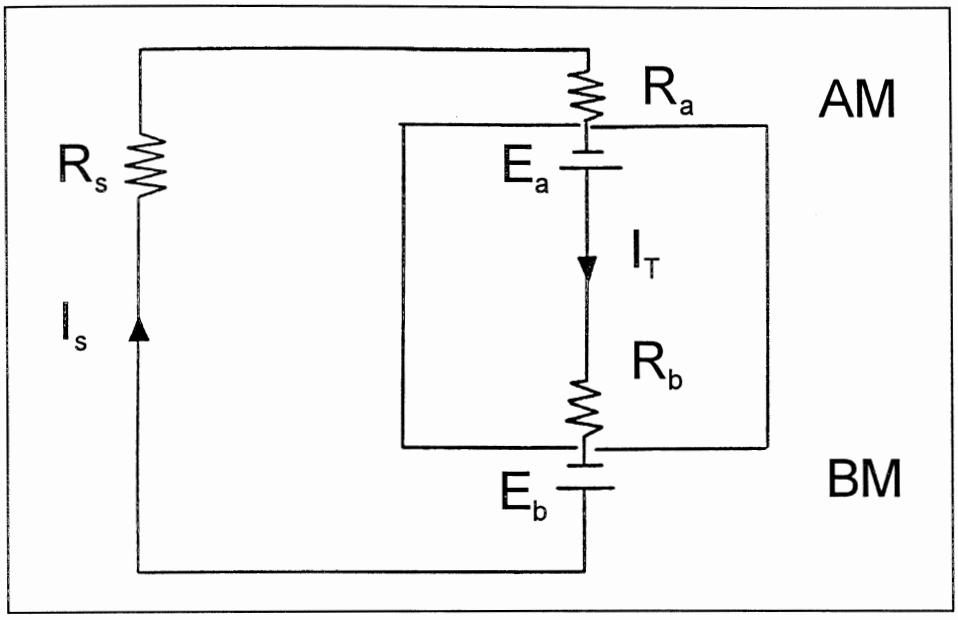

Fig. 4.1. Thévenin equivalent electrical circuit model of transport across an epithelial layer/barrier (Modified from Helman and Fisher, 1977). Abbreviations are as follows:
AM & BM: Apical and Basolateral Membrane respectively.
$R_{a\&b}$:Slope resistance of the apical and basolateral membranes
$E_{a\&b}$:Thévenin electromotive force of the apical and basolateral membranes
I_T : Transepithelial current
R_s : Shunt resistance (that resistance to flow of ions between cells)
I_s : Shunt current flowing through the shunt

The EMF can therefore be estimated directly from values of E_b as described by Helman and Fisher (1977). Microelectrode impalement studies carried out by Els and Mahlangu (1987) on frog skin were able to better characterise the typical values for R_a and R_b in this model sodium transporting tissue. These studies determined that increases in the concentration of intracellular cAMP resulted in stimulated sodium transport currents brought about primarily as a result of the lowering of the apical membrane resistance (R_a) with little effect on the EMF or R_b. The study provided electrical support for the theory that cAMP was acting as the

secondary messenger in the hormonal control of sodium transport. A basic means of tracking changes in Na^+ transport is to measure the electrical changes occurring across the epithelium. By mounting an epithelium in a modified four-electrode Ussing chamber and applying a voltage clamp measurements of the short-circuit current (I_{SC}) flowing across the epithelium can be made. The Ussing chamber equipment is designed to incorporate a voltage and current electrode on either side of a bathed epithelial layer (see Chapter 2). Voltage clamping is the ability to continuously maintain the tissue at a transepithelial voltage of zero (short circuit the tissue) in order to monitor only the current flowing across the epithelium and therefore to eliminate the flow of ions between cells. This technique was used to obtain the macroscopic electrical evidence for effects of elevated cAMP levels.

4.1.2. Electrical recordings

A number of refined electrophysiological techniques have been developed in order to get a better insight into the electrical functioning of membranes and channels. As previously mentioned, one of the earlier techniques involved the use of electrode impalement of epithelial cells in order to separate electrical information coming from either the apical or basolateral membranes of cells.

4.1.3. Patch Clamp

A enhancement on electrode work was pioneered by Neher and Sackmann (1976) and involved the use of membrane patch clamping. The technique makes use of very fine, polished glass pipettes which can be placed directly onto cell membranes to form a very tight seal. This so called gigaohm or Giga-seal (Sigworth and Neher, 1980) enables electrical recordings to be made from single ion channels located directly beneath the sealed 0.5-1μm diameter of the pipette.

Formation of the giga-seal effectively isolates the membrane patch both electrically and chemically and allows the current flowing through single channels to be recorded. The patch can thus be voltage clamped by applying voltage to the patch pipette (Lewis and Donaldson, 1990).

Various configurations of membrane patches have been developed in order to isolate and study the direct effects of various conditions on isolated ion channels. These include the cell-attached patch, where the whole cell is attached to the membrane under the pipette. Second the whole cell patch in which suction is applied to the membrane in contact with the pipette in order to rupture the membrane and allow the pipette direct access to the inside of the cell. The third configuration is the excised patch, after forming the seal the pipette is withdrawn from the surface of the cell and the piece of membrane attached by means of the giga-seal is ripped from the membrane of the cell and access is then possible to the inner surface of the membrane. Finally the inside out patch involves obtaining a whole-cell configuration and then pulling the pipette away. The pieces of membrane then naturally reseal, but in a reverse orientation ensuring the inner leaflet is then exposed to the inside of the pipette. A schematic illustration of the various patch configurations is depicted in figure 4.2.

These configurations allow researchers to expose ion transporters to a range of different ionic environments, agonists and antagonists. The versatility has provided a wealth of information about various ion channels and have enabled the precise single channel characteristics of different transporters to be resolved. In particular estimates of the single channel conductance, channel selectivity and open time probability can be determined and thus provides a fingerprint to identify particular channels in different cell and tissue types.

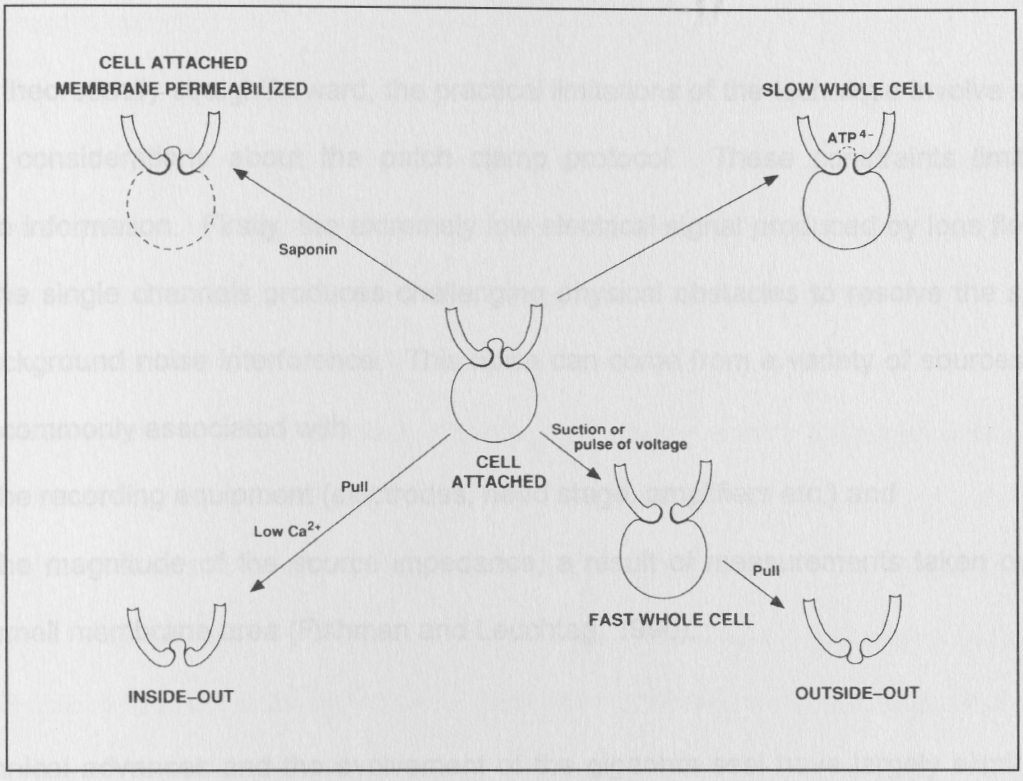

Fig. 4.2. Schematic diagram depicting the different patch configurations available. (From Lewis and Donaldson, 1990).

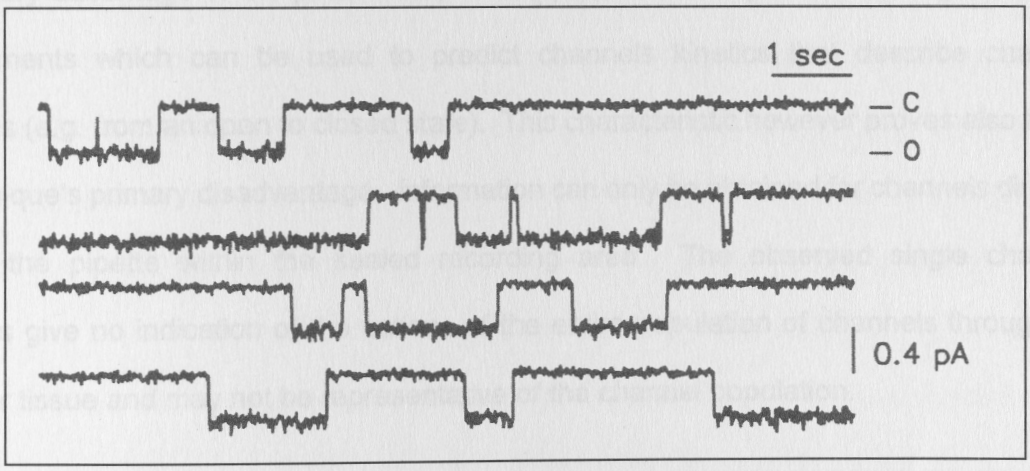

Fig. 4.3. Typically representative single channel recording taken from a Na+ channel in A6 cells. C represents the recording from the channel in the closed state and o in the open state. The magnitude of the deflection is the amount of conductivity or single channel current. (From Eaton and Marunaka, 1990).

Although theoretically straightforward, the practical limitations of the technique involve some important considerations about the patch clamp protocol. These constraints limit the obtainable information. Firstly, the extremely low electrical signal produced by ions flowing through the single channels produces challenging physical obstacles to resolve the signal above background noise interference. This noise can come from a variety of sources, but are most commonly associated with

i) the recording equipment (electrodes, head stage, amplifiers etc.) and

ii) the magnitude of the source impedance, a result of measurements taken over a small membrane area (Fishman and Leuchtag, 1990).

Both technical advances and the evolvement of the gigaohm seal have largely eliminated problematic noise sources and produce traces which are easily analysable (figure 4.3).

The primary advantage of the patch clamp technique is the ability to obtain single channel measurements which can be used to predict channels kinetics that describe channel transitions (e.g. from an open to closed state). This characteristic however proves also to be the technique's primary disadvantage. Information can only be obtained for channels directly beneath the pipette within the sealed recording area. The observed single channel properties give no indication of the actions of the entire population of channels throughout the cell or tissue and may not be representative of the channel population.

4.1.4. Current fluctuation

Early on in investigations surrounding the electrical activity of sodium channels, it was noted that channels fluctuate randomly between an open and a closed state. This fluctuation is readily demonstrated by patch clamp (see fig. 4.3. above). Conceptually the single channel fluctuations recorded at the patch clamp level could be extrapolated to a whole cell or tissue level where channels would be randomly opening and closing across the entire epithelium. The transepithelial current recording of sodium ion flux across a voltage-clamped epithelium would therefore comprise the summed activity of all the selective sodium ion channels in the membranes of the epithelium. When such recordings were made on excitable tissue the resulting "noise" or current fluctuations were readily demonstrated and could theoretically be analysed. These random or stochastic events are however not easy to analyse and it was realised that Fourier analysis would be a valuable tool to extract information from the complex random data (Fishman and Leuchtag, 1990).

An easier way of handling data collected temporally is to convert it into a frequency domain by fast Fourier transformations (FFT). This process produces data which can be represented graphically by plotting an amplitude versus frequency spectrum. When the amplitudes are plotted as the mean square values the graph is termed a power density spectrum (PDS) (Fishman and Leuchtag, 1990). Three types of "noise" or fluctuation components are commonly recorded from voltage-clamped epithelia. These are 1) low frequency noise or 1/f noise, 2) Lorentzian or relaxation noise and 3) amplifier noise (van Dreissche and van Deynse, 1990). The origin of the 1/f noise is not always clear, and this dominates the lower frequency end of the data collected. The Lorentzian noise is of most interest from a biological point of view as it originates from fluctuations produces by the random opening and

closing of channels which interrupt the flow of ions and thus the current flowing through the channels. Finally, the amplifier noise is at the high end of the frequency following the Fourier transform and can thus be readily filtered out.

4.1.5. Theoretical background (fluctuation analysis)

The Lorentzian component of the noise therefore contains data about the opening and closing of channels in the epithelia. The transition of channels from an open to a closed state can be theoretically defined by the rate coefficients α and β in the equation;

$$\text{Closed} \underset{\alpha}{\overset{\beta}{\rightleftharpoons}} \text{Open} \qquad \text{(Eq. 4.1)}$$

The channel open probability (or the chance of detecting the channel in the open state) can thus be defined as:

$$\beta' = \beta/(\alpha+\beta) = N_o/N_T \qquad \text{(Eq. 4.2)}$$

Where N_T represents the total pool of active channels or the average mean open (N_o) plus closed (N_c) states of the channel (Helman and Kizer, 1990).

When data are collected from an epithelium which is voltage clamped changes in the mean macroscopic rate of sodium ion transport (I_{Na}) result from fluctuations between open and closed states of the sodium channels and is further dependant on the number of channels (N_T) and the single channel current (i_{Na}) according to the equation:

$$\sigma^2_{I_{Na}} = N_T i^2_{Na} \beta'(1-\beta) \qquad \text{(Eq. 4.3)}$$

where $\sigma^2_{I_{Na}}$ is the variance of the mean sodium transport rate and

$$I_{Na} = \beta' N_T i_{Na} \qquad \text{(Eq. 4.4)}$$

and

$$i_{Na} = \frac{\sigma^2_{i_{Na}}}{I_{Na}(1-\beta')} \qquad \text{(Eq. 4.5)}$$

In the case of ion channels, the "noise" or fluctuations in recording resulting from the flow of ions through the channel follow an exponential kinetics and produce a Lorantzian curve of the form:

$$S(f)=S_o/[1 + (f/f_c)^2] \qquad \text{(Eq. 4.6)}$$

Where S_o and f_c are the low-frequency plateau and corner frequency of the Lorentzian PDS respectively.

4.1.6. Blocker introduction

It is theoretically possible to determine the PDS of any frequency of interest, but practically frequencies of less than 0.1 Hz prove to problematic due to 1/f noise (Helman and Kizer, 1990). For sodium channels of excitable tissue such as nerve, this is not a problem due to the fact that the channels flicker between the open and closed states fairly rapidly (milliseconds) and are above the range of interfering noise signals, but in epithelial cells channel opening can be several seconds in duration. The spontaneous Lorentzain resulting from these slow flickering events would appear in the background 1/f noise and therefore be lost in the instrumentation noise.

In order to counteract this setback in epithelial cells, researchers have made use of specific blockers in order to artificially occlude the ion channel of interest (in this case the sodium

channel) and produce a more rapid flickering of the channel according to the binding kinetics of the compound to the channel (Baxendale and Helman, 1986; Helman and Baxendale, 1990; Kleyman and Cragoe, 1988; Li *et al.*, 1985, 1987; Lindemann and Van Driessche, 1977; Van Driessche and Zeiske, 1980; Zeiske and Van Driessche, 1984). In the case of sodium channels two specific blockers namely amiloride and CDPC (6-chloro- 3,5-diaminopyrazine-2-cardoxamide) have been extensively used.

4.1.7. Models for blocker interactions

In order to account for the properties of blocker interaction on the channel a four state model needs to be considered and is represented as:

$$\text{Closed-blocked} \underset{\gamma}{\overset{\delta}{\rightleftharpoons}} \text{Closed} \underset{\alpha}{\overset{\beta}{\rightleftharpoons}} \text{Open} \underset{k_{bo}}{\overset{k_{ob}}{\rightleftharpoons}} \text{Blocked} \qquad \text{(Eq. 4.7)}$$

Where k_{ob} and k_{bo} are the transition rates or rate coefficients of the open to blocked and blocked to open state respectively and are functions of the particular blocker being used. Conceptually however it can be argued that a closed-blocked channel would not have any sodium flux and therefore not contribute to the observed PDS. In order to simplify the equations a simpler three-state model has been proposed as follows:

$$\text{Closed} \underset{\alpha}{\overset{\beta}{\rightleftharpoons}} \text{Open} \underset{k_{bo}}{\overset{k_{ob}}{\rightleftharpoons}} \text{Blocked} \qquad \text{(Eq. 4.8)}$$

Most of the useful data collected in this scenario would arise from the Lorentzian PDS resulting from the blocker frequencies. Assuming that the changes in single channel characteristic vary linearly with linear changes in blocker concentration it is possible to extrapolate back to the unblocked state and determine the single channel parameters by

collecting data at increasing blocker concentrations and making use of the equations outlined below (derived by Lindemann and Van Driessche, 1977).

This method, commonly referred to as the staircase protocol, requires data collection to occur during steady states in the experimental protocol. Due to the fact that the low-frequency plateau and corner frequency (S_o and f_c) of the blocker arise from fluctuations of the channels from the open and blocked states the single channel current for a particular concentration of blocker (i_{Na}^{B}) can be calculated directly as

$$i_{Nz}^{B} = \frac{S_o^B (2\pi f_c^B)^2}{4 I_{Na}^B k_{ob}[B]} \qquad \text{(Eq. 4.9)}$$

The open channel density at a particular blocker concentration [B] is

$$N_o^B = I_{Na}^B / i_{Na}^B \qquad \text{(Eq. 4.10)}$$

These values for open channel number do not reflect the pool of open channels that are blocked (N_{ob}) at each of the blocker concentrations. These data can be calculated according to the law of mass action as:

$$\begin{aligned} N_{ob} &= N_{oB}(1+[B]/K_B) \\ &= N_{oB} + N_b \end{aligned} \qquad \text{(Eq. 4.11)}$$

where N_b are the number of blocked channels and N_{oB} the number of open channels in a blocked state. The three-state model allows for the estimation of channel open probability, a measure of channel open time, at each blocker concentration and by extrapolating back to zero by linear regression analysis, the open probability of the channels can be obtained (Eq.4.12).

$$P_O = \frac{[1-(N_{oB}/N_o)]}{(N_o/N_{oB})([B]/K_B)} = \frac{N_o/N_{oB}-1}{[B]/K_B} \qquad \text{(Eq. 4.12)}$$

Finally, the total channel density (N_T) which constitutes the sum of the electrically active open and closed channels in the absence of blocker can be derived by:

$$N_T = N_o + N_c \qquad \text{(Eq. 4.13)}$$

The staircase protocol provided valuable information of single channel characteristics acting across an entire epithelium, but was restrictive in that these data could only be obtained during steady state conditions. Due to the fact that a number of blocker concentrations were employed in order to perform linear regressions on the values some time was required to collect the necessary data.

4.1.8. Pulse inhibition protocol

A modification on the technique was proposed and implemented some time later (Helman *et al.*, 1998). The consistency of data obtained by the staircase protocol gave researchers the confidence to make certain assumptions as to the way the epithelium would react to blocker concentrations. In the new protocol only two blocker concentrations were utilised to obtain two data points from which to extrapolate. The apical surface of the epithelium was constantly bathed in a medium containing 10 μM CDPC and periodically pulsed with one containing 30 μM CDPC. Noise analysis was performed at these two blocker concentrations and data use to derive all the values discussed above.

The method has been termed the pulse-inhibition protocol due to the nature of the experiment and has been utilised in these time course investigations. The major advantage of the protocol (details discussed below) is the fact that measurements can be obtained very rapidly and therefore during transient events rather than at static steady state periods. More data can be collected more quickly from the epithelium and thus sudden changes in channel kinetics can be obtained. However the technique is not without problems and the sacrifice of many data points means assumptions and safeguards need to be in place to ensure accuracy of data obtained.

4.1.9. Considerations for the pulse-protocol

First, the time needed to totally replace the one solution present in the chamber with the second at the higher concentration ranges from 40 to 60 seconds. This was due to the mixing of the solutions at first in the chamber and the presence of unstirred layers preventing fast replacement of the old solution. Cells have been found however to respond rapidly to any inhibition in sodium flux by autoregulatory means (Chou and Els, 1997). A rapid inhibition in current is followed by an autoregulatory increase in sodium transport after 30 to 60 seconds. It was therefore important to ensure that true minimum values for the data were obtained during the pulse inhibition. This was accomplished by using a non-linear curve fitting routine to fit the measured data and account for baseline variations and the delayed autoregulatory increases (see fig.4.4). In order to track these small but rapid changes, I_{SC} values were recorded every 10 seconds during the noise analysis acquisition phase for use in the curve-fitting routine.

The particular methodology and calculations involved in obtaining data by the pulse-inhibition protocol of noise analysis have been previously described in detail (Helman *et al.*, 1998) and are discussed briefly in the Materials and Methods section (see below).

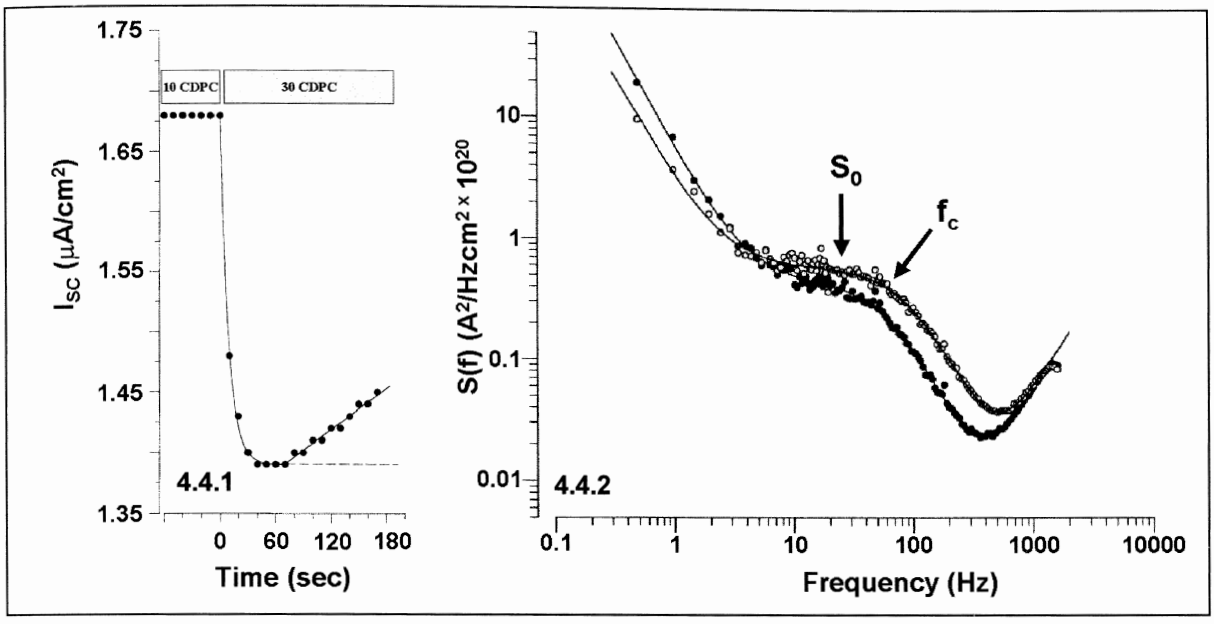

Fig. 4.4. The pulse-inhibition protocol of noise analysis required certain considerations. True minima (dashed line) of the inhibition pulse after the introduction of 30 μM CDPD (4.4.1) were obtained from the fitted curve before autoregulation commenced. A typical PDS of both 10 μM CDPC (black circles) and 30 μM CDPC (grey circles) is presented in 4.4.2. The S_0 (plateaux) and f_c (corner frequency) values are obtained from the fitted spectra (see equation 4.6) at the points indicated. In this example the f_c for 10 μM and 30 μM CDPC was 60.7 and 87.6 respectively. Note log scale in 4.4.2. (modified from Helman *et al.*, 1998)

4.1.10. Advantages and disadvantages of current fluctuation analysis

It is therefore possible by the method of noise analysis to obtain much of the same data as single channel methods, but the information relates to the whole channel population in an epithelial monolayer. The physiological responses of the entire population of channels can be investigated under a number of experimental conditions in order to get a better holistic understanding of sodium channel biology. There are a number of drawbacks to this technique however. The first is that fluctuation analysis makes certain assumptions based on theoretical models of channel kinetics. The correct kinetic "scheme" needs to be determined in order to extrapolate data for particular ion channels (Eaton and Marunaka, 1990). As no direct kinetic data can be obtained for channels using this technique, it is often of great value to employ both single-channel and current fluctuation analysis when working in an unknown paradigm.

Secondly, if channels are found to fluctuate between an open and closed state very slowly (seconds), the use of channel blockers needs to be employed. This poses additional constraints on the technique as suitable blockers need to be found which will bind to the channel in a reversible fashion (in order to generate the flicker needed for noise analysis) and be selective only for the channel under investigation.

Thirdly, there needs to be sufficient current flowing through the channels of interest in order to generate a signal which is detectable above background noise. The signal needs to be adequately resolved to thus be amplified and filtered in order for perform the FFT. Changes in ionic driving forces would also cause changes in calculated single channels currents.

Fourth, as discussed the measured current fluctuations are obtained under voltage clamped conditions. The assumption made here is that the resistance in series across the membrane is small in relation to the cell membrane resistance. In other words in the case of an epithelial monolayer of A6 epithelial cells it is assumed that the resistance of the basolateral membrane is much smaller than the apical membrane resistance. Were this not the case, an increased series resistance would reduce the current required to clamp the membrane and therefore also the amplitude of the current fluctuations (van Driescche and van Deynse, 1990).

In the case of epithelial sodium channels however, much data has already been obtained by both noise analysis and patch-clamp methods. The kinetic data from patch-clamping compares favourably with noise-analysis data and therefore reinforces the three-state model outlined above. This makes noise analysis a particularly attractive tool to study the regulation of the total population of sodium channels in model epithelia. There are also

suitable blockers for the channel and model epithelia particularly of the kidney produce sodium currents which are readily detectable.

In order to address the specific limitations of patch clamp technique, Eaton and Marunaka (1990) suggested a hybrid technique which combined the best of both the patch clamp and noise/fluctuation analysis methods. In 1991 Marunaka and Eaton produced a measure to quantified the channel activity by expressing it as the product of the number of channels and the open probability according to the equation:

$$NP_O = \sum_{n=0}^{N} \frac{nt_n}{T} \qquad \text{(Eq. 4.14)}$$

Where T is the total recording time and N is the number of open channels, n is the number of channels open. NP_o is therefore the measure of channel activity. Complications do arise however when the P_o is very low.

This chapter reports the results of data obtained from A6 epithelia stimulated by increasing cAMP levels, firstly by simple short current (I_{SC}) measurements and secondly by noise analysis. The two methods provide information about the response to an acute stimulation at both the tissue and cellular (channel) level and serve to quantify the visual results presented in the previous chapter.

4.2. MATERIALS AND METHODS

4.2.1. Cell culture

Once again the same cell culture methodology was employed as discussed in Chapter 2. Only cells grown on filter supports to an electrically competent age were used. All cells were treated in the same way whether to obtain data by basic I_{SC} or noise analysis.

4.2.2. Ussing chamber preparation and tissue mounting

The preparation of Ag/AgCl electrodes and mounting of tissues into a modified Ussing chamber has been described in the general materials and methods section (see Chapter 2)

4.2.3. Short-circuit current measurements

The Ussing chamber was housed in a shielded (Faraday) cage which was grounded. The clamp apparatus was powered by a 12V DC battery to reduce noise. Mounted epithelia were continuously short-circuited with a low noise voltage clamp (clamped at 0mV) and current recorded on a strip-chart recorder (linear 1200, Anatech Instruments Ltd.,South Africa).

It was of interest to determine the ionic nature of the A6 response to forskolin as this cell line differed slightly from previous studies using A6 cells. To investigate the sodium transport, 100 μM amiloride was added apically to the A6 mounted epithelia in order to inhibit the epithelial sodium channels. By doing this the contribution of the sodium current to the total recorded transepithelial current could be determined. The response to cAMP in other well studied model epithelia like toad bladder and cortical collecting ducts produced a large increase in water permeability (Grantham and Burg, 1962; Hays and Leaf, 1962; Orloff *et al.*,

1962), unlike A6 epithelia which show no water permeability and probably do not express water channels (Crowe *et al.*, 1995). The A6 cells have however been reported to alter Cl^- transport in response to cAMP stimulation (Chalfant *et al.*, 1993; Yanase and Handler, 1986a). This is achieved by expression of Cl^- channels in the apical membranes of the cells (Marunaka and Eaton, 1990; Nakahari and Marunaka, 1995). Results from these investigations would seem to indicate that this Cl^- response is lacking in these cells and this needed to be kept in mind when investigating the regulation of sodium by current fluctuation analysis.

4.2.4. Current fluctuation analysis

In order to record the small signal obtained from the epithelium a low-noise voltage clamp, electrical amplifiers and filters were needed. The mounted epithelium was voltage clamped to 0mV. Current input into the voltage clamp was by differential amplifier (DA) which amplified the signal 100 times. A feedback amplifier (FBA) was responsible for clamping the tissue at the desired voltage (in this case 0mV). The output current was next fed through pre-filters, aliasing filters and amplifiers with adjustable gain control and finally sent to a current to voltage converter (CA).

To detect current fluctuations, the AC and DC components of the recorded current were separated by a high-pass rectifying current filter and the AC component was then amplified 1000 times. The remaining signal was passed through anti-aliasing filtering and a low-pass filter to remove the high amplitude AC signal. Finally the signal was converted from an analogue to a digital one by and A/D converter (RTI 800, Analog Devices Inc., Mass, USA).

The fundamental frequency of 0.5 Hz was used to derive the PDS. In order to perform the FFT the PDS of 2048 fequencies were obtained from 50 data sweeps. The collected and

digitised data were stored on the acquisition computer for later analysis. Spectra containing relaxation noise (channel fluctuations) were fitted by non-linear, least square regression analysis. The equations derived above for noise analysis were adapted to apply to the specific conditions of the pulse-inhibition protocol. As two blocker concentration were utilised the fitted PDS curves each produced a f_c which could be used to determine the k_{ob} and k_{bo} rate coefficients from the slopes and the intercepts of rate concentration plots and the blocker equilibrium coefficient (K_B) by the following equation:

$$2\pi f_c = k_{ob}[B]+k_{bo} \qquad \text{(Eq. 4.15)}$$

KB was calculated from the quotient $\frac{k_{bo}}{k_{ob}}$ at each time point.

Single channel currents were calculated by:

$$i_{Na}^{B} = \frac{S_0(2\pi f_c)^2}{4I_{Na}^{B}k_{ob}B} \qquad \text{(Eq. 4.16)}$$

and the channel open probability (P_o) was determined from the fractional inhibition of the blocker sensitive I_{SC} at the two blocker concentrations used, 10 µM and 30 µM CDPC (Eq. 4.17).

$$P_O = \left[\frac{1-\left(I_{Na}^{30}/I_{Na}^{10}\right)}{B^{30}\left(I_{Na}^{30}/I_{Na}^{10}\right)-B^{10}}\right]K_B \qquad \text{(Eq. 4.17)}$$

Open channel densities at 10 µM CDPC (N_o^{10}) were calculated as:

$$N_o^{10} = \frac{I_{Na}^{10}}{i_{Na}^{10}} \qquad \text{(Eq. 4.18)}$$

The N_o in the absence of blocker could be extrapolated from equation 4.19.

$$N_o^{10}(1+P_oB^{10}/K_B) \qquad \text{(Eq. 4.19)}$$

Finally the total pool of functional channels (N_T) in both closed or open states in the absence of blocker was calculated as $N_T = \frac{N_O}{P_O}$ (Eq.4.20)

The time course of the current fluctuation analysis experiments of forskolin stimulation was kept consistent and pluses were given at set 10 minute intervals in order to obtain single channel data. A typical trace of one such experiment is presented in figure 4.5. The epithelium was first voltage clamped and then the 10 μM CDPC solution perfused on the apical membrane. Following a 30-minute stabilisation period 2.5 μM forskolin was added to the basolateral medium which produced a maximal response within 40 minutes. The forskolin was washed out and the epithelia allowed to return to basal levels before 100 μM amiloride was added to the apical membrane perfusate to determine the contribution of sodium to the overall recorded current. The epithelium was pulsed at 10 minute intervals with 30 μM CDPC during which time noise analysis measurements were taken. After data collection at 30 μM CDPC was complete, the solution was switched back to 10 μM CDPC. Time zero was taken as the time at which forskolin was added to the epithelium.

Due to slight differences in I_{SC} from culture to culture it was difficult at times to pool data. The nature of the responses remained similar despite differences in baseline transport values and in order to get a cleaner set of comparable data, the information obtained from the current fluctuation was plotted as experimental versus baseline control values. The convention was adopted to assign the data point immediately prior to the addition of forskolin as the control value from which deviations higher or lower were calculated. In this way experimental results were expressed in terms of increases or decreases from this baseline point and each experiment acted as its own control. Therefore, both absolute single channel data and relative changes are presented below.

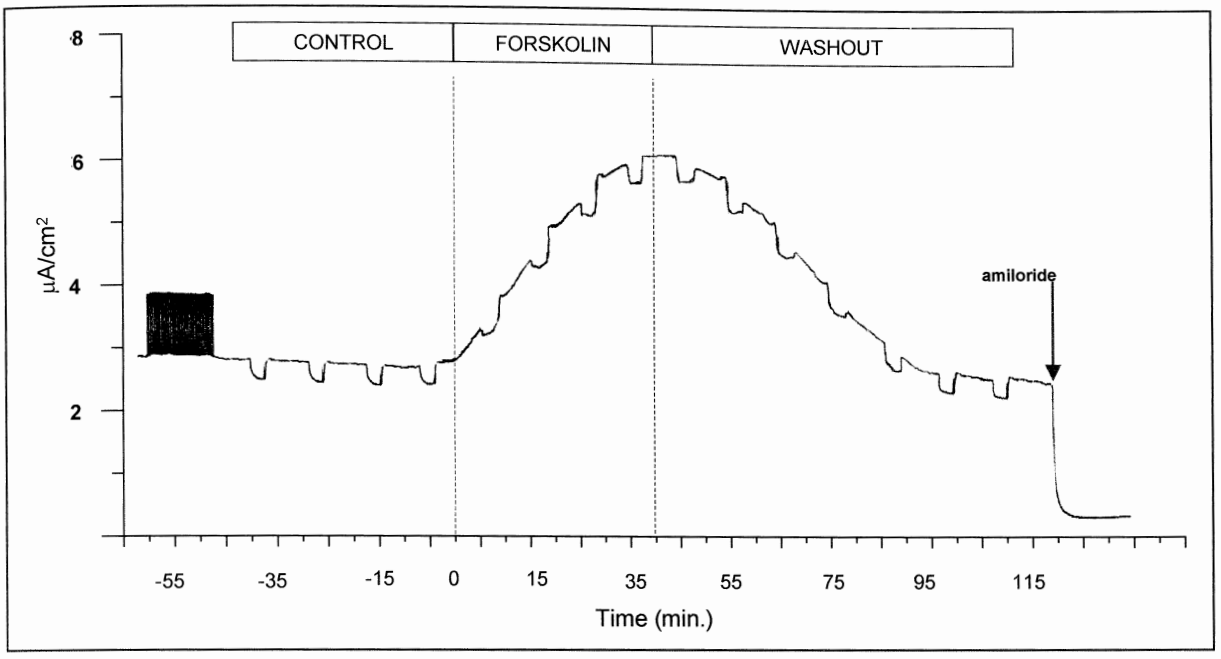

Fig. 4.5. A typical short-circuit current trace from a voltage clamped A6 monolayer used for current fluctuation analysis. Cells were allowed to stabilise (control period indicated) in the Ussing chamber and stimulated with 2.5 µM forskolin (period indicated by the box). At various points cells were pulsed with 30 µM CDPC (deflections). Finally 100 µM amiloride was added to determine the contribution of sodium to the overall current recorded. Note that the initial rapid Cl^- response seen in other investigations with A6 (Chalfant *et al.*, 1993) at the addition of forskolin is lacking

4.3. RESULTS

4.3.1. Short circuit current

In order to get an indication of the electrical response of A6 cells to forskolin stimulation, simple I_{SC} measurements were made on the cultured monolayers. As described, the voltage clamped epithelia were constantly perfused and stimulated with 2.5 μM forskolin. The strip chart trace of a typical current fluctuation analysis experiment is presented in figure 4.5. However to investigate the contribution of sodium transport to the recorded current, amiloride was added at differing times to short-circuited epithelia. One such experiment is presented in figure 4.6.

It can clearly be seen that there is a rapid increase in transepithelial current following the addition of forskolin, but no transient Cl^- current is observed. Amiloride was added before, during and after forskolin addition as indicated. At every point, amiloride inhibited the majority of the recorded current indicating a minimal contribution of chloride transport to the total recorded current.

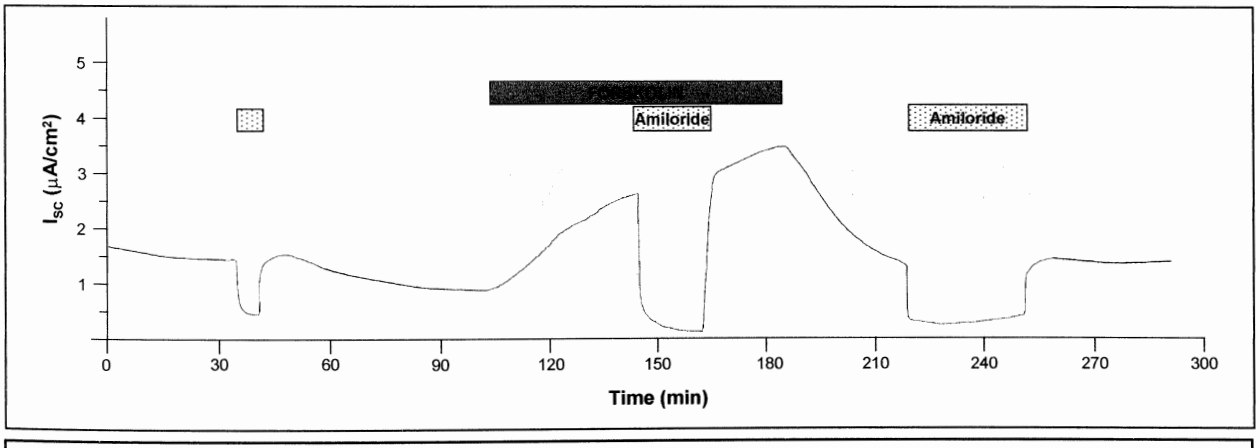

Fig. 4.6. A short-circuit current trace from a voltage clamped A6 monolayer. Cells were allowed to stabilize in the Ussing chamber and stimulated with 2.5 μM forskolin (period indicated by the dark box). At various points 100 μM amiloride (light hatched box) was added to determine the contribution of sodium to the overall current recorded.

A closer examination of the trace presented illustrates three very important characteristics of the A6 cells. The forskolin stimulation produced a rapid increase in transepithelial current, the effects of which are evident within 5 minutes following the addition of forskolin. It has been reported that in A6 cells forskolin activates chloride channels typically within the first 5 minutes of forskolin addition (Păunescu and Helman, 2001). Although with our source of A6 cells no transient increases in I_{SC} were observed within this crucial 5 min period (figure 4.6), we can not rule out the possibility that some Cl^- channels had been activated. In retrospect, a better experiment would have been to add forskolin to amiloride-treated tissues. However the addition of 100μm amiloride at the peak of forskolin stimulation effectively eliminated approximately >90% of the short-circuit current, suggesting that sodium current is the main component of the total recorded I_{SC} at this stage. As amiloride also inhibited the I_{SC} to near zero values after 60 min forskolin washout, the A6 cells used in our experiments was an eminently suitable model for studies on sodium transport as well as for studies on ENaC trafficking.

4.3.2. Current fluctuation analysis

Once the characteristic responses to forskolin stimulation had been demonstrated and cAMP stimulation could be seen to directly effect sodium transport, it was of interest to determine the nature of this response. The electrophysiological technique of noise analysis provided the ability to undertake such measurements. Several pieces of data could be obtained by this technique (as described above) and these are presented in the figures below. Figures 4.7-4.9 provide data as obtained from 14 separate experiments, expressed in the particular units for each. From figure 4.7. the increase in short-circuit current (an example of which is presented in fig. 4.5) can be seen to be predominantly as a result of an increase in macroscopic sodium current.

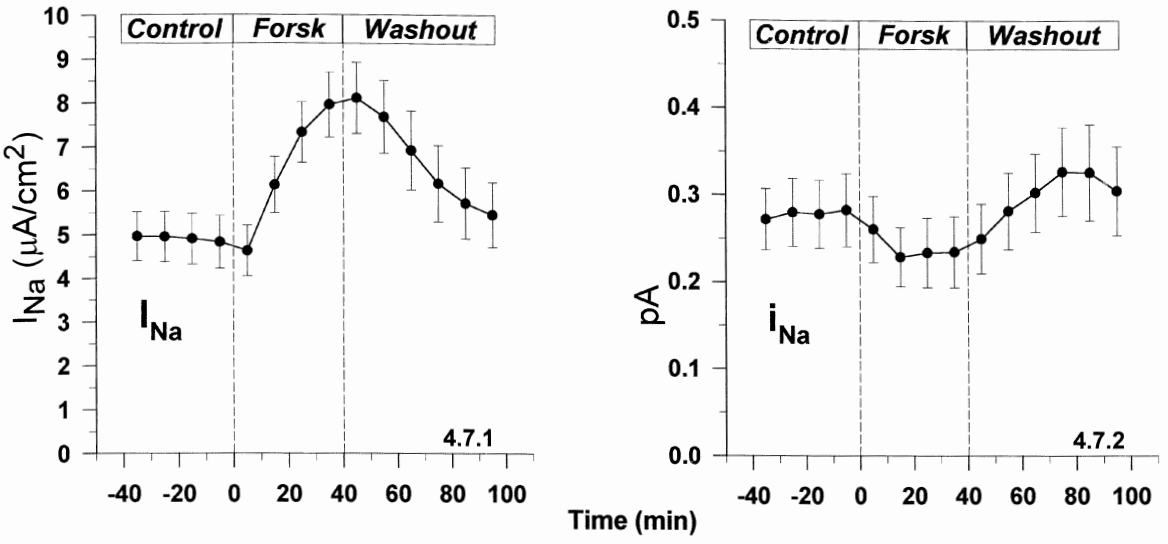

Fig. 4.7. The macroscopic sodium current response to forskolin stimulation is presented in 4.7.1 with units expressed for exposed filter area in the Ussing chamber. Forskolin was introduced for the period indicated after which it was washed out. The increase in overall current is at odds with the single channel sodium current, i.e. current flowing through individual sodium channels shown in fig.4.7.2. Data obtained from 14 separate experiments with error bars representing standard errors of the mean (S.E.)

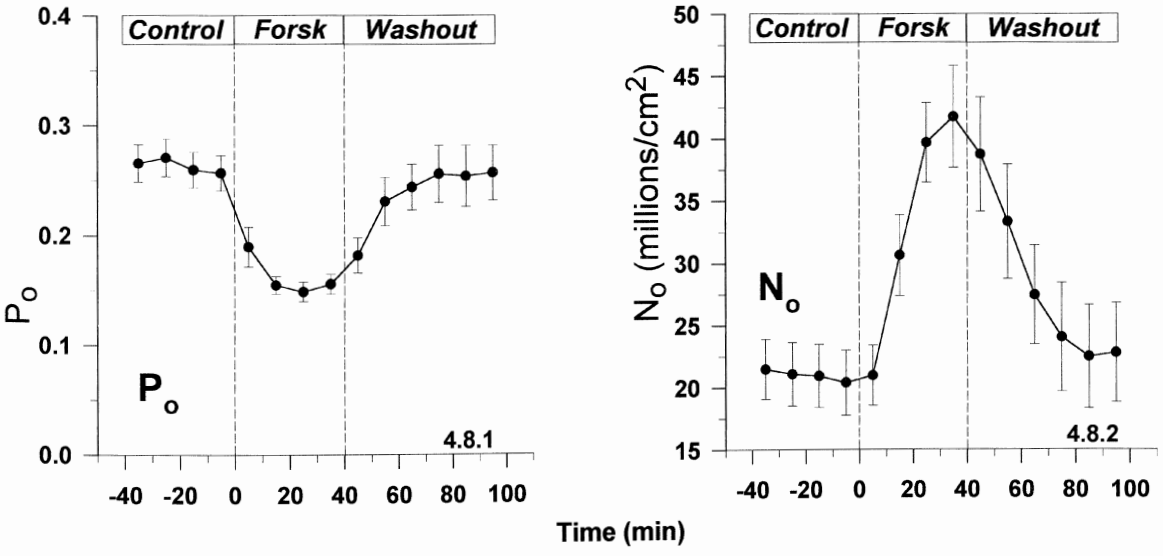

Fig. 4.8. The open probability for channels during the experimental protocol is presented in figure 4.8.1. The adjacent figure (4.8.2) summarises data obtained for the number of open channels per exposed filter area in the Ussing chamber. Data obtained from 14 separate experiments with S.E. bars.

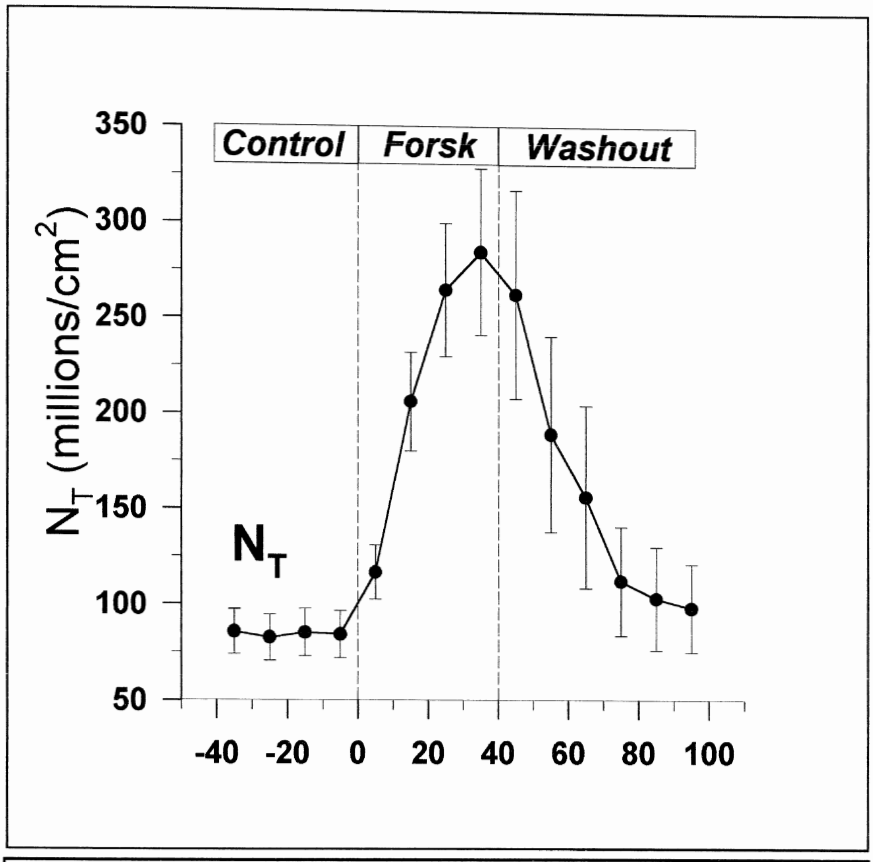

Fig. 4.9. Average values calculated for total channel number (N_T) during control, forskolin stimulation and washout are presented. Units reflect area of exposed filter in the Ussing chamber. Data obtained from 14 separate experiments with error bars representing S.E.

Following these results, data from the same experiments are expressed as experimental versus control (see materials and methods above) as each culture acted as its own control (figures 4.10 - 4.11). The second set of figures serve to better illustrate the forskolin response as they eliminate random variations from culture to culture as a result of slightly different starting values.

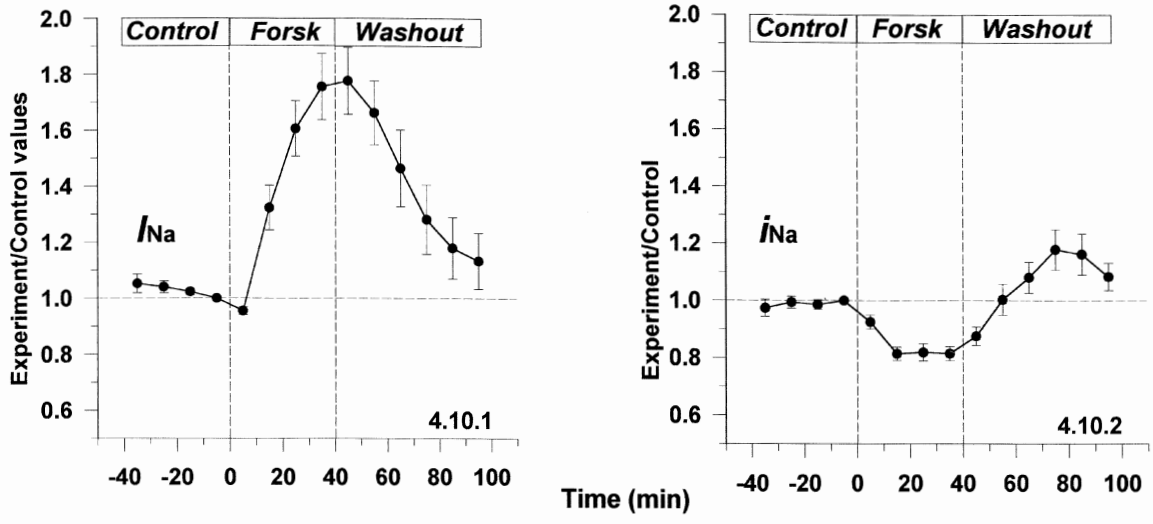

Fig. 4.10. The macroscopic sodium current (I_{Na}) and single channel current (i_{Na}) data expressed as experimental versus control values (see material and methods for explanation). n = 14 for separate unpaired experiments with error bars representing S.E.

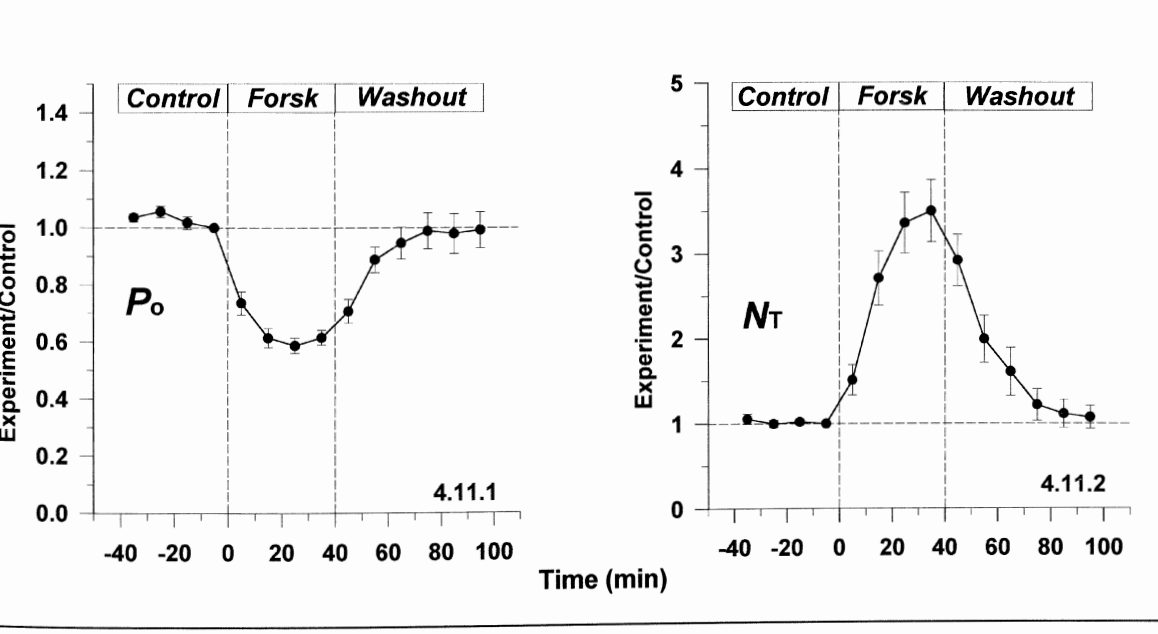

Fig. 4.11. The experimental versus control changes for P_o (fig.4.11.1) and N_T (fig.4.11.2) data from 14 independent experiments (results presented above). Standard error bars as indicated

The observed increase in macroscopic current cannot be attributed to a change in the transport rates of the channels themselves. The data indicate that the single channel current (i_{Na}) at the peak of the forskolin response was approximately 20% lower than the starting value as it fell from 0.283 ±0.042pA per channel to 0.229 ±0.034 pA per channel. The P_o data indicated the same trend with values dropping to under 61.5 ±2.6% of the starting control levels. These two parameters were however in contrast to the N_o and N_T data obtained. Both the open channel number and the total channel number increased dramatically with a 3.5 fold increase observed in the case of N_T. In quantitative terms this represented an increase from 84.35 ±12.25 million channels/cm^2 to 284.83 ±43.60 million channels/cm^2.

One of the considerations of the noise analysis technique is the fact that these values for various single channel parameters are calculated from the fractional inhibition of the sodium channels. In order for the various calculations to be made, it is assumed that the blocker interaction with the channel does not vary significantly throughout the experiment. This assumption can be tested however by monitoring the rate coefficients of k_{ob}, k_{bo} and the K_B values throughout the experiment. A dramatic shift in any of these values would indicate a change in the blocker/channel interaction or the emergence of a different channel with dissimilar blocker kinetics. The values for these three measurements are plotted in figure 4.12 and 4.13 and illustrate that the introduction of forskolin caused no significant changes in the CDPC-blocker/ENaC interaction indicating channels recruited by cAMP stimulation had the same blocker kinetics as those present in the membrane before forskolin stimulation.

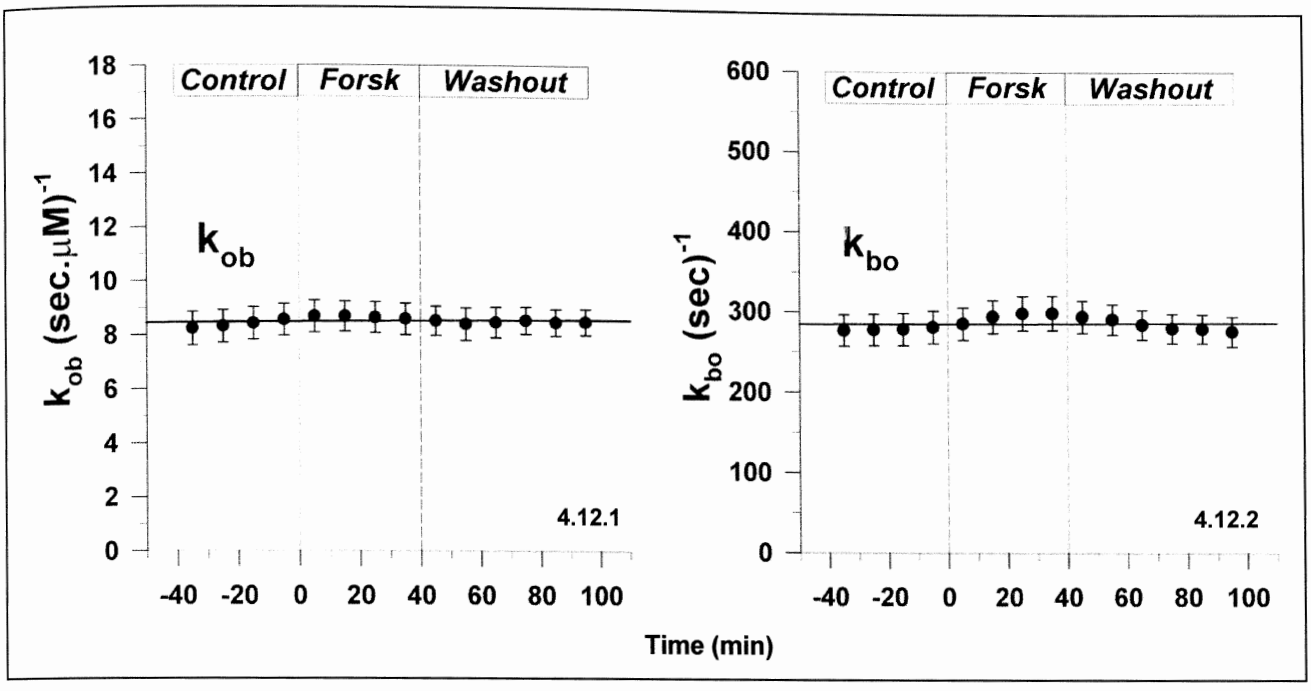

Fig. 4.12. Averaged blocker kinetic values for kob (4.12.1) and kbo (4.12.2) throughout the course of the protocol are illustrated. The linear regression for the data points (solid line) was plotted to compare extrapolated points with previously obtained data (Sigma Plot, SPSS, Chicago, USA). n=14 ± S.E.

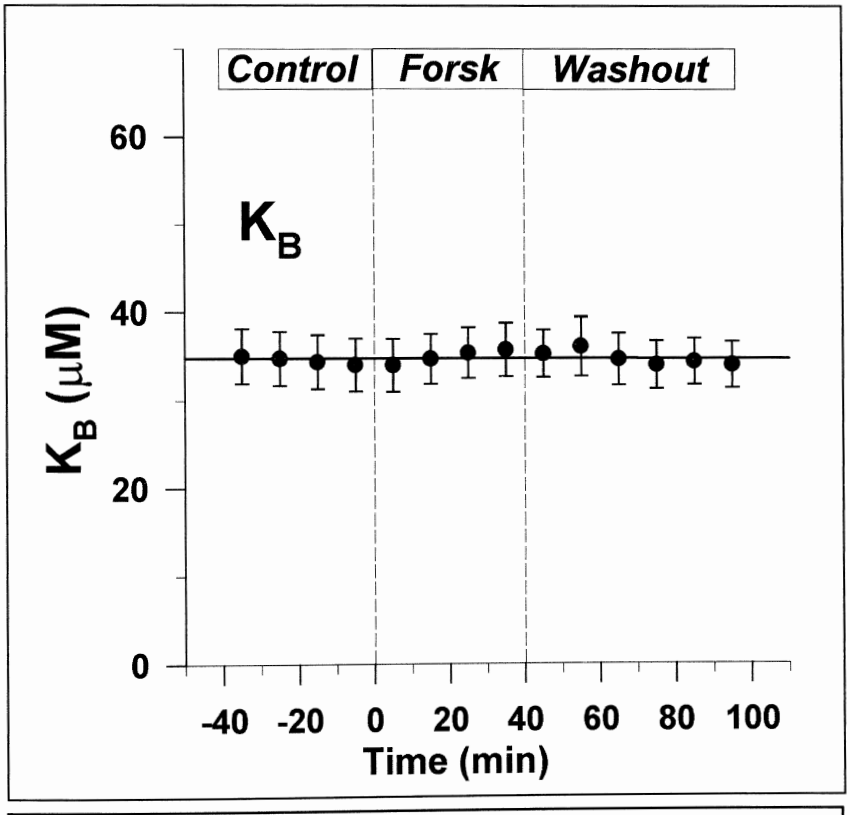

Fig. 4.13. Average blocker affinity values plotted over the experimental timecourse with fitted linear regression (solid line) plotted as before. CDPC blocker affinity did not alter significantly during the experiments. n=14 ±S.E..

The data obtained under control and stimulated conditions as graphed above are summarised in table 4.1. Two data points are listed, namely the control values just prior to forskolin introduction and those obtained at the point of maximum response (35min).

	I_{Na} ($\mu A/cm^2$)	i_{Na} (pA)	N_o ($10^6/cm^2$)	P_o	N_T ($10^6/cm^2$)	k_{ob} (rad/s.μM)	k_{bo} (rad/s)	K_B (μM)
Control	**4.83 ±0.06**	**0.283 ±0.042**	**20.40 ±2.63**	**0.257 ±0.016**	**84.35 ±12.35**	**8.56 ±0.59**	**281.56 ±20.01**	**34.09 ±3.00**
Stimulated	**7.96 ±0.74**	**0.235 ±0.041**	**41.77 ±4.09**	**0.156 ±0.009**	**284.83 ±43.60**	**8.59 ±0.58**	**299.39 ±21.40**	**35.81 ±3.04**

Table 4.1. Summarised results of control and stimulated Na^+ channel parameters. Values are expressed as means and S.E. (n=14).

4.4. DISCUSSION

4.4.1. Forskolin effects on sodium transport

Simple I_{SC} measurements illustrate the rapid nature of the cAMP-mediated response in the A6 cells. As described, the response was mainly due to a large increase in Na^+ current. Results from the noise analysis serve to confirm this. The I_{Na} plotted in fig. 4.7.1 illustrates the rapid increase in Na^+ current as a result of forskolin stimulation. This is true in all cases irrespective of the culture baseline I_{SC} values. When experimental versus control data are plotted (fig. 4.10.1) a 1.77 ±0.12 fold increase in I_{Na} is over control values was recorded. An investigation into the cause of this large increase reveals that it was not as a result of an increase in individual single channel currents. The i_{Na} actually decreases during the stimulation period, at its lowest point ending up only 81.5 ±2.4% of the original starting value.

The regulation of sodium conductance through the apical sodium channels is directly proportional to the product of the single channel conductance of each channel, the number of conducting channels and the open probability of each channel. Results for the channel open probability indicate a reduction in the average open time with P_o falling to 58.7 ±2.7% of the control value. According to the scheme then, the only property which could account for increased current was a greater number of active channels present at the apical membrane. This fact is illustrated in the results for both the N_o and N_T where the values of each increased 213 ±18.3% and 350 ±36.5% respectively. The product of the three parameters, N_T, P_o and i_{Na} therefore equals the total observed increase in sodium current, which at 35 minutes is 1.77 ±0.12 fold greater than control. The large increase in the number of active channels at the apical membrane resulted in the increased sodium transport, the characteristic cAMP-mediated response.

The control values for I_{Na} reported here were in line with previous studies (summarised in Helman and Kizer, 1990; Helman *et al.*, 1998) with a slightly lower value reported by Bindels *et al.* (1988). The calculated control i_{Na} was however slightly lower than data reported by Helman and Keizer (1990). An approximation of single channel conductance can be made from the i_{Na} by substituting into the following equation:

$$\gamma = \frac{i_{Na}}{(V_m - E_{Na})} \qquad \text{(Eq. 4.21)}$$

where E_{Na} is calculated from the Nernst potential for sodium (Ganong, 1991) as:

$$E_{Na} = 58 \log \frac{[Na^+]_o}{[Na^+]_i} \qquad \text{(Eq. 4.22)}$$

Substituting the mean control i_{Na} of 0.28 pA (table 4.1) and approximations for intracellular and extracellular Na+ concentrations of 14.5 mM and 110 mM respectively (Els and Helman, 1991) with membrane potential of approximately 71 mV (Koeppen *et al.*, 1983) produces an approximation of 2.25 pS for single channel conduction. This is slightly lower than previously reported values in A6 cells and other model tissues (reviewed by Garty and Palmer, 1997), but falls in line with the idea that these channels are members of the low conductive highly Na^+ selective group discussed in the opening chapter.

4.4.2. Blocker interactions

This increase in channel number could be as a result of recruitment of electrically silent channels resident in the apical membrane or insertion of active channels into the apical membrane from a sub-apical pool. Channels emerging electrically at the apical membrane did not differ from those already present as the CDPC binding kinetics did not change significantly throughout the course of the experiments and could therefore be considered to be the same

channels. The rate coefficients and binding kinetics of CDPC were essentially unchanged (see figures 4.12 & 4.13, and table 4.1) in control and stimulated states and values did not differ significantly for any k parameter. From table 4.1 values of control rate coefficients are very similar to reports from A6 cells using this same technique (Helman *et al.*, 1998) and also from studies using the staircase protocol of blocker induced noise analysis (see above) where a larger range of CDPC concentrations were used (Baxendale-Cox *et al.*, 1997). This further supported the use of the pulse-protocol of noise analysis as a reliable method to track dynamic changes in the A6 cells in response to forskolin.

These forskolin-induced results from current fluctuation parallel findings in other model tissues (Els and Helman, 1991; Helman *et al.*, 1983; Krattenmacher *et al.*, 1988; Li *et al.*, 1982) which were confirmed by patch clamp techniques in A6 (Marunaka and Eaton, 1991). The mechanism which results in the increased channel number is however not as clear. The introductory chapter focused on the two possibilities more fully, but in order to dissect out the intracellular process another method needed to be employed. Although the noise analysis provided important information regarding the timing and nature of the cAMP response it could not be utilised to study intracellular trafficking mechanisms.

The next three chapters focus on protocols which attempt to find evidence for the recruitment hypothesis (previously outlined) as a mechanism to account for the increase in channel numbers observed from these electrophysiological studies.

CHAPTER 5

FLUID-PHASE MARKER UPTAKE

5.1. INTRODUCTION

The electrophysiological results above indicated that following an increase in intracellular cAMP by forskolin, there was the rapid increase in total channel number (N_T) at the apical surface of the A6 cells. On removal of the forskolin stimulation N_T was observed to decline over time close to control baseline values, supporting the hypothesis that ENaC numbers are regulated by trafficking to and from the apical membrane. Trafficking implies both the exocytic insertion and the endocytic removal of channels. As a first approach to find evidence for trafficking the endocytic process in A6 cells was investigated by making use of fluid-phase endocytic markers. The idea of using endocytic markers was that if the channels were retrieved into the cells by regulated endocytosis it would be possible that some extracellular fluid (ECF) on the apical membrane would be withdrawn into the vesicles with the channels. By loading the ECF with a marker (either fluorescent or chemical) it could be possible to detect changes in endocytic retrieval when compared to control data. Such techniques have been successfully employed to study endocytosis in other cell types (Thilo *et al.*, 1995) with the use of fluorescein-labelled dextran and horseradish peroxidase as fluid-phase markers.

Quantitation of the uptake of marker in unstimulated, control cells and forskolin pre-stimulated cells could provide important information about rates of uptake or differences in endocytic kinetics between experimental and control groups. A problem with this approach however, is that it relies on internalisation of marker not directly associated with the sodium channels. It

could be possible that the method would be sensitive enough to detect even small alterations in the kinetics of endocytic trafficking that would be consistent with the relatively quite large changes in channel densities as demonstrated in the electrophysiological results. If the increase in channel number was brought about by a change in the kinetics of delivery of channels to the apical membrane it would be reasonable to assume that the decrease in channel number following stimulus withdrawal would similarly result from an exocytic channel removal event.

The information obtained from marker studies only addressed the internalisation or retrieval events of apical membrane and possibly ENaC following the removal of stimulation. An attempt was however made to obtain evidence for insertion events by enzymatic labelling (see footnote[1]).

Two separate marker-uptake studies were performed in order to obtain both absolute changes and kinetic data from the uptake of markers. Despite some complications, the approach provided initial evidence for changes in trafficking kinetics and aided in the design of studies to follow.

---

[1] Proteins glycoconjugates on the apical surface were labelled to attempt to detect differences in protein expression levels. Enzymatic cleavage exposed N-acetyl-glucosamine moieties as labelling sites which were radioactively labelled before or after stimulation. In this way a plot of labelled surface proteins in control and stimulated cells could be compared. This attempt proved to be unsuccessful however and results will therefore not be presented here, but was the first approach at finding evidence for possible ENaC insertion events.

5.2. MATERIALS AND METHODS

5.2.1. Cell Culture

The general cell culture conditions have been outlined above. Cells cultured on filter supports for 14 days were used initially in all uptake studies. Variations in culture conditions in order to address high background levels were undertaken and will be outlined in detail below. Cells used in these experiments were cultured in parallel with the inserts used for electrophysiological measurements and samples were divided randomly between the two protocols so that cells from similar batches could be compared.

5.2.2. Fluid-Phase Marker Uptake

Cells grown on filter supports were divided into 4 groups as outlined in table 5.1 below.

Group	2.5 µm Forskolin	28°C	4°C	Description
Experimental	√	√	-	Stimulated, endocytosis
Control Group 1	-	√	-	Unstimulated, Baseline endocytosis
Control Group 2	√	-	√	Stimulated, on ice (no endocytosis)
Control Group 3	-	-	√	Unstimulated on ice (no endocytosis)

Table 5.1. Experimental design scheme

Filter inserts were divided into one of four groups. Experimental cells were incubated with 2.5 µm forskolin in DMEM following the same time course used in the electrophysiological investigations. Following stimulation inserts were washed and basolateral solution replaced

with DMEM without forskolin and allowed to return to control state over 40 min. During this retrieval stage, apical DMEM was replaced with DMEM containing 1 mg/ml HRP (Servac, South Africa) in the presence of 1 mg mannan and 3mg/ml FITC-dextran (Sigma, St Louis, USA) conjugate (Mr = 71,200, 0.005 mol/mol glucose). This experimental design has been presented previously in studies involving endocytosis (Thilo, 1985; Thilo, *et al.*, 1995). To ensure that only conjugated FITC was present in the incubation medium, the FITC conjugated at a 20 fold stock concentration in PBS, was run through a sephadex column (G50) to separate the unconjugated FITC from the FITC-dextran (FITC-D) as it was found that the unconjugated FITC was responsible for a high level of non-specific background signal.

Control groups were marker loaded in an identical manner to forskolin pre-treated cells, but were either held on ice at 4°C (to prevent endocytosis) or did not receive any forskolin stimulation according to the scheme outlined in table 5.1. All measurements were carried out on paired inserts. Following the 40 minute retrieval the cells were placed on ice to prevent any further endocytic activity and washed thoroughly with ice cold DMEM (three 10 minute washes). The cells were then prepared for marker quantitation of either HRP or FITC-D. Results are expressed as percentage of the cold unstimulated control cells (group 1).

i) *HRP Detection*

Filter inserts were punched out from the Millipore cups and placed in separate 20ml plastic tubes. Cells were incubated on ice with HEPES buffer at pH 7.4 to which 0.5% triton-X 100 was added to solubilise the cell membranes in order to release internalised HRP. The level of internalised HRP was measured by employing a widely used protocol first reported by Steinman and Cohn in 1972 to assay HPR in macrophages.

As HRP converts H_2O_2 to H_2O and $O^{\bullet}$, the technique makes use of a photochemical free radical-sensitive compound, 2,2'-azino-di-(3-ethylbenzthiazoline sulphonate) (ABTS) which

turns blue, to detect free radicals produced by the action of HRP. The substrate solution for the reaction contained 0.55mg/ml ABTS in a phosphate/citrate buffer (20 mM Na_2HPO_4, 110 mM NaCl, 20 mM $C_6H_8O_7 \cdot H_20$(citric acid) 150 mM NaCl) at pH 4.3, to which 0.003% H_2O_2 and 0.1% triton-X100 was added. The HRP solubilised cells were incubated in this solution for precisely 5 minutes per sample after which the reaction was stopped by the addition of 0.01%NaN_3 in 100 mM citric acid. The azides in the solution are able to mop up excess free radicals. The solutions were centrifuged to precipitate the cell particulate matter and the coloured product was measured on identical volumes from each sample with a Unicam SP1800 ultraviolet spectrophotometer at a wavelength of 420nm.

ii) *FITC measurement*

In principle the measurement of FITC was more straight forward as the moiety is self-fluorescent and no additional procedures were required to detect a signal. However, in practice an important consideration needed to be realised before making final measurements. As FITC is a fluorophore, it requires a specific excitation wavelength of light and emits photons at a different, longer wavelength (Stoke's shift, see chapter 2 for more details). The small sub-cellular debris and particles released by the action of triton-x100 in the solution however scattered the incident or excitation light to some degree and caused a light-scattering peak which partially overlaped the emission spectra of the FITC. In order to correct for this, a standard curve was constructed for each experimental batch of cells by making a series dilution of cell samples which were not incubated with FITC and recording the light scattering levels at the emitted wavelength for each cell sample volume. A fitted standard curve was used to correct cell samples containing FITC by subtracting the fluorescent intensities (as a result of scatter) for each sample from the recorded fluorescence intensity. Fluorescence was measured in a 1 ml glass cuvette using a Perkin-Elmer fluorescence spectrophotometer type 203, with excitation at 470 nm and emission at 515nm.

5.2.3. Time course of uptake

The protocol for internalisation of HRP and FITC just outlined provides information about absolute changes in internalised marker after 40 minutes retrieval. Far more informative data would be generated by tracking uptake of marker over time. In this regard, a similar protocol was followed as above with a variation being that filters were harvested at fixed time points after removal of forskolin stimulation and start of HRP uptake. Times selected for initial investigations were 5, 10, 20 and 40 minutes. Only HRP uptake was tracked in these investigations due to the problems with high background contaminations when using FITC.

5.2.4. Resistance measurements

In order to find an explanation for the binding of marker to the filter (see background discussion later), even though marker was only added to the apical medium, the resistances of the cells cultured on the filter cups was recorded at both 25°C and 0°C over time with the aid of chopstick electrodes and the Millicel-ERS (Millipore, Bedford, MA, USA) voltmeter. The device allows for *in situ* measurement of both open circuit voltage and resistance across cultures on filter inserts. Resistance measurements were taken on unstimulated cultures at each temperature at 5 minute intervals. Results are expressed as percentage of starting values.

5.2.5. Cell Suspensions

One major complication which arose during the FITC and HRP uptake studies was a high level of variable background contamination of both HRP and FITC in the samples. Initially in an effort to reduce this, the FITC was column purified (as described) and a number of different sample tubes were tried. After some investigation it was determined that much of this contamination was as a result of absorption onto the Millipore-HA filter support the cells were

cultured on. This support is integral to cell development to maturity however and even with extensive washing protocols the background levels were not sufficiently reduced. This problem combined with the fact that the background contamination was highly variable from one sample to another and could therefore not be readily accounted for, required the elimination of the filter altogether from the protocol in an effort to obtain cleaner data.

Cultured cells were therefore lifted by treating with 0.05%:0.02% trypsin:EDTA (as described in chapter 2) and collected in DMEM in a 20ml plastic centrifuge tube. The cells in suspension were treated in the same manner as outlined above, with the following variations. Only two groups of cells were used, experimental and control. The experimental group was stimulated with 2.5 μm forskolin for 30 minutes in the tube while the control group received no stimulation. After 30 minutes cells were washed by spinning down under mild centrifugation (1000 X *g*) to minimise damage and resuspended thrice with cold (4°C) DMEM. Cells were then resuspended in warm DMEM containing 3mg/ml column purified FITC-D as described above, and allowed to retrieve FITC. At set intervals a 20 μl sample of the cell suspension was withdrawn from the tubes, placed on ice in a 1 ml tube and a double volume of cold DMEM added to the cells to dilute the marker before washing the cells. This was done to ensure that if any marker was taken up while the cells cooled down and endocytosis halted it would add a negligible signal to the internalised pool. Cells were again washed three times by centrifugation. On the second resuspension cells were transferred to a fresh tube, in order to avoid further contamination of the signal by free FITC which may have adhered to the sides of the tube, and pelleted for the final wash with 1 mg/ml bovine serum albumin (BSA) to further reduce the risk of background contamination from the tubes. Samples were taken from the cell suspension at time points of 5, 10, 20 and 40 minutes after removal of forskolin and incubation with FITC.

Before proceeding with the Triton-X100 incubation to release the internalised FITC, a fraction of the suspended volume (1 μm) of cells was counted using a Coulter-counter in order to quantify the cell density in the sample. In this way inconsistencies in cell number removed from the cell suspension could be accounted for. After counting, Triton-X100 was added to the samples to solubilise the membranes (see above) and release the marker. A sample of the FITC-D solution was retained for the construction of a standard curve by serial dilution so that data expressed in the results is in the form nanolitres of marker per million cells.

5.3. RESULTS

5.3.1. Marker uptake

For absolute marker uptake the cells which, theoretically, should have the lowest marker levels are those kept on ice which had no prior forskolin stimulation. For this reason the control level of this group of cells (group one) was set as the baseline to which other marker levels were compared. The graphs of the various groups for both the HRP and FITC fluid-phase markers are presented in figure 5.1 as a percentage of this control. Due to the high background contamination, standard errors are relatively large, however the room temperature unstimulated and stimulated (group 3 & 4) groups differed significantly ($p<0.05$, t-statistic = 2.80) from control group 2 in the case of the HRP marker levels. While both did not differ from control group 1 at $p\leq0.05$ a trend did emerge in most cases where the levels of forskolin pre-stimulated experimental cells (group 4) tended to exhibit a higher internalised marker level than any of the control groups.

Samples measured for internalised FITC-D did not show significant differences at $p\leq0.05$. The p-values were significant however at $p\leq0.1$. Even though this is not generally accepted as statistically significant for biological data, it provided impetus for expanding the study in an attempt to resolve the uptake of marker in the A6 cells.

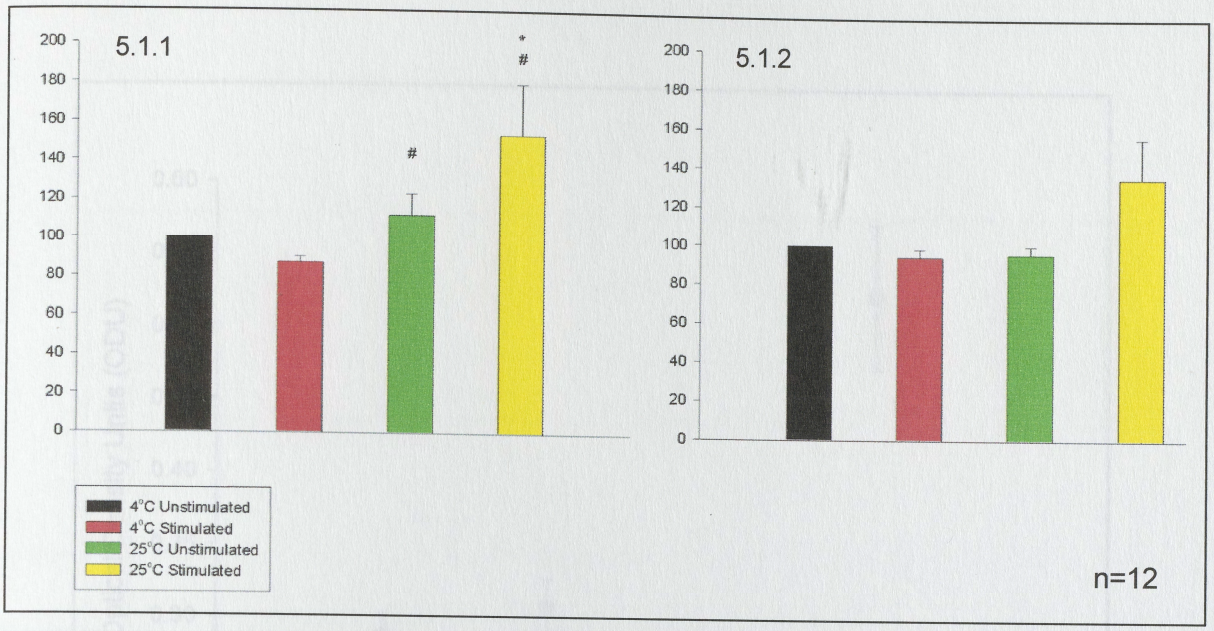

Fig.5.1. Levels of internalised fluid-phase marker in three control and one experimental group. Results are expressed as a percentage of the cold unstimulated control group 1 (black bar) + standard error of the mean (see Materials and Methods section for more detail). Levels of internalised HPR (fig.5.1.1) in experimental group 4 (yellow bar) were significantly different (* symbol at $p<0.05$) from control groups 2&3, but not group 1. The unstimulated control cells kept at room temperature (group 3, green bar) also had significantly greater levels of internalised HRP (# symbol $p<0.05$) than group 2 cells (red bar) kept on ice. Although there was a difference in the various groups of FITC-D internalised marker (fig.5.1.2) this was only significant at a p-value ≤ 0.1. The same trend was however evident when compared to the HRP data.

5.3.2. Time course of marker uptake

Another set of data were obtained for uptake of marker over time. This protocol too was hampered by the background contamination, but results from a successful experiment are presented in figure 5.2. Note that the samples at each time point are paired and thus points represent the average and standard error for the paired cultures. These data were obtained following removal of forskolin stimulation and measurement of intracellular levels of HRP by the protocol described above.

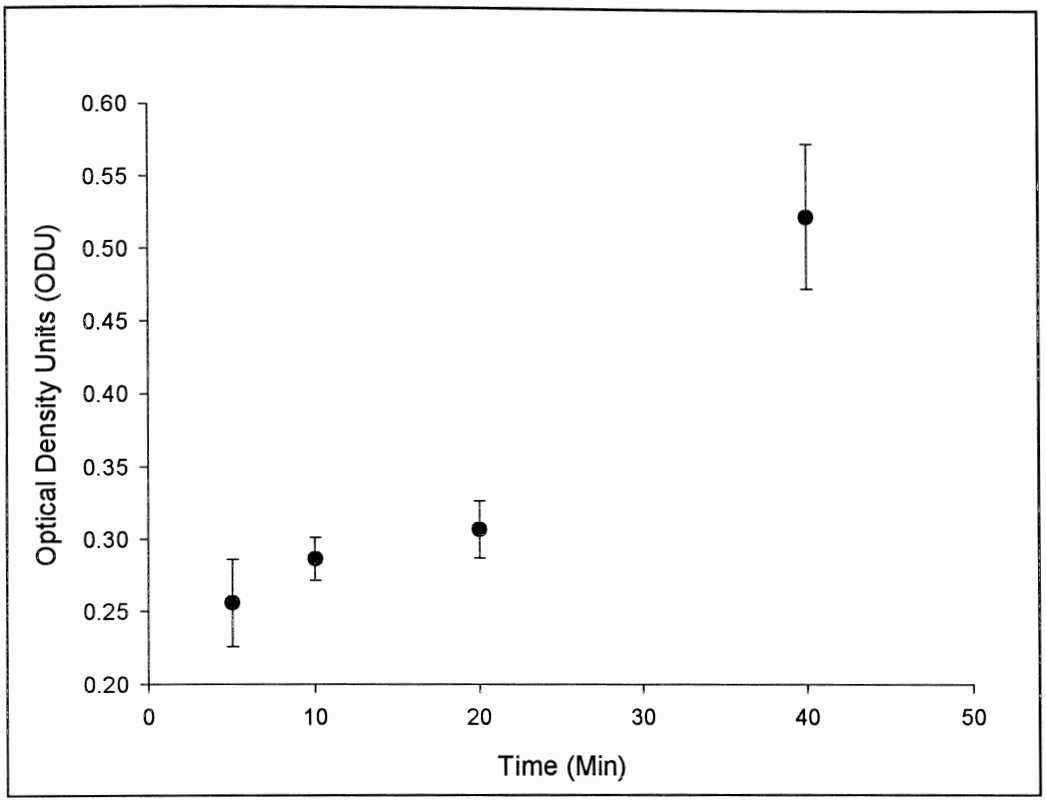

Fig.5.2. Levels of internalised HRP marker were tracked over time. Paired inserts were treated identically and harvested at 5, 10, 20 and 40 minutes following forskolin washout to record internalised HRP levels. The points plotted represent levels of HRP as arbitrary optical density units (as measured from the spectrophotometer and corrected as described) at set time points with the error bars (± S.E.) for the paired inserts.

5.3.3. Background contamination

The high background contamination prompted a search for a possible explanation into the reason for inconsistent labelling and a modification in the experimental protocol in an effort to reduce the non-specific marker levels. By examining the transcellular resistances it was clear that inserts kept on ice for extended periods exhibited a slow decrease in the transcellular resistance over time. Results for 4 inserts are presented in figure 5.3.

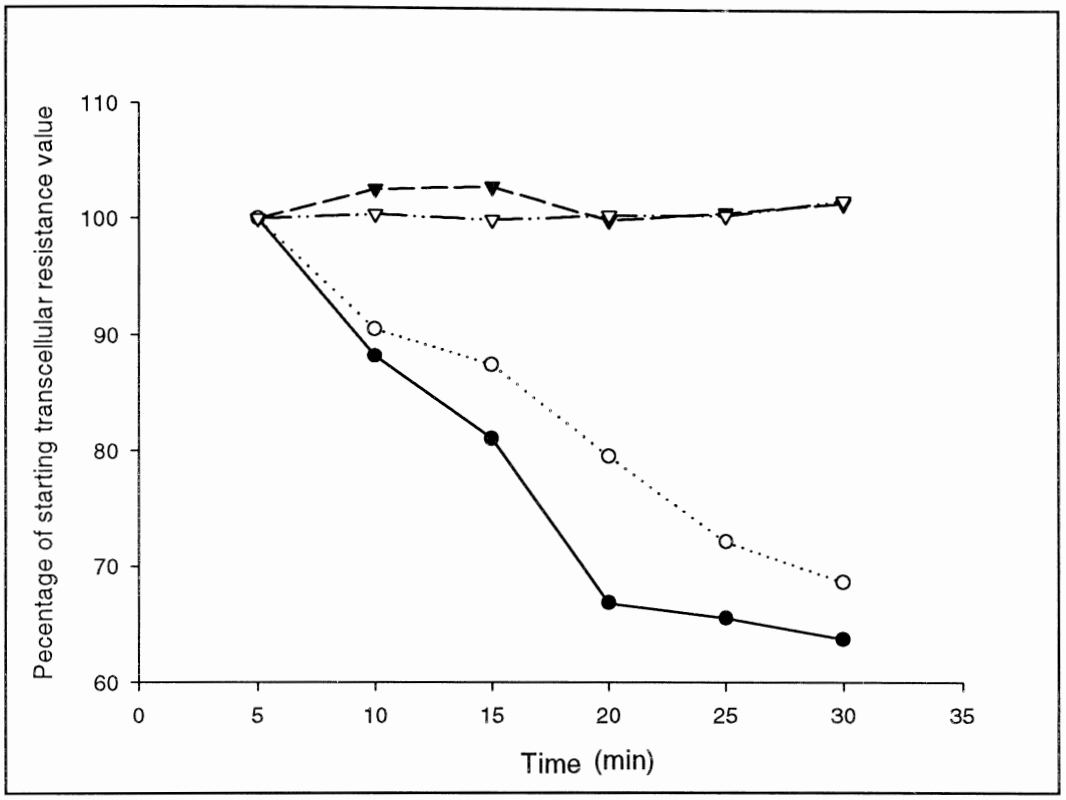

Fig.5.3. Transcellular resistance in four inserts were measured at 5 minute intervals for 30 minutes. Values are expressed as percentage of first recorded resistance reading (all inserts had initial resistances of between 1-2 kΩ). Resistance in the two control inserts (open and closed triangles) remained fairly constant over this period, while the inserts kept in cold DMEM (open and closed circles) can be seen to drop to below 70% of the starting value.

The decline in transcellular resistance indicated the possibility that the paracellular pathway between the cells was becoming more accessible and that the tight epithelial layer was becoming leaky. The markers were found to bind very strongly with the filter supports cells were cultured on and access to these filters may have accounted for the background contamination observed in all experiments.

With these problems and in order to eliminate as much background as possible, the cells were lifted from the culture substrate and experiments were performed on cells in a DMEM suspension. In this case it was possible to get a more accurate determination of the endocytic uptake of marker over time, but at the sacrifice of a polarised monolayer. The uptake curves for control and forskolin prestimulated cultures are illustrated in figure 5.4. Cells that received a forskolin stimulation before marker uptake proceeded had significantly higher uptake of maker at all time points ($p<0.01$, paired student's t-test) when compared to control data. Data from 5 experiments were pooled and averages and standard errors of the mean presented. Control uptake was fitted by a first order linear regression while experimental curve was fitted by a second order regression (Sigma Plot 2000, SSPS, Chicago, IL, USA).

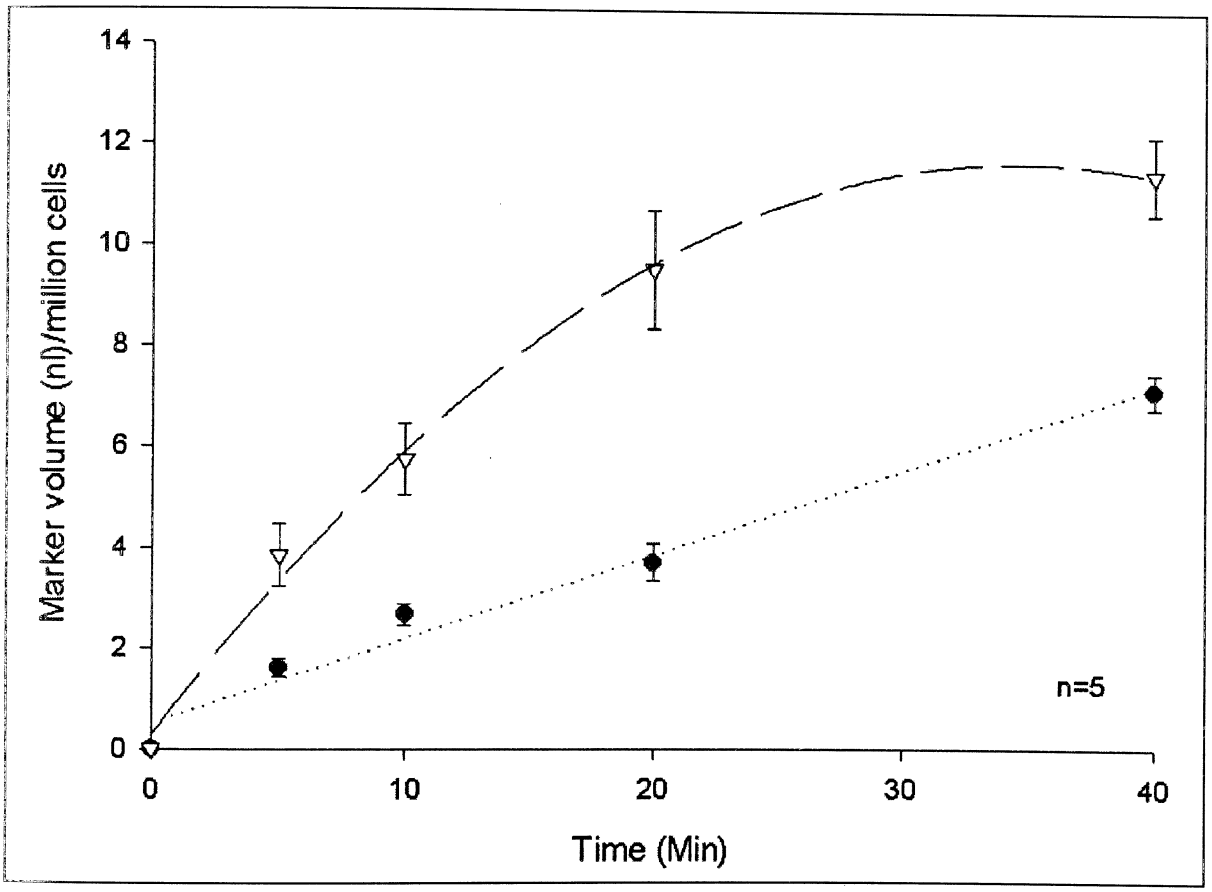

Fig.5.4. Uptake of fluid-phase marker in A6 cells in suspension over time. Values express uptake as marker volume (nl) per million cells. Samples were collected at 5, 10, 20 and 40 minutes. Levels of internalised marker in control cells (closed circles) can be seen to increase at a constant linear rate over time (dotted line is the best fit regression with $r^2=0.979$). Experimental cells (open triangles) which had been prestimulated with forskolin exhibited a more rapid marker retrieval rate and greater overall internalisation of marker than unstimulated controls. Dashed line represents best fit least squared regression ($r^2=0.995$) of the data (Sigma Plot 2000). Results are the average values with S.E. error bars as indicated.

5.4. DISCUSSION

Following the electrophysiological results it was important to obtain information about the mechanisms of ENaC regulation demonstrated to occur electrically under the influence of cAMP. As a first approach, the endocytic uptake of fluid-phase markers was investigated in an attempt to gain insight into the possible trafficking machinery at play within the A6 cells. Initial efforts were however hampered by the consistently high level of background fluid-phase marker contamination in the cell cultures. Such fluid-phase uptake protocols have been employed previously in both toad bladder (Coleman and Wade, 1994) and in A6 cells and are reported specifically for HRP in A6 cells in papers by Verrey and others (1993, 1995). In these studies HRP was reported to be successfully employed as an endocytic marker on A6 cells grown on filter supports. The authors experienced similar problems however and mentioned in the paper published in 1995 that data needed to be corrected for background values which were subtracted from the experimental values and could be as high as 45% of the experimental value. In the present study, the background level was never consistent from one filter to another and it was felt that subtracting the background value obtained from a control sample may not reflect the actual background found in the experimental culture.

5.4.1. Background marker contamination

Several approaches were attempted to reduce this background signal, but as it can be seen from figure 5.1, the levels remained high. Although significant differences between experimental and control groups were found in the HRP data (between groups 2, 3 and 4), this was not always the case for the FITC data. A trend of marker uptake in the forskolin treated cultures did emerge however, and this is better illustrated in figure 5.2 by tracking the HRP internalisation over time.

A possible explanation for the background contamination was that the markers may have become trapped within the filter support on which the cells were cultured. In order for this to become a problem, the markers needed access to the filters themselves. As the markers were added from the apical side of a confluent, tight monolayer, this did not initially appear likely. However when the transepithelial resistances (R_T) were measured in the cultures over time, they were seen to fall from to about 60% of initial starting values after 30 minutes. Similar, longer term effects have been reported by Hayslett, *et al.* (1995) when treating A6 cells to a cold loading protocol. The cells were shown to recover from the cold treatment, but to levels which were lower than baseline, even after they had been given time to recover in warm medium. This loss in resistance may go some way in explaining the occurrence of background contamination. However this was not the only source of background. The markers have a tendency to bind to certain plastics and for this reason, the addition of BSA in all incubating media and extensive washing protocols were designed. In addition, the FITC-D was column purified, and it was found by this process that there was a significant (>40%) level of unconjugated fluorescence in the solution made from powdered stock. In the end, these measures were not sufficient to resolve marker uptake on such a small scale and a different approach was adopted.

5.4.2. Cell suspensions

By removing the filter supports from the protocol the immediate advantage was the removal of much of the background contamination. This was however at the cost of a polarised monolayer. The importance of culturing the model A6 cells on filter supports as well as considerations about the type of filters used has been noted in chapter two. By lifting cells from the filter, the electrical monolayered configuration was lost and markers had access to both apical and basolateral domains. This would not be a problem if the cells had no endocytic activity from the basolateral domain, but this is not necessarily the case. The time course data

obtained is however much more quantitative as cells were counted and actual volumes of marker taken up by the cells could be calculated. When these results are compared to similar studies performed by Verrey *et al.*, it is apparent that the levels of uptake are much higher that those reported in both Verrey studies (1993, 1995). Under control conditions, the authors report an uptake of HRP labelled medium of about 0.01nl/minute/filter (of 4.7cm^2) for a 10 minute uptake. It can be approximated that there are 1x10^6 cells/cm^2 on a confluent filter so converting the values to cubic meters (for later comparisons) the data equate to approximately, 3.19x10^{-24}m^3/cell/minute. In similar results presented by Verrey *et al* in 1995, cells were stimulated with arginine vasotocin (AVT), the amphibian neurohypophyseal hormone and cAMP agonist. Here, once again converting the data to reflect uptake per cell, the stimulated cells internalised approximately 5.53x10^{-24}m^3/cell/min from the apical membrane.

From results presented here, under control conditions, the average uptake can be calculated from the slope of the fitted curve (figure 5.4). Here a value of approximately 1.78x10^{-22}m^3/cell/min is obtained, over 50 times higher than results reported by Verrey and others in 1995. What needs to be considered though, is that the data calculated from the earlier study reflect only apical HRP uptake. The authors make the point that basolateral internalisation in A6 cells in their results presented in 1993 reflect a 20-32 times faster endocytic rate. If the results from the present study are adjusted to account for this finding, assuming the higher rate, a marker uptake rate from the apical membrane of 5.56x10^{-24}m^3/cell/minute can be calculated. This value is in line with the previously reported results, but illustrates the complication in attempting to extract relevant information on possible ENaC trafficking mechanisms by using the cell suspension protocol.

This complication notwithstanding, there was a significantly higher level ($p<0.05$) and faster initial rate of endocytic retrieval of fluid-phase marker in cells which had been pre-stimulated with forskolin (see figure 5.4). The retrieval of marker after 40 minutes in the experimental

tissue was 1.6 fold higher than the control cells. Results from Verrey *et al* (1993) also find an increase in apical and basolateral endocytosis after AVT stimulation. Results from these initial investigations suggested that forskolin was definitely exerting an effect on endocytic rates, but due to experimental limitations, the exact nature of these effects could not be dissected.

A different approach was therefore required. It was of interest to continue to work on live cells rather than fixed or harvested samples in order to better compare data obtained with electrophysiological results. The fact that cells both on inserts or in suspension were destroyed in order to measure internalised marker meant that at no time could the entire endocytic process be continuously observed in one cell. Attention was therefore shifted back to cells cultured on filter supports, to ensure a physiologically relevant model was maintained, and with the aid of confocal microscopic techniques, to be discussed in the proceeding chapter, it was possible to further re-investigate the endocytic process in living A6 cells. In so doing, a clearer picture of the nature and time course of endocytosis could be obtained and these results could then be readily compared to the electrical data obtained. Chapter six outlines the exact nature of these experiments, but the results presented in this chapter provided impetus to continue to look at endocytic rates as results indicated that endocytosis was regulated by forskolin in some way.

CHAPTER 6

ENDOCYTOSIS VIEWED BY CONFOCAL MICROSCOPY

6.1. INTRODUCTION

Maker uptake studies indicated that the decrease in N_T following removal of a forskolin stimulus event may well be due to an increase in vesicular endocytic trafficking. According to the hypothesis under investigation, ENaC regulation mechanisms would involve the insertion (by exocytosis) and retrieval (by endocytosis) of channel containing vesicles. An alteration in the rate of turnover of sodium channels, either by increasing exocytic events or by decreasing endocytic retrieval or a combination of both could effect this change in channel number. The results presented in the previous chapter indicated that cAMP resulted in alteration in trafficking rates whether from the apical or basolateral membrane or both. Conceptually, if an increase in channel density were brought about by increased residence time of channels in the apical membrane during constant stimulation there would need to be a rapid retrieval event following removal of the stimulus.

In order to obtain more conclusive evidence for these events in real time, attention was shifted to microscopic techniques. Due to the inherent problems with marker uptake studies (large background contamination, variable loading into cells and the fact that cells were destroyed to obtain information) it was of interest to use the confocal microscope in order to work on living tissue in real time. By doing so the initial, inconclusive evidence for changes in endocytic trafficking events could be better characterised. Theoretically the use of the confocal microscope would allow three dimensional (3-D) images to be constructed of living cells with

the ability to image vesicles trafficked from the apical membrane. A further advantage of the confocal microscope was the ability to perform serial optical sections and thus ascertain the relative position of vesicle trafficking within the living cells.

6.1.1. Aims

By making use of specific fluorophores to label apical membranes of cultured A6 cells it was possible to image live cells in 3-D in real time with the use of confocal microscopy. The aim of these investigations were therefore to investigate the mechanisms of endocytic uptake following removal of a cAMP stimulatory event and track the movement of vesicles in live epithelia over time. Having obtained these data, it was also of interest to compare the rates of endocytosis with the electrophysiological data to get some idea of the possible involvement of ENaC in trafficking events.

6.2. MATERIALS AND METHODS

6.2.1. Cell culture

Cells were cultured on permeable filter supports as described previously (Chapter 2) until a confluent transporting monolayer was formed.

6.2.2. Membrane labelling

In order to visualise the intracellular movement of apical membrane vesicles, real-time confocal imaging of apical membranes in monolayers of A6 cells was performed. Apical cell membranes were stained with the fluorescent marker FM4-64 (N-(3-triethylammoniumpropyl)-4-(6-4 diethylamino)phenyl)hexatrienyl)pyridinium dibromide (Molecular Probes; Leiden, Netherlands). This very specific lipophyllic styryl dye has been widely used to visualise the movement of membranes in a number of experimental models (Betz *et al.*, 1996). The FM4-64 has a unique characteristic that it fluoresces weakly while in aqueous solutions and very strongly when lipid bound. To visualize the endocytic retrieval of apical membrane during a period of forskolin washout, cells on culture inserts were pre-stimulated with 2.5 μM forskolin in DMEM at room temperature for 35 minutes prior to membrane labelling. Following stimulation, monolayers of cells were chilled by washing in cold (4°C) DMEM to immediately inhibit membrane trafficking. Inserts were washed (two 5 minute washes) on ice in cold DMEM. Thereafter, the apical medium was replaced with cold medium (4°C) containing 16 nM of FM4-64 prepared in cold DMEM (4 μM stock solution in dH_2O) and kept on ice for 30 minutes to label the apical membrane.

6.2.3. Confocal chamber assembly

The cells were then washed (two washes of 5 minutes), punched out of the inserts and placed in DMEM in an inverted position on a glass coverslip (31 mm diam., 0.15 mm thick; Biophysical Technologies, Baltimore, MD, USA) in a specially designed chamber for viewing on the confocal microscope. A schematic diagram of the chamber assemblage is depicted in figure 6.1.

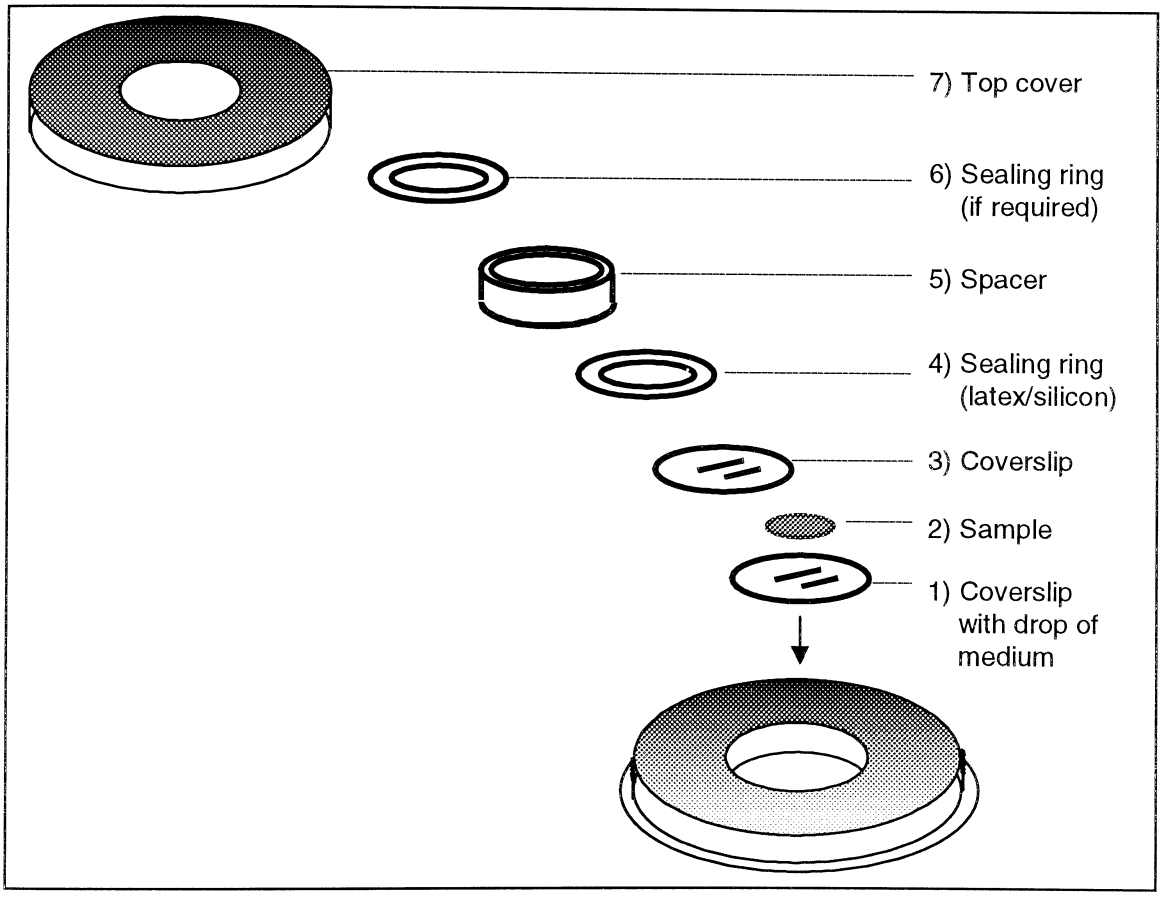

Fig. 6.1. Schematic illustration of the confocal chamber assemblage. The sealed configuration prevented medium leakage onto the microscope objective lens and the sample was placed in DMEM between two coverslips.

A thin layer of medium prevented the cells from being squashed against the coverslip. The chamber was sealed with a silicone O-ring to prevent leakage or membrane movement whilst

imaging. Control cells were similarly treated, except that they were kept in DMEM without any forskolin for 35 minutes before membrane labelling.

6.2.4. Confocal imaging

Confocal images were obtained using a Zeiss LSM 410 inverted single laser confocal imaging system equipped with a Zeiss (x63) Planachromat oil immersion objective (NA=1.4) and a (x100) Plan Nuofluar objective (NA=1.3) that were used for obtaining all images. The FM4-64 fluorophore was excited by illuminating the cells with a krypton-argon laser using the 568 nm excitation line which was close enough to the peak absorption wavelength of 559 nm for FM4-64. The scan times varied between 8-64 s, made up of 4-16s individual sweeps (with a line average of 2 to 4 times to provide the best image).

To minimize photobleaching, images were collected using 20% of maximum laser power, at an attenuation no higher than 10, while the pinhole size was kept at the smallest position possible. Photobleaching under these conditions was minimal for the initial scans which meant cells could be effectively imaged in the chamber for up to 2 hours. Typically only 60 minutes of imaging was ever performed. Cell cultures were screened so that tissues with minimal autofluorescence were used in all cases. As the cell heights on the filter varied (see figure 6.5), the convention was adopted to begin optical sectioning from the appearance of the top of the apical membrane of the tallest cells. From this point 1 μm thick optical sections were taken until the filter support was imaged.

6.2.5. Time course of vesicle uptake and depth analysis

For time course investigations, scans were done at 10 min intervals and the 3-D data were represented as overlaid xy images. In some cases it was necessary to exclude the first optical

section (most apical) as the fluorescence emanating from the coverslip produced too much non-specific fluorescent signal to observe the underlying sections. In order to get an idea of the localisation of internalised membranes, 3-D images were constructed from multiple Z-scans to obtain an artificially colour coded 3-D stack (using the Zeiss, LSM-410 confocal software) so that colour represented depth in the final image (see results).

6.2.6. Vesicle counts

In order to get a semi-quantitative measure of the appearance of the vesicles within the cells, internalised vesicles were manually counted after image acquisition and processing. The counts were obtained using Image Tool (version 2.0) developed at the University of Texas by Don Wilcox and colleagues in 1995 (University of Texas, Health Science Center, San Antonio, USA). Vesicles were counted in as many cells as possible in the field of view and averaged. In all cases there were never fewer than 10 cells counted and the maximum number of cells counted in one image was 125.

From all experiments performed two sets of data were extracted. The first were counts of intracellular vesicles from a number of separate experiments at a fixed time point. As a time-series of vesicle uptake was not always possible (due to timing inconsistencies or photobleaching) images from separate unpaired tissues were taken 55 minutes after forskolin washout (last time point in the time course protocol) and vesicles counted. This gave information for overall vesicle endocytosis in experimental and control tissues, but no indication of the rates of endocytosis. In a smaller pool of experiments the time course of appearance of vesicles in control and forskolin pre-stimulated cells was determined by counting vesicle numbers at 10 minute intervals following the endocytic retrieval phase.

6.2.7. ENaC labelling and imaging

In some experiments, presumptive Na^+ channels in apical membranes were labelled with fluorescent-tagged amiloride (BODIPY-FL amiloride; Molecular Probes; Leiden, Netherlands) at a concentration of 5 µl/ml in DMEM (from a 0.4 µM stock solution prepared in DMSO). The marker's optimal absorption wavelength is 504 nm and it emits at 511 nm. Since BODIPY-amiloride was co-localized with derivatives of membrane labelled with FM4-64, emitted fluorescent light of the two different wavelengths was captured on two separate channels. The excitation wavelengths available for multichannel imaging were 568nm for FM4-64 and 488nm for BODIPY-amiloride. Although this was not at the optimal absorption wavelength for either probe, there was sufficient emitted light for co-localisation imaging. The emitted fluorescent light was separated by passing through a band pass and long pass filter to differentiate between emitted light of each fluorophore. For FM4-64, emitted light was of a wavelength slightly above 733nm and was captured by using a long pass 590nm filter. BODIPY-amiloride emitted light maximally at 511 nm and was detected by passing light through a band pass filter (515-565 nm), which was the closest filter set to the emitted light of interest. There was no cross-talk between the two channels as filter cutoffs were sufficiently separated to minimise signal bleed-through. All colours were artificially assigned by the Zeiss software after capturing, with the convention chosen of FM4-64 label in red and BODIPY-amiloride in green.

Cross-sectional confocal images, 512 x 512 pixels in size, were captured and stored on magneto-optical disk and transferred to a PC for computer analysis. In order to construct 3-D images of the cells, serial optical sections were taken in the z-plane at 1 µm intervals. Data stacks of the optical sections were reconstructed using Zeiss LSM 410 software. Post-capture processing involved only the manipulation of contrast and brightness and gamma settings of the images in order to obtain the best image (by visual assessment) for printing. For higher

magnification, images were digitally magnified using the LSM software, but never more than 2.5 times the optical magnification obtained.

6.2.8. Autofluorescent imaging

To determine the extent of autofluorescence within the live A6 cells themselves, unlabelled cells cultured in the same manner as before were mounted in the chamber and subjected to the same intensity excitation wavelength from the 488nm and 568nm laser lines. Using the same filter settings as for the co-localisation studies (FM4-64 and BODIPY-amiloride), the signal generated by autofluorescent elements were assigned a red and green colour for these two lines respectively. Any detected fluorescence would be as the result of native proteins and bodies within the cells which fluoresce when excited. In addition to cultures on filters, cells cultured on coverslips were used to enable rapid screening of cell lines of different passage number. These investigations enabled cultures to be selected which had the least autofluorescent signal and were therefore best to image. In addition to the fluorescence signal, contrast microscopy was utilised for cells grown on coverslips in order to view the outlines of the cells to ascertain the relative position of the autofluorescent signal.

6.2.9. Differential Interference Contrast (DIC) microscopy

In order to localise autofluorescence within the cells, DIC, which makes use of polarised transmitted light to view unstained specimens, was employed. The DIC images of cells cultured on coverslips were superimposed with the red and green fluorescence signals to determine the location of the autofluorescent signals obtained. This type of imaging could not be performed with cells cultured on filters as the filter itself would be in the light path for transmitted light and thus make DIC imaging impossible. In filter grown cells, only the fluorescent signal was imaged.

6.3. RESULTS

The purpose of undertaking confocal imaging of live cells was to obtain real-time qualitative data of membrane trafficking. By imaging the internalisation of labelled apical membrane over time, some idea of the effects of forskolin pre-stimulation on endocytic uptake could be obtained. Before these investigations could be undertaken however, technical difficulties in dealing with live cells in confocal microscopy needed to be resolved.

6.3.1. Autofluorescence

One major pitfall in working with live cell fluorescence is the fact that autofluorescent particles can often contribute quite substantially to a false positive signal. In order to determine the extent of autofluorescence within the A6 cells, cultures were imaged without the presence of fluorophores. Cells cultured on coverslips for 5 days were imaged by fluorescence and DIC microscopy and are presented in figure 6.2. An extreme example of unwanted inclusions and autofluorescence is presented in figure 6.3.

In figure 6.3 a single cell has been imaged and only the signal generated in the "green" channel is presented. Note the large number of small inclusions near the apical surface which could easily be mistaken for labelled vesicles. As the cell was not labelled, there should have been little, or no autofluorescent signal. Screening cells to be used in experiments allowed batches of cells to be selected with minimal autofluorescent signals. The cells presented in figure 6.4 were found to have a small and at times undetectable autofluorescent signal. It was important to select cells best suited for live cell imaging and this meant that highly autofluorescent culture batches could not be used.

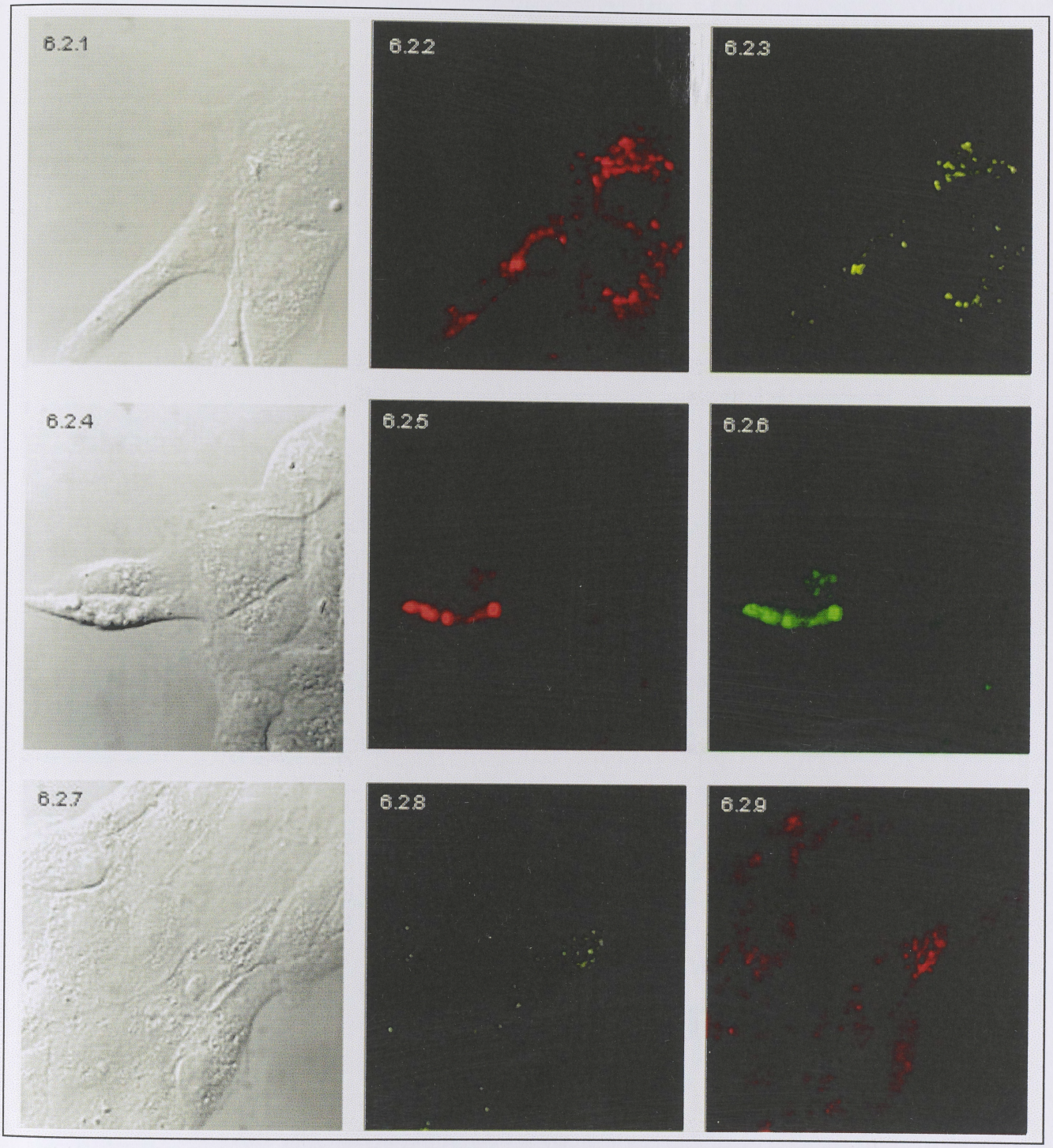

Fig.6.2. Autofluorescent signals detected in A6 cells grown on glass coverslips. Note the large inclusions in both the red and green channels that from the DIC images (6.2.1, 6.2.4, 6.2.7) can be seen to be located within the cells. Scalebar represents 10μm.

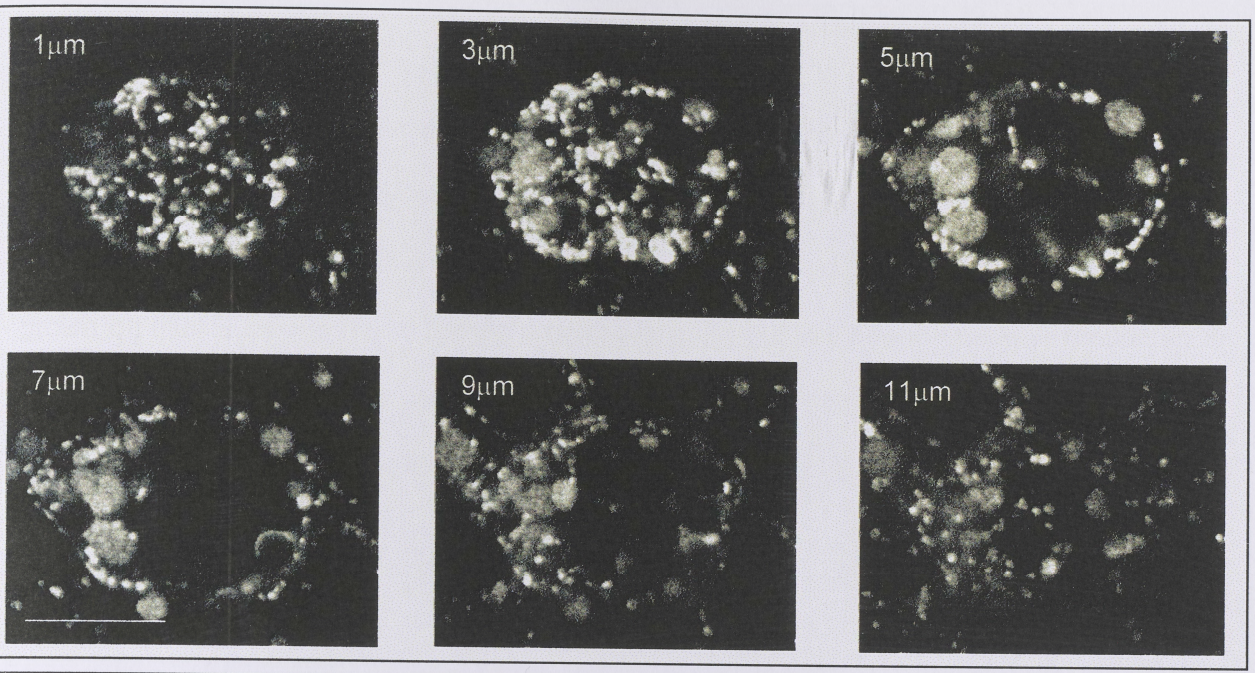

Fig.6.3. A series of optical sections taken from a single highly autofluorescent cell is illustrated. Depths of the section from the apical membrane are indicated. No artificial colouration has been added to the greyscale images. Scalebar represents 5μm.

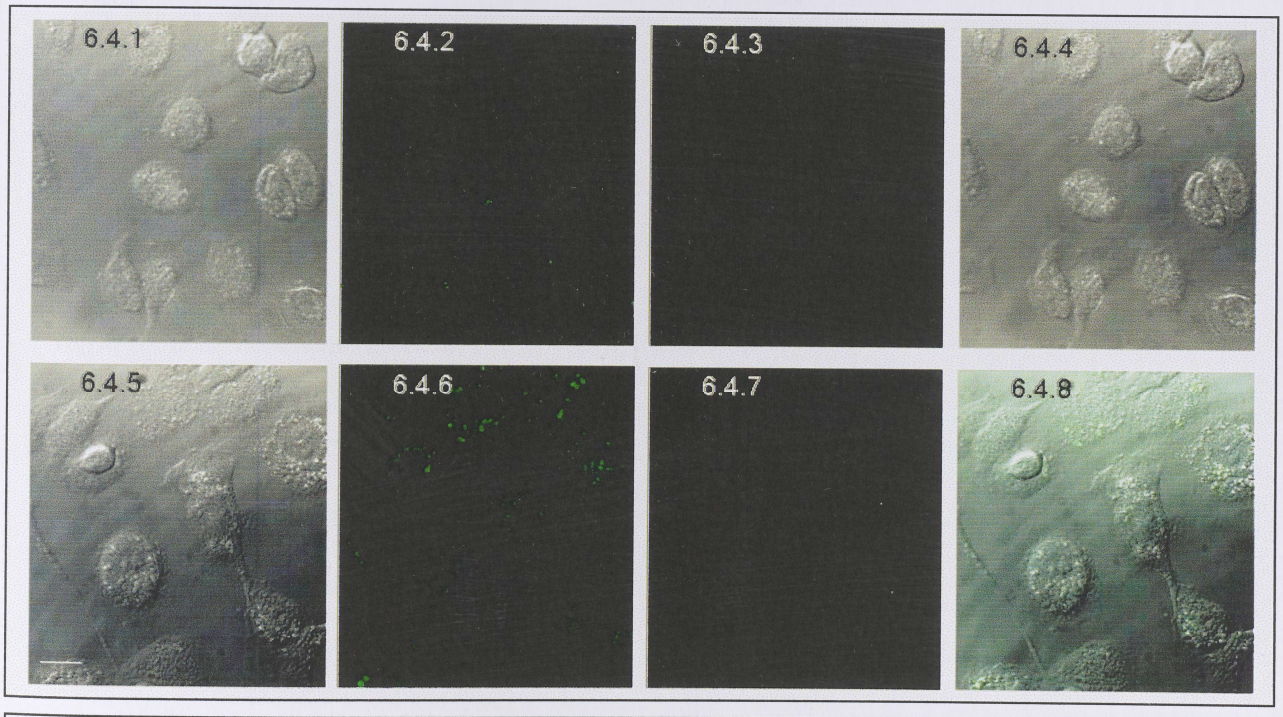

Fig.6.4. A6 cells cultured on glass coverslips for 5 days were imaged by fluorescence and DIC. Both green (6.4.2 & 6.4.6) and red (6.4.3 & 6.4.7) channels showed marked reduction in autofluorescent signals with an overlay of all 3 images presented in 6.4.3 & 6.4.8. The scalebar represents 5μm.

6.3.2. Cell heights

Autofluorescence was not the only consideration for live cell imaging, the variability in height of cells within the monolayer proved to be problematic. This non-uniform topology is represented schematically in a theoretical cross section taken through a monolayer of cells grown on filter supports (fig. 6.5). An extreme example of this phenomenon is presented in figure 6.6. The convention used in this study was to assign the starting point for optical sectioning (0 μm) as that focal plane where the appearance of the apical membrane of the tallest cell became visible.

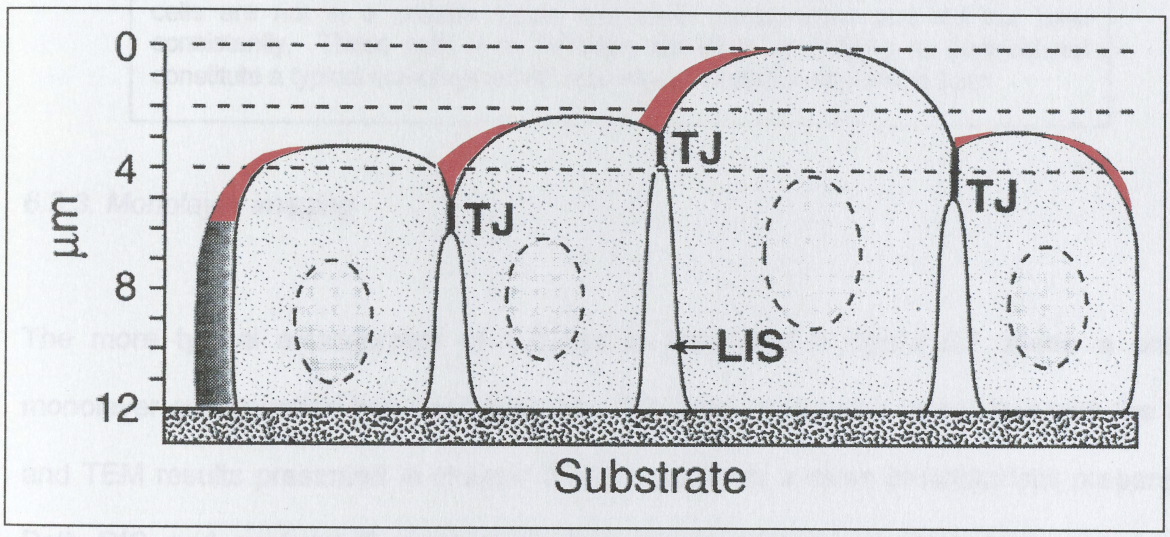

Fig.6.5. Schematic illustration of a 2-D cross section through an epithelial cell monolayer. Optical sectioning was started at the tallest cells and taken at 1 μm intervals. TJ = tight junctions and LIS = lateral intracellular space. (From Butterworth *et al*, 2001).

Although this convention was convenient for most of the samples, cultured cells did not always exhibit a uniform flat monolayer configuration. An example of this is presented in figure 6.6 where it can be seen that cells were piled up and a domed configuration is apparent. There are also several gaps in the monolayer. Notice too that the cells higher up stained better with the fluorophore (FM4-64).

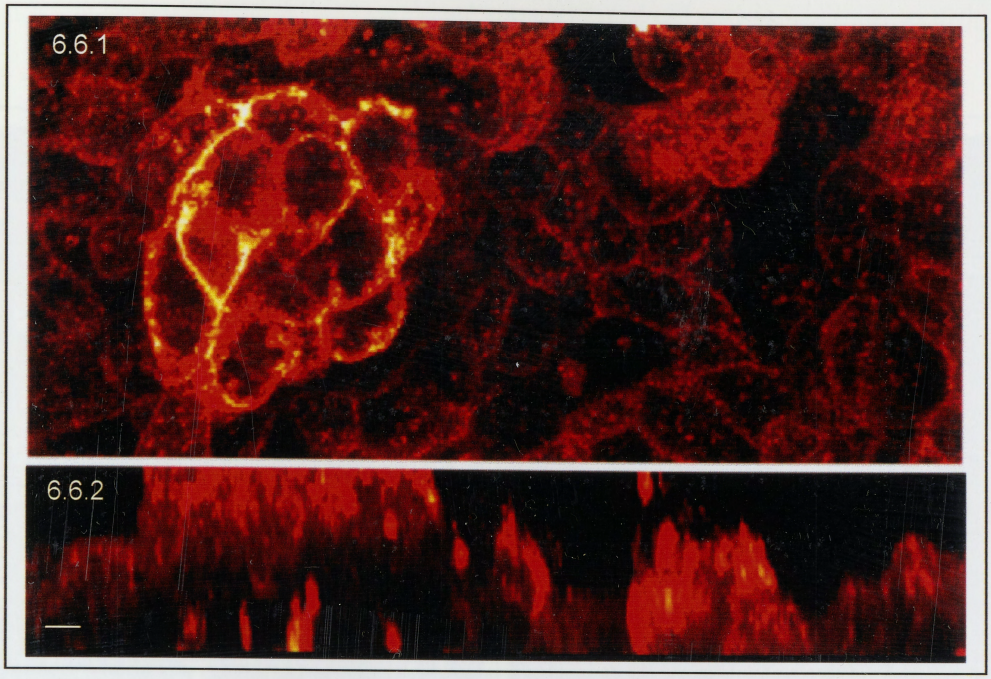

Fig.6.6. A 3-D reconstruction of A6 cells cultured on a permeable filter support. The image was constructed from 1μm serial optical sections. Figure 6.6.1 represents the x-y view (from above) while 6.6.2 the x-z view (from the side). The cells are not in a uniform single monolayer configuration and did not label consistently. These cells were therefore not ideal for imaging as they did not constitute a typical monolayered A6 epithelium. Scalebar represents 5μm

6.3.3. Monolayer imaging

The more typical arrangement of cultures is presented in figure 6.7 where a uniform monolayer configuration has been imaged. This type of image is consistent with the SEM and TEM results presented in chapter 3 and represents a more characteristic preparation. Both DIC and confocal fluorescent images are presented and characterise the type of cultures which were used in these investigations.

A similar image to figure. 6.6 of a more uniform, monolayered culture is displayed in figure 6.8. Note that cells are on the same level and uniformly labelled with FM4-64. There are no gaps in the culture and cells are not piling on top of each other as was the case in fig. 6.6. The labelling is easier to analyse in these cells as depth determination is more consistent (see depth analysis below).

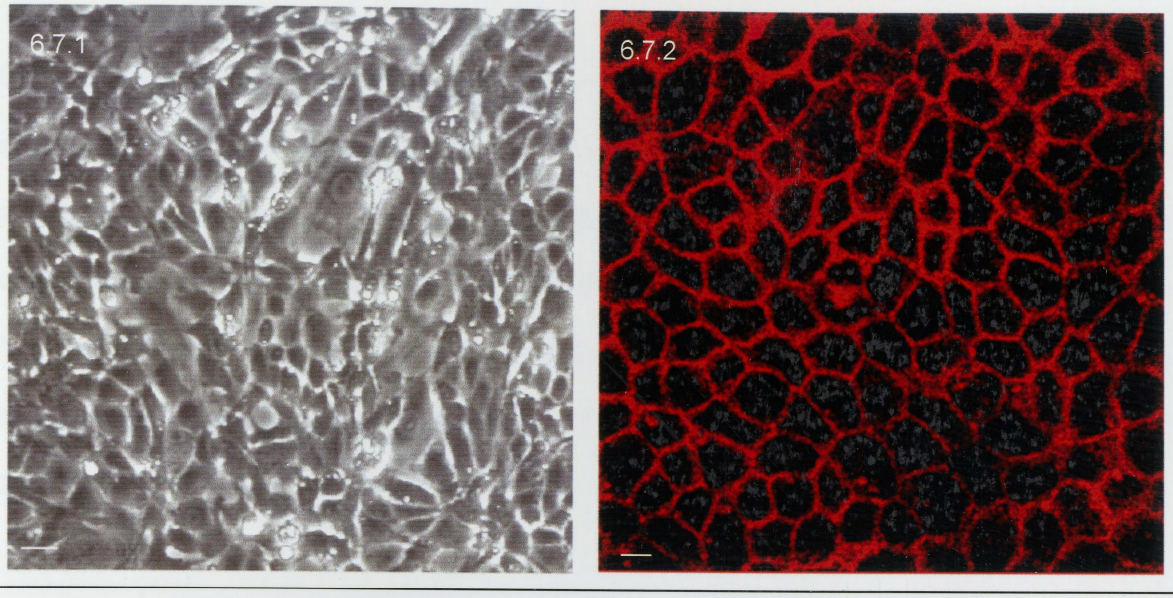

Fig.6.7. Typical monolayer arrangement of A6 cultures used in these investigations. Figure 6.7.1 is an image of unlabelled cells cultured on plastic culture flasks and imaged with DIC while 6.7.2 is an image of cells cultured on filters and imaged by confocal microscopy. The image generated in 6.7.2 is an optical section taken 5μm from the apical surface. Cells were labelled with FM4-64 as described above. The scalebar represents 10μm.

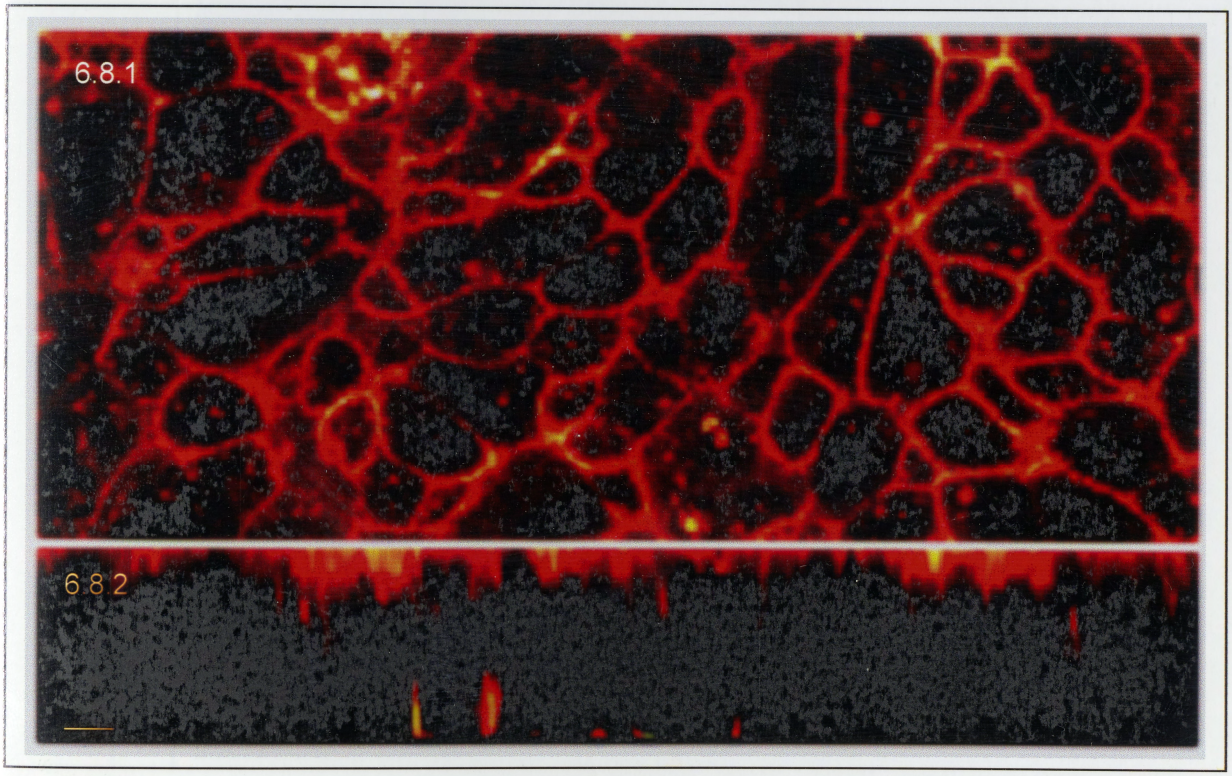

Fig.6.8. A 3-D reconstruction of A6 cells cultured on a permeable filter support. The 3-D image was constructed from 1μm serial optical sections. Figure 6.8.1 represents the x-y view (from above) while 6.8.2 the x-z view (from the side). The cells are in a single monolayer configuration and uniformly labelled and therefore ideal for image analysis. Scalebar represents 5μm

Once suitable and consistent imaging of monolayers was achieved, it was possible to track endocytic membrane retrieval following forskolin removal. The appearance of labelled membrane, in the form of vesicles was readily detected as bright punctate staining within the cells. An example of the internalised apical membrane in vesicular form is illustrated in figure 6.9 (this was also evident in figures 6.6 & 6.8). By using the particular confocal chamber setup described above it was possible to track the appearance of vesicles over time in live cells.

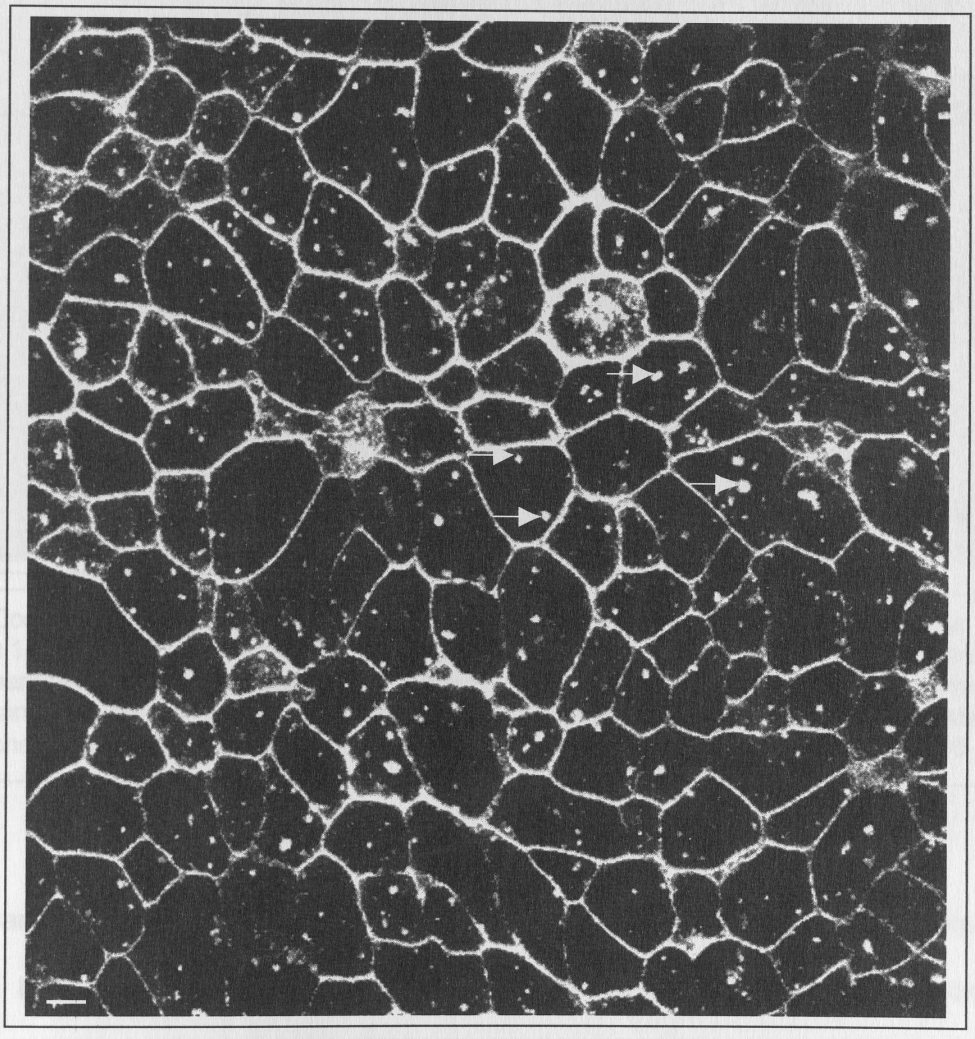

Fig.6.9. Optical section of an A6 monolayer taken 4μm beneath the apical surface. The greyscale image has not been artificially coloured so that the internalised labelled membrane in the form of vesicles (arrows) are more clearly visible. The internalised membrane signal is clearly visible in most cells in the form of vesicles (not all indicated). The scalebar represents 5 μm.

6.3.4. Effect of forskolin on endocytosis

A fixed-time comparison between the uptake of vesicles in control and forskolin pre-stimulated cells is presented in figure 6.10. The image was taken 4 μm beneath the apical membrane (single optical section) after 40 minutes of retrieval. It is clear that cells which had received a forskolin pre-stimulation contained far more internalised vesicles when compared to the unstimulated control.

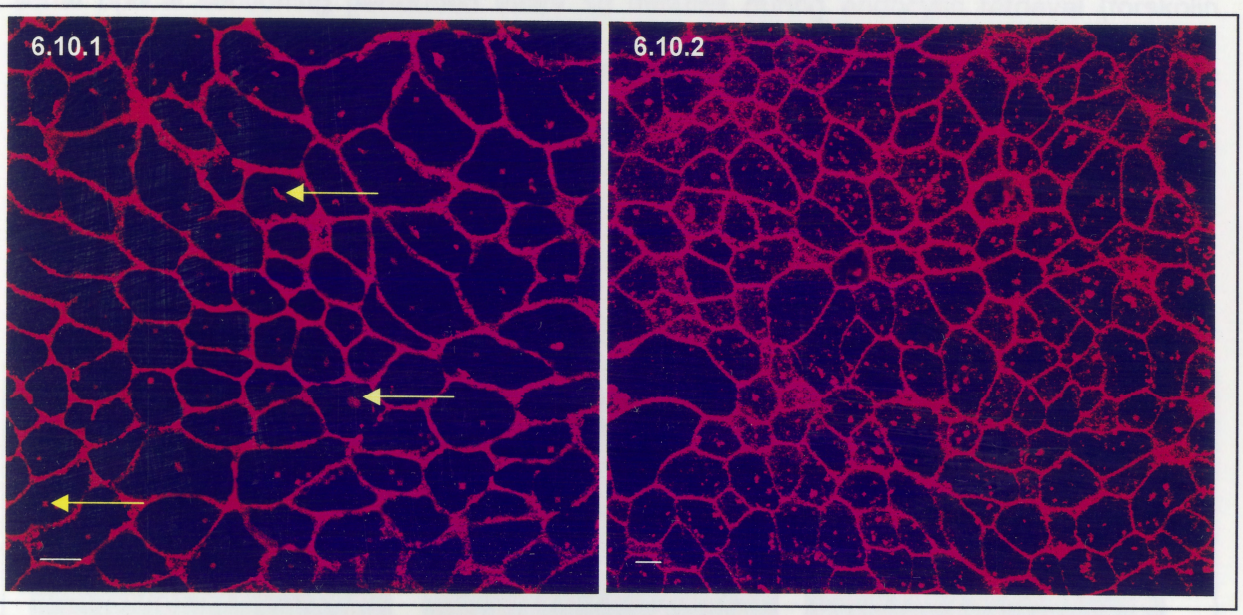

Fig.6.10. Comparison between vesicle uptake in prestimulated and unstimulated A6 epithelia. Control cells in 6.10.1 exhibit far fewer internalised vesicles (arrows) than the forskolin pre-stimulated cells in 6.10.2. Experimental cells were treated with forskolin for 30 minutes after which the stimulation was washed out and both control and experimental epithelia retrieved apical membrane for 40 minutes. The optical sections shown were taken 4 μm beneath the apical membrane and scalebars represent 5 μm.

In nine separate unpaired tissues the numbers of vesicles internalised after 55 minutes were counted in both control and forskolin pre-stimulated tissues. The average number of intracellular vesicles in the control (unstimulated) tissues was 6.05 ±0.669 (SEM) and in the forskolin pre-stimulated, 17.12 ±2.13 (SEM). A student's t-test confirmed that these data were statistically significantly different ($p<0.0002$, t-statistic = -4.95).

6.3.5. Time course of vesicle uptake

Due to the fact the imaging was done on live cells it was possible in many cases to observe the accumulation of vesicles over time. By taking serial optical sections and producing a 3-D image, the number of vesicles appearing within the cells was tracked over extended periods (up to one hour). This was done in both forskolin pre-stimulated (experimental) and unstimulated (control) cells. An example of results of uptake in a pre-stimulated tissue is laid out in figure 6.11. Here apical membranes of forskolin pre-treated cultures were labelled and serial optical sectioning performed every 10 minutes during endocytic retrieval (forskolin removed). It is clear that vesicles, internalised from the apical membrane, accumulate intracellularly over the 55 minute time course and cells are heavily filled with vesicles at the last time point.

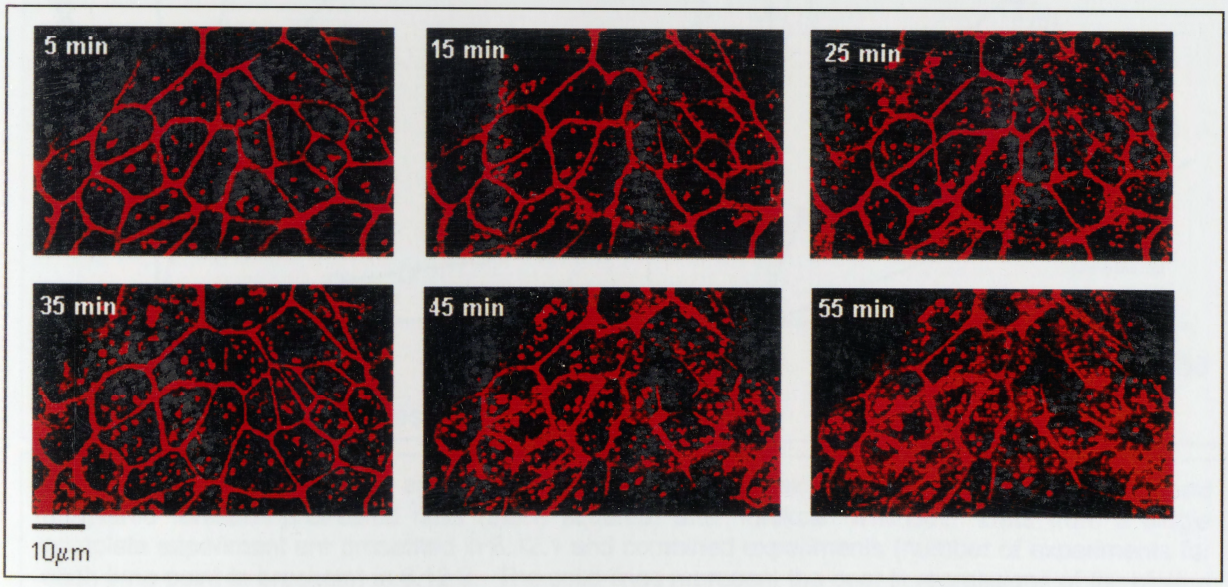

Fig.6.11. Serial optical were used to generate 3-D confocal micrographs. The xy images are composed of nine optical sections each of 1μm. The first 1μm optical section was excluded from the reconstructed images (to avoid coverslip fluorescence). The images illustrate the time-course of appearance of vesicles within the A6 cells after forskolin washout. Imaging commenced 5 minutes after removal of forskolin and images were acquired every 10 minutes.

6.3.6. Vesicle counts

The endocytosed vesicle counts were expressed as numbers of vesicles per cell over time (for sampled time points). Rates of endocytosis were estimated from the fitted plots of the time-course data and are plotted in figure 6.12. One single complete experiment and the combined data are presented on separate curves. It is clear from both the single and combined plots that the baseline rate of uptake in control cells increased dramatically when cells were pre-treated with forskolin.

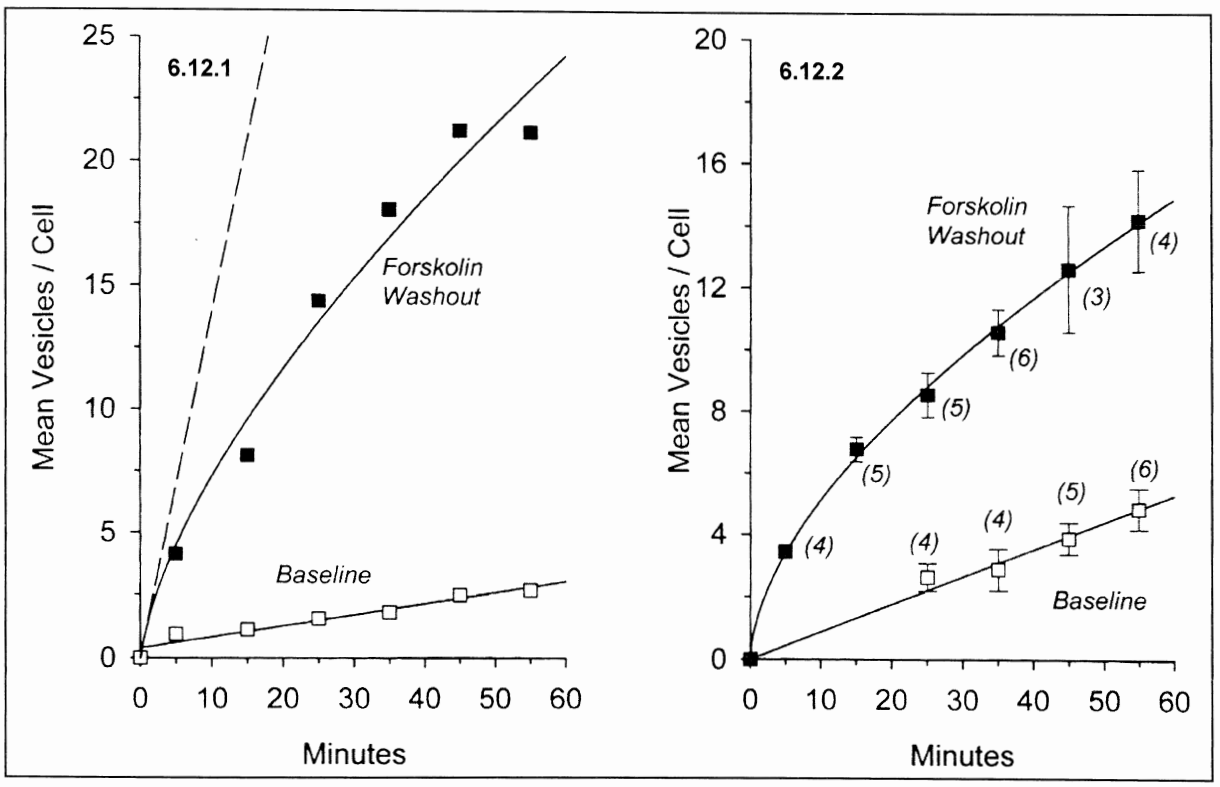

Fig. 6.12. Time course of appearance of endocytosed vesicles in control (white square) and nonpaired forskolin pretreated cells (black squares) after forskolin washout. Data from a single complete experiment are presented in 6.12.1 and combined experiments (number of experiments for each time point in brackets) in 6.12.2. The solid lines represent the best fit regressions of the plotted data. For both 6.12.1 & 6.12.2 the control data were fit linearly with r^2=0.97 (6.12.1) and r^2=0.96 (6.12.2). For forskolin pretreated tissues the solid lines are best fit to equation $y=a+bx^c$ (Table Curve, SPSS, Chicago, USA). For 6.12.1. this fit produced an r^2=0.97 and an r^2=0.99 in the case of 6.12.2. The dashed line in 6.12.1 represents an approximation of the endocytic rate in the experimental tissue before forskolin was removed. Note from the solid fitted curve (6.12.2) in forskolin pre-treated cells that the rate of endocytosis decreases with time and approached the baseline by 60 minutes.

The accumulation of vesicles under control, unstimulated conditions increased essentially linearly over the 55 minute time course and averaged 4.8 ±0.7 (S.E.) vesicles per cell at 55 minutes. This result is consistent with a constant low-rate, steady state turnover of vesicles at the apical membrane and represents a vesicle endocytic rate of 0.086 ±0.01 (S.E.) vesicles per cell per minute. The situation is quite different in the forskolin-pretreated tissues however. It is clear from the fitted curves in figures 6.12.1 and 6.12.2 that the rates of internalisation of membrane were far greater than control tissues. The initial sharp rise in retrieval rates can be seen to plateau off after 35 minutes approaching control values by 55 minutes. The combined data indicate that after 55 minutes however, the rate of retrieval was still elevated in the forskolin pre-treated cells.

In the case of the forskolin pre-treated tissues in the combined data (6.12.2) the endocytic rates in terms of vesicles per minute could be calculated for different time points as the first derivate of the fitted curve. These values at 1, 5 and 55 minutes were 0.77, 0.4 and 0.15 vesicles per cell per minute respectively. When these values are compared to baseline rates (0.086±0.01) it is clear that forskolin pre-treatment resulted in an initial 9-fold increase in vesicle endocytic rate which plateaued off and at 55 minutes was less than two-fold higher than the baseline rate.

6.3.7. Channel number decline and vesicle accumulation

Although no comment could be made at this point about the association of ENaC with the internalised vesicles, a study of the rates of channel number decline and vesicle internalisation was quite revealing. Data obtained from noise analysis (chapter 4) for total channel number (N_T) is plotted in figure 6.13.1 with only the forskolin washout portion of the data displayed. The points were fit by least-square regression to the exponential decline. Next, vesicle accumulation (as in 6.12) is plotted on the same curve in figure 6.13.2.

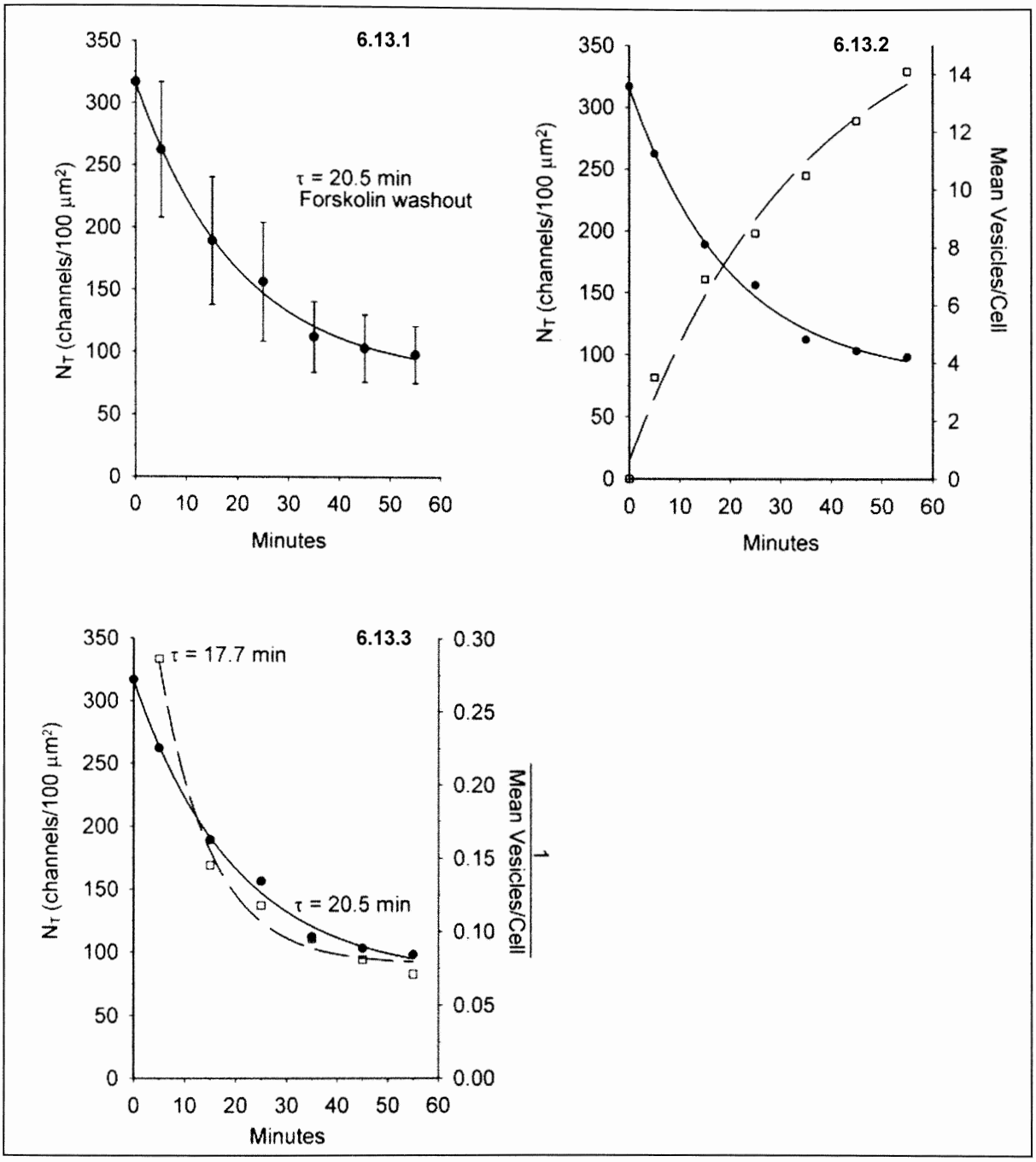

Fig. 6.13. Time course of the disappearance (electrically) of functional channel densities (N_T) from the apical membrane following forskolin washout is plotted in 6.13.1. The solid line is the least-square regression fit of an exponential time dependant decline of N_T with a time constant of 20.5 minutes. A combined plot of channel disappearance (solid line) and vesicle appearance (dashed line) is plotted in 6.13.2 where the standard error bars have been excluded for clarity (note separate axes). The time constant for appearance of vesicles was calculated from the fitted curve (Table Curve, SPSS, Chicago, USA) to be 17.7 minutes. To better compare the rates, vesicle uptake was plotted as reciprocal values in 6.13.3 and curves fitted as before (again on separate axes).

The exponential decline of N_T was found to have a time constant of 20.5 minutes. When inverse vesicle density is plotted over time in 6.13.3 (in order to better compare rates) the fitted data were found to exhibit a time constant of 17.7 minutes. These two rates parallel one another very closely with time constant of vesicle accumulation only slightly faster than N_T disappearance.

6.3.8. Depth analysis

One of the features of confocal microscopy is the ability to construct 3-D images from the optical sections and then to manipulate these images in virtual space. The Zeiss 410 LSM software provided the option to construct 3-D images and then to assign colours to represent the depth of the fluorescent signal. This "depth analysis" produces a visual representation of the relative position of the signal in 3-D space. Such images were constructed for control and forskolin pre-treated tissues and are presented in figure 6.14. In addition to the colour depth analysis, the 3-D stack can be rotated to present an x-z image rather than the overhead x-y orientation (see figures 6.6 and 6.8). By placing the cells "on their side" it is possible to look "through" a cross section of the entire epithelium to better gauge the location of vesicles beneath the membrane. The corresponding x-z plane for each coloured depth analysis is provided beneath the x-y plane in fig. 6.14.

From the various images presented several features can be noted. First, as presented above there is a greater vesicle density in the forskolin pre-treated tissues after the first 10 minutes of washout. From the depth analysis it is clear that the vesicles in both the control and forskolin treated tissues were initially located fairly close to the apical surface (within 5μm). However, after 60 minutes a number of differences could be observed between the tissues.

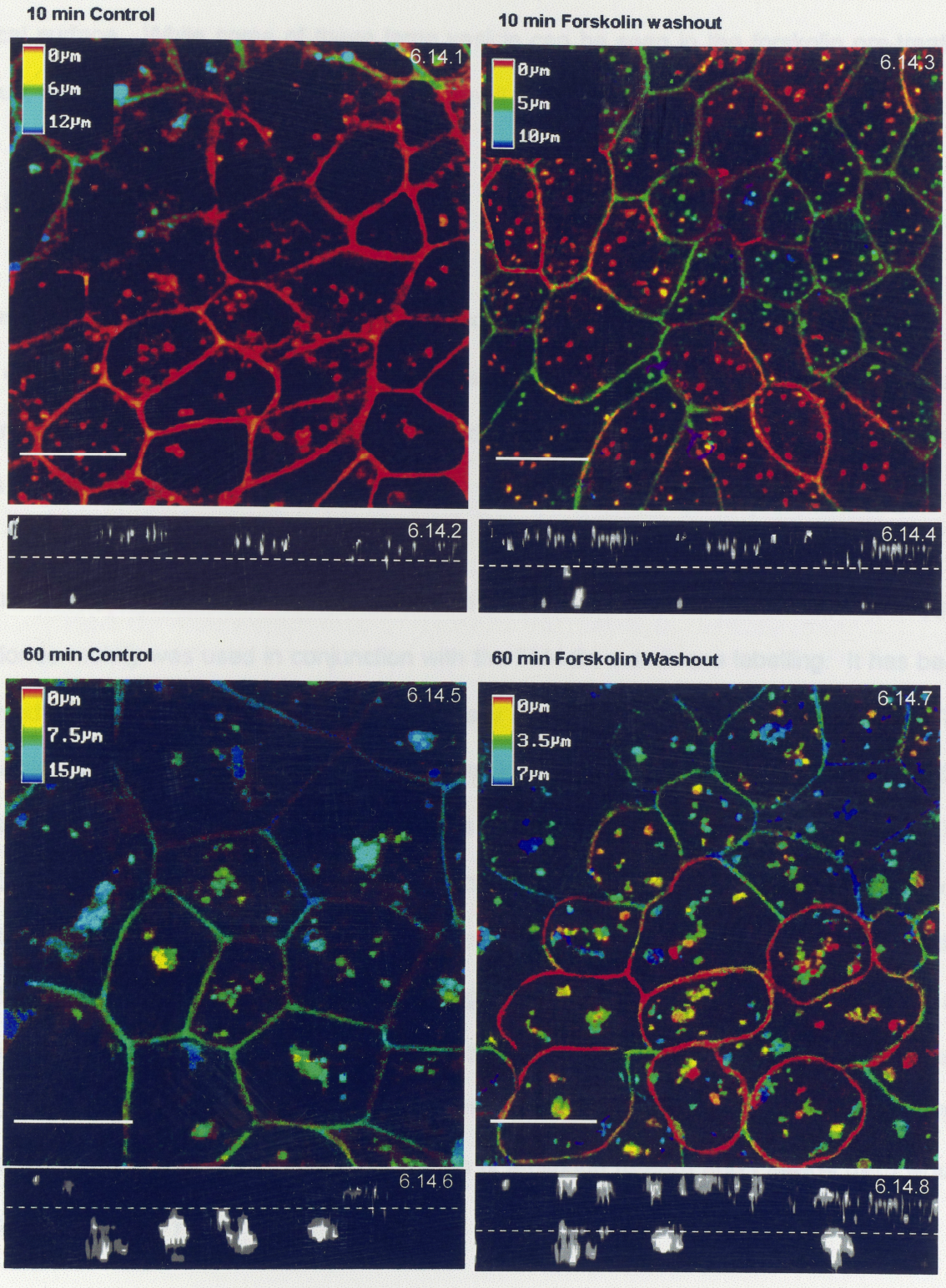

Fig.6.14. Depth analysis of 3-D stacks in control and forskolin pretreated cells at 10 and 60 minutes after forskolin washout are presented. Serial optical sections of the fluorescent FM4-64 signal were overlaid to produce a 3-D colour map. The colours in the x-y plane (6.14.1, 6.14.3, 6.14.5, 6.14.7) were artificially assigned according to the scale (top left) . Note that not all scales are identical. The corresponding x-z (6.14.2, 6.14.4, 6.14.6, 6.14.8) images are shown beneath the x-y planes. The dashed lines in the x-z images represent the 5th optical section (5 µm beneath the apical membrane). The scalebar represents 10 µm.

In the control cells large vesicles formed deep within the cells, located beneath 5 μm from the apical surface. While some of these large vesicle can be seen in the forskolin pre-treated tissue, there was still a significant number of small vesicles close to the apical membrane.

6.3.9. ENaC and vesicles

Thus far results have been presented for vesicular internalisation only with no reference to the channels or their involvement in this process. It would be attractive to speculate that the channels were associated with the internalised vesicles, but from the data presented there was no direct evidence for this.

In an attempt to label sodium channels in the apical membrane, a fluorescently-tagged amiloride moiety was used in conjunction with the FM4-64 membrane labelling. It has been pointed out previously that amiloride specifically inhibits epithelial sodium channels. The possible binding of a fluorescently-tagged amiloride could give some indication of the location of the channels when forskolin was washout out and vesicles retrieved. The BODIPY-amiloride produced by Molecular Probes was a suitable marker for imaging with FM4-64 as the fluorescent emission spectrum was sufficiently far removed from the membrane probe to attempt double imaging. Figure 6.15 presents the results of an experiment were both fluorophores were used. The image is from a forskolin pre-treated tissue, which was labelled with BODIPY-amiloride and FM4-64 and imaged 20 minutes after forskolin washout. Note that the colocalisation of amiloride (green) and FM4-64 (red) would produce an orange/yellow signal.

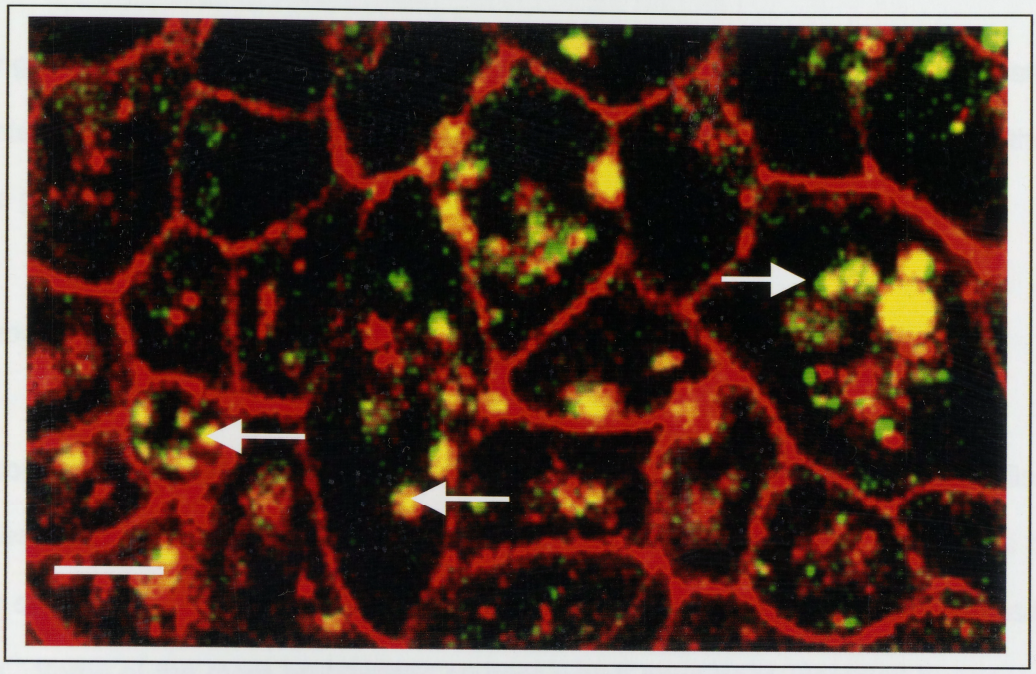

Fig.6.15. Colocalisation of apical membrane (red) with bodipy-amiloride (green) is evident in yellow areas (arrows). The optical section was taken 4 μm beneath the apical membrane, 20 min after forskolin removal. The scalebar represents 10μm.

6.4. DISCUSSION

Following from initial fluid-phase marker uptake attempts to find evidence for trafficking mechanisms in A6 cells, these investigations focused on confocal microscopic methods to view the processes occurring in living cells.

6.4.1 Troubleshooting

Some consideration had to be given to problems arising when working with live cells. The difficulties of autofluorescence were highlighted in figures 6.2 and 6.3. Viable cells have a number of potential intracellular fluorescent molecules which are derived from a variety of sources. Some of the more problematic sources which have been identified by researchers are listed in table 6.1 below.

Compound	Localisation/Source	Excitation Range (wavelength)	Emission Range (wavelength)
Amino Acid residues (aromatic rings)	Most proteins	200-340nm	360-370nm & 455nm
Reduced pyridine nucleotides	NADH, NADPH usually concentrated in the mitochondria (sometimes in the cytoplasm)	~360nm	~460nm
Flavins	Riboflavin, FAD bound to co-enzymes mostly in the mitochondria	445-470nm	~520nm
Lipofuscin	Pigment which accumulates with cell age	UV and 490nm	~450nm and >545nm

Table 6.1. Common autofluorescent sources in live cells. The compound type and common localisation are listed with a range of excitation and emission wavelengths. (Complied from Aubin, 1979; Benson *et al*., 1979; Yongkind *et al.*, 1982)

Lipofuscin autofluorescence is often the most problematic due to its broad excitation and emission spectra (Barden, 1978; Dowson, 1982, 1983) and was probably the major source of autofluorescence detected in these A6 cells. The spectra of lipofuscin overlaps that of the fluorophores used in this investigation and can there become particularly problematic when trying to distinguish fluorescence from specific labelling and non-specific autofluorescence (see fig. 6.3). Similar problems have been reported particularly in fluorescent imaging of the CNS of many animals (Correa *et al.*, 1980; Kalyuzhny and Wessendorf, 1998; Moore, 1981; Partanen *et al.*, 1980; Santer *et al.*, 1980).

The autofluorescent problem could be minimised however when cultures were screened and younger cultures (cells with fewer passages) with little or no autofluorescence were used (fig. 6.4). Once the autofluorescence issues had been resolved, the uniformity of the monolayers had to be addressed. Problems with uneven monolayers and non-uniform cultures (fig. 6.6) meant that not all cultures were suitable for data collection. The convention to use the appearance of signal from the tallest cells as the fist optical section (0 μm) was adopted to account for height variability of cells in many cultures In an ideal scenario, flat monolayers with uniformly arranged cells were used (as presented in figs. 6.7 and 6.8). The disadvantage was that not all preparations were suitable for analysis, resulting in a relatively low number of pooled experiments for vesicle uptake studies. This disadvantage was overcome to some extent by the large numbers of cells imaged on each filter. By counting up to 120 cells per image, a consistent pattern of vesicle endocytosis emerged.

Note too that in many cases the membrane label can be seen to be fairly deep within the cell layer (cell outlines are clear even beneath the apical membrane). This may reflect the domed nature of the cells (figure 6.5.) but may also be due to the labelling protocol which required cells to be kept on ice for 30 minutes. As demonstrated in Chapter 4, cold treatment had an adverse effect on transepithelial resistance, and it is possible that some of the FM4-

64 label may have had access to the lateral membrane. The possible "slide" of label down the side of cells was not very extensive however, as in no case were cell outlines ever seen to the level of the filter support.

6.4.2. Vesicle endocytosis

A common trend emerged when experimental cells, pre-treated with a forskolin, were compared to the untreated controls. Figure 6.10 illustrated the marked difference in accumulation of vesicles in experimental and control tissues following a 40 minute retrieval period. Manual counting of the imaged vesicles confirmed these observations. The time course of this appearance is presented in the next figure (fig.6.11) which illustrated that live cells could be effectively tracked over time. By comparing the rates of vesicle accumulation in control and forskolin pre-treated cultures it was readily apparent that the forskolin pre-stimulation drastically altered the rate of vesicle internalisation. Fitted curves of the vesicle retrieval rates (fig.6.12) indicated that at five minutes after forskolin withdrawal, there was an initial five-fold increase in vesicle uptake when compared to controls. When this rate was extrapolated to time zero the increase over control was even higher at about nine-fold over control/baseline rates. What these data indicated were that the forskolin stimulus resulted in alterations to the rate of apical membrane turnover.

At steady states the rate of exocytosis and endocytosis needs to be the same in order to maintain channel number. If the increase in channel numbers was brought about by trafficking mechanisms, strategies employed by the cell to increase plasma channel numbers could include the increase in exocytosis, with no concomitant change in steady state endocytosis, or a decrease in endocytosis with no change in exocytic rates or a combination of both. As endocytic rates after removal of forskolin were found to be elevated it is most unlikely that forskolin caused the rates of endocytosis to be inhibited. The elevated rate of

endocytosis due to forskolin stimulus withdrawal would therefore had to have been matched by an elevated exocytic rate in order to achieve increased channel number.

A more likely scenario would involve an increase rate of exocytosis which would be followed in time by increased endocytic rate in order to maintain steady-state stimulated values. In other words, a time lag in the increase in endocytosis following the stimulated increase in exocytic rates would result in an initial increase in channel densities at the apical membrane. Once the endocytic retrieval rate matched the elevated exocytic delivery, an new steady-state equilibrium, raised above baseline, would have been reached. When the exocytic impetus (forskolin stimulation) was removed, the rate of exocytosis (delivery of channels) would probably fall and, due to the fact that endocytic rates were still very high, channels would be retrieved from the membrane until such time as the endocytic rate again matched that of exocytosis to re-establish a steady-state and baseline values. The cAMP/PKA pathway would therefore most probably act at increasing exocytosis in addition to the increased endocytosis reported here.

Support for this idea can be found in another model kidney cell line, the Madin-Darby canine kidney (MDCK) cells. Pimplikar and Simons (1994) demonstrated that activation of PKA stimulated apical, but not basolateral transport in the MDCK cells. Hansen and Casanova (1994) illustrated an increase in both apical secretion and transcytosis in MDCK cells stimulated with cAMP. In addition, the vacuolar apical compartment (VAC) in these cells (Vega-Salas *et al.*, 1988) was exocytosed under the influence of cAMP (Brignoni *et al.*, 1995).

6.4.3. Membrane capacitance measurements

The assumption that exocytic rates are increased by forskolin has not been demonstrated by the data here, and is merely a theoretical speculation based on the rates of endocytosis. Evidence for increases in exocytic events has however been obtained by performing capacitance measurements in A6 cells. Conceptually, an increase in exocytosis would result in a net gain of plasma membrane at the apical surface. This gain in surface area can theoretically be quantified from impedance analysis by performing capacitance measurements. An increase in apical membrane capacitance may indicate an increase in membrane surface area (Erlij *et al.*, 1999). These measurements are not without complications and several assumptions need to be made when collecting data and analysing results (Păunescu and Helman, 2001a). However, bearing in mind that there are some limitations, results from several studies seem to indicate that apical membrane surface area does increase when A6 cells are stimulated by the forskolin/cAMP/PKA pathway (Atia *et al.*, 1999; Erlij *et al.*, 1999; Păunescu and Helman, 2001b; Zeiske *et al.*, 1998). Similar results were also found when cells were treated with other agonists such as insulin, prostaglandins and other factors (Erlij *et al.*, 1994; Jans *et al.*, 2000; Niisato *et al.*, 2000; Păunescu and Helman, 2001b).

From the current investigations it is not clear what the effects of forskolin on exocytic events are. Due to the fact that it was not possible to re-stimulate cells once inside the confocal chamber, it was also not feasible to attempt to label intracellular membranes to look for exocytic events. A flow-through chamber may well be a suitable tool to address the insertion events in live cell microscopy and there are a number of fluorophores available now to attempt to do such work.

6.4.4. Is ENaC involved?

No indication of ENaC involvement could be assumed from imaging labelled membrane. An attempt was made to co-localise ENaC with these internalised vesicles by using a fluorescently-tagged amiloride (fig. 6.15). The use of antibodies to label ENaC at the apical surface in order to observe changes in channel densities has been attempted by others with some success (Benos *et al.*, 1992; Kleyman *et al.*, 1994; Morris *et al.*, 1998). The results were however variable and one of the necessities of the labelling protocol usually involved the fixation of the cells to be labelled. It was therefore not possible to obtain data from living cells and difficult to get an idea of the time course of possible shuttling mechanisms as presented above. The tagged-amiloride results were however not entirely satisfactory due to the nature of the amiloride/sodium channel interaction. It has been pointed out that amiloride is a fairly specific channel blocker (with a binding concentration in the nanomolar range), and while amiloride is able to bind very well to the sodium channel the process is reversible and it is possible for the tagged amiloride to uncouple from the sodium channel. This would result in an unspecific signal being internalised and imaged. In addition, amiloride has been shown to bind to other transporters, even though less specifically, which could also lead to non-specific labelling (see Chapter 1).

The rates of functional ENaC disappearance and vesicle appearance are however very closely matched (see fig. 6.13). Assuming therefore, for the purposes of the current discussion that each of the endocytosed vesicles contained channels, and that on removal of forskolin stimulation the ENaCs in the apical membrane were retrieved intracellularly into these vesicles, then from the vesicle counts as a first approximation each vesicle would contain about 10 channels. From the electrophysiological data it was found that the number of functional channels per cell was quite low, consistent with a low number of endocytosed vesicle densities. The idea that many channels may be clustered into one vesicle are

compatible with patch clamp studies (Marunaka and Eaton, 1991) where clustering of ENaC in the apical cells membranes was observed. Therefore delivery of channels to the apical membrane may well occur by insertion of ENaC-containing vesicles producing clusters of channels at the cell surface.

6.4.5. Vesicle destinations

Figure 6.14 makes use of the ability to reconstruct 3-D images from the optical sections obtained with the confocal to ascertain where the vesicles become localised within the cells once they are endocytosed. It is clear once again that the forskolin pre-treated tissues internalise a higher number of vesicles. It can be readily demonstrated by observing the x-z images that at 10 minutes after washout, vesicles in both the control and experimental tissues are located near the apical membrane (within 5 μm). With time however, vesicles in the control tissues seem to migrate deeper into the cells (beneath 5 μm), coalescing to form larger structures with a few vesicles remaining close to the apical surface. The mechanism for vesicle processing has been extensively characterised in the MDCK epithelial cell line (reviewed by Mostov *et al.*, 2000) and suggests that vesicles either eventually pass through a degradative pathway, fusing with other vesicles and lysosomes in order for the vesicular contents to be destroyed or are recycled via the Golgi apparatus (Brignoni *et al.*, 1995; Orzech *et al.*, 1999).

In the forskolin pre-treated experimental tissues however, a different population of vesicles can be observed which remained fairly close to the surface of the cells. There are indeed some of the larger and deep vesicular bodies within these cells, but of interest, a large number of smaller vesicles do not proceed down this pathway. In terms of the recycling hypothesis it would be attractive to suggest that should these vesicles contain channels, they would be ideally suited for a second round of stimulation by exocytic insertion.

6.4.6. Two pools of channels

Studies on A6 cells and other model tissues, making use of brefeldin A (BFA) support the idea of different channel populations. The effect of BFA is to inhibit delivery of proteins produced in the golgi apparatus to their intended targets (Pelham, 1991). Treatment of cells with BFA basically destroys the golgi apparatus and halts delivery of transcribed proteins (Lippincott-Schwartz *et al.*, 2000; Wagner *et al.*, 1994). This makes it a particularly useful tool to dissect the downstream regulatory mechanisms of a variety of proteins. It should be noted that BFA treatment would effect all proteins indiscriminately regardless of the intended intracellular destination. In studies on A6 cells treated with BFA it was noted that destruction of the golgi apparatus had no effect on the response of the cells to either insulin or forskolin, both acute activators of sodium transport (Coupaye-Gerard *et al.*, 1994). It was suggested in this paper that as it had been recently demonstrated that insulin produced an increase in open probability (Marunaka *et al.*, 1992), and there were no observable alterations in responses of BFA-treated cells when compared to untreated controls, the action of forskolin may well follow the same mechanism, that is direct activation with no trafficking involvement. A similar study in toad bladder looked at BFA treatment and repeated rounds of forskolin stimulation (Weng and Wade, 1994). This study also noted little effect of BFA on responses to forskolin stimulation. In order to look a the effects of BFA treatment on single channel parameters, Fisher and colleagues (1996) once again made use of BFA-treated A6 cells and noise analysis to investigate effects of BFA treatment on single channel parameters. This work demonstrated that after three hours the number of open channels (N_O) in the apical membrane had declined to about 40% of starting values. The effects of forskolin treatment was however not investigated in this last study.

At first glance the forskolin-BFA studies seem to favour the hypothesis that forskolin may be activating membrane resident channels to increase sodium transport. However, when single

channel parameters were recorded it was observed that active channel number at the apical membrane declined with prolonged BFA treatment. The results from these studies can be explained in the light of the confocal investigations presented here. If channels are indeed contained in observed labelled vesicles then there appears to be two populations of vesicles and therefore two channel populations. The first population would probably comprise a constitutively delivered population of channels, derived from production and delivered via the Golgi body to the apical membrane. The density of channels resident at the apical membrane would therefore be kept constant by a constant turnover of apical membrane from production of surface proteins (ENaC-containing vesicles being inserted and removed at the same rate). Channels removed from the membrane would be processed deep within the cells, either destined for degradation or re-entry into the production pathway (i.e. routed through the Golgi apparatus). The appearance of the deep large membrane structures in the control tissues would support this idea. When A6 cells were treated for an extended period with BFA there was a steady decline in recorded I_{SC} (Coupaye-Gerard *et al.*, 1994) which could be attributed to a decline in active channel numbers at the apical membrane (Fisher *et al.*, 1996). This rundown would be expected if constitutive endocytosis was not matched by continual delivery from production.

The acute response by forskolin stimulation need not necessarily implicate resident channel activation. If a pool of channels was stored beneath the apical membrane, it may not be affected by the BFA treatment (which affects mainly the Golgi apparatus) and the vesicles may well be available for exocytosis. In fact, it is highly plausible that the apical vesicles observed in the depth analysis presented above is such a pool. Increases in apical channel densities due to raised cAMP levels would therefore be derived from exocytosis of these channel-containing vesicles. On removal of stimulation the channels may well re-enter this pool, available for another round of stimulation. Not all the channels would be able to re-enter the cytoplasmic pool though, as some may be destined for degradation or may not be

efficiently recycled. As the size of the recycling pool is probably fixed, and if this pool could not be augmented by production of new channels and delivery from the Golgi body (as would be the case in BFA treated cells), repeated rounds of stimulation would produce ever diminishing responses. This was indeed observed in the studies on toad bladder by Weng and Wade (1994) where subsequent rounds of forskolin stimulation resulted in smaller and smaller I_{SC} responses until the BFA was removed and delivery of newly synthesised channels restored.

In light of the results presented here, the BFA studies can therefore be argued to support the hypothesis of trafficking as a mechanism for ENaC regulation. The fact that ENaC was not conclusively associated with the vesicular movements remained problematic. In order for the hypothesis to be confirmed, it needed to be shown conclusively that ENaC was indeed involved in the membrane trafficking demonstrated here. It was also of importance to attempt to obtain this information in live cells so that results presented to date from a variety of techniques could be compared. In this regard, a green fluorescent protein (GFP) construct was produced so that channel subunits were labelled directly with GFP and tracked in live cells. This final approach is presented in the next chapter which describes the production of GFP-ENaC cell lines and the use of confocal microscopy to follow ENaC within the cells.

CHAPTER 7

GFP-ENaC

7.1. INTRODUCTION

The data presented in the previous chapter alluded to the possibility of sodium channels being regulated by vesicular trafficking. The trafficking mechanism is certainly in place within the A6 epithelia and is under the regulation of the cAMP secondary messenger cascade. Results presented indicate an alteration in rates of membrane turnover which corresponds to the time course of removal of channels recorded electrically. These data support the idea of channel trafficking, and in an attempt to show channels were involved in this regulated recycling, a tagged sodium channel blocker was used to label channels. The colocalisation of the tagged blocker and internalised membrane was demonstrated. The tag was however not satisfactory for a number of reasons and another more suitable method of channel labelling was required. An ideal candidate for tagging proteins for use in live cell imaging is the green fluorescent protein (GFP) derived from the bioluminescent jellyfish *Aequorea victoria*.

7.1.1. GFP

The unique characteristic of bioluminescent jellyfish is the production of light when energy is transferred from a Ca^{2+}-activated photoprotein, aequorin to the green fluorescent protein (Morin and Hastings, 1971; Shimomura *et al.*, 1962; Ward *et al.*,1980). By cloning and expressing the GFP in non-native cells it is possible to use the fluorescence produced by the protein as a unique reporting system. Expressed in either eukaryotic or prokaryotic cells and illuminated by blue or UV light, GFP yields a bright green fluorescence. Light-stimulated GFP fluorescence is species-independent and does not require any cofactors, substrates, or

additional gene products from *A. victoria*. Additionally, detection of GFP and its variants can be performed in living cells and tissues as well as fixed samples. These unique characteristics made GFP an ideal candidate to use in this study. It was of particular interest to continue working with living cells to get a direct indication whether trafficking of ENaC was responsible for the regulation of sodium channel densities.

By using GFP it was theoretically possible to label the various channel subunits by constructing a fusion protein consisting of the fluorescent moiety in GFP and the channel protein subunit itself. Insertion of this plasmid into the A6 cells and selection of cells which expressed the GFP-ENaC fusion protein could produce a stable clonal cell line expressing fluorescent channel subunits. Once such a stable cell line was produced, these cells could then be treated in the same way as the A6 epithelia before and the GFP signal used as a marker to track the movement of channels within the live cells in response to changes in cAMP levels. In order to understand the limitations of GFP in live cell imaging however, some attention should be paid to the characteristics of GFP itself.

7.1.2. GFP Properties and Structure

The GFP chromophore consists of a cyclic tripeptide derived from Ser-Tyr-Gly in the primary protein sequence (Cody *et al.*, 1993). GFP is only fluorescent when embedded within the complete GFP protein with amino acids 7–229 (out of 238) required for fluorescence (Li *et al.*, 1997). Nascent GFP is not fluorescent, since chromophore formation occurs post-translationally. The chromophore is formed by a cyclisation reaction and an oxidation step that requires molecular oxygen (Heim *et al.*, 1994). The wild type GFP (wt GFP from the jellyfish) absorbs UV and blue light with a maximum peak of absorbance at 395 nm and a minor peak at 470 nm and emits green light maximally at 509 nm, with a shoulder at 540 nm (Ward *et al.*, 1980). In this study a variation on the wt GFP, called enhanced GFP (EGFP)

produced by Clontech Laboratories Inc. (Palo Alto, CA, USA) was used. In expression studies using wt GFP it was found that much of the GFP produced was found in insoluble, non-fluorescent inclusion bodies. EGFP on the other hand is expressed as a soluble, fluorescent protein (Clontech Handbook, Living Colors User Manual, 2000). As mentioned in chapter 6, photobleaching is a major concern in fluorescence microscopy. GFP has been shown to be more stable than the commonly used fluorescein to photobleaching (Niswender *et al.*, 1995; Wang & Hazelrigg, 1994). In addition the EGFP variant is stable over a wide pH range (pH 7-11.5) and in the presence of a number of chemicals (SDS, mild gluteraldehyde or formaldehyde fixation) over extended periods of time (greater than 24 hours). The A6 cells, cultured at 27°C was also not a problem for GFP expression. *E. coli* expressing GFP showed stronger fluorescence when grown at 24°C or 30°C compared to 37°C (Heim *et al.*,1994). Mammalian cells expressing GFP have also been seen to exhibit stronger fluorescence when grown at 30–33°C compared to 37°C (Ogawa *et al.*, 1995; Pines, 1995).

7.1.3. GFP as a Reporter Molecule

Probably the most useful feature of GFP is the ability to produce protein chimeras, by molecular methods, to fluorescently tag the protein of interest. Many of the GFP studies have made use of expression systems like *Xenopus sp.* oocytes or cells which readily express transfected proteins, like HeLa cells. Transient expression systems have also been used to greatly increase the number of proteins of interest and to study the produced proteins within a small window of transient expression within these systems. In this study however, it was decided that expression of a GFP-ENaC chimera in the A6 cells would be of greater value than expression in a non-epithelial system as so much data had already been obtained on sodium channel regulation in the A6 cell line. In addition, a stable cell line, constitutively expressing EGFP-ENaC would produce far fewer copies of the chimeric protein than a transient

expression system thereby reducing the chance that the regulatory mechanisms within the cells would become swamped and thus making study more physiologically relevant. In collaboration with Dr's Blazer-Yost and Rhodes at Indiana University, University of Purdue in Indianapolis, IN, USA, (IUPUI), EGFP-ENaC-subunit expressing clonal A6 cell lines were produced (as described in materials and methods) in order to study the regulation of fluorescently-tagged channels in live cells.

7.1.4. GFP Detection

The excitation and emission spectra for EGFP are depicted in figure 7.1. The ability to detect a GFP signal using the confocal microscope depends on a number of factors. The brightness of all fluorophores can be calculated and is approximately equal to the product of the extinction coefficient (E_m) and quantum efficiency (ϕ) of the molecule. The extinction coefficient of a fluorochrome is the amount of light that it absorbs at a particular wavelength. The molar extinction coefficient is defined as the optical density of a 1 M solution of the fluorochrome measured through a 1 cm light path. Enhanced GFP contains a double-amino-acid substitution Phe-64 to Leu and Ser-65 to Thr (Cormack *et al.*, 1996). Based on spectral analysis, EGFP fluoresces 35-fold more intensely than wt GFP when excited at 488 nm (Cormack *et al.*, 1996; Yang *et al.*, 1996), due to an increase in its extinction coefficient and a higher efficiency of chromophore formation. The E_m for EGFP is 55,000 $cm^{-1}M^{-1}$ at 489nm excitation, compared with 9,500 $cm^{-1}M^{-1}$ for wt GFP. The quantum efficiency is close to 60% (or 0.6) for EGFP, with excitation peak at 489nm and emission peak at 508nm (Cormack *et al.*, 1996; Yang *et al.*, 1996). In addition to the physical characteristics of GFP, the minimum detectable fluorescence depends on the amount of available fluorophore in the scanned field (i.e. the concentration of the fluorophore), the thickness of the specimen and the efficiency of detectors in the system. It is difficult to predict if a system is able to detect the available signal and most often this is tested empirically on the confocal system to be used even if it could

theoretically be calculated. A different confocal system was used in these studies (see material and methods) that possessed several advantages over the previously described Zeiss 410 system used for the membrane uptake studies to better image the EGFP-ENaC expressed within the A6 cells.

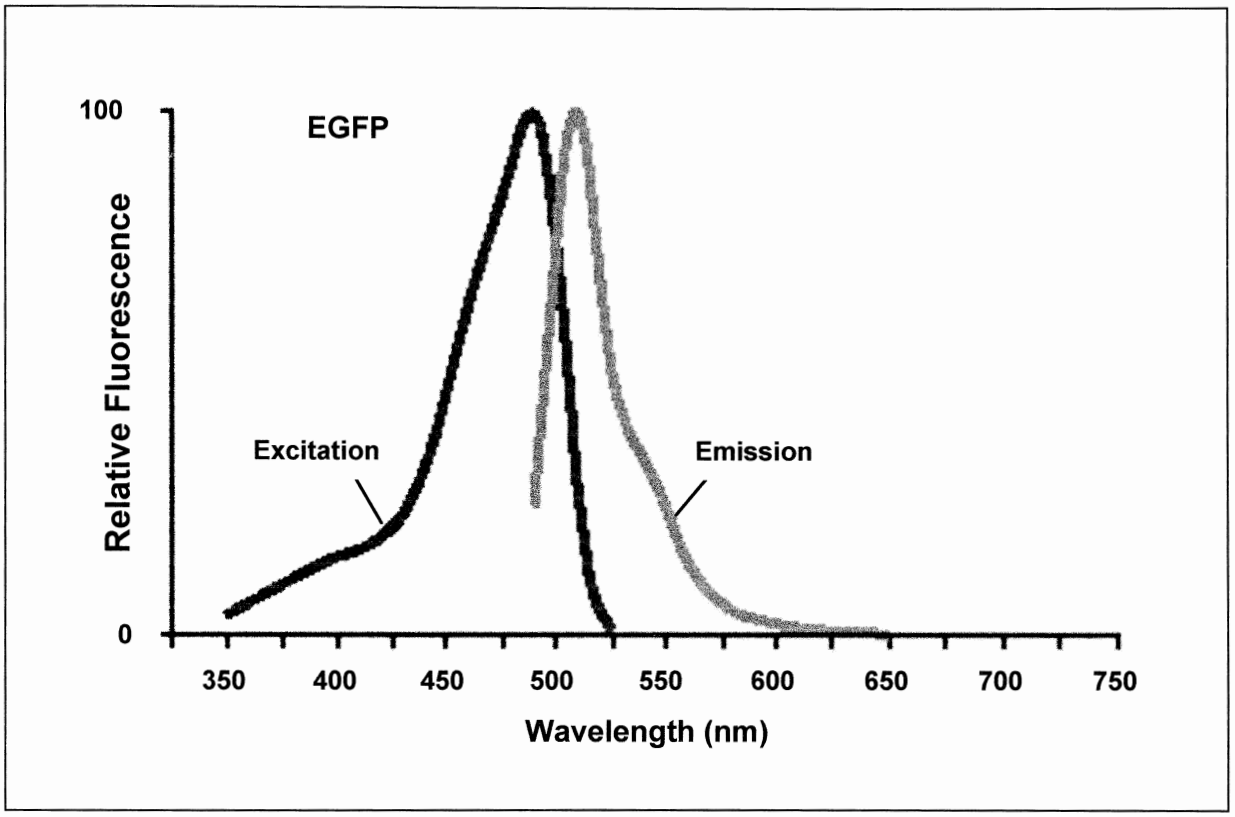

Fig.7.1. Excitation and emission spectra for the EGFP fluorescence. (Modified from Patterson *et al.*, 1997).

7.1.5. EGFP Filtering

As mentioned previously, the choice of filter in fluorescence microscopy is very important in order to maximise detection of relatively weak signals emitted by the fluorophore under investigation. The ability to exclude undesirable wavelengths of light which may not emanate from the fluorophore itself is often limited by the physical characteristics of the filter employed.

The bandpass filters commonly used in fluorescence microscopy can often lead to crosstalk between different channels/filters and undesirable light (noise) from artefacts and the light source itself can also be problematic. The spectra presented in fig.7.1 illustrate the small Stoke's shift between excitation and emission spectra for EGFP. There is a measure of crosstalk around 500nm with the Stoke's shift less than 20nm.

Glass bandpass filters used previously would have resulted in some overlap and crosstalk as the filter would have allowed undesirable wavelengths of light to be detected. The Leica TCS – NT system used for EGFP imaging utilised an acousto-optical tunable filter (AOTF) which greatly reduced crosstalk, eliminated some of the non-specific fluorescence and allowed a greater degree of control in filtering desired wavelengths of light (Wachman *et al.*, 1997).

The AOTF consists of a transparent optical crystal with an ultrasonic wavefield. The crystal can be made to vibrate at a selected frequency, causing the diffraction of light at particular desired wavelengths (Wachman *et al.*, 1997). The vibrations basically set up a diffraction grating for light passing through the crystal. The arrangement allows for both the selection of wavelengths to be filtered as well as the intensity of light to allow through the filter. This flexibility therefore allows for the adjustment of light intensity for various fluorophores to compensate for the relative brightness of different fluorophores and helps to reduce photobleaching in specimens with sensitive fluorophores. The disadvantages of the AOTF are that the bandpass filter is limited to 2nm minimum width and secondly, due to the fact that light is linearly polarised when passed through the filter, only the incident light in the polarised plane would pass through the filter.

Despite these minor disadvantages however, by making use of the AOTF a very narrow bandpass filter could be selected for the EGFP signal and multiple-colour imaging was possible by setting the filter to obtain the best image for both the EGFP and FM4-64 signals.

7.2. MATERIALS AND METHODS

The production of the GFP-ENaC cell lines was carried out in Indianapolis, IN, USA by collaborators at IUPUI, and properties of the cloned cell have very recently been described (Blazer-Yost *et al.*, 2001).

7.2.1. Cell Culture

A6 cells were grown and seeded onto Millipore HA filters for confocal imaging as described previously. For initial I_{SC} measurements to characterise the A6 clone, the cells were subcultured onto 24 mm Transwell tissue culture-treated inserts (Costar, Cambridge, MA) for at least 12 days. In addition to these data, I_{SC} measurements were carried out on cloned cells which were cultured on Millipore-HA filters (as described in chapter 2).

7.2.2. Green fluorescent protein expression vector construction

Complementary DNAs (cDNAs) encoding *Xenopus* ENaC alpha (xENaCα) and beta (xENaCβ) channel subunits were cloned from A6 cell cDNA by the polymerase chain reaction (PCR) using oligonucleotide primers based on the sequences described by Puoti *et al.* (1997) and *Pfu* DNA polymerase (Stratagene, La Jolla, CA, USA). cDNAs were first subcloned into pBluescript KS II- (Stratagene) using standard procedures and confirmed by DNA sequencing using the Sanger dideoxy method and Sequenase (Amersham, Piscataway, NJ. USA). Expression vectors for xENaCα-EGFP and EGFP-xENaCβ were generated by cloning PCR products into the Xho I/Bam HI sites of pEGFP-N1 and the Eco RI/Bam HI sites of pEGFP-C1 (Clontech, Palo Alto, CA, USA), respectively. Oligonucleotides were: 5'-gcgctcgagaggacgcctggagatatctgagac-3' (sense), 5'-cgggatcccttctacctccattctcctcatag-3' (antisense) for xENaCα-EGFP and 5'-cggaattctatgaagaggctgaagcgatatttcacc-3' (sense), 5'-

cgggatcccgcttgtagtgtcgtttaattctc-3' (antisense) for EGFP-xENaCβ. A schematic representation of the cloning vector contruction is illustrated in figure 7.2. Plasmids were purified by two rounds of caesium chloride gradient centrifugation and confirmed by DNA sequencing.

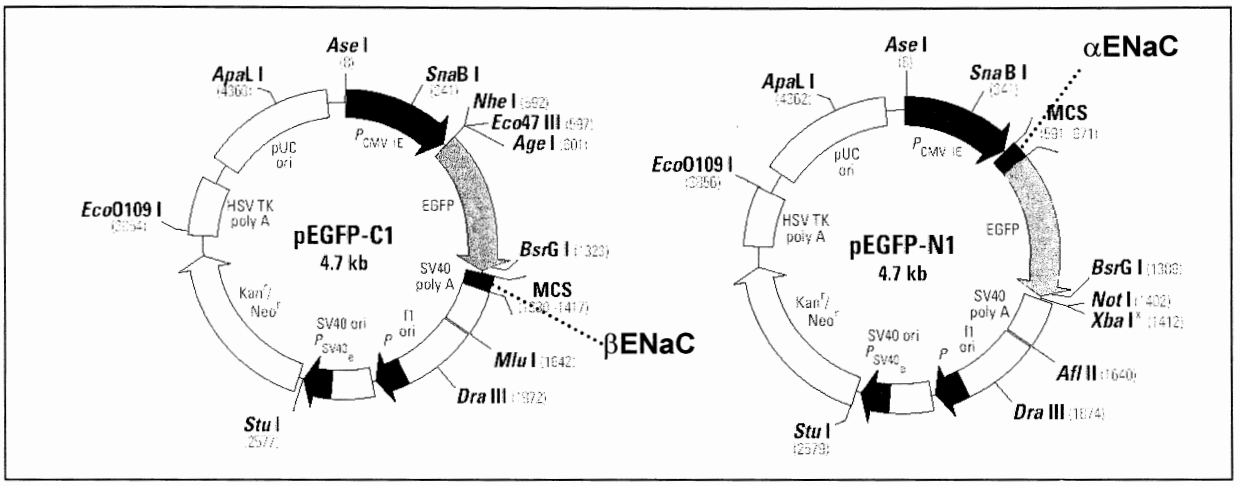

Fig.7.2. Schematic vector map indicating the cloning site for βENaC and αENaC into the EGFP vector, pEGFP-C1 and N1 respectively. (Vector maps modified from the Clontech Livingcolors manual)

7.2.3. A6 cell transfection

A6 cells were seeded onto plastic Petri dishes and grown to approximately 20% confluency. Transfection with the EGFP protein expression vectors was accomplished by incubating the cells with DNA (4 μg/100 mm^2 dish) and lipofectamine (Life Technologies) in serum-free media overnight. The following day, the mixture was replaced with normal serum-containing media and the cells were grown to confluence. The cells were trypsinized and replated on Petri dishes at a concentration equal to 10% confluent density in the presence of a toxic (2 mg/ml) concentration of Geneticin (Gibco BRL, Rockville, MD, USA). Under these conditions, it was possible to identify clones arising from single cells which had incorporated ENaC-EGFP

expression vector containing a neomycin resistance gene. When individual clones had grown to colonies of 100-200 cells, they were trypsinised using cloning cylinders (Bel-Art Products, Pequannock, NJ, USA), seeded onto 25 cm^2 flasks and maintained in 0.5 mg/ml Geneticin. The individual clones were maintained as normal A6 cells, but were kept under selective pressure with the addition of 0.5 mg/ml Geneticin to the culture media. Cells seeded onto filter inserts were fed with normal A6 media.

7.2.4. Transfection controls (Null vectors)

In order to compare the expression pattern of chimera plasmid constructs with standard EGFP within the A6 cells, cultures were transfected as described above with a vector containing only the EGFP plasmid (as obtained from the manufacturer). As no ENaC DNA was incorporated into the vector, this served to confirm that the A6 cells were capable of producing the EGFP at detectable levels and to localise the pattern of expression of EGFP alone within the cells. In order to get an idea of transfection efficiency, transiently trasfected cultures were observed 48 hours after plasmid introduction and imaged for EGFP expression. The cells were fixed briefly in a 1% paraformaldehyde Ringer's solution (30 minutes), washed twice and the nuclei of the cells stained with 300nM stock solution Hoechst 33342 (Molecular Probes, Leiden, Netherlands) for 10 minutes. Cells were washed twice in cold Ringer's solution and mounted on slides for conventional fluorescence microscopy. The bisbenzimide dye, Hoechst 33342 is cell-permeant, binds to the minor groove of DNA and fluoresces bright blue upon binding (Molecular Probes, Leiden, Netherlands). One major advantage of the dye is that it does not bind to RNA in the cytoplasm, so no RNase treatment is necessary to view the cell nuclei clearly. The imaging needed to be carried out by conventional fluorescent microscopy due to the nature of the Hoechst stain. The excitation wavelength of the dye is approximately 350nm with maximum emission at about 470nm which is in the ultra violet range and can not be excited with the Kr/Ar laser setup of the confocal microscope. For two colour imaging, the

fluorophores were excited by a Xenon lamp and the Hoechst fluorophore filtered with a standard DAPI filter cube. The EGFP was filtered and imaged separately with an FITC filter cube and images were overlaid using Paint Shop Pro (v7.01, JASC Software Inc., USA). All images were obtained using a 64X oil immersion objective (N.A.=1.4). Due to the fact that standard fluorescence was used, no optical sectioning was performed on these samples with the nuclear stain. The images obtained served to localise the relative position of EFGP with regard to the nuclear position and better quantitate transfection efficiency. The system also allowed for rapid screening of transfected cultures before moving to the more elaborate live cell work on the confocal microscope.

7.2.5. Electrophysiology

Initial clonal electrophysiological characterisation, carried out at IUPUI, were performed using a closed Ussing chamber setup (no flow through) to asses the cells responses to a variety of hormonal agonists. In these investigations, cells were stimulated with either insulin, ADH or forskolin. At the end of the stimulation, 10 mM amiloride was introduced to the apical membrane to determine the contribution of sodium transport to the total I_{SC}. In addition to these initial investigations, the electrical response to forskolin stimulation was recorded at the University of Cape Town in order to compare these with previously obtained data for untransfected A6 cells. The electrophysiological monitoring ensured that the introduction of additional labelled ENaC subunits did not interfere with the previously observed responses to elevated cAMP levels. Cells cultured on filters were mounted into an 4-electrode Ussing chamber (as previously described), continuously perfused with DMEM and voltage clamped to record the short-circuit current. The epithelia were stimulated with 2.5μM forskolin introduced in the basolateral medium (as before) and washed out after the peak response had plateaued off. The relative contribution of sodium ion transport to overall recorded current was

determined by the addition of 100 μM amiloride at the end of the forskolin stimulation and washout events.

7.2.6. Confocal Microscopy

For confocal microscopy, cloned A6 cells, cultured on Millipore millicell HA permeable supports in DMEM for at least 14 days were washed in cold DMEM after which the apical membranes were labelled for 30 min on ice with the FM 4-64 at a final concentration of 16μM. The procedure employed was as described in Chapter 6 for membrane trafficking studies. Following plasma membrane labelling, excess fluorphore was washed off in two cold DMEM washes (5 minutes each) to reduce background fluorescence. Next, approximately 0.75cm^2 area of filter was punched out of the supports and the cells and transferred to the confocal chamber where tissues were mounted apical surface down for imaging.

Laser scanning confocal microscopy (LSCM) was performed using an inverted Leica TSC-NT confocal imaging system equipped with a x63 Plan APO 1.2 NA water immersion objective used for all imaging. For the dual imaging of EGFP and FM 4-64, fluorescent images were collected by exciting the fluorophores with a Kr-Ar laser at 478 nm (for EGFP) and at 568 nm (for FM4-64). Emissions from EGFP and FM 4-64 were filtered with the AOTF with a band-pass filter set to 510-530 nm (for EGFP) and 690-730 nm (for the FM4-64) respectively. Serial optical z-sections were collected at 0.3 μm intervals, with an optimal scan time that varied between 8 and 32 sec, using 4 to 16 line averages depending on the intensity of the fluorescence and the degree of photobleaching observed. The EGFP signal emitted in the 520nm range was assigned a green colour, while those excited with the 568 nm line were labelled red. An overlay of collected images at each depth was performed to produce the final double-labeled images (Leica TSC-NT software). As the EGFP-ENaC signal most often

emitted at a lower level than the FM 4-64, EGFP signal was optimised by increasing the photomultiplier gain until levels in both channels appeared approximately equal. Laser power was kept below 50% to minimize photo damage, with optimal pinhole size automatically determined for the objective. Under these conditions there was minimal autofluorescence from the preparation and no bleed-through between emitted fluorophore channels.

In order to follow the localisation of the labelled channels over time and under the influence of forskolin, serial optical sectioning was performed every 5 minutes from the beginning of the image acquisition protocol. The reconstructed 3-D images would then represent a 3-D view of the cells over time and movements of the GFP within the cells could be monitored. One disadvantage of taking so many scans in such a short period was that inevitable photobleaching did occur. This was more prevalent in the case of the FM4-64 than the EGFP, as EGFP is more resistant to photobleaching (see above), but the increased intensity of FM4-64 signal over EGFP meant that this was not totally destroyed before the end of each experiment.

A similar protocol for forskolin stimulation and washout was employed as described before (Chapter 6). The washout experiment followed the same protocol and time course used for the membrane uptake experiments already discussed. In addition however, the effect of stimulation of the A6 cell by forskolin was also observed. For this, cells on ice were incubated with DMEM containing 2.5μM forskolin before the filter inserts were punched out and placed in the chamber with the same DMEM containing 2.5μM forskolin, at room temperature. Effects of forskolin stimulation could be observed once cells were allowed to reach room temperature. In practice, the time taken to mount the cells in the chamber, prepare the chamber on the confocal specimen stage and find a suitable region from which to acquire images was sufficient for the cells to recover and respond to the forskolin stimulus (~ 5-7 min). With this protocol the effects of both forskolin stimulation and washout of stimulus could be observed.

As the level of detectable EGFP was often low, 3-D images, presented side on (x-z plane) were not merely orthogonal sections (taken at a specific slice on the x-y plane) but was all the signal in the field of view. What this means is that when x-z views are presented, the image is a side on look through the entire cell layer (between 5 to 10 cells) rather than 1 cell. The reason for doing this was to enhance the available signal by looking at all the cells in view and get a better appreciation for the behaviour of the cells as an epithelium. This concept is depicted pictorially in figure 7.11.

7.2.7. WGA-Rhodamine Labelling

Previously, some difficulties were experienced in obtaining clean apical membrane images from live cell imaging using the confocal chamber. In some cases the most apical section needed to be exluded due to high levels of background contamination arising from the coverslip. In order to better localise the EGFP signal with respect to the apical membrane, fixed cell cultures on filter supports were labelled with a conjugated wheat germ agglutinin. By fixing the cells and preparing the filters as a standard slide preparation, filters could be more easily manipulated without timing concerns of the live cell microscopy and thus more ideal images obtained. Wheat germ agglutinin (WGA) selectively binds to N-acetylglucosamine and N-acetylneuraminic acid (sialic acid) residues which are particularly abundant on most cell membranes (Molecular Probes, Leiden, Netherlands). In solution, wheat germ agglutinin exists as a heterodimer with a molecular weight of approximately 38,000 daltons and is normally cationic under physiological conditions. Cells were kept on ice and a DMEM solution containing tetramethylrhodamine-WGA (Molecular Probes, Leiden, Netherlands) at a final concentration of 5 µg/ml was introduced to the apical membrane to obtain a specific label for the apical residues alone. Following labelling, cells were washed twice in cold DMEM (for 5 minutes each) without WGA and fixed in a 1% paraformaldehyde medium for 1hr on ice. Fixation was performed after WGA labelling rather than before labelling to ensure

that the membranes were not damaged and WGA could not enter the cells. Once fixed, cells were again washed twice in cold DMEM, filter inserts with cells cut from the filter cups and mounted on standard light microscope slides. The peak excitation and emission spectra for WGA-rhodamine was 555nm and 580nm respectively and the 568nm laser excitation line was suitable for producing WGA fluorescence. Collected fluorescence was filtered at 575-590nm for this fluorophore and EGFP collected as above. The same techniques for serial optical sectioning and 3-D analysis was employed as described above.

7.3. RESULTS

A number of clonal lines were obtained which expressed EGFP to a greater or lesser extent, and two of these were selected for study in greater detail as they were found to express the highest levels of EGFP-ENaC. The two cell lines expressed a tagged α- and β-ENaC respectively

7.3.1. Electrophysiology

In order to determine whether the cloned cells responded in an electrically similar manner as the parental cell line, I_{SC} measurements on filter-grown monolayers were performed. Results indicated that both insulin and antidiuretic hormone caused an increase in sodium current, and that the basal current of the cloned cells was always higher than the parental line. Results for the influence of insulin on the parental and $\tilde{\alpha}$ENaC clonal lines are presented in figure 7.3. It is clear that although the baseline, unstimulated I_{SC} is elevated in the transfected cell line, the response to insulin stimulation is essentially unchanged. Similarly, the responses of both α- and β-ENaC clones to ADH is presented in figure 7.4 where the basal currents are higher, but ADH effects are not increased proportionally. Finally, results obtained at IUPUI from stimulation of cells by forskolin is presented in figure 7.5. Here data from typical experiments for parental, the α- and β-ENaC clones are presented on the same axis. It is once again clear that the clonal lines have a higher basal current, but that the responses are similar to the parental cell line.

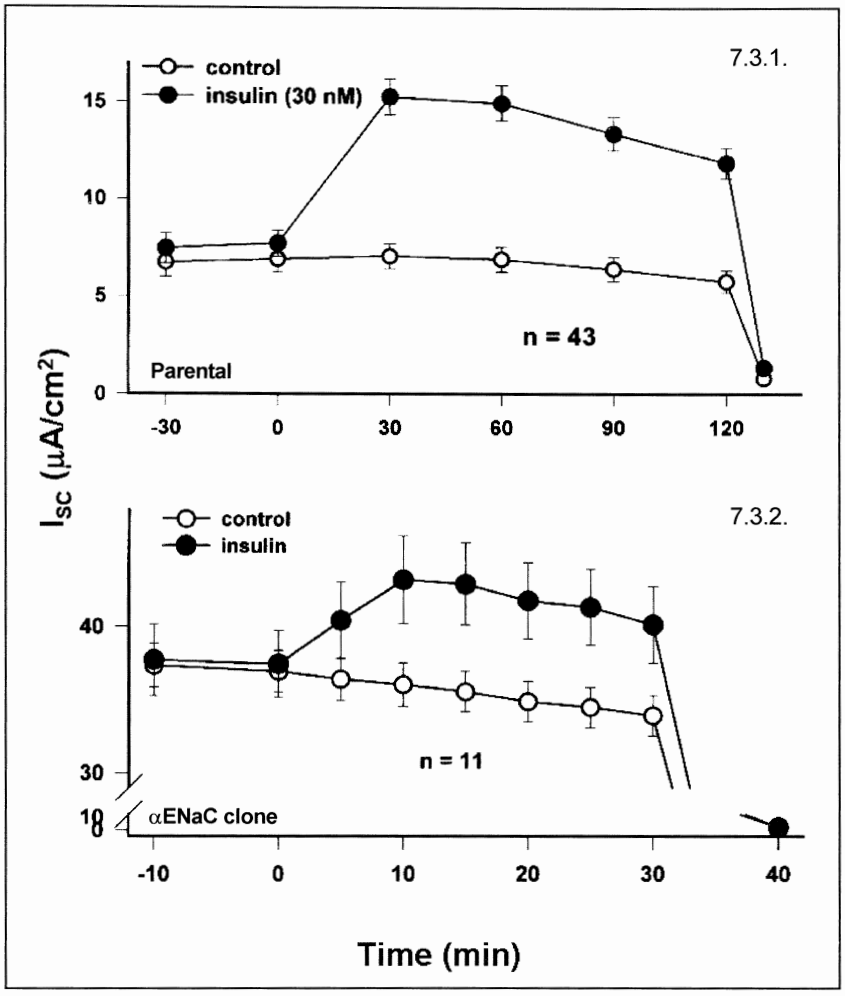

Fig.7.3. An electrophysiological comparison between transfected and parental A6 cell lines. The I_{SC} response of the parental A6 cells to a 30nM insulin stimulation is presented in 7.3.1. Following 120 minutes stimulation, 10μM amiloride was added to the apical medium to inhibit the sodium derived I_{SC}. A similar response was observed in the EGFP α-ENaC clonal cell line (7.3.2) where amiloride was added after 30 minutes stimulation. Note that the basal I_{SC} was significantly enhanced, but that the change in I_{SC} under the influence of insulin was essentially the same.

To compare the effects of forskolin on the cloned cells with previously reported results for A6 epithelia (chapter 4), cloned cells were mounted in flow-through Ussing chambers (as described) and stimulated with forskolin in the same way as the untransfected A6 cells had been.

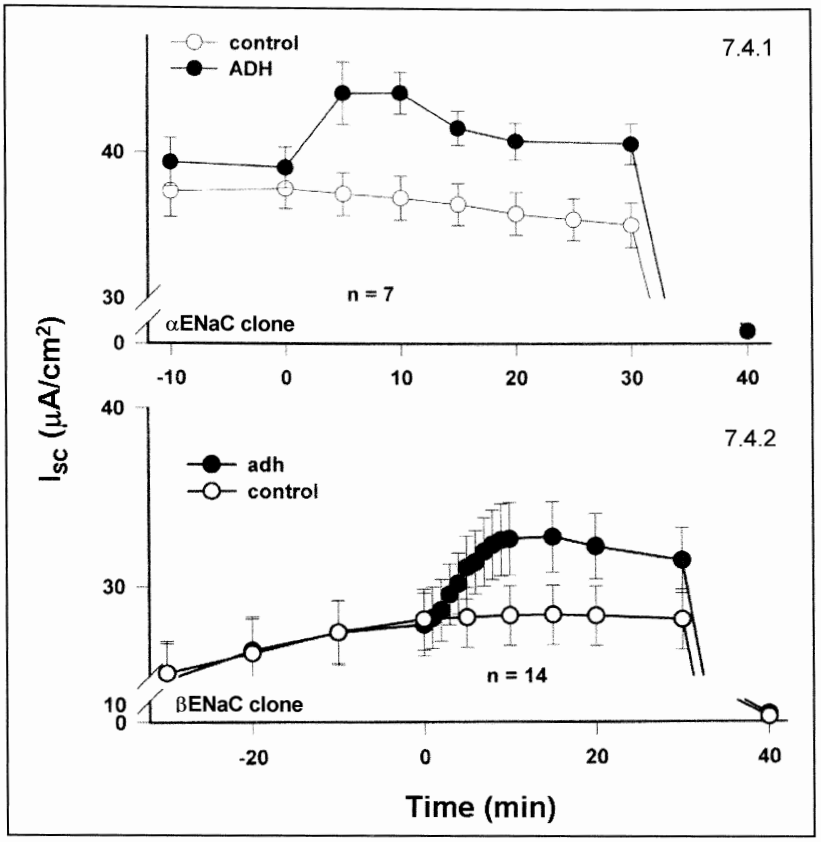

Fig.7.4. The response of the selected clonal cell lines to 25mU/ml ADH stimulation. The I_{SC} response of the αENaC-EGFP cells is presented in 7.4.1. and the EGFP-βENaC in 7.4.2. Amiloride (10 μM) was added to the apical medium after 30

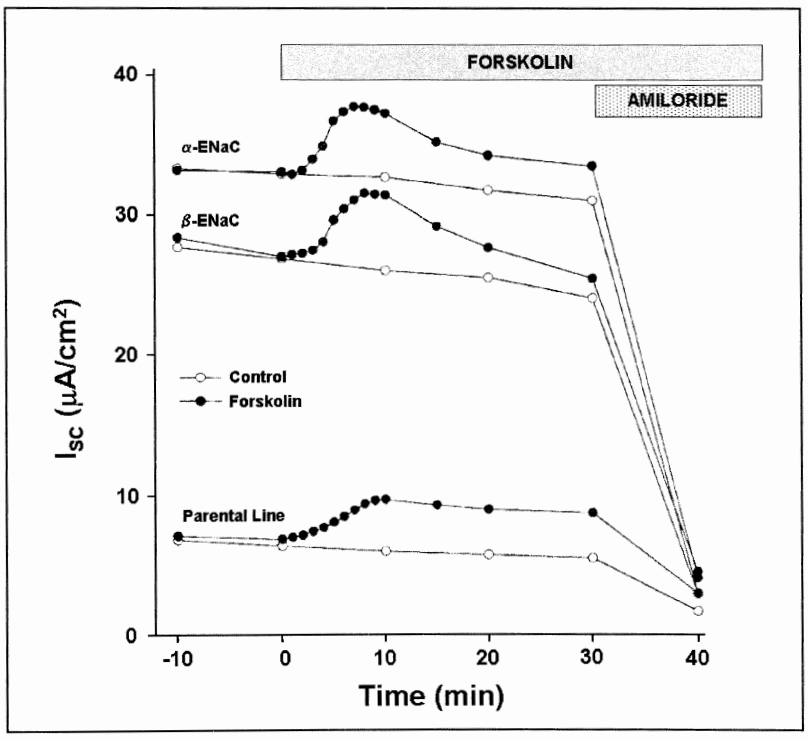

Fig.7.5. The I_{SC} response of the clonal and parental cell lines a to 2.5 μM forskolin stimulation. After 30 minutes 10 μM amiloride was added to the apical medium.

In agreement with responses observed in the laboratory in the USA, figures 7.6 and 7.7 illustrate that the epithelia respond in a similar manner to forskolin as the non-transfected A6 cells presented previously and that this follows the same time course as previously observed. The I_{SC} was however not as high as had been recorded when the cells were cultured on the Transwell filters in a closed system and may reflect differences due to variations in culture and experimental setup (Candia *et al.* 1993; Helman and Liu, 1997). The high I_{SC} and transepithelial open circuit voltages are congruent with the idea that a larger number of channel subunits were expressed in the cloned cells possibly resulting in a greater number of functional channels.

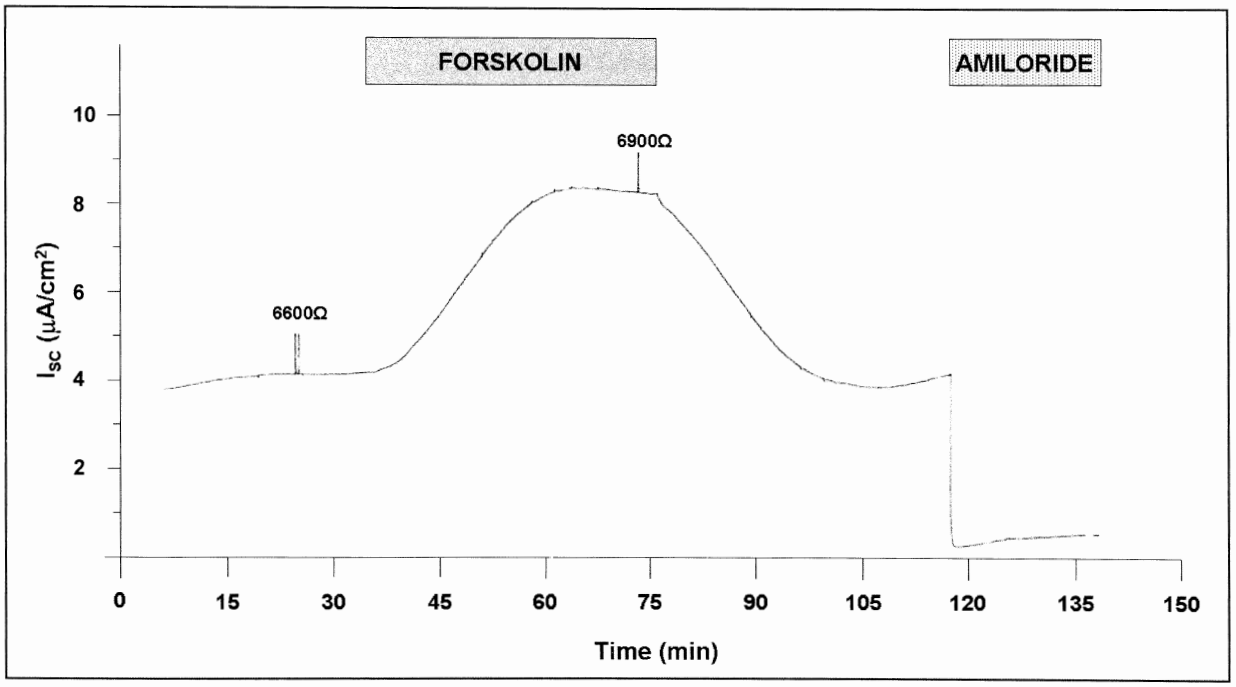

Fig.7.6. Strip-chart trace of a typical I_{SC} recording of the cloned EGFP-βENaC expressing A6 epithelia. The cells respond to forskolin with a time-course consistent with non-transfected A6 cells. The addition of amiloride (100 μM) indicates that the current is predominantly a sodium current. Before and during forskolin stimulation, a short 3mV pulse was applied across the epithelium to determine the transepithelial resistance. The values are indicated above each pulse.

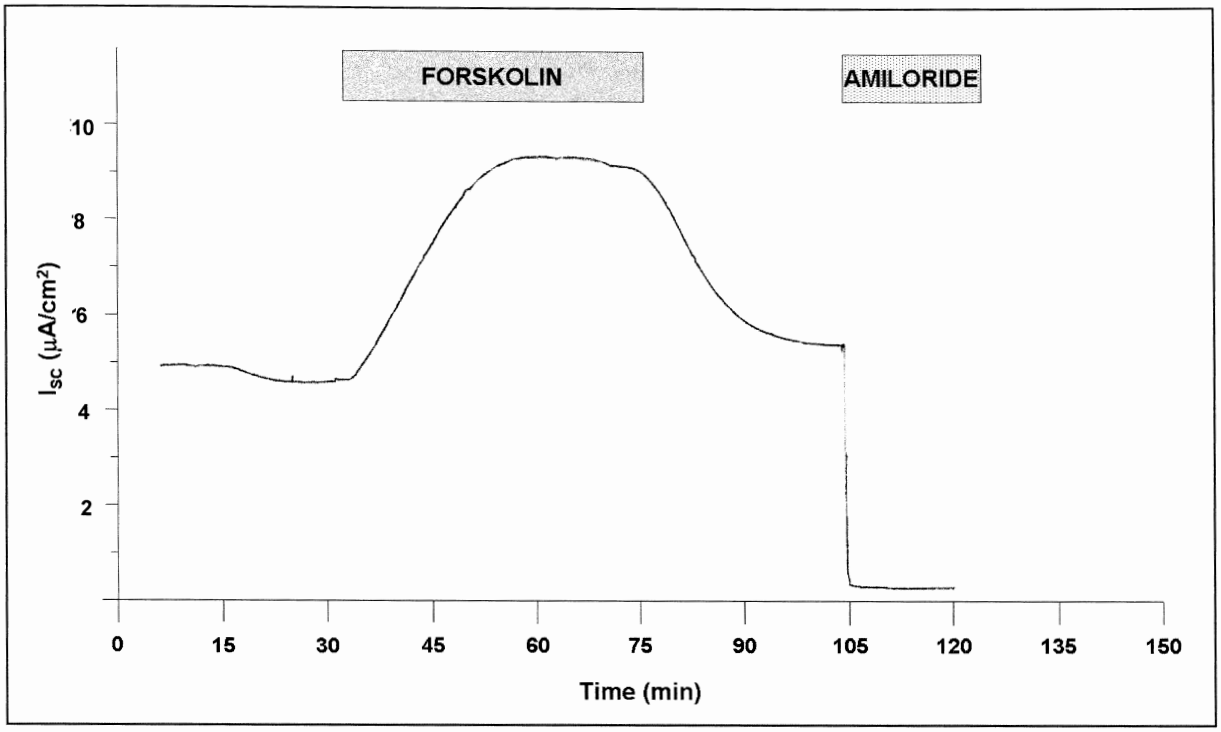

Fig.7.7. Strip-chart trace of an I_{SC} recording of the cloned αENaC-EGFP expressing A6 epithelia. The cells respond to forskolin with a time-course consistent with non-transfected A6 cells. Amiloride addition (100 μM) at the end of the trace indicates the proportion sodium current to the total I_{SC}.

7.3.2. EGFP Expression

To test whether the A6 epithelial cells were capable of expressing the EGFP construct, cells were transiently transfected with the unmodified EGFP-C1 vector as obtained by the manufacturers. Examples of highly expressive cells are presented in figure 7.8. It is clear that the cell which incorporate the vector are readily able to produce the GFP, but that this signal is not localised to any specific domain of the cells. The endoplasmic lattice structure can actually be made out in the transfected cell indicating general cytoplasmic localisation. Transfection efficiency was also not very high (>10%) demonstrating the need for selective media to obtain stable clonal lines.

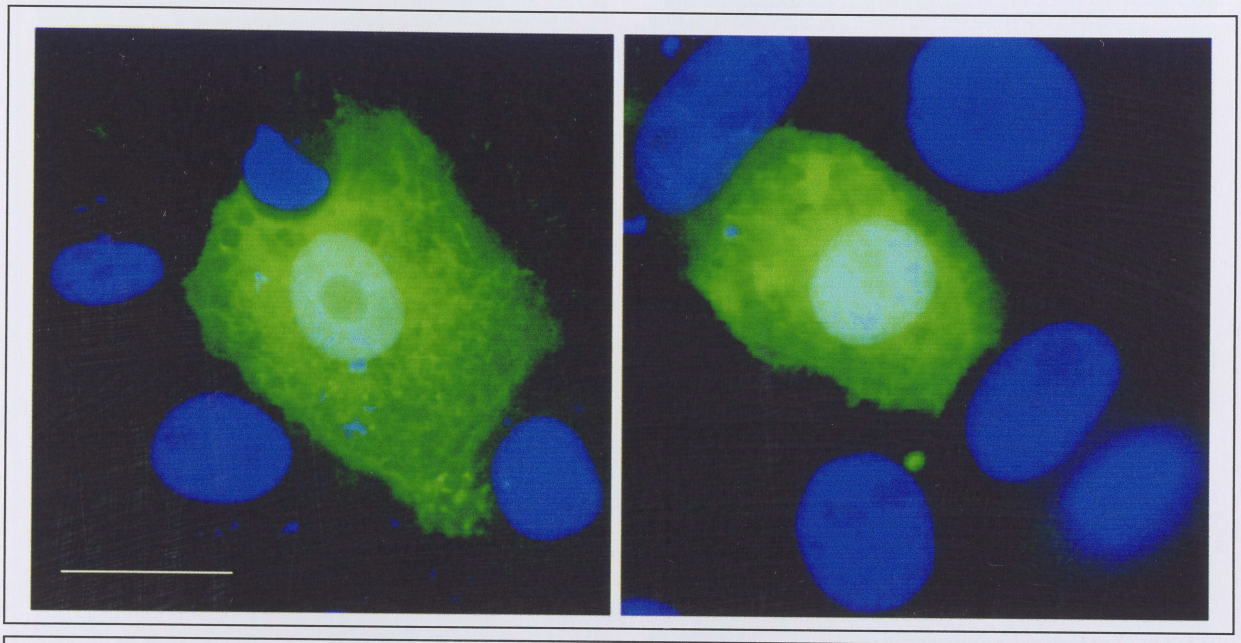

Fig.7.8. A6 cells transiently transfected with the EGFP vector (null vector). Cell nuclei were stained with Hoechst (blue) demonstrating that not all cells were successfully transfected. The EGFP is not specifically localised within the cells and the endoplasmic lattice structure is clearly visible in the cell on the left. Scale bar indicates 5 μm

7.3.3. EGFP-ENaC Imaging

In order to obtain qualitative information from the cloned cells it was important that the EGFP expressed in the cells could be readily imaged. Both clonal lines produced GFP (confirmed by Southern and Western blotting performed in Dr. Blazer-Yost's laboratory), and this signal was detected by the confocal microscope as illustrated in figure 7.9 and 7.10. The αENaC clonal cell line exhibited a better general EGFP expression with more fluorescence present, but it was possible to detect the GFP in both the αENaC and βENaC clones.

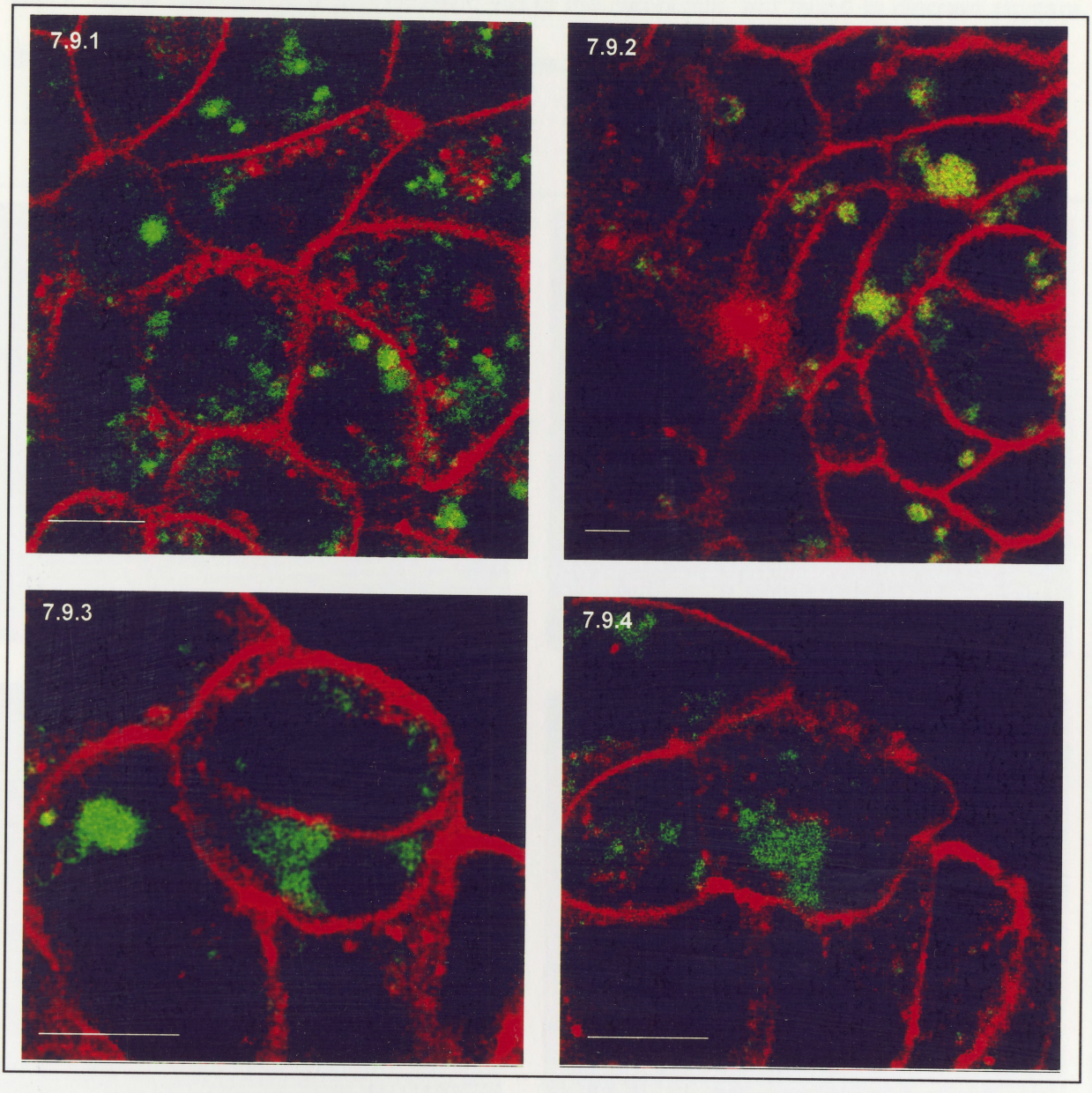

Fig.7.9. Confocal images taken from the αENaC-EGFP A6 clonal cell line. Membrane is labelled with FM4-64 (red) and the EGFP-ENaC (green) is visible within the cells. Note the accumulation of GFP in vesicular structures beneath the membrane. The optical sections were taken 2-6μm beneath the apical membrane. Scalebar represents 5 μm in each case.

Serial optical sectioning further permitted the localisation of the EGFP within the cells to be determined. In most cases EGFP signal was located nearer the apical domain of the cloned cells. This is more readily demonstrated in figures 7.13-7.15. In both clonal cell lines, the

EGFP signal was not generally localised within the cytoplasm, but found in discreet clusters (possibly vesicles) beneath the apical membrane.

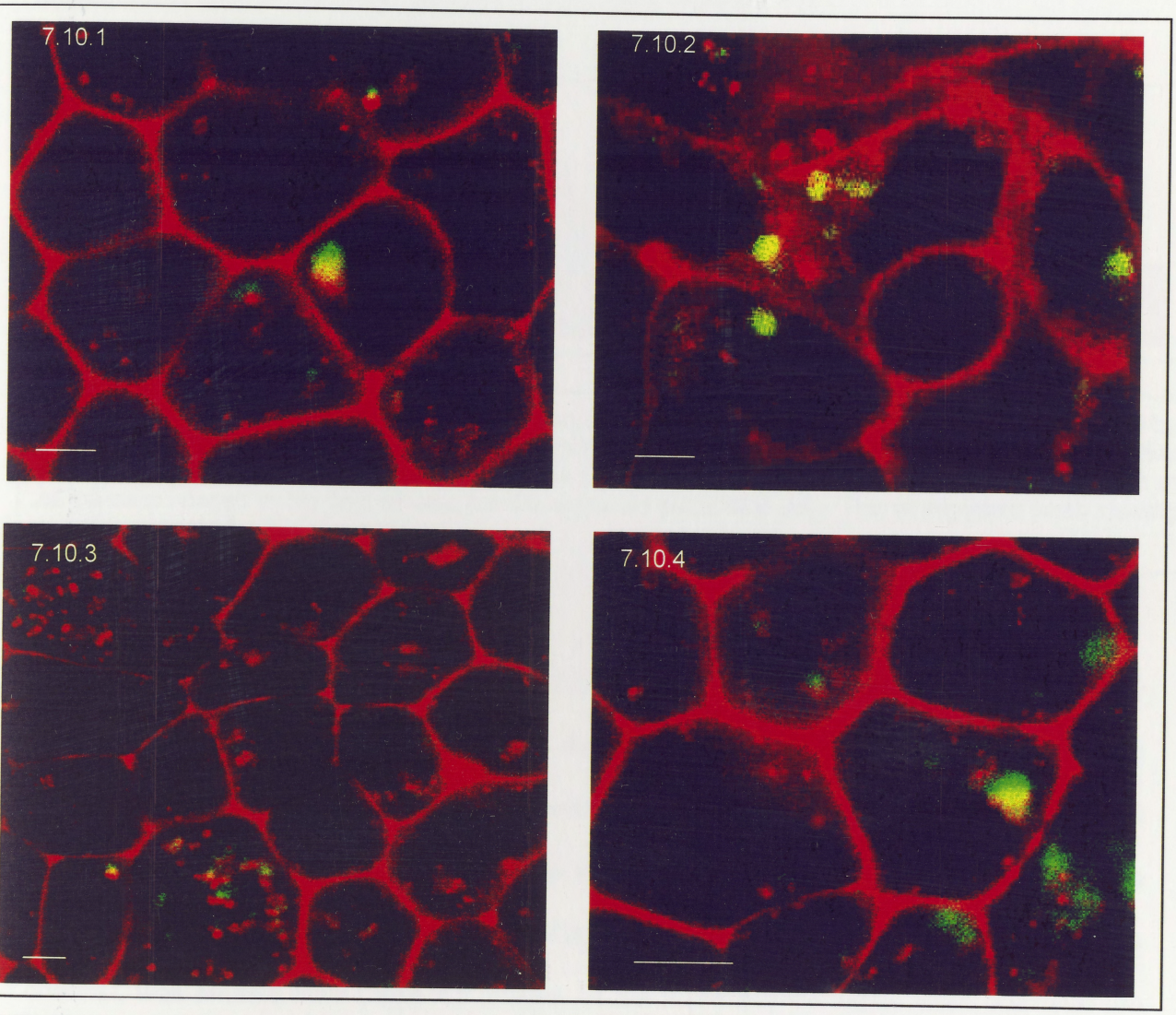

Fig.7.10. Confocal images taken from the EGFP-βENaC A6 clonal cell line. Membrane is labelled with FM4-64 (red) and the EGFP-ENaC (green) is clearly visible within the cells. The optical sections were all taken 2-6μm beneath the apical membrane. Scalebar represents 5 μm in each case.

To visualise the relative position and movement of signals within the cells in the z-axis, the serial optical sections were reconstituted to produce a 3-D image which could be manipulated in virtual space. By orientating the 3-D monolayer such that the cells were viewed side on the movement of GFP signal could be viewed more easily (figure 7.11).

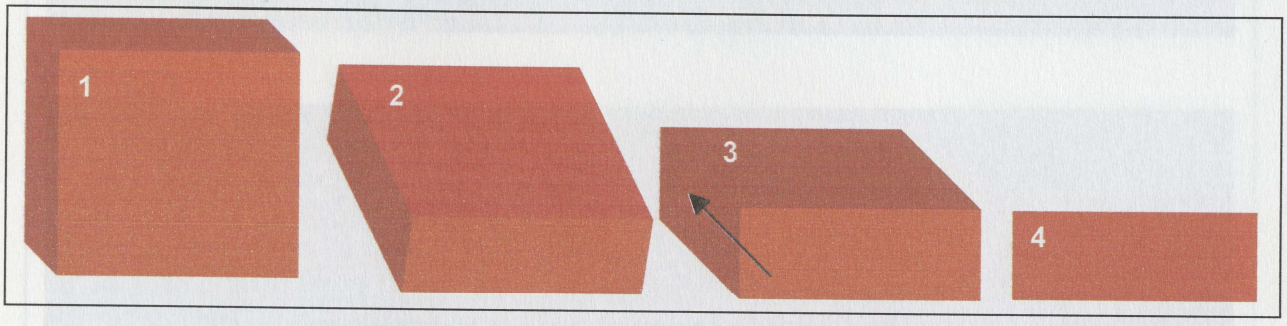

Fig.7.11. Schematic illustration of the orientation of the x-z plane. The monolayer of cells is depicted by the simple 3-D box (1). The box is rotated (2) until it is on its side (3&4) to illustrate the viewing perspective (arrow) of the x-z plane. Note that side-on view is not an orthogonal section, but rather an accumulation of all the cells imaged in the field of view (i.e the entire z-y plane side on). This is important when viewing results presented for EGFP movement.

The advantage of viewing all the cells from the side was that the EGFP signal from the entire imaged area was apparent in the x-z image. As the EGFP signal was far less when compared to the FM4-64 fluorophore and at times at the limits of detection by the confocal system, it was an advantage to accumulate the entire signal in one side view. In order to get an idea of the location and movement of the EGFP-ENaCs the FM4-64 signal, acquired on a separate channel, was omitted from these x-z images as the more intense signal often obscured the EGFP signal. The effects of the addition of forskolin on both the clonal cell lines over time is presented in figures 7.12 and 7.13. The x-z views presented comprise snapshots at set time points following the onset of image acquisition, but do not present all the time points at which optical sectioning was performed (the designed protocol prescribed sectioning every 5 minutes).

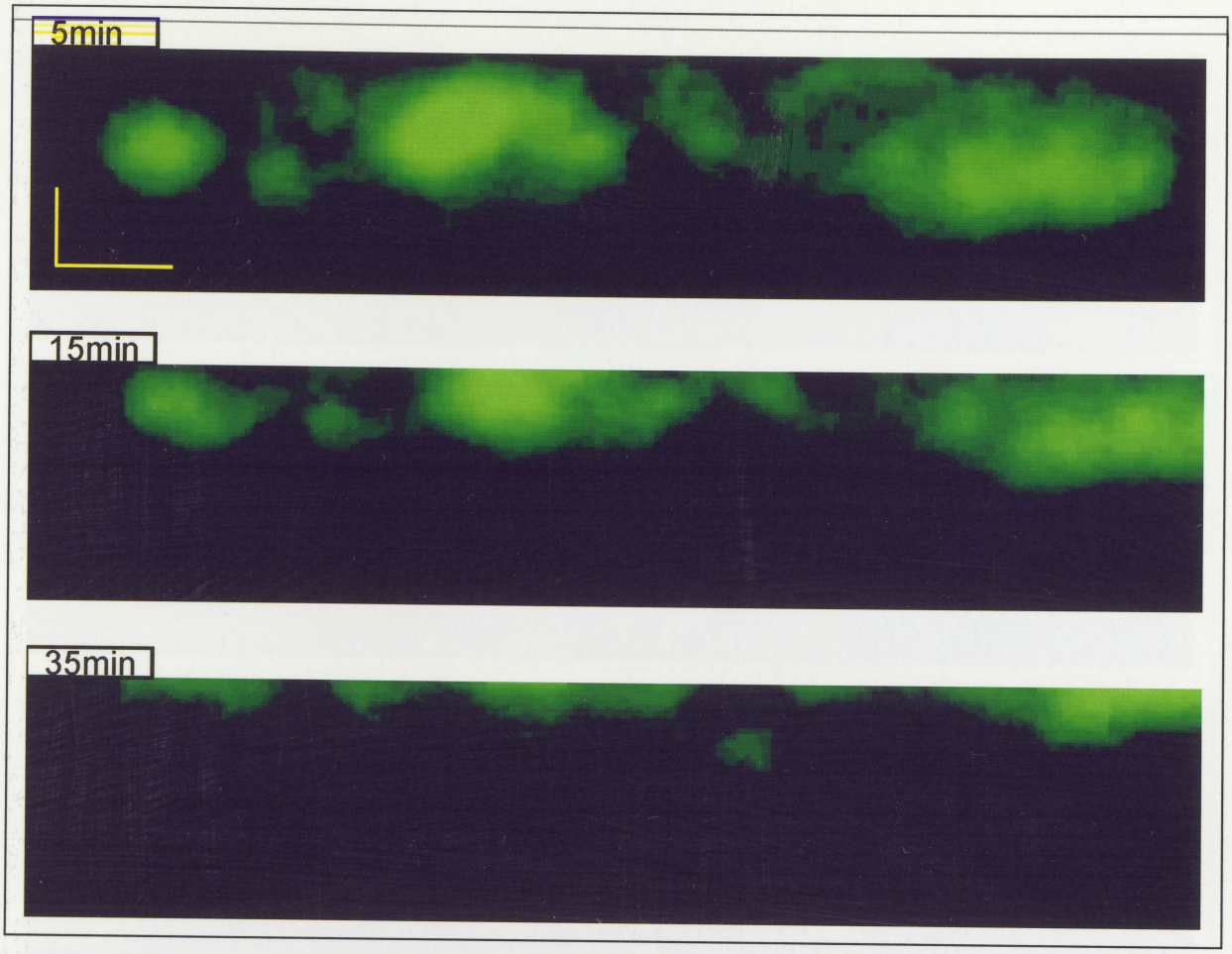

Fig.7.12. The effect of forskolin stimulation on **EGFP-βENaC** localisation within the cell monolayer. The labelled ENaC subunit can be seen to traffic from a sub-apical location within the cells approximately 5 μM from the apical membrane toward the apical surface. Most of the ENaC trafficking to the apical surface had occurred by 35 minutes. The scalebar represents 5μm in both planes.

It is clear from the snapshots presented that the tagged ENaC subunits relocate from within the cell towards the apical membrane. Forskolin stimulation resulted in trafficking of ENaC to the surface within 40 minutes, consistent with the electrical responses recorded previously. The trafficking phenomenon is apparent in both the α- and β-ENaC clonal lines. This evidence for the first time directly implicated ENaC trafficking in response to cAMP stimulation. Following the forskolin stimulation it was important to observe the effects after stimulus withdrawal.

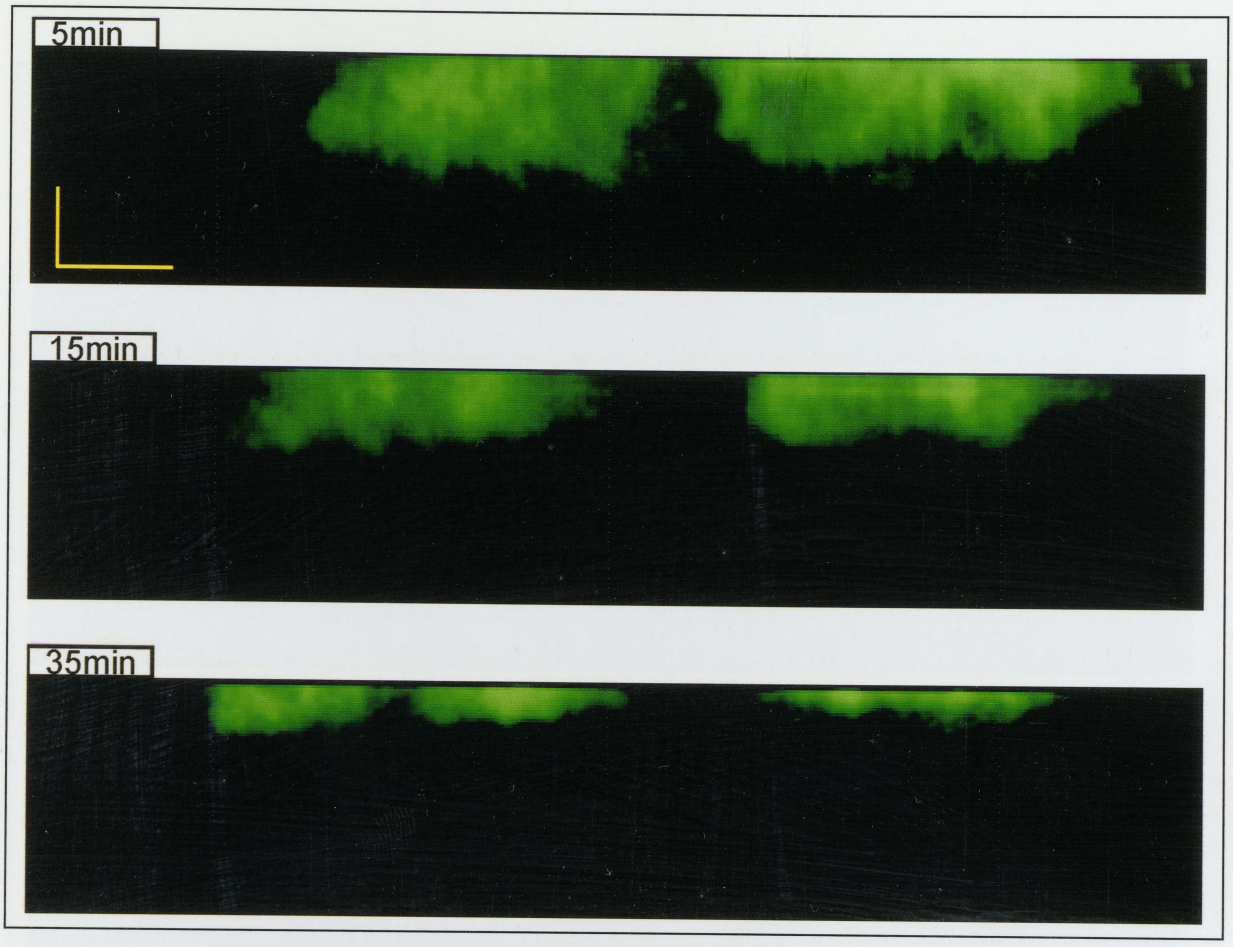

Fig.7.13. The effect of forskolin stimulation on αENaC-EGFP localisation within the cell monolayer. The labelled ENaC subunit can be seen to traffic from a sub-apical location within the cells toward the apical membrane. Most of the ENaC trafficking to the apical surface had occurred by 35 minutes. The scalebar represents 5 μm in both planes.

The evidence presented thus far strongly indicated that regulation of sodium ion transport occurs by trafficking of ENaC to and from the apical membrane. However no direct evidence for this had been demonstrated. Figure 7.14 illustrates the movement of αENaC-EGFP following the removal of forskolin stimulation. Note the difference in time course, with the final image presented at 45 minutes after removal of forskolin. It is clear that tagged ENaC subunits were retrieved into the cells with the majority of the signal internalised after 45 minutes.

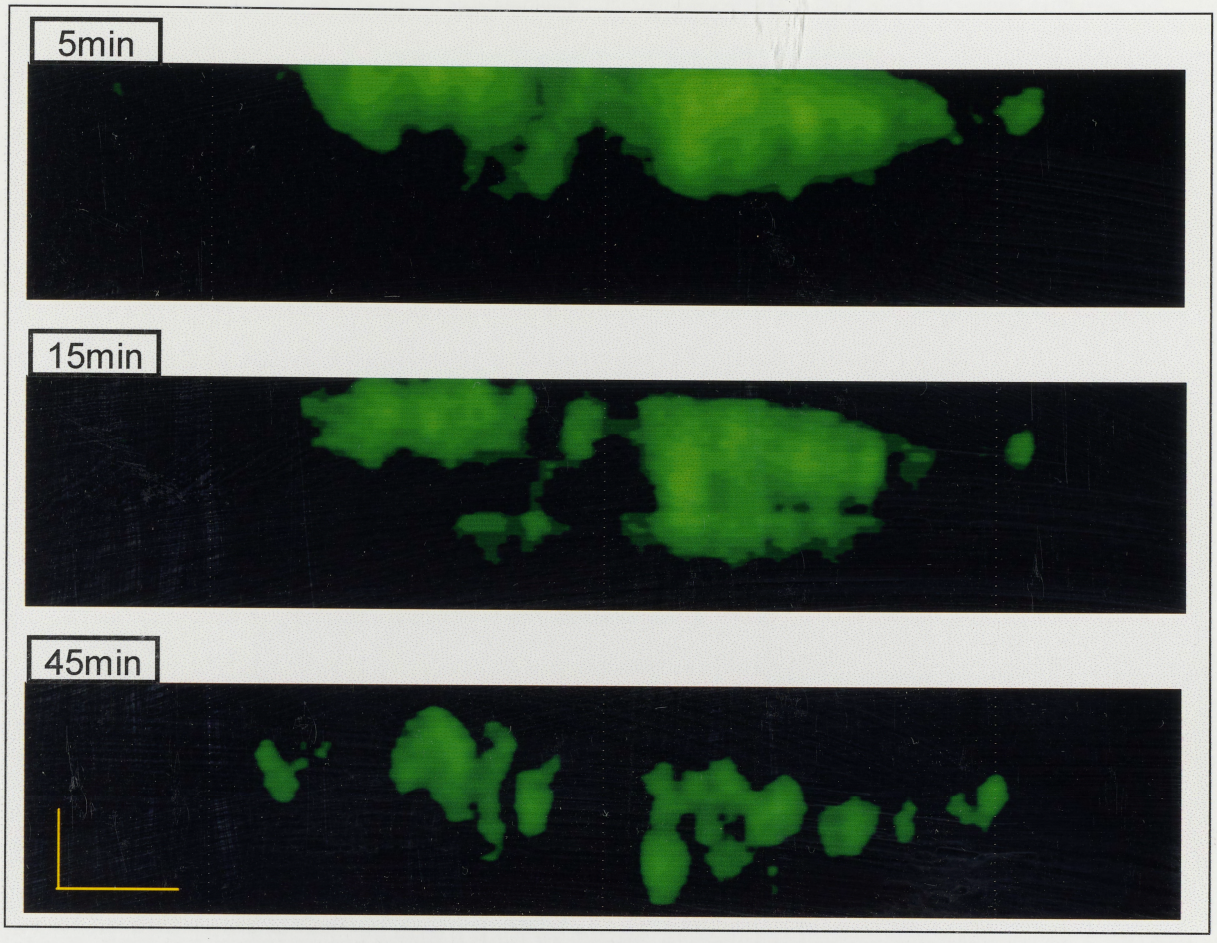

Fig.7.14. Sequential snapshot images taken at times indicated above each image following removal of forskolin stimulation. The EGFP-αENaC localisation within the cell monolayer can be seen to move from the apical domain deeper into the cells. Note that the time points differ from those presented in figs.7.12 & 7.13. The scalebar represents 5 μm in both planes.

Due to the technical constraints imposed by live cell imaging it was rarely possible to obtain satisfactory images from the apical surface of the cells. The large autofluorescent signal eminating from the chamber coverslip produced a non-specific noise signal in the very apical optical sections obtained. An example of the domed apical surface labelled with FM4-64 of the EGFP-βENaC cells is presented in figure 7.15. It can be seen that the GFP signal is associated with the membrane as this first apical slice contains both red (FM4-64) and green

(EGFP) signal. This type of image was not always obtainable and vital information about the apical membrane/GFP interaction was often lost as the most apical section was not usable.

In order to confirm that the GFP was indeed associated with the apical surface (i.e. channels are inserted into the apical membrane) a different approach was employed.

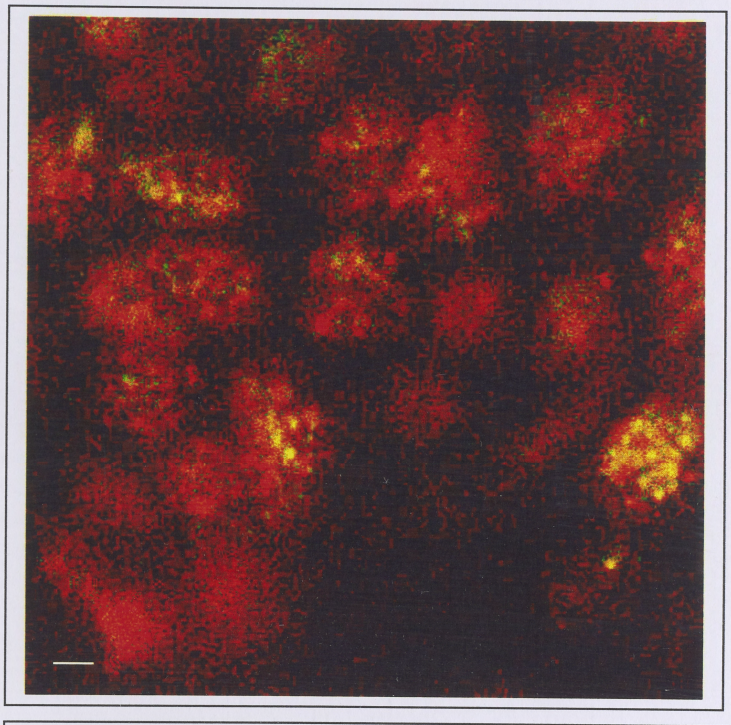

Fig.7.14. Double labelling of FM4-64 and EGFP at the apical surface of the EGFP-βENaC clonal cells. The channel subunits appear at the domed apical surface with this image representing the first optical section in an ideal experiment. Scalebar represents 5 μm.

Presented in figure 7.15, the double labelling of apical membrane with WGA-rhodamine and EGFP confirms the presence of EGFP in and directly beneath the apical membrane.

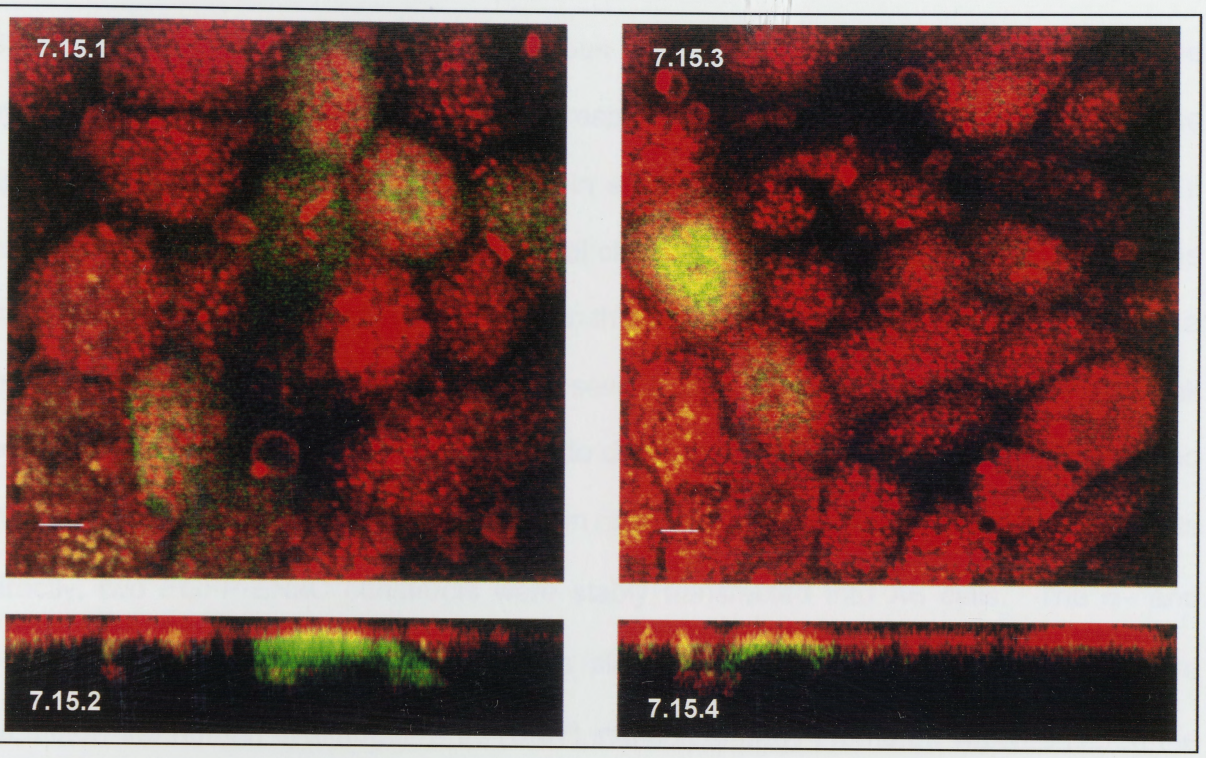

Fig.7.15. Confocal migrographs taken from fixed EGFP-αENaC clonal cells cultured on filter supports. The apical membrane was labelled with WGA-rhodamine and the filters mounted on slides. The domed tops of the apical surface can be seen in the optical section taken in the xy plane in 7.15.1 & 7.15.3. An orthogonal x-z slice produced from the 3-D stack is presented beneath each xy plane (7.15.2 & 7.15.4) to illustrate the localisation of ENaC in and directly beneath the apical membrane. Scalebar represents 5 μm.

This protocol was not ideal however for trafficking investigations as it needed to be performed on fixed cells mounted on slides and unlike the live cell work, no dynamic information could be obtained from the preparation.

7.4. DISCUSSION

7.4.1. GFP clone characterisation

Studies undertaken and described in previous chapters provided indirect evidence for the hypothesis that trafficking mechanisms are responsible for regulating ENaC numbers at the apical membrane. The regulated increase in endocytosis after forskolin stimulus washout corresponded in time to the decrease in total channel number at the apical surface. Some suggestion that channels could be involved in this trafficking was obtained by labelling with a fluorescently tagged amiloride moiety, but several limitations prevented a conclusive link being made. Results presented here provide direct evidence for the first time of regulated trafficking of ENaC by forskolin stimulation. In order to view the movement of ENaC subunits directly, two EGFP-ENaC constructs were stably transfected into A6 cells. The α– and β–ENaC subunits were incorporated into a plasmid containing EGFP and a constitutive promotor, the human cytomegalovirus (CMV) immediate early promoter, which ensured the constant production of the EGFP constructs within the cloned cells. This increase in available ENaC subunits produced an increase in basal currents of the A6 cells when compared to the parental line. This is understandable when one considers that a larger number of available subunits would quite possibly lead to a larger number of assembled channels being constructed by the cells.

7.4.2. Hormonal response

The increase in basal transport was not however indicative of an increased response to hormonal stimulation. The hormones insulin, ADH and direct AC stimulation elicited a response from the transfected cells, but this was not augmented to the same extent as the basal current. In all cases the I_{SC} increases were very similar to the parent cell line and compared favourably with results presented in Chapter 4. The increase in I_{SC} following

forskolin addition was about 4-5 $\mu A/cm^2$ which was similar to results for untransfected A6 cells presented previously. What the electrophysiological results demonstrated were that the transfected cells were still able to respond in a physiological manner, in a similar time course and to the same extent as untransfected parental lines.

The interesting phenomenon of increased basal current, but no concurrent increase in hormonal response raises the possibility that if the regulated acute response to cAMP occurs by shuttling channels located in an intracellular pool to the apical membrane, the size of this pool is finite and tightly regulated. The increase in basal transport rates was probably as the result of more active channels delivered to the apical membrane. A sudden increase in channel subunit production would probably force the cells into producing and assembling more channels which would raise the numbers delivered to the apical membrane. At some point the levels of production and delivery would be balanced by endocytosis and degradation and a new elevated basal transport rate would have been established.

This constitutive delivery pathway was however distinct from the acute response pathway to hormonal stimulation. According to the hypothesis of channel delivery, channels would be derived from an intracellular pool beneath the apical membrane. This pool can be seen to be in operation when the EGFP signal is tracked after cells were stimulated with forskolin (figures 7.12 and 7.13). From the electrophysiological responses, the pool size appears however to be fixed as the channels delivered to the apical membrane produced the same response as untransfected A6 cells. These results support the findings reported in Chapter 6 where it was suggested that there are two pools of channels which are regulated independently.

7.4.3. Direct channel activation?

The idea of direct channel activation to explain increases in sodium transport is also disputed by these results. It is clear that there are more channels resident in the apical membrane due to the increased basal current, and it would therefore be expected that this increase in resident channels would result in an augmented response to cAMP activation if apical resident channels were activated directly. This was not the case in the responses observed with the transfected cells.

7.4.4 EGFP localisation

The EGFP signal presented in figures 7.9 and 7.10 illustrate a distinct vesicular-like localisation of the tagged-ENaC subunits within the cells consistent with the vesicular machinery presented in the previous chapter. This localisation was not observed when EGFP was transfected alone. It must be noted however that even though the cultures were maintained under continuous positive selective pressure and the cultures originated from a clonal cell line, not all the cells are seen to contain green fluorescence. The reasons for this could be a variable level of production in each cell, and even if GFP was produced it may have fallen beneath the level of detection of the confocal microscope system.

This fact was kept in mind when trafficking of EGFP-ENaC was investigated as the paucity of signal in individual cells would mean that movement of the signal could be missed in many cells. In order to maximize the chances of observing the EGFP-ENaC movement, the entire imaged field was observed side on in the xz-plane in figures 7.12-7.14. The influence of forskolin on ENaC regulation is illustrated in these figures. It is clear in both clonal lines that the EGFP-ENaCs are trafficked to the apical membrane when stimulated by forskolin. It appears however that not all the signal reached the apical surface, but it should be kept in

mind that as in the FM4-64 endocytic uptake investigations (Chapter 6) the epithelial layer is not perfectly flat and height variations are problematic in live cell work. On removal of forskolin stimulation the GFP signal is seen to move from the apical surface back to intracellular compartments.

An additional limitation with the live-cell confocal setup was the strong non-specific signal near the apical surface of the cells which originated from the coverslip itself. One of the advantages of the confocal already discussed is that it can effectively reduce and often eliminate out of focus fluorescence. This feature does have limitations and, as discussed previously, the pinhole size accounts for much of this sensitivity. In order to obtain images from the weak EGFP signal it was often necessary to open the pinhole to allow more light to reach the detectors. This had the disadvantage of allowing more out of focus light in and a noisier signal was obtained. In most cases this necessitated the removal of the first optical section from the 3-D stack. This was not always the case as illustrated in figure 7.14 where the apical surface of the cells is illustrated, but was of sufficient concern to require an additional protocol to be employed in order to view the apical surface of the cells.

To this end, a rhodamine-conjugated WGA was used to label the surface of the A6 cells and cells fixed and mounted on slides for imaging. Images obtained in this manner are presented in figure 7.15 and the association of EGFP-ENaC with the apical membrane is clearly visible. In addition the relative location of the EGFP signal directly beneath the apical membrane is also apparent.

7.4.5. Conclusions

The results in this study would support the idea that ENaC is trafficked to and from the apical membrane in response to forskolin stimulation and removal of stimulus as the localisation of EGFP-ENaC can be seen to change in a time course consistent with electrical data obtained.

In studies by Chalfant *et al.* (1999) the authors present evidence for an endocytic motif on the amino end of the ENaC subunits which would support the idea of trafficking observed in these studies. Mutating the amino-terminus of the subunits prevented delivery of channels to the surface of oocytes.

The size of the pool of stored channels appears to remain constant even with an increase in channel production. This would suggest a tightly regulated machinery within the A6 cells. In support of this idea, studies by Valentijn and colleagues (1998), demonstrated that in an oocyte overexpression system, many of the expressed subunits were in fact degraded and never reached the membrane to participate in sodium transport.

CHAPTER 8

DISCUSSION AND SUMMARY

8.1. GENERAL DISCUSSION

8.1.1 The use of A6 cells

The aim of this study was to examine the mechanism of rapid hormonal regulation of sodium ion channels in renal epithelia. The renal cell line, A6, derived from *Xenopus laevis* was used as a model for mammalian cortical collecting duct (CCD) cells. A number of previous studies which made use of A6 cells showed that this cultured cell line does indeed constitute a reliable model for the principal cell in the CCD and has thus been extensively used to characterise the transepithelial sodium ion transport in tight epithelia (Beron *et al.*, 1995; Bindels *et al.*, 1988; Butterworth *et al.*, 2001; Cantiello *et al.*, 1989; Chalfant *et al.*, 1993; Crowe *et al.*, 1991, 1995; Fidelman *et al.*, 1982; Handler *et al.*, 1981a,b; Johnson *et al.*, 1986; Keeler and Wong, 1986; Kemendy *et al.*, 1992; Kleyman *et al.*, 1994; Marunaka *et al.*, 1994; Perkins and Handler, 1981; Rokaw *et al.*, 1996b; Sariban-Sohraby *et al.*, 1983; Thomas and Mintz, 1987; Verrey *et al.*, 1987; Wills and Millinoff, 1990; Yanase and Handler, 1986b).

Cultured epithelia can be grown under defined conditions, with defined growth media, and are therefore not affected by factors such as seasonality, dietary complications, supply or availability, geographical and individual variations which are considerations that need to be addressed when living animal models are used (Helman and Liu, 1997). The A6 cells are responsive to both amphibian and mammalian hypophyseal hormones, AVT and ADH/AVP respectively (Ali *et al.*, 1998, Bindels *et al.*, 1988; Doi and Marunaka, 1995; Kleyman *et al.*,

1994; Marunaka and Eaton, 1991; Nakahari and Marunaka, 1995) as well as a number of other secondary messengers like insulin, aldosterone, and prostoglandins (Bindels *et al.*, 1988; Blazer-Yost *et al.*, 1982, 1998; Edinger *et al.*, 1999; Helman *et al.*, 1998; Kemendy *et al.*, 1992; Kleyman *et al.*, 1992, 1994; Marunaka and Eaton, 1991).

Due to the extensive characterisation of the cell line and the fact that certain protocols had been well defined in this laboratory all investigations were carried out using A6 cells so that results from experiments employing a number of different techniques could be readily compared.

8.1.2 Hypotheses for ENaC regulation

Due to the controversy surrounding the nature of ENaC regulation as studied in a number of model tissues of the CCD (see introductory chapter and below), the aim of this study was to investigate the possible regulation of ENaC by trafficking or shuttling mechanisms. The idea is not without precedent however as similar regulation is found to be in operation for other transporters in a variety of tissues. For example, the GLUT-4 glucose transporter in skeletal muscle (Guma *et al.*, 1995), the cystic fibrosis transmembrane conductance regulator (CFTR), the anionic channel found in a number of secreting epithelia like lung and distal colon (Tousson *et al.*, 1996) and aquaporin 2 (AQP-2), the water channel in the kidney collecting duct (Marples *et al.*, 1995). In the case of ENaC, two differing views on possible cAMP-dependant regulation have emerged.

The first suggests that channels, resident in the apical plasma membrane are acted on directly, possibly by phosphorylation in order to activate sodium ion transport in these inactive (silent) channels. Evidence has been presented to support the hypothesis in a number of studies. Sariban-Sohraby *et al.* (1988) demonstrated an AVT-dependant phosphorylation of a peptide

associated with a purified ENaC complex. Direct phosphorylation of channels was demonstrated in studies using ENaCs reconstituted in planar lipid bilayers (Ismailov *et al.*,1994; Oh *et al.*, 1993). Several studies using toad bladder, another CCD model tissue were also suggestive of direct activation (Levine *et al.*, 1981; Palmer and Lorenzen, 1983; Stetson *et al.*, 1982; Taylor *et al.*, 1978). The possibility exists that because these studies make use of different experimental models, differences between results presented here and these studies could be ascribed to differences in experimental model. Not so for a study by Morris *et al.* (1998). Investigations to look at the acute effects of AVP, were performed on the A6 cell line itself. In their paper, following evidence presented from immunolocalisation and cytoskeletal disruptions, the authors state in their discussion of their results that Na^+ channels are not acutely redistributed to the apical membrane from a cytoplasmic pool.

In further support of the direct phosphorylation idea was the finding that the carboxy-tails of ENaC β and γ subunits could be phosphylated directly by protein kinase A (PKA), the downstream messenger of the AC/cAMP cascade (Shimkets *et al.* 1998). In addition, PKC, aldosterone and insulin were all shown to phosphorylate these subunits of ENaC in the same study. In a related study aimed a clarifying some of the effects of various protein kinases on ENaC activity, Volk *et al.* (2000) demonstrated that PKC had a direct effect in regulating human ENaC kinetics which were expressed in the *Xenopus sp.* oocyte model system. A less specific PKA inhibitor however used in the Volk study seemed to have no effect on ENaC activity.

The other hypothesis often presented as an alternative to direct activation is that on acute cAMP-stimulation, ENaCs are recruited from subapical pools and inserted into the plasma membrane in an active form. The idea of ENaC recruitment has some support from radioiodination studies in A6 cells (Kleyman *et al.*, 1994) and patch clamp studies performed on A6 (Marunaka and Eaton, 1991). Earlier work done by Garty and Edelman (1983) using toad bladder demonstrated the emergence of new (unaltered) channels on AVP stimulation

after membrane trypsinisation had effectively destroyed ENaC function at the apical surface. The AVP response was not diminished significantly, suggesting that these channels had been inaccessible to the proteolytic effects of trypsin, possibly being stored beneath the apical membrane in storage pools. It has also been demonstrated that Nedd4 binding with ENaC acts as a signal for the retrieval and degradation of channels in the apical membrane as a means of regulating functional channel densities at the apical surface (Harvey and Kumar, 1999; Staub *et al.*, 1997b; Staub *et al.*, 2000) in line with the regulated insertion and retrieval hypothesis investigated here.

Although these two hypotheses appear to be contradictory, a closer inspection of evidence for direct phosphorylation raises a number of important issues. As mentioned, most of the studies were performed on non-native tissues or non-epithelial models. Several accessory proteins and the machinery necessary for trafficking events to occur are lacking in the lipid bilayer model and may be deficient in oocyte systems. In the A6 study best suited to compare with the current work (Morris *et al.*, 1998), limitations in terms of experimental technique are evident. Their conclusion that ENaC trafficking does not occur from intracellular pools was drawn mainly from the immunolocalisation studies. The antibodies used were polyclonally derived and therefore less suited for precise localisation studies than equivalent mouse monoclonal antibodies would be. The concentrations of antibody used were also very high (1:20) possibly indicating a lack of specificity. In addition, the cells were imaged using conventional fluorescence microscopy with no image deconvolution or 3-dimensional reconstruction. The authors themselves comment on the inadequacy of the imaging technique used to derive the conclusions on the lack of trafficking. In their summation, they state that, "...immunofluorescence resolution is insufficient (to) rule out shuttling of Na^+ channels between the cell membrane and the cytoplasmic region immediately underlying it". In the case of the MDCK study on PKA phosphorylation of ENaC subunits (Shimkets *et al.*,1998), the results indicate that both β and γ subunits are phosphorylated by PKA. In separate studies however, it

was found that direct phosphorylation by PKA did not translate into direct modulation of ENaC activity (Awayda *et al.*, 1996).

8.1.3. Cytoskeletal Involvement

Evidence for a recruitment scenario is however also plagued with unanswered questions. The hypothesis of channel recruitment from sub-apical pools probably requires the involvement of cytoskeletal elements in order to traffic ENaC-loaded vesicles to the cell surface. Here too contradictory evidence has been reported. Investigations initially focussed on the possibility that actin, microtubules or both these cytoskeletal elements would be involved if trafficking were occurring in ENaC regulation. It could therefore reasonably be expected that disruption of these elements would lead to an alteration in cAMP-mediated ENaC regulation and consequently the I_{SC} response. This has not always been the case however. By making use of colchicin, a microtubule disrupter, Taylor and colleagues (1978) showed no alteration in the I_{SC} response to AVP despite alterations in water transport in the toad bladder. Similar results were reported on studies with frog skin (Els and Chou, 1993) where colchicin had no apparent effects on channel autoregulation. Studies on A6 cultures using both colchicin and nacodozole, another microtubule disrupter, showed no effect of either drug on AVP-stimulated I_{SC} responses (Morris *et al.*, 1998). In contrast however, Verrey *et al.* (1995) reported that continuous treatment of A6 cells with nacodozole or a colchicin treatment resulted in disruptions of both protein delivery to, and retrieval from, the apical membrane. In addition the authors demonstrated a decreased sodium conductance in both control and AVT stimulated groups as a result of microtubule disruption.

The results from studies of actin depolymerisation/disruption have been equally obscure. In support of a recruitment scenario, the same paper by Verrey *et al.* (1995) once again provided evidence for a microfilament (actin) role in ENaC regulation. Treatment of A6 cultures with

cytochalasin D (an actin depolymerisor) resulted in augmented transepithelial conductance and increased protein secretion, implying a possible barrier function to actin in ENaC delivery. The treatment also increased endocytic uptake in the cells. However, the cytochalasin D treatment reduced the amiloride sensitive sodium response to AVT. In contrast to these findings, Chou and Els (1997) reported no significant alteration in the I_{SC} response to AVP when frog skin was treated with cytochalasin B. Studies on toad urinary bladder by Palmer and Lorenzen (1983) produced a similar result that microfilament disruption did not effect sodium transport, but it was found to effect water transport in this tissue. In addition to model tissue studies, a number of investigations have been carried out using lipid bilayers to demostrate a direct interaction of actin with ENaC subunits. Jovov and colleagues reported direct effects on ENaC kinetics when actin was introduced into a reconstituted artificial lipid bilayer system (Jovov *et al.*, 1999). Further studies of ENaC reconstituted in lipid bilayers (Berdiev *et al.*, 2001) implicate a role for actin in ENaC regulation. Finally, the gating of ENaC by actin and the site of actin regulation on the β-ENaC subunit has recently been identified using a similar technique (Copeland *et al.*, 2001).

From these studies it appears once again that the mode of ENaC regulation is still far from clear. Contradictory evidence has been demonstrated in a variety of model systems. Although the use of different systems may in part explain some of the discrepancies in results, it must also be kept in mind that the two hypotheses need not be mutually exclusive. In fact a range of strategies may be employed by various cell types to regulate ENaC. Direct ENaC phosphorylation for example may "prime" the channel for interactions with trafficking machinery. Non-coordinate expression and regulation of channel subunits has been proposed (Valentijn *et al.*, 1998; Weisz *et al.*, 2000) as another possible regulatory mechanism.

8.2. SUMMARY

With the issue of ENaC regulation not fully dissected, and due to the fact that evidence for trafficking had to date only been indirectly obtained, investigations carried out in this study focussed directly on the issue of acute ENaC regulation by recruitment. In this regard ENaC would need to be inserted from sub-apical pools into the plasma membrane by exocytosis and retrieved by endocytosis following a fairly rapid timecourse not associated with channel production. It is under these assumptions that the investigations detailed below were carried out.

8.2.1. Adenylate Cyclase in A6 Cells

As the effects of ADH/AVP on ENaC were being investigated, early experiments involved arginine vasopressin (AVP) as an agonist. It was found however, that a more pronounced response was observed when the drug forskolin, which acts directly on adenylate cyclase (AC), was employed. Consequently, all investigations made use of similar concentrations of forskolin to elicit a cAMP-mediated response. No evidence was available though for the localisation of AC in A6 cells. As all investigations were to be carried out using forskolin, to better characterise its action, the first results presented (chapter three) used cytochemical techniques to examine the nature and location of the action of forskolin. These results illustrated a number of novel findings relating specifically to A6 cells.

Firstly, localisation of AC in the membranes of mature A6 cultures established a predominantly lateral position for AC activity. Little signal was detected in the basal membranes, possibly due to cell-filter interactions and no signal was ever found on the apical surface of mature cultures. It has also been noted previously that the cells cultured on filter supports take a period from seven to fourteen days to form a mature transporting monolayer (Helman and Liu, 1997). By

investigating the AC activity in maturing A6 cultures a distinct trend in the AC localisation emerged.

The second finding of note therefore was the fact that AC localisation in immature cultures was far more random and not restricted to specific domains of the immature cells. This is probably due to the fact that in immature cultures, cells have not developed a polarised orientation with a distinct apical and basolateral membrane, separated by tight junctions. This is readily demonstrated in the immature cultures by the localisation of AC around almost the entire cellular membrane in cells underlying other cells. Before a monolayered configuration is achieved then, it appears that AC activity can be found wherever there is cell-to-cell contact.

The levels of AC activity were also estimated by making use of a radioactive labelling protocol. At all ages of culture, stimulated cells were found to produce higher levels of cAMP than the unstimulated controls. The level of AC activity was however highly variable in the younger cultures. This probably reflected the variable nature of the AC localisation demonstrated for the younger cultures. What is clear from the results were that the level of cAMP production increased with culture maturation. Consequently, the highest forskolin-induced cAMP levels were reported in cultures of 21 days. This production is significantly greater than similar cultures of only five days.

In all, the AC localisation and activity results reported in chapter three establish that an AC/cAMP secondary messenger pathway is in operation within the cells and that the action of forskolin is via this PKA pathway. The AC is located laterally and actions of agonists like forskolin increase levels of cAMP production. Of importance is the fact that uniform and consistent AC localisation and forskolin responsiveness was only observed in more mature cultures (older than seven days). These results illustrated the need to work with mature transporting cultures in order to obtain reliable, reproducible responses to forskolin stimulation.

8.2.2. Electrophysiology

At the foundation of all the investigations were the electrophysiological results presented in chapter four. The specific pulse protocol of current fluctuation analysis first described by Helman and others (1998), was used to obtain both temporal macroscopic and single-channel data from the A6 epithelial cells under the influence of hormonal stimulation. The investigations established a number of baseline parameters and gave an indication of the single channel responses to forskolin stimulation. Many of the protocols were centred around results obtained from this technique which investigated specifically the rapid response to forskolin (i.e. the elevated intracellular cAMP levels). Tissues mounted in an Ussing chamber under short-circuit conditions indicated I_{SC} rapidly increased by the action of forskolin to a level about twice the original value over a period of about 30 minutes and was consistent with results from other AVT/AVP studies (Morris *et al.*, 1998). When forskolin was removed, I_{SC} dropped back to control values, but at a slightly slower rate and thus took over 40 minutes to return to baseline. Consequently, future protocols ensured sufficient time for both stimulation (to reach a maximum) and washout of stimulus (to return to baseline) in order to be compared to the electrophysiological data.

Of more interest however, was the nature of the I_{SC} response. As information about single-channel parameters could be calculated from the measured data, the single channel parameters responsible for the I_{SC} response could be ascertained. By employing the specific ENaC channel blocker amiloride during all phases of the protocol (control, stimulated and washout events) it was found that sodium ion flux contributed the majority (>90%) of the measured I_{SC}. Thus ENaC was the primary transporter for determining the electrical response observed and discussions of I_{SC} essentially refer to I_{Na} (the macroscopic sodium ion current). So what effect did forskolin have on ENaC?

The two most important findings concerning single channel parameters were that the channel open probability (P_o) fell during forskolin stimulation and that both the number of open channels (N_o) and the total channel number (N_T) increased dramatically over this time. Taking each of these findings separately, they provide strong evidence in support of the recruitment hypothesis. Firstly, the fact that P_o fell during forskolin stimulus strongly refutes the idea that a direct phosphorylation of ENaC contributes to increased sodium transport. For this to be the case, it would be expected that P_o would increase with forskolin stimulation. If phosphorylation were involved in alterations of channel gating, this increase would be detected by an increase in the P_o of the channels. In addition, the single channel currents also fell after the addition of forskolin. This would not be expected if phosphorylation were augmenting sodium transport. The only time a change in P_o would not be detected would be if closed channels were phosphorylated to an open state and the electrically "silent" channels would then be detected as soon as they started transporting. In the same way the increase in channel density at the apical membrane is very likely the result of arrival of new, active channels. The only condition that could account for an increase in channel number by activation through phosphorylation, would once again be if "silent" channels resident in the membrane were activated and started transporting.

Unfortunately, the electrophysiological noise-analysis technique could not distinguish between activation of resident channels and recruitment of stored channels. It is only the active channels which produce a signal, and as long as the active channels (inserted or phosphorylated) are identical, nothing would distinguish one scenario from the other. Therefore, even though the single channel evidence was suggestive of channel recruitment, there was no way of demonstrating unequivocally by noise analysis that this was actually taking place. Nevertheless, the technique provided important information about the time course and extent of forskolin stimulation in A6 epithelia and the effect of forskolin of single channel parameters.

8.2.3. Marker Uptake Studies

In order to find evidence for the involvement of channel recruitment as a means of acute ENaC regulation, the first studies focussed on endocytosis and attempted to use fluid-phase marker uptakes as a probe for this process. Although other similar studies had been performed on A6, using HRP as a marker (Verrey *et al.*, 1993, 1995), several additional components were added to the protocol. One of these was the use of a second marker in addition to HRP, namely conjugated FITC with the potential aim of performing pulse-chase and re-release type investigations. Attempts to use the double markers as indicators of endocytosis were however hampered by the high background problems experienced. A number of adjustments were made to the protocols used in an attempt to reduce the background signal, but despite this the data obtained were far from ideal, and the double marker loading could never be used as originally intended. A second difference in these investigations when compared to earlier work was the acquisition of data over time rather than at the end of an endocytic event.

The information gathered was not entirely without substance and differences in endocytosis were evident. Cells, which received a period of initial forskolin stimulation, took up more marker when compared to the control, unstimulated cells. The rate of endocytosis was also seen to increase under the influence of forskolin when this stimulus was removed and the time course of marker uptake was followed. In the case of these time course investigations, the experiments needed to be performed on cell suspensions, which made comparisons with electrophysiological data impossible as cells had lost the monolayer configuration.

The marker uptake studies did point to the fact that forskolin was in some way involved in alterations of endocytosis. No comments could be inferred about the role of ENaC in the endocytic movements, but it was evident that the machinery involved in protein trafficking was implicated. A further drawback of the marker uptake experiment was the fact that cells needed

to be harvested and destroyed to obtain internalised marker measurements. A more suitable type of investigation was employed in the confocal membrane labelling studies as actions of live transporting cells on filter supports could be viewed directly, in real time and in three dimensions.

8.2.4. Confocal Studies

By making use of live cells in a monolayer configuration, and using a specially designed sealed confocal chamber, it was possible to obtain information about endocytic uptake in the A6 epithelia. The membrane marker, FM4-64 used in all investigations, was desirable in that only the apical membrane of the A6 cell layer could be labelled for study. By tracking the internalisation of labelled membrane in the form of vesicles a clear picture of the role of endocytosis in forskolin pre-stimulated cells could be formed. Several unique findings from this work emerged.

Firstly, there was a distinct difference in endocytosis between cells which had been stimulated with forskolin, washed and allowed to internalise membrane and those which had no pre-stimulation. A greater internalisation of vesicles (i.e. higher vesicle density) can be seen in the experimental cells after the same period of internalisation when compared to controls.

Secondly, by tracking the appearance of vesicles over time it is clear that the rate of endocytosis was also increased under the influence of a forskolin pre-stimulation. The internalisation rate of vesicles was highest right after the forskolin removal (almost a nine-fold increase over control) and gradually plateaued out to rates similar to those of control cells over time. Of interest though was the fact that when the time course of vesicle accumulation was compared to the electrophysiological data, endocytic retrieval corresponded very well to the

disappearance electrically of channels as measured by the total channel number in the electrophysiological results.

The third observation, made possible by the unique characteristics of confocal microscopy, was that the localisation of vesicles within the cells could be ascertained. By performing 3-D reconstructions on labelled cells with internalised vesicles it was possible to determine the fate of vesicles derived from the apical membrane. In control cells, the vesicles appeared to migrate deeper into the cells and coalesce to form larger structures, consistent with the idea of vesicular processing and lysosomal formation observed in other studies of endocytosis. The forskolin pre-treated cells however displayed two distinct vesicle populations. The deeper and larger vesicles observed in the control cells were still found in the experimental cells, but a second more apically located group was also observed. This second group was found close to the apical membrane and vesicles remained in this pool even 60 minutes after the beginning of the endocytic imaging protocol. In the work presented by Morris and colleagues (1998) done on A6 cells using immunofluorescence, the authors indicate that if a sub-apical pool were present in the A6 cells it would need to be located very close to the apical membrane. Due to technical limitations in their methodology the authors were not able to detect this pool and therefore favoured the idea of direct channel activation over channel recruitment as the mechanism for forskolin activation of ENaC. In results presented here, the use of laser confocal microscopy has allowed for a more precise localisation of intracellular organelles and the a distinct vesicle pool has been detected when cells were treated with forskolin. It would be attractive to suggest that this may well be the pool involved in ENaC recruitment, but as only membrane was fluorescently labelled, no indication of ENaC localisation was obtained from these experiments.

This drawback notwithstanding, the data once again indicated that the endocytic machinery was indeed affected by the action of forskolin in a timecourse consistent with earlier electrophysiological results.

With no information available for the involvement of ENaC in this process, an attempt was made to label the channels themselves by making use of a fluorescently-tagged amiloride moiety. The advantage of using such a tag was that it could be applied directly to living cells with no need for fixation and secondary antibody labelling. A second antibody step would certainly be required were antibodies used due to the small numbers of channels available to tag (based on the electrophysiological evidence). This amiloride tag did show colocalisation with internalised membrane, intimating the possibility that ENaC was involved in the endocytic shuttling observed with the FM4-64 marker. Considerations about the nature of the tag cast doubt on the absolute certainty of the colocalised entities though, as amiloride is able to freely disassociate from ENaC and consequently the fluorescent tag may not be a reliable indicator of the presence of ENaC. There was a possibility that the tagged amiloride was merely internalised into the apically-derived vesicles in a free unbound form, and not tagged to ENaC itself. This possibility was somewhat diminished however by the washing protocol used just prior to imaging. The unbound marker would most likely have been removed by the washes and therefore not internalised with the membrane, but the possibility still remained that there was some unbound tag in the internalised vesicles. In addition to this amiloride is also known to bind to other transporters and this would mean that even if bound it may still not have provided information about ENaC itself.

As a result of the difficulties in linking ENaC to the trafficking mechanisms demonstrated to this point, it was decided to decisively label the ENaC subunits by making use of green fluorescent protein.

8.2.5. GFP-ENaC

By making use of an A6 cell line transfected with GFP-ENaC constructs, it was possible to view the direct regulation of the channels in living cells. The transfected cells exhibited increases in levels of sodium transport, which was to be expected with an overproduction of ENaC subunits. The fact that the GFP-tagged subunits were transfected with a constitutive promotor resulted in a constant overproduction of channel subunits. This was evident in the elevated baseline transport rates of the various selected clones above the parental controls. The particular A6 clone used for transfection differed slightly from those used in the studies presented to this point from this laboratory at the University of Cape Town. One of the major differences was the fact that there was a poor response to ADH in these particular cells. Once transfected however, the cells did respond to ADH in a similar manner to A6 cells in this laboratory. Of interest though was the observation that the magnitude of the hormonal response was not proportionally augmented in the transfected cells in contrast to the baseline transport which was markedly increased. Further investigations of the clones at the University of Cape Town demonstrated that the cells responded in the same manner to a forskolin stimulation as had previously been noted, and in the same timeframe as before. In addition, the predominant contribution to the measured I_{SC} was sodium transport via sodium channels noted by the addition of amiloride at the end of each investigation.

It was possible to image the GFP in living cells by confocal microscopy and labelling of the various clones demonstrated an apically localised ENaC pool. Under the influence of forskolin, the pool of localised ENaC could be tracked in 3-D space and was seen to traffic to the apical membrane. On removal of stimulation, the apically located ENaC was moved back into the cells in a timecourse consistent with electrophysiological data. This novel finding was extremely valuable in bringing together the evidence presented by the other techniques.

Up to this point, all evidence for channel trafficking was gathered by indirect methods. Other studies attempting to find evidence for ENaC recruitment were based on indirect methods, used non-epithelial model systems or fixed cell preparations. For the first time, evidence for ENaC recruitment to the apical membrane and removal from the apical surface, under acute stimulation and removal of the stimulus respectively, was obtained in living cells in real time.

8.3. CONCLUSIONS

The combined evidence from electrophysiological, marker uptake, membrane-imaging and live cell GFP-ENaC studies can be used to provide a model for ENaC regulation by the cAMP secondary messenger pathway in A6 cells. Evidence from the various techniques supports the hypothesis of ENaC recruitment from intracellular storage pools. A model of ENaC regulation has been depicted in figure 8.1 and incorporates much of the information gathered by the techniques discussed above and can be summarised as follows:

1) ENaCs are stored in pools beneath the apical membrane and ENaC numbers in these storage pools are augmented either directly by production or indirectly from endocytic retrieval from the apical surface. The GFP-tagged ENaC was localised beneath the apical membrane when imaged by confocal microscopy.

2) There appear to be two distinct pathways for delivery of ENaC in A6 cells. The first is a constitutive and possibly unregulated pathway which delivers channels to the surface without input from the cAMP-dependant secondary messengers. Evidence for this was gained from the transfected A6 cells in which an increased baseline current was observed as a consequence of increased constitutive production.

3) The rates of exocytosis and endocytosis under unstimulated conditions are in equilibrium so that the number of channels resident in the apical membrane remains constant. The evidence for constant membrane turnover can be found in the marker uptake and labelled-membrane confocal studies, which demonstrated constant endocytic retrieval under unstimulated conditions.

4) Membrane retrieved from the surface is destined for degradation well beneath the apical membrane as seen in the deep coalesced vesicles in the confocal studies.

5) Acute stimulation by forskolin results in increase ENaC numbers at the apical membrane from delivery from the storage pool to the apical membrane. This was demonstrated by the current-fluctuation analysis and the imaging the GFP-tagged ENaC subunits.

6) On removal of stimulation, the additional EnaCs which were inserted by exocytosis and are no longer required, are removed from the membrane by fluid-phase endocytic retrieval. The movement of ENaC from the apical surface was observed in the GFP-tagged subunits and endocytosis was demonstrated by fluid-phase and apical membrane marker uptake.

7) The rate of endocytosis after stimulus removal is increased to facilitate the retrieval of ENaC from the apical membrane. This was demonstrated in particular by the confocal labelled-membrane studies on live cells.

8) Once retrieved, a large proportion of the vesicles return to the storage pool area directly beneath the apical membrane, as demonstrated by 3-D confocal analysis.

9) The size of this regulated pool appears to remain constant, despite enhanced channel production, as the size of response in GFP-ENaC cloned cells was not enhanced by increased channel production.

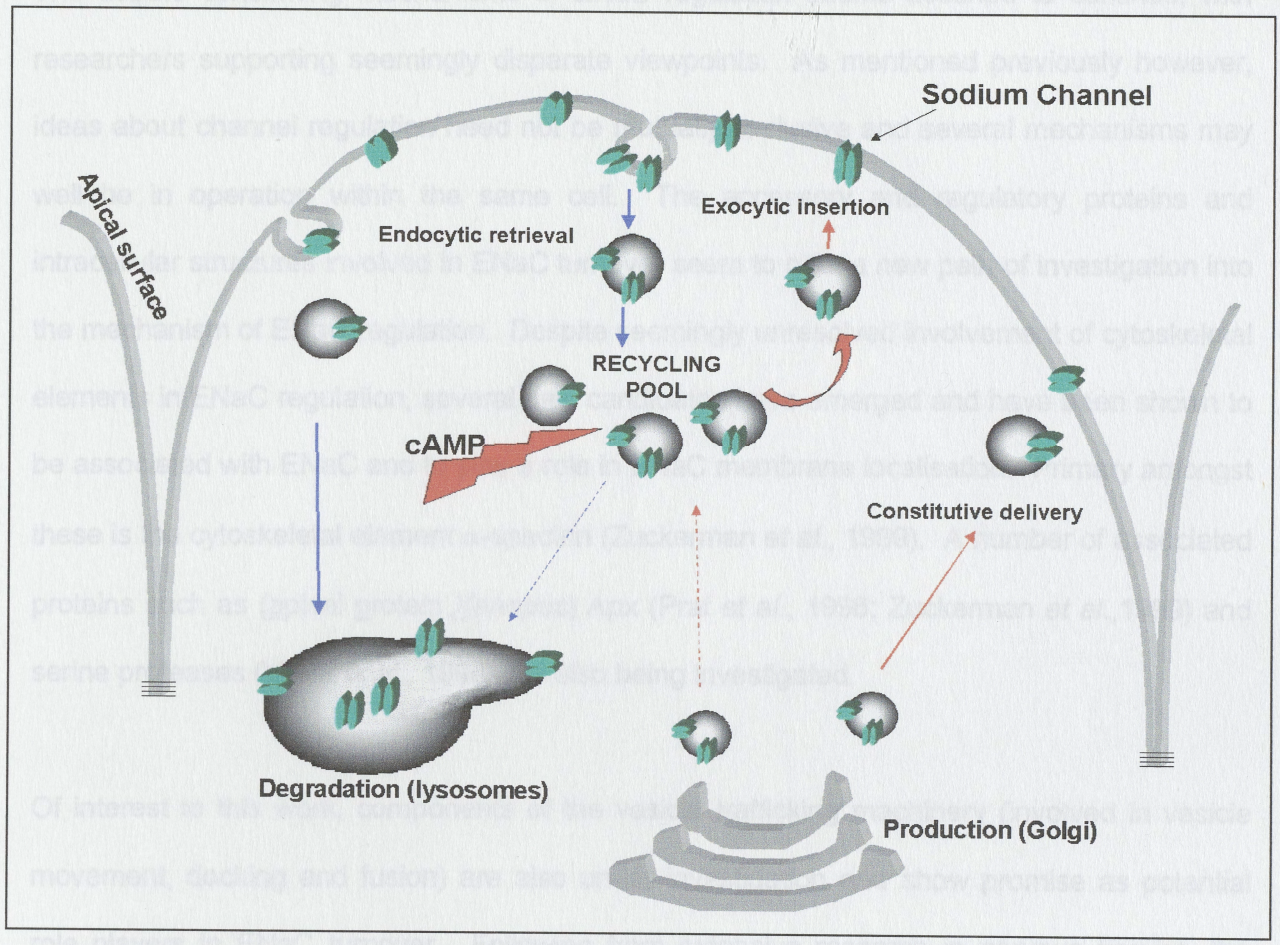

Fig.8.1. Schematic model depicting the mechanism of cAMP-dependant regulation of ENaC in the cultured A6 cell line

8.4. FUTURE WORK

The debate concerning mechanisms of ENaC regulation seems destined to continue, with researchers supporting seemingly disparate viewpoints. As mentioned previously however, ideas about channel regulation need not be mutually exclusive and several mechanisms may well be in operation within the same cell. The accessory and regulatory proteins and intracellular structures involved in ENaC turnover seem to offer a new path of investigation into the mechanism of ENaC regulation. Despite seemingly unresolved involvement of cytoskeletal elements in ENaC regulation, several new candidates have emerged and have been shown to be associated with ENaC and to play a role in ENaC membrane localisation. Primary amongst these is the cytoskeletal element α-spectrin (Zuckerman *et al.*, 1999). A number of associated proteins such as (apical protein *Xenopus*) Apx (Prat *et al.*, 1996; Zuckerman *et al.*,1999) and serine proteases (Vallet *et al.*, 1998) are also being investigated.

Of interest to this work, components of the vesicle trafficking machinery (involved in vesicle movement, docking and fusion) are also under investigation and show promise as potential role players in ENaC turnover. Following from extensive research in nervous tissues, the (soluble N-ethylmaleimide-sensitive factor attachment protein receptor) SNARE family of proteins have recently been shown to affect ENaC regulation in an oocyte model system, in particular the SNARE syntaxin 1a (Juanjuan *et al.*, 1999; Saxena *et al.*, 1998) and these same proteins have recently been identified in A6 epithelia. Small GTPases (Rab and Ras proteins) associated with the endocytic machinery may also be involved in the ENaC regulatory process (Mastroberardino *et al.*, 1998; Somsel Rodman and Wandinger-Ness, 2000). The cytoplasmic tails of ENaC subunits are implicated in determining their turnover as interactions with these intracellular portions and interacting proteins like the ubiquitin ligase, Nedd4 has been investigated (Abriel *et al.*, 1999; Goulet *et al.*, 1998; Staub *et al.*, 1996,1997a, 2000).

These studies make most sense when viewed within the context of regulated ENaC recruitment and turnover at the apical membrane and it is in these various lines where future work seems likely to progress and expand our understanding of ENaC and its regulation.

REFERENCES

Abramcheck, F.J., Van Driessche, W. and Helman, S.I. (1985). Autoregulation of apical membrane Na^+ permeability of tight epithelia. Noise analysis with amiloride and CGS 4270. *Journal of General Physiology*. **85**: 555-582.

Abramow, M., Beauwens, R and Cogan, E. (1987). Cellular events in vasopressin action. *Kidney International. Supplemental*. **32**: S56-S66.

Abriel H. and Horisberger, J.D. (1999). Feedback inhibition of rat amiloride-sensitive epithelial sodium channels expressed in *Xenopus laevis* oocytes. *Journal of Physiology*. **516**: 31-43.

Abriel, H., Loffing, J., Rebhun, J.F., Pratt, J.H., Schild, L., Horisberger, J.-D., Rotin, D and Staub, O. (1999). Defective regulation of the epithelial Na^+ channel by Nedd4 in Liddle's syndrome. *Journal of Clinical Investigation*. **103**: 667-673.

Ahn, Y.J., Brooker, D.R., Kosari, F., Harte, B.J., Li, J., Mackler, S.A. and Kleyman, T.R. (1999). Cloning and functional expression of the mouse epithelial sodium channel. *American Journal of Physiology*. **277**: F121-F129.

Alberts, B., Bray, D. and Lewis, J. (1989). The plasma membrane. In: *Molecular Biology of the Cell*. 2nd edition. Garland Publishing, New York. pp. 275-280.

Ali, N., Kantachuvesiri, S., Smallwood, J.I., Macala, L.J., Isales, C., Ji, J., Reilly, R. and Hayslett, J.P. (1998). Vasopressin-induced activation of protein kinase C in renal epithelial cells. *Biochimica et Biophysica Acta*. **1402**: 188-196.

Almeida, A.J. and Burg, M.B. (1982). Sodium transport in the rabbit connecting tubule. *American Journal of Physiology*. **243**: C842-C847.

Alvarez de la Rosa, D., Canessa, C.M., Fyfe, G.K. and Zhang, P. (2000). Structure and regulation of amiloride-sensitive sodium channels. *Annual Review of Physiology*. **62**: 573-594.

Ammar, A., Roseau, S. and Butlen, D. (1992). Pharmacological characterization of V_{1a} vasopressin receptors in the rat cortical collecting duct. *American Journal of Physiology*. **262**: F546-F553.

Anderson, J.M. and Stevenson, B.R. (1992). The molecular structure of the tight junction. In: *Tight Junctions*. Creijido, M. (ed.). CRC Press, Boca Raton. pp. 77-90.

Anderson, J.M. and Van Itallie, C.M. (1995). Tight junctions and the molecular basis for regulation of paracellular permeability. *American Journal of Physiology.* **269**: G467-G475.

Ando, Y. and Asano, Y. (1993). Functional evidence for an apical V_1 receptor in rabbit cortical collecting duct. *American Journal of Physiology.* **264**: F467-471.

Ando, Y., Tabei, K. and Asano, Y. (1991). Luminal vasopressin modulates transport in the rabbit cortical collecting duct. *Journal of Clinical Investigation.* **88**: 952-959.

Asher, C., Singer, D., Eren, R.,Yeger, O., Dascal, N. and Garty, H. (1992). NaCl dependent expression of an amiloride-blockable Na^+ channel in *Xenopus sp.* oocytes. *American Journal of Physiology.* **262**: G244-G248.

Asher, C., Wald, H., Rossier, B.C. and Garty, H. (1996). Aldosterone-induced increase in the abundance of Na^+ channel subunits. *American Journal of Physiology.* **271**: C605-C611.

Atia, F., Zeiske, W and Van Driessche, W. (1999). Secretory apical Cl^- channels in A6 cells: possible control by cell Ca^{2+} and cAMP. *Pflügers Archiv: European Journal of Physiology.* **434**: 344-353.

Aubin, J. (1979). Autofluorescence of viable cultured mammalian cells. *Journal of Histochemical Cytochemistry.* **27**: 36-43.

Ausiello, D. (1991). G-protein function in vasopressin-sensitive epithelia. In: *Vasopressin.* Volume 208. Jard, S. and Jamison, R. (eds). Collogue INSERM/John Libbey Eurotext Ltd. pp. 135-145.

Ausiello, D.A., Stow, J., Cantiello, H.F., de Almeida, J.B. and Benos, D.J. (1992). Purified epithelial Na^+ channel complex contains the pertussis toxin sensitive G_{ai-3} protein. *Journal of Biological Chemistry.* **267**: 4759-4765.

Awayda, M.S. (1999). Regulation of the epithelial Na^+ channel by intracellular Na^+. *American Journal of Physiology.* **277**: C216-C224.

Awayda, M.S., Ismailov, I.I., Berdiev, B.K., Fuller, C.M. and Benos, D.J. (1996). Protein kinase regulation of a cloned epithelial Na^+-channel. *Journal of General Physiology.* **108**: 49–65.

Balda, M. S., Gonzalez-Mariscal, R. G., Contreras, M., Macias-Silva, M.,Torres-Marquez, M. E., Garcia-Sainz, J. A. and Cereijido, M. (1991). Assembly and sealing of tight junctions: possible participation of G-proteins,phospholipase C, protein kinase C and calmodulin. *Journal of Membrane Biology.* **122**: 193-202.

Barden, H. (1978). Further histochemical studies characterizing the lipofuscin component of human neuromelanin. *Journal of Neuropathology and Experimental Neurology.* **37**: 437-451.

Bastl, C.P. and Hayslett, J.P. (1992). The cellular action of aldosterone in target epithelia. *Kidney International.* **42**: 250-264.

Baxendale, L.M. and Helman, S.I. (1986). Sodium concentration dependence of apical membrane single channel Na^+ current and density of nondepolarized frog skin (three state model). *Biophysical Journal.* **49**: 160a.

Baxendale-Cox, L.M., Duncan, R.L., Liu, X., Baldwin, K., Els, W.J. and Helman, S.I. (1997). Steroid hormone-dependant expression of blocker-sensitive ENaCs in apical membranes of A6 epithelia. *American Journal of Physiology.* **273**: C1650-C1656.

Benjamin, W.B. and Singer, I. (1974). Aldosterone-induced protein in toad urinary bladder. *Science.* **186**: 269-272.

Benos, D.J. (1982). Amiloride: a molecular probe of sodium transport in tissues and cells. *American Journal of Physiology.* **242**: C131-C145.

Benos, D.J., Mandel, L.J. and Simon, S.A. (1980). Cation selectivity and competition at the sodium entry site in frog skin. *Journal of General Physiology.* **76**: 233-247.

Benos, D.J., Cunningham, S., Baker, R.R., Beason, K.B., Oh, Y. and Smith, P.R. (1992). Molecular characteristics of amiloride-sensitive sodium channels. *Review of Physiology Biochemistry and Pharmacology.* **120**: 31-113.

Benos, D.J., Saccomani, G. and Sariban-Sohraby, S. (1987). The epithelial sodium channel. Subunit number and location of the amiloride binding site. *Journal of Biological Chemistry.* **262**: 10613-10618.

Benson, H.C., Meyer, R.A. and Zaruba, M.E. (1979). Cellular autofluorescence – is it due to flavins? *Journal of Histological Cytochemistry.* **27**: 44-48.

Bentzel, C. J., Hainau, S., Ho, S., Hui, S. W., Edelman, A., Anagnostopoulos, T. and Benedetti, E. L. (1980). Cytoplasmic regulation of tight junction permeability: effect of plant cytokines. *American Journal of Physiolology.* **239**: C75-C89.

Berdiev, B.K., Latorre, R., Benos, D.J. and Ismailov, I.I. (2001). Actin modifies Ca^{2+} block of epithelial Na^+ channels in planar lipid bilayers. *Biophysical Journal.* **80**: 2176-2186.

Beron, J., Mastroberardino, L. Spillmann, A. and Verrey, F. (1995). Aldosterone modulates sodium kinetics of Na,K-ATPase containing an alpha 1 subunit in A6 kidney cell epithelia. *Molecular Biology of the Cell.* **6**: 261-271.

Betz, W.J., Mao, F. and Smith, C.B. (1996). Imaging exocytosis and endocytosis. *Current Opinions in Neurobiology.* **6**: 365-371.

Bindels, R.J.M., Schafer, J.A. and Reif, M.C. (1988). Stimulation of sodium transport by aldosterone and arginine vasotocin in A6 cells. *Biochimica et Biophysica Acta.* **972**: 320-330.

Bindslev, N., Cuthbert, A.W., Edwardson, J.M. and Skadhauge, E. (1982). Kinetics of amiloride action in the hen coprodaeum *in vitro*. *Pflügers Archiv: European Journal of Physiology.* **392**: 340-346.

Blazer-Yost, B.L. and Cox, M. (1988). Insulin-like growth factor I stimulates renal epithelial Na^+ transport. *American Journal of Physiology.* **255**: C413-C417.

Blazer-Yost, B.L., Geheb, M., Preston, A., Handler, J. and Cox, M. (1982). Aldosterone-induced proteins in renal epithelia. *Biochimica et Biophysica Acta.* **719**: 158–161.

Blazer-Yost, B., Cox, M. and Furlanetto, R. (1989). Insulin and IGF-I receptor-mediated Na^+ transport in toad urinary bladders. *American Journal of Physiology.* **257**: C612-C620.

Blazer-Yost, B.L., Liu, X. and Helman, S.I. (1998). Hormonal regulation of ENaCs: insulin and aldosterone. *American Journal of Physiology.* **274**: C1373–C1379.

Blazer-Yost, B.L., Butterworth, M.B., Hartman, A.D., Parker, G.E., Faletti, C.J., Els, W.J. and Rhodes, S.J. (2001). Charaterization and imaging of A6 epithelial cell clones expressing fluorescently labeled ENaC subunits. *American Journal of Physiology.* **281**: C624-C632.

Boucher, R.C and Gatzy, J.T. (1983). Characteristics of sodium transport by excised rabbit trachea. *Journal of Applied Physiology.* **55**: 1877-1883.

Bradford, A.L., Ismailov, I.I., Achard, J.-M., Warnock, D.G., Bubien, J.K. and Benos, D.J. (1995). Immunopurification and functional reconstruction of Na^+ channel complex from rat lymphocytes. *American Journal of Physiology.* **269**: C601-C611.

Breyer, M.D. (1991). Feedback inhibition of cyclic adenosine monophosphate-stimulated Na^+ transport in the rabbit cortical collecting duct via Na^+-dependent basolateral Ca^{2+} entry. *Journal of Clinical Investigation.* **88**: 1502-1510.

Briffeuil, P., Thibaut-Vercruyssen, R. and Ronveaux-Dupal, M.-F. (1994). Ciliation of the bovine aortic endothelial cells in culture. *Atherosclerosis.* **106**: 75-81.

Brignoni, M., Pignataro, O.P., Rodriguez, M.L. Alvarez, A., Vega-Salas, D.E., Rodriguez-Boulan, E. and Salas, P.J. (1995). Cyclic AMP modulates the rate of "constitutive" exocytosis of apical membrane proteins in Madin-Darby canine kidney cells. *Journal of Cell Science.* **108**: 1931-1943.

Bubien, J.K., and Warnock, D.G. (1993). Amiloride-sensitive sodium conductance in human B lymphoid cells. *American Journal of Physiology.* **265**: C1175-C1183.

Butterworth, M.B., Helman, S.I. and Els, W.J. (2001). cAMP-sensitive endocytic trafficking in A6 epithelia. *American Journal of Physiology.* **280**: C752-C762.

Candia, O., Mia, A.J. and Yorio, T. (1993). Influence of filter supports on transport characteristics of cultured A6 kidney cells. *American Journal of Physiology.* **265**: C1479-C1488.

Canessa, C.M., Horisberger, J.-D. and Rossier, B.C. (1993). Epithelial sodium channel related to proteins involved in neurodegeneration. *Nature.* **361**: 467-470.

Canessa, C.M., Schild, L., Buell, G., Thorens, B., Gautschi, I., Horisberger, J.-D. and Rossier, B.C. (1994a). Amiloride-sensitive epithelial Na^+ channel is made of three homologous subunits. *Nature.* **367**: 463-467.

Canessa, C.M., Mérillat, A.-M. and Rossier, B.C. (1994b). Membrane topology of the epithelial sodium channel. *American Journal of Physiology.* **267**: C1682-C1690.

Canessa, C.M., Horisberger, J.-D., Schild, L. and Rossier, B.C. (1995). Expression cloning of the epithelial sodium channel. *Kidney International.* **48**: 950-955.

Cantiello, H.F. (1995). Role of the actin cytoskeletonon epithelial Na+ channel regulation. *Kidney International.* **48**: 970-984.

Cantiello, H.F., Patenaude, C.R. and Ausiello, D.A. (1989). G-protein subunit, α_i-3, activates a pertussis toxin-sensitive Na^+ channel from the epithelial cell line A6. *Journal of Biological Chemistry.* **264**: 20867-20870.

Cereijido, M., González-Mariscal, L., Contreras, R.G., Gallardo, J.M., García-Villegas, R. and Valdés, J. (1993). The making of a tight junction. *Journal of Cell Science, Supplement.* **17**: 127-132.

Chalfant, M.L., Coupaye-Gerard, B. and Kleyman, T.R. (1993). Distinct regulation of Na^+ reabsorption in Cl^- secretion by argenine vasopressin in the amphibian cell line A6. *American Journal of Physiology.* **264**: C1480-C1488.

Chalfant, M.L., Denton, J.S., Langloh, A.L., Karlson, K.H., Loffing, J., Benos, D.J. and B.A. Stanton, B.A. (1999). The NH_2 terminus of the epithelial sodium channel contains an endocytic motif. *Journal of Biological Chemistry.* **274**: 32889-32896.

Chalfie, M. and Wollinsky, E. (1990). The identification and suppression of inherited neurodegeneration in *Caenorhabditis elegans. Nature.* **345**: 410-416.

Champigneulle, A., Siga, E., Vassent, G. and Imbert-Teboul, M. (1993). V_2-like vasopressin receptor mobilizes intacellular Ca^{2+} in rat medullary collecting tubules. *American Journal of Physiology.* **265**: F35-F45.

Chang, S.S., Grunder, S., Hanukoglu, A., Rosler, A., Mathew, P.M., Hanukoglu, I., *et al.* (1996). Mutations in subunits of the epithelial sodium channel cause salt wasting with hyperkalaemic acidosis, pseudohypoaldosteronism type 1. *Nature Genetics.* **12**: 248-253.

Chen, H.I., Einbond, A., Kwak, S.-J., Linn, H., Koepf, E. Peterson, S., Kelly, J.W. and Sudol, M. (1997). Characterization of the WW domain of human Yes-associated protein and its polyproline-containing ligands. *Journal of Biological Chemistry.* **272**: 17070-17077.

Chou, C.L., Yip, K.P., Michea, L., Kador, K., Ferraris, J.D., Wade, J.B. and Knepper, M.A. (2000). Regulation of aquaporin-2 trafficking by vasopressin in the renal collecting duct. Roles of rynodine-sensitive Ca^{2+} and calmodulin. *Journal of Biological Chemistry.* **275**: 36839-36846.

Chou, K.-Y. and Els, W.J. (1997). Effects of disassembly of actin microfilaments on the AVP-induced regulation of sodium channel densities in frog skin epithelium. *Biology of the Cell.* **89**: 285-294.

Chraïbi, A., Vallet, V., Firsov, D., Kharoubi Hess, S., Horisberger, J.-D. (1998). Protease modulation of the activity of the epithelial sodium channel expressed in *Xenopus sp.* oocytes. *Journal of General Physiology.* **111**: 127-38.

Civan, M.M., Peterson-Yantorno, K. and O'Brien, T.G. (1988). Insulin and phorbol ester stimulate conductive Na^+ transport through a common pathway. *Proceedings of the National Academy of Sciences of the USA.* **85**: 963-967.

Civan, M.M., Peterson-Yantorno, K., George, K. and O'Brien, T.G. (1989). Interactions of TPA and insulin on Na^+ transport across frog skin. *American Journal of Physiology.* **256**: C569-C578.

Clauss, W. and Skadhauge, E. (1988). Modulation of Na^+ and Cl^- transport by mineralocorticoids. *Comparative Biochemistry and Physiology.* **90**: 583-589.

Clauss, W., Arnason, S.S., Munck, B.G. and Skadhauge, E. (1984). Aldosterone-induced sodium transport in the lower intestine. Effects of varying NaCl intake. *Pflügers Archiv: European Journal of Physiology.* **401**: 354-360.

Clauss, W., Durr, J.E., Guth, D. and Skadhauge, E. (1987). Effects of adrenal steroids on Na^+ transport in the lower intestine (Corprodeum) of the hen. *Journal of Membrane Biology.* **96**:141-152.

Cody, C. W., Prasher, D. C., Westler, W. M., Prendergast, F. G. and Ward, W. W. (1993). Chemical structure of the hexapeptide chromophore of *Aequorea* green-fluorescent protein. *Biochemistry.* **32**: 1212–1218.

Coleman, R.A. and Wade, J.B. (1994). ADH-induced recycling of fluid-phase marker from endosomes to the mucosal surface in toad bladder. *American Journal of Physiology.* **267**: C32-C38.

Copeland, S.J., Berdiev, B.K., Ji, H.L., Lockhart, J., Parker, S., Fuller, C.M. and Benos, D.J. (2001). Regions in the carboxy terminus of alpha-bENaC involved in gating and functional effects of actin. *American Journal of Physiology.* **281**: C231-240.

Cormack, B. P., Valdivia, R. and Falkow, S. (1996). FACS-optimized mutants of the green fluorescent protein (GFP). *Gene.* **173**: 33–38.

Correa, F.M., Innis, R.B., Rouot, B., Pasternak, G.W. and Snyder, S.H. (1980). Fluorescent probes of alpha- and beta-adrenergic and opiate receptors: biochemical and histochemical evaluation. *Neuroscience Letters.* **16**: 47-53.

Coupaye-Gerard, B., Kim, H.J., Singh, A. and Blazer-Yost, B.L. (1994). Differential effects of brefeldin A on hormonally regulated Na^+ transport in a model renal epithelial cell line. *Biochimica et Biophysica Acta.* **1190**: 449-456.

Crowe, W.E., Ehrenfeld, J., Brochiero, E. and Wills, N.K. (1995). Apical membrane sodium and chloride entry during osmotic swelling of renal (A6) epithelial cells. *Journal of Membrane Biology.* **144**: 81-91.

Cutler, L.S. (1983). Cytochemical methods for the localization of adenylate cyclase. A review and evaluation of the efficiency of the procedures. *Journal of Histochemistry and Cytochemistry.* **31**: 85-93.

Cutler, L.S. and Christian, C.P. (1980). Cytochemical localization of adenylate cyclase. *Journal of Histochemistry and Cytochemistry.* **28**: 62-65.

Davis, W.L., Jones, R.G. and Googman, D.B. (1987). Electron microscopic cytochemical localization of adenylate cyclase in amphibian urinary bladder epithelium: effects of antidiuretic hormone. *Journal of Histochemistry and Cytochemistry*. **35**: 103-111.

Davidson, M.W. and Abramowitz, M. (1989). Optical Microscopy. *Olympus America, Inc. Melville, New York*. pp1-41.

De Keyzer, Y., Auzan, C., Lenne., F., Beldjord, C., Thibonnier, M., Bertagna, X. and Clauser, E. (1994). Cloning and characterization of the human V3 pituitary vasopressin receptor. *FEBS Letters*. **356**: 215-220.

Denker, B.M. and Nigam, S.K. (1998). Molecular structure and assembly of the tight junction. *American Journal of Physiology*. **274**: F1-F9.

Dinudom, A., Harvey, K.F., Komwatana, P., Young, J.A., Kumar, S. and Cook, D.I. (1998). Nedd4 mediates control of an epithelial Na^+ channel in salivary duct cells by cytosolic Na^+. *Proceedings of the National Academy of Sciences of the USA*. **95**: 7169-7173.

Doi, Y. and Marunaka, Y. (1995). Antidiuretic hormone decreases the intracellular pH in distal nephron epithelium (A6) by inhibiting Na^+/H^+ exchange. *General Pharmacology*. **26**: 723-726

Dowson, J.H. (1982). The evaluation of autofluorescence emission spectra derived from neuronal lipopigment. *Journal of Microscopy*. **128**: 261-270.

Dowson, J.H. (1983). Autofluorescence emission spectra of neuronal lipopigment in a case of adult-onset ceroidosis (Kufs' disease). *Acta Neuropathologica*. **59**: 241-245.

Driscoll, M. and Chalfie, M. (1991). The mec-4 is a member of a family of *Caenorhabditis elegans* genes that can mutate to induce neuronal degeneration. *Nature*. **349**: 588-593.

Drudin, D.G. and Nelson, W.J. (1996). Origins of cell polarity. *Cell*. **84**: 335-344.

Duc, C.N., Farman, N., Canessa, C.M., Bonvalet, J.-P. and Rossier, B.C. (1994). Cell-specific expression of epithelial sodium channel α, β and γ subunits in aldosterone-responsive epithelia from the rat: localization by *in situ* hybridisation and immunocytochemistry. *Journal of Cell Biology*. **127**: 1907-1921.

Duffy, J.L. and Suzuki, Y. (1968). Ciliated human renal proximal tubule cells. *American Journal of Pathology*. **53**: 609-616.

Eaton, D.C. and Marunaka, Y. (1990). Ion channel fluctuations: "Noise" and single-channel measurements. In: *Channels and Noise in Epithelial Tissues*. Helman, S.I. and Van Driessche, W. (eds.). In: *Current Topics in Membranes and Transport*. Volume 37. Bronner, F. (ed.). Academic Press, New York. pp. 61-116.

Ecelbarger, C.A., Chou, C.-L., Lolait, S.J., Knepper and DiGiovanni, S.R. (1996). Evidence for dual signalling pathways for V_2 vasopressin receptor in rat inner medullary collecting ducts. *American Journal of Physiology*. **270**: F623-F633.

Edinger, R.S., Rokaw, M.D. and Johnson, J.P. (1999). Vasopressin stimulates sodium transport in A6 cells via a phosphatidylinositide 3-kinase-dependent pathway. *American Journal of Physiology*. **277**: F575: F579.

Els, W.J. and Chou, K.-Y. (1993). Sodium-dependent regulation of epithelial sodium channel densities in frog skin: a role for the cytoskeleton. *Journal of Physiology*. **462**: 447-464.

Els, W.J. and Helman, S.I. (1981). Vasopressin, theophylline, PGE_2, and indomethacin on active Na^+ transport in frog skin: studies with microelectrodes. *American Journal of Physiology*. **241**: F279-F288.

Els, W.J. and Helman, S.I. (1989). Regulation of epithelial sodium channel densities by vasopressin signalling. *Cell Signalling*. **1**: 533-539.

Els, W.J. and Helman, S.I. (1991). Activation of epithelial Na^+ channels by hormonal and autoregulatory mechanisms of action. *Journal of General Physiology*. **98**: 1197-1220.

Els, W.J. and Mahlangu, A.F.D. (1987). Microelectrode studies on the effects of exogenous cyclic adenosine monophosphate on active sodium transport in frog skin. *Journal of Physiology*. **388**: 547-539.

Erlij, D., De Smet, P. and Van Driessche, W. (1994). Effect of insulin on area and Na^+ channel density of apical membrane of cultured toad kidney cells. *Journal of Physiology*. **481**: 533-542.

Erlij, D., De Smet, P. Mesotten, D. and Van Driessche, W. (1999). Forskolin increases apical sodium conductance in cultured toad kidney cells (A6) by stimulating membrane insertion. *Pflügers Archiv: European Journal of Physiology*. **438**: 195-204.

Eskandari, S., Snyder, P.M., Kremna, M., Zampighi, G.A., Welsh, M.J. and Wright, E.M. (1999) Number of subunits comprising the epithelial sodium channel. *Journal of Biological Chemistry*. **274**: 27281-27286.

Fidelman, M.L., May, J.M., Biber, T.U. and Watlington, C.O. (1982). Insulin stimulation of Na^+ transport and glucose metabolism in cultured kidney cells. *American Journal of Physiology*. **242**: C121-C123.

Findling, J.W., Raff, H., Hansson, J.H. and Lifton, R.P. (1997). Liddle's syndrome: prospective genetic screening and suppressed aldosterone secretion in an extended kindred. *Journal of Clinical Endocrinology and Metabolism*. **82**: 1071-1074.

Firsov, D., Gautschi, I., Merillat, A.-M., Roddier, B.C. and Schild, L. (1998). The heterotetrameric architecture of the epithelial sodium channel (ENaC). *EMBO Journal*. **17**: 344-352.

Firsov, D., Robert-Nicoud, M., Gruender, S., Schild, L. and Rossier, B. C. (1999). Mutational analysis of cysteine-rice domains of the epithelium sodium channel (ENaC). *Journal of Biological Chemistry*. **274**: 2743-2749.

Fischer, H. and Clauss, W. (1990). Regulation of Na^+ channels in frog lung epithelium: a target for aldosterone action. *Pflügers Archiv: European Journal of Physiology*. **416**: 62-67.

Fisher, R.S., Grillo, F.G. and Sariban-Sohraby, S. (1996). Brefeldin A inhibition of apical Na^+ channels in epithelia. *American Journal of Physiology*. **270**: C138-C147.

Fishman, H.M. and Leuchtag, H.R. (1990). Electrical noise in physics and biology. In: *Channels and Noise in Epithelial Tissues*. Helman, S.I. and Van Driessche, W. (eds.). In: *Current Topics in Membranes and Transport*. Volume 37. Bronner, F. (ed.). Academic Press, New York. pp. 4-36.

Frindt, G. and Windhager, E.E. (1990). Ca^{2+}-dependent inhibition of sodium transport in rabbit cortical collecting tubules. *American Journal of Physiology*. **258**: F568-F582.

Frindt, G., Silver, R.B., Windhager, E.E. and Palmer, L.G. (1993). Feedback regulation of Na^+ channels in rat CCT. II. Effects of inhibition of Na^+ entry. *American Journal of Physiology*. **264**: F565-F574.

Frindt, G., Palmer, L.G. and Windhager, E.E. (1995). Feedback regulation of Na^+ channels in rat CCT. IV. Mediation by activation of protein kinase C. *American Journal of Physiology*. **270**: F371-F376.

Frindt, G., Palmer, L.G. and Windhager, E.E. (1996). Feedback regulation of Na^+ channels in rat CCT. IV. Mediation by activation of protein kinase C. *American Journal of Physiology*. **270**: F371-F376.

Frings, S., Purves, R.D. and MacKnight. (1988). Single-channel recordings from the apical membrane of the toad urinary bladder epithelial cell. *Journal of Membrane Biology*. **106**: 157-172.

Fuchs, W., Hvidd-Larsen, E., Lindemann, B. (1977). Current-voltage curve of sodium channels and concentration dependence of sodium permeability in frog skin. *Journal of Physiology*. **267**: 137166.

Fuller, C.M., Awada, M.S., Arrate, M.P., Bradford, A.L., Morris, R.G., Canessa, C.M. and Rossier, B.C. (1995). Cloning of a bovine renal epithelial Na^+ channel subunit. *American Journal of Physiology*. **269**: C641-C654.

Fyfe, G.K. and Canessa, C.M. (1998). Subunit composition determines the single channel kinetics of the epithelial sodium channel. *Journal of General Physiology*. **112**: 423-432.

Ganong, W.F. (1991). *Review of Medical Physiology*. 15th Edition. Prentice-Hall, Englewood Cliffs, New Jersey. pp.26-40.

Ganote, C.E., Grantham, J.J., Moses, N.L., Burg, M.B. and Orloff, J. (1968). Ultrastructural studies of vasopressin effect on isolated perfused renal-collecting tubules of the rabbit. *Journal of Cell Biology*. **36**: 355-367.

Garty, H. (1986). Mechanisms of aldosterone action in tight epithelia. *Journal of Membrane Biology*. **90**: 193-205.

Garty, H. (1992). Regulation of Na^+ permeability by aldosterone. *Seminars in Nephrology*. **12**: 24-29.

Garty, H. and Benos, D.J. (1988). Characteristics and regulatory mechanisms of the amiloride-blockable Na^+ channel. *Physiological Reviews*. **68**: 309-373.

Garty, H. and Edelman, I.S. (1983). Amiloride-sensitive trypsinization of apical sodium channels. Analysis of hormonal regulation of sodium transport in toad bladder. *Journal of General Physiology*. **81**: 785-803.

Garty, H. and Palmer, L.G. (1997). Epithelial sodium channels: function, structure, and regulation. *Physiological Reviews*. **77**: 359-396.

Geheb, M., Hercker, E., Singer, I. and Cox, M. (1981a). Subcellular localization of aldosterone-induced proteins in toad urinary bladder. *Biochimica et Biophysica Acta*. **641**: 422-426.

Geheb, M., Huber, G., Hercker, E. and Cox, M. (1981b). Aldosterone-induced proteins in toad urinary bladders. Identification and characterization using two-dimensional polyacrylamide gel electrophoresis. *Journal of Biological Chemistry*. **256**: 11716-11723.

Geheb, M., Alvis, R., Hercker, E. and Cox, M. (1983). Mineralocorticoid-specificity of aldosterone induced protein synthesis in giant-toad (*Bufo marinus*) urinary bladders. *Biochemistry Journal*. **214**: 29-35.

Gensler, S., Sander, A., Korngreen, A., Traina, G., Giese, G. and Witzmann, V. (2001). Assembly and clustering of acetylcholine receptors containing GFP-tagged epsilon or gamma subunits: selective targeting to the neuromuscular junction in vivo. *European Journal of Biochemistry*. **268**: 2209-2217.

Gogelein, H. and Greger, R. (1986). Na^+-selective channels in the apical membrane of rabbit late proximal tubules (pars recta). *Pflügers Archiv: European Journal of Physiology*. **406**: 198-203.

Goldstein, O., Asher, C. and Garty, H. (1997). Cloning and induction by low NaCl intake of avian intestine Na^+ channel subunits. *American Journal of Physiology*. **272**: C270-C277.

Goulet, C.C., Volk, K.A., Adams, C.M., Prince, L.S., Stokes, J.B. and Snyder, P.M. (1998). Inhibition of the epithelial Na^+ channel by interaction of Nedd4 with a PY motif deleted in Liddle's syndrome. *Journal of Biological Chemistry*. **273**: 30012-30017.

Grantham, J.J. and Burg, M.B. (1962). Effect of vasopressin and cyclic AMP on permeability of isolated collecting tubules. *American Journal of Physiology*. **211**: 255-259

Guma, A., Zierath, J.R., Walberg-Henriksson, H. and Klip, A. (1995). Insulin induces translocation of GLUT-4 glucose transporters in human skeletal muscle. *American Journal of Physiology*. **268**: E613–E622, 1995.

Gumbiner, B., Lowenkopf, T. and Apatira, D. (1991). Identification of a 160-kDa polypeptide that binds to the tight junction protein ZO-1. *Proceedings of the National Academy of Sciences of the USA*. **88**: 3460-3464.

Gustafson, C.E., Levine, S., Katsura, T., McLaughlin, M., Aleixo, M.D. Tamarappoo, B.K., Verkman, A.S. and Brown, D. (1998). Vasopressin regulated trafficking of a green fluorescent protein-aquaporin 2 chimera in LLC-PK1 cells. *Histochemistry and Cell Biology*. **110**: 377-386.

Hamilton, K.L., and Eaton, D.C. (1986). Regulation of single sodium channels in renal tissue: a role in sodium homeostasis. *Federation Proceedings*. **45**: 2713-2717.

Handler, J.S., Preston, A.S. and Orloff, J. (1972). Effect of ADH, aldosterone, ouabain, and amiloride on toad bladder epithelial cells. *American Journal of Physiology.* 222: 1071-1074.

Handler, J.S., Perkins, F.M. and Johnson, J.P. (1981a). Hormone effects on transport in cultured epithelia with high electrical resistance. *American Journal of Physiology.* **240**: C103-C105.

Handler, J.S., Preston, A.S., Perkins, F.M., Matsumura, M., Johnson, J.P. and Watlington, C.O. (1981b). The effect of adrenal steroid hormones on epithelia formed in culture by A6 cells. *Annals of the New York Academy of Sciences.* **372**: 442-454.

Hansen, S.H. and Casanova, J.E. (1994). Gs alpha stimulates transcytosis and apical secretion in MDCK cells through cAMP and protein kinase A. *Journal of Cell Biology.* **126**: 677-687.

Hansson, J.H., Nelson-Williams, C., Suzuki, H., Schild, L., Shimkets, R., Lu, Y., *et al.* (1995). Hypertension caused by a truncated epithelial sodium channel gamma subunit: genetic heterogeneity of Liddle syndrome. *Nature Genetics.* **11**: 76-82.

Harvey, K.F., and Kumar, S. (1999). Nedd4-like proteins: an emerging family of ubiquitin-protein ligases implicated in diverse cellular functions. *Trends in Cell Biology.* **9**: 166–169.

Hays, R.M. and Leaf, A. (1962). Studies on the movement of water through the isolated toad bladder and its modification by vasopressin. *Journal of General Physiology.* **45**: 905-919.

Hayslett, J.P., Macala, L.J., Smallwood, J.I., Kalghatgi, L., Gassala-Herraiz, J. and Isales, C. (1995). Vasopressin-stimulated electrogenic sodium transport in A6 cells is linked to a Ca^{2+}-mobilizing signal mechanism. *Journal of Biological Chemistry.* **270**: 16082-16088.

Heck, G.L., Mierson, S. and Desimone, J.A. (1984). Salt transduction occurs through an amiloride-sensitive transport pathway. *Science.* **233**: 403-405.

Heim, R., Prasher, D. C. and Tsien, R. Y. (1994). Wavelength mutations and posttranslational autoxidation of green fluorescent protein. *Proceedings of the National Academy of Sciences of the USA.* **91**: 12501–12504.

Helman, S.I. and Baxendale, L.M. (1990). Blocker-related changes of channel density: Analysis of a three-state model for apical Na^+ channels for frog skin. *Journal of General Physiology.* **95**: 647-678.

Helman, S.I. and Fisher, R.S. (1977). Microelectrode studies of the active Na^+ transport pathway of frog skin. *Journal of General Physiology.* **69**: 571-604.

Helman, S.I. and Kizer, N.L. (1990). Apical sodium ion channels of tight epithelia as viewed from the perspective of noise analysis. In: *Channels and Noise in Epithelial Tissues.* Helman, S.I. and Van Driessche, W. (eds.). In: *Current Topics in Membranes and Transport.* Volume 37. Bronner, F. (ed.). Academic Press, New York. pp. 117-157.

Helman, S.I. and Liu, X. (1997). Substrate-dependant expression of Na^+ transport and shunt resistance in A6 epithelia. *American Journal of Physiology.* **273**: C434-C441.

Helman, S.I. and Miller, D.A. (1971). In vitro techniques for avoiding edge damage in studies of frog skin. *Science*. **173**: 146-148.

Helman, S.I., Cox, T.C. and Van Driessche, W. (1983). Hormonal control of apical membrane Na^+ transport in epithelia. Studies with fluctuation analysis. *Journal of General Physiology*. **82**: 201-220.

Helman, S.I., Liu, X., Baldwin, K., Blazer-Yost, B.L. and Els, W.J. (1998). Time-dependent stimulation by aldosterone of blocker-sensitive ENACs in A6 epithelia. *American Journal of Physiology*. **274**: C947-C957.

Horisberger, J.-D. and Rossier, B.C. (1992). Aldosterone regulation of gene transcription leading to control of ion transport. *Hypertension*. **19**: 221-227.

Howell, S.I., and Whitfield, M. (1972). Cytochemical localization of adenylate cyclase activity in rat islands of Langerhans. *Journal of Histochemistry and Cytochemistry*. **20**: 873-879.

Hunter, M., Horisberger, J.-D., Stanton, B.A. and Giebisch, G. (1987). The collecting tubule of *Amphiuma*. I. Electrophysiological characterization. *American Journal of Physiology*. **253**: F263-F272.

Inoue, J., Iwaoka, T, Tokunaga, H., Takamune, K., Naomi, S., Araki, M. *et al.* (1998). A family with Liddle's syndrome caused by a new missense mutation in the beta subunit of the epithelial sodium channel. *Journal of Clinical Endocrinology and Metabolism.* **83**: 2210-2213.

Imbert-Teboul, M., Charbardes, D. and Morel, F. (1980). Vasopressin and catecholamines sites of action along rabbit, mouse and rat nephron. *Contributions in Nephrology*. **21**: 41-47.

Irusta, P.M. and DiMaio, D. (1998). A single amino acid substitution in a WW-like domain of diverse members of the PDGF receptor subfamily of tyrosine kinases causes constitutive receptor activation. *EMBO Journal*. **17**: 6912-6923.

Ismailov, I.I., McDuffie, J.H. and Benos, D.J. (1994). Protein kinase A phosphorylation and G protein regulation of purified renal Na^+ channels in planar bilayer membranes. *Journal of Biological Chemistry*. **269**:10235–10241.

Itoh, M., Nagafuchi, A., Yonemura, S., Kitani-Yasuda, T., Tsukita, S. and Tsukita S. (1993). The 220-kDa protein colocalising with cadherins in non-epithelial cells is identical to Zo-1, a tight junction associated protein in epithelial cells: cDNA cloning and immunolocalization. *Journal of Cell Biology*. **124**: 491-502.

Jans, D., Simaels, J., Cucu, D., Zeiske, W. and Van Driessche, W. (2000). Effects of extracellular Mg^{2+} on transepithelial capacitance and Na^+ transport in A6 cells under different osmotic conditions. *Pflügers Archiv: European Journal of Physiology.* 439: 504-512.

Jesaitis, L.A. and Goodenough, D.A. (1994). Molecular characterization and tissue distribution of ZO-2, a tight junction protein homologous to ZO-1 and the *Drosophila* disk-large tumor suppressor protein. *Journal of Cell Biology*. **124**: 949-961.

Jeunemaitre, X., Bassilana, F., Persu, A., Dumont, C., Champigny, G., Lazdunski, M., *et al.* (1997). Genotype-phenotype analysis of a newly discovered family with Liddle's syndrome. *Journal of Hypertension.* **15**: 1091-1100.

Johnson, J.P., Jones, D. and Wiesmann, W.P. (1986). Hormonal regulation of Na^+-K^+-ATPase in cultured epithelial cells. *American Journal of Physiology.* **251**: C186-C190.

Johnson, R.A. and Salomon, Y. (1991). Assay of adenyl cyclase catalytic activity. *Methods in Enzymology.* **195**: 3-21.

Jongkind, J.F., Verkerk, A., Visser, W.J. and van Dongen, J.M. (1982). Isolation of autofluorescent "aged" human fibroblasts by flow sorting. *Experimental Cell Research.* **138**: 409-417.

Jordan, K., Solan, J.L., Dominguez, M., Sia, M., Hand, A., Lampe, P.D. and Laird, D.W. (1999). Trafficking, assembly, and function of a connexin43-green fluorescent protein chimera in live mammalian cells. *Molecular Biology of the Cell.* **10**: 2033-2050.

Jovov, B., Tousson, A., Ji, H.-L., Keeton, D., Shlyonsky, V., Ripolli, P.-J., Fuller, C.M. and Benos, D.J. (1999). Regulation of epithelial Na^+ channels by actin in planar lipid bilayers and in the *Xenopus sp.* oocyte expression system. *Journal of Biological Chemistry.* **274**: 37845-37854.

Juanjuan, Q., Peters, K.W., Liu, C., Wang, J.-M., Edinger, R.S., Johnson, J.P., Watkins, S.C. and Frizzell, R.A. 1999. Regulation of the amiloride-sensitive epithelial sodium channel by syntaxin 1A. *Journal of Biological Chemistry.* **274**: 30345-30348.

Kalyuzhny, A.E. and Wessendorf, M.W. (1998). Relationship of mu- and delta-opioid receptors to GABAergic neurons in the central nervous system, including antinociceptive brainstem circuits. *Journal of Comparative Neurology.* **392**: 528-547.

Keeler, R. and Wong, N.L. (1986). Evidence that prostaglandin E2 stimulates chloride secretion in cultured A6 renal epithelial cells. *American Journal of Physiology.* **250**: F511-F515.

Kellenberger, S., Gautschi, I., Rossier, B.C. and Schild, L. (1998). Mutations causing Liddle syndrome reduce sodium-dependent downregulation of the epithelial sodium channel in the *Xenopus sp.* oocyte expression system. *Journal of Clinical Investigation.* **101**: 2741-2750.

Kemendy, A.E., Kleyman, T.R. and Eaton, D.C. (1992). Aldosterone alters the open probability of amiloride-blockable sodium channels in A6 epithelia. *American Journal of Physiology.* **263**: C825-C837.

Kirsten, E., Kirsten, R., Leaf, A. and Sharp, G.W.G. (1968). Increased activity of enzymes of the tricarboxylic acid cycle in response to aldosterone in the toad bladder. *Pflügers Archiv: European Journal of Physiology.* **300:** 213-225.

Kirsten, E., Kirsten, R. and Sharp, G.W.G. (1970). Effects of sodium transport stimulating substances on enzyme activities in the toad bladder. *Pflügers Archiv: European Journal of Physiology.* **316**: 26-33.

Kleyman, T.R. and Cargoe, E.J. Jr. (1988). Amiloride and its analogs as tools in the study of ion transport. *Journal of Membrane Biology.* **150**: 1-21.

Kleyman, T.R., Kraehenbuhl, J.P. and Ernst, S.A. (1991). Characterization and cellular localization of the epithelial Na^+ channel. Studies using an anti-Na^+ channel antibody raised by an anti-idiotypic route. *Journal of Biological Chemistry.* **266**: 3907-3915.

Kleyman, T.R., Coupaye-Gerard, B. and Ernst, S.A. (1992). Aldosterone does not alter apical cell-surface expression of epithelial Na+ channels in the amphibian cell line A6. *Journal of Biological Chemistry.* **267**: 9622-9628.

Kleyman, T.R., Ernest, S.A. and Coupaye-Gerard, B. (1994). Arginine vasopressin and forskolin regulate apical cell surface expression of epithelial Na^+ channels in A6 cells. *American Journal of Physiology.* **266**: F506-F511.

Knauf, H. (1972). The isolated salivary duct as a model for electrolyte transport studies. *Pflügers Archiv: European Journal of Physiology.* **333**: 82-94.

Knowles, M.R., Murray, G., Shallal, J., Askin, F., Ranga, V., Gatzy, J and Boucher, R. (1984). Bioelectric properties and ion flow across excised human bronchi. *Journal of Applied Physiology.* **56**: 868-877.

Koechlin, N., Pisam, M., Poujeol, P., Tauc, M. and Rambourg, A. (1991). Conversion of a rabbit proximal convoluted tubule (PCT) into a cell monolayer: Ultrastructural study of cell dedifferentiation and redifferentiation. *European Journal of Cell Biology.* **54**: 224-236.

Koefoed-Johnsen, J.P. and Ussing, H.H. (1958). The nature of the frog skin potential. *Acta Physiologica Scandinavica.* **42**: 298-308.

Koeppen, B.M. (1986). Conductive properties of the rabbit outer medullary collecting duct: outer stripe. *American Journal of Physiology.* **250**: F70-F76.

Koeppen, B.M., Biagi, B.A. and Giebisch, G.H. (1983). Intracellular microelectrode characterization of the rabbit cortical collecting duct. *American Journal of Physiology.* **244**: F35-F47.

Komwatana, P., Dinudom, A., Young, J.A. and Cook, D.I. (1996). Cytosolic Na^+ controls an epithelial Na^+ channel via the G_o guanine nucleotide-binding regulatory protein. *Proceedings of the National Academy of Sciences of the USA.* **93**: 8107-8111.

Kosari, F., Sheng, S., Li, J., Mak, D.-O., Fosket, K. and Kleyman, T.R. (1998). Subunit stoichiometry of the epithelail sodium channel. *Journal of Biological Chemistry.* **273**: 13469-13474.

Krattenmacher, R., Fisher, H., Van Driessche, W. and Clauss, W. (1988). Noise analysis of cAMP-stimulated Na^+ current in frog colon. *Pflügers Archiv: European Journal of Physiology.* **412**: 568-573.

Kroll, B., Bremer, S., Tummler, B., Kottra, G. and Fromter, E. (1991). Sodium dependence of the epithelial sodium conductance expressed in *Xenopus laevis* oocytes. *Pflügers Archiv: European Journal of Physiology.* **419**:101-107.

Lang, M.A., Muller, J., Preston, A.S. and Handler, J.S. (1986). Complete response to vasopressin requires epithelial organization in A6 cells in culture. *American Journal of Physiology*. **250**: C138-C145.

Levine, S.D., Kachadorian, W.A., Levin, D.N. and Schlondorff, D. (1981). Effects of trifluoperazine on function and structure of toad urinary bladder. *Journal of Clinical Investigation*. **67**: 662–671.

Lewis, S.A. and Alles, W.P. (1986). Urinary kallikrein: a physiological regulator of epithelial Na^+ absorption. *Proceedings of the National Academy of Sciences of the USA*. 83: 5345-5348.

Lewis, S.A. and Clausen, C. (1991). Urinary proteases degrade epithelial sodium channels. *Journal of Membrane Biology*. **122**: 77-88.

Lewis, S.A. and Diamond, J.M. (1976). Na^+ transport by rabbit urinary bladder, a tight epithelium. *Journal of Membrane Biology*. **28**: 1-40.

Lewis, S.A. and Donaldson, P.J. (1990). Patch clamp of cation channels. In: *Channels and Noise in Epithelial Tissues*. Helman, S.I. and Van Driessche, W. (eds.). In: *Current Topics in Membranes and Transport*. Volume 37. Bronner, F. (ed.). Academic Press, New York. pp. 215-247.

Li, J.H.-Y., Palmer, L.G., Edelman, I.S. and Lindemann, B. (1982). The role of sodium-channel density in the natriferic response of the toad urinary bladder to an antidiuretic hormone. *Journal of Membrane Biology*. **64**: 77-89.

Li, J.H.-Y., Cragoe, E.J. Jr. and Lindemann, B. (1985). Structure-activity relationship of amiloride analogs as blockers of epithelial Na^+ channels. Pyrazine-ring modifications. *Journal of Membrane Biology*. **83**: 45-56.

Li, J.H.-Y., Cragoe, E.J. Jr. and Lindemann, B. (1987). Structure-activity relationship of amiloride analogs as blockers of epithelial Na^+ channels: II. Side-chain modifications. *Journal of Membrane Biology*. **95**: 171-185.

Li, X., Zhang, G., Ngo, N., Zhao, X., Kain, S. R. and Huang, C.-C. (1997). Deletions of the *Aequorea victoria* green fluorescent protein define the minimal domain required for fluorescence. *Journal of Biological Chemistry*. **272**: 28545–28549.

Liddle, G.W., Bledsoe, T. and Coppage Jr., W.S. (1963). A familial renal disorder simulating aldosteronism but with negligible aldosterone secretion. *Transactions of the Association of American Physicians*. **76**: 199-213.

Lindemann, B. (1984). Fluctuation analysis of sodium channels in epithelia. *Annual Review of Physiology*. **46**: 497-515.

Lindemann, B. (1995). Sweet and salty: transduction in taste. *News in Physiological Science*. **10**: 166-170.

Lindemann, B. (1996). Taste reception. *Physiological Reviews*. **76**: 719-766.

Lindemann, B. and Van Driessche, W. (1977). Sodium-specific membrane channels of frog skin are pores: current fluctuations reveal high turnover. *Science*. **195**: 292-294.

Ling, B.N. and Eaton, D. C. (1989). Effects of luminal Na^+ on single Na^+ channels in A6 cells, a regulatory role for protein kinase C. *American Journal of Physiology.* **256**: F1094-F1103.

Ling, B.N., Hinton, C.F. and Eaton, D.C. (1991). Amiloride-sensitive sodium channels in rabbit cortical collecting tubule primary cultures. *American Journal of Physiology.* **261**: F933-F944.

Lingueglia, E., Voilley, N., Waldmann, R., Lazdunski, M. and Barbry, P. (1993). Expression cloning of an epithelial amiloride-sensitive Na^+ channel. *FEBS Letters.* **318**: 95-99.

Lippincott-Schwartz, J., Roberts, T.H. and Hirschberg, K. (2000). Secretory protein trafficking and organelle dynamics in living cells. *Annual Review of Cell and Developmental Biology.* **16**: 557-589.

Liu, J., Conklin, B.R., Blin, N., Yun, J. and Wess, J. (1995). Identification of a receptor/G-protein contact site critical for signalling specificity and G-protein activation. *Proceedings of the National Academy of Sciences of the USA.* **92**: 11642-11646.

Loffing, J., Loffing-Cueni D., Macher A., Hebert S.C., Olson B., Knepper M.A., Rossier B.C. and Kaissling, B. (2000). Localization of epithelial sodium channel and aquaporin-2 in rabbit kidney cortex. *American Journal of Physiology.* **278**: F530-F539.

Lolait, S.J., O'Carroll, A.-M., McBride, O.W., Konig, M., Morel, A. and Brownstein, M.J. (1992). Cloning and characterization of a vasopressin V2 receptor and possible link to nephrogenic diabetes insipidus. *Nature.* **357**: 336-339.

MacKnight, A.D., DiBona, D.R. and Leaf, A. (1980). Sodium transport across toad urinary bladder: a model "tight" epithelium. *Physiological Reviews.* **60**: 615-715.

Madara, J. L. (1988). Tight junction dynamics: is paracellular transport regulated? *Cell.* **53**: 497-498.

Maeda, Y., Han, J.S., Gibson, C.C. and Knepper, M.A. (1993). Vasopressin and oxytocin receptors coupled to Ca^{2+} mobilization in rat inner medullary collecting duct. *American Journal of Physiology.* **265**: F15-F25.

Marples, D., Knepper, M.A., Christensen, E.I. and Nielsen, S. (1995). Redistribution of aquaporin-2 water channels induced by vasopressin in rat kidney inner medullary collecting duct. *American Journal of Physiology.* **269**: C655–C664.

Marunaka, Y. and Eaton, D.C. (1991). Effects of vasopressin and cAMP on single amiloride blockable Na^+ channels. *American Journal of Physiology.* **260**: C1071-C1084.

Marunaka, Y., Hagiwara, N. and Tohda, H. (1992). Insulin activates single amiloride-blockable Na^+ channels in a distal nephron cell line (A6). *American Journal of Physiology.* **263**: F392-F400.

Marunaka, Y., Tohda, H., Hagiwara, N. and Nakahari, T. (1994). Antidiuretic hormone-responding nonselective cation channel in distal nephron epithelium (A6). *American Journal of Physiology.* **266**: C1513-C1522.

Mastroberardino, L., Spindler, B., Forster, I., Loffing, J., Assandri, R., May, A. and Verrey, F. (1998). Ras pathway activates epithelial Na^+ channel and decreases its surface expression in *Xenopus sp.* ooctyes. *Molecular Biology of the Cell.* **9**: 3417-3427.

McDonald, F.J., Price, M.P., Snyder, P.M. and Welsh, M.J. (1995). Cloning and expression of the beta- and gamma-subunits of the human epithelial sodium channel. *American Journal of Physiology.* **268**: C1157-C1163.

McNicholas, C.M. and Canessa, C.M. (1997). Diversity of channels generated by different combinations of epithelial sodium channel subunits. *Journal of General Physiology.* **109**: 681-692.

Mingxia, H. and Chalfie, M. (1994). Gene interactions affecting mechanosensory transduction in *Caenorhabditis elegans*. *Nature.* **367**: 467-470.

Minuth, W.W., Struck, M., Zwanzig M. and Gross, P. (1989). Action of aldosterone on citrate synthase in cultured renal collecting duct cells. *Renal Physiology and Biochemistry.* **12**: 85-95.

Mitic, L.L. and Ancerson, J.M. (1998). Molecular architecture of tight junctions. *Annual Review of Physiology.* **60**: 121-142.

Moore, R.Y. (1981). Fluorescence histochemical methods. In: *Neuroanatomical Tract-tracing Methods.* Heimer L. (ed.). Plenum Press, New York. pp. 457-458.

Morel, A., O'Carroll, A.-M., Brownstein, M.J. and Lolait, S.J. (1992). Molecular cloning and expression of a rat V1a arginine vasopressin receptor. *Nature.* **356**: 523-526.

Morin, J. G. and Hastings, J. W. (1971). Energy transfer in a bioluminescent system. *Journal of Cell Physiology.* **77**: 313–318.

Morris, R.G., Tousson, A., Benos, D.J. and Schafer, J.A. (1998). Microtubule disruption inhibits AVT-stimulated Cl^- secretion but not Na^+ reabsorption in A6 cells. *American Journal of Physiology.* **274**: F300-F314.

Mostov, K.E., Verges, M. and Altschuler, Y. (2000). Membrane traffic in polarized epithelial cells. *Current Opinion in Cell Biology.* **12**: 483-490.

Nagel, W. (1978). Effects of antidiuretic hormone upon electrical potential and resistance of apical and basolateral membranes of frog skin. *Journal of Membrane Biology.* **42**: 99-122.

Nagel, W. and Crabbé, J. (1980). Mechanism of action of aldosterone on active sodium transport across toad skin. *Pflügers Archiv: European Journal of Physiology.* **385**: 181-187.

Nakada, T., Koike, H., Akiya, T., Katayama, T., Kawamata, S., Takaya, K. and Shigematsu, H. (1987). Liddle's syndrome, an uncommon form of hyporeninemic hypoaldosteronism: functional and histopathological studies. *Journal of Urology.* **137**: 636-640.

Nakahari, T. and Marunaka, Y. (1995). ADH-evoked $[Cl^-]$i-dependent transient in whole cell current of distal nephron cell line A6. *American Journal of Physiology.* **268**: F64:F72.

Navar, L.G. (1984). Regulation of body fluid balance. In *Edema*. Staub, N.C. and Taylor, A.E. (eds.). Raven Press, New York. pp. 319–352.

Navar, L.G. and Hamm, L.L. (1999). The kidney in blood pressure regulation In: *Atlas of Diseases of the Kidney.* Volume 3. Schrier, R.W. (ed.). Blackwell Science. New York. pp. 1-22.

Neher, E. and Sackman, B. (1976). Single channel currents recorded from membrane of denervated frog muscle fibres. *Nature*. **260**: 779-802.

Niisato, N., Van Driessche, W., Liu, M. and Marunaka, Y. (2000). Involvement of protein tyrosine kinase in osmoregulation of Na^+ transport and membrane capacitance in renal A6 cells. *Journal of Membrane Biology*. **175**: 63-77.

Niswender, K. D., Blackman, S. M., Rohde, L., Magnuson, M. A. and Piston, D. W. (1995). Quantitative imaging of green fluorescent protein in cultured cells: comparison of microscopic techniques, use in fusion proteins and detection limits. *Journal of Microbiology*. **180**: 109–116.

O'Brodovich, H. (1995). The role of active Na^+ transport by lung epithelium in the clearance of airspace fluid. *New Horizons*. **3**: 240-247.

Ogawa, H., Inouye, S., Tsuji, F. I., Yasuda, K. and Umesono, K. (1995). Localization, trafficking, and temperature-dependence of the *Aequorea* green fluorescent protein in cultured vertebrate cells. *Proceedings of the National Academy of Sciences of the USA*. **92**: 11899–11903.

Oh, Y., Smith, P.R., Bradford, A.L., Keeton, D. and Benos, D.J. (1993). Regulation by phosphorylation of purified epithelial Na^+ channels in planar lipid bilayers. *American Journal of Physiology*. **265**: C85–C91.

Orloff, J., Handler, J.S. and Preston, A.S. (1962). The similarity of effects of vasopressin, adenosine-3'-5'-phosphate (cyclic AMP) and theophylline on the toad bladder. *Journal of Clinical Investigation*. **41**: 702-709.

Orzech, E., Schlessinger, K., Weiss, A., Okamoto, C.T. and Aroeti, B. (1999). Interactions of the AP-1 Golgi adaptor with the polymeric immunoglobulin receptor and their possible role in mediating brefeldin A-sensitive basolateral targeting from the trans-Golgi network. *Journal of Biological Chemistry*. **274**: 2201-2215.

Palmer, L.G. (1982). Ion selectivity of the apical membrane Na^+ channel in the toad urinary bladder. *Journal of Membrane Biology*. **67**: 91-98.

Palmer, L.G. (1984). Voltage-dependant block by amiloride and other monovalent cations of apical Na^+ channels in the toad urinary bladder. *Journal of Membrane Biology*. **80**: 153-165.

Palmer, L.G. (1992). Epithelial Na^+ channels: function and diversity. *Annual Review of Physiology*. **54**: 51-66.

Palmer, L.G. and Frindt, G. (1986). Epithelial sodium channels: charaterization by using the patch-clamp technique. *Federation Proceedings*. **45**: 2708-2712.

Palmer, L.G. and Frindt, G. (1992). Regulation of apical membrane Na^+ and K^+ channels in rat renal collecting tubules by aldosterone. *Seminars in Nephrology.* **12**: 37-43.

Palmer, L.G. and Lorenzen, M. (1983). Antidiuretic hormone-dependent membrane capacitance and water permeability in the toad urinary bladder. *American Journal of Physiology.* **244**: F195–F204.

Palmer, L.G., Li, J.H.-Y., Lindemann, B. and Edelman, I.S. (1982). Aldosterone control of the density of sodium channels in the toad urinary bladder. *Journal of Membrane Biology.* **64**: 91-102.

Palmer, L.G., Sackin, H. and Frindt, G. (1998). Regulation of Na^+ channels by luminal Na^+ in rat cortical collecting tubule. *Journal of Physiology.* **509**: 151-162.

Partanen, M., Santer, R.M. and Hervonen, A. (1980). The effect of ageing on the histochemically demonstrable catecholamines in the hypogastric (main pelvic) ganglion of the rat. *Histochemical Journal.* **12**: 527-535.

Patterson, G. H., Knobel, S. M., Sharif, W. D., Kain, S. R. and Piston, D. W. (1997). Use of the green fluorescent protein and its mutants in quantitative fluorescence microscopy. *Biophysical Journal.* **73:** 2782–2790.

Păunescu, T.G. and Helman, S.I. (2001a). cAMP activation of apical membrane Cl^- channels: theoretical considerations for impedance analysis. *Biophysical Journal.* **81**: 838-851.

Păunescu, T.G. and Helman, S.I. (2001b). Pge(2) activation of apical membrane Cl^- channels in A6 epithelia: impedance analysis. *Biophysical Journal.* **81**: 852-866.

Pelham, H.R. (1991). Multiple targets for brefeldin A. *Cell.* **67**: 449-451.

Perkins, F.M. and Handler, J.S. (1981). Transport properties of toad kidney epithelia in culture. *American Journal of Physiology.* **241**: C154-C159.

Peter, J., Burbach, H., Adan, R.A., Lolait, S.J., van Leeuwen, F.W., Mezey, E., Palkovits, M. and Barberis, C. (1995). Molecular neurobiology and pharmacology of the vasopressin/oxytocin receptor family. *Cellular and Molecular Neurobiology.* **15**: 573-595.

Pimplikar, S.W. and Simons, K. (1994). Activators of protein kinase A stimulate apical but not basolateral transport in epithelial Madin-Darby canine kidney cells. *Journal of Biological Chemistry.* **269**: 19054-19059.

Pines, J. (1995). GFP in mammalian cells. *Trends in Genetics.* **11**: 326–327.

Pirozzi, G., McConnell, S.J., Uveges, A.J., Carter, J.M., Sparks, A.B., Kay, B.K. and Fowlkes, D.M. (1997). Identification of novel human WW domain-containing proteins by cloning of ligand targets. *Journal of Biological Chemistry.* **272**: 14611-14616.

Ploem, J.S. (1993). Fluorescence Microscopy. In: *Fluorescent and Luminescent Probes for Biological Activity. A Practical Guide to Technology for Quantitative Real-Time Analysis.* Mason, W.T. (ed.). In: *Biological Techniques. A series of Practical Guides to New Methods in Modern Biology.* Sattelle, D.B. (ed.). Academic Press, London. pp. 1-11.

Pough, F.H., Heiser, J.B. and McFarland, W.N. (1989). *Vertebrate Life*. 3rd Edition. Macmillan Publishing. New York. pp904.

Prat, A.G., Ausiello, D.A. and Cantiello, H.F. (1993). Vasopressin and protein kinase A activate G protein-sensitive epithelial Na^+ channels. *American Journal of Physiology*. **265**: C218-C223.

Prat, A.G., Holtzman, E.J., Brown, D., Cunningham, C.C., Reisin, I.L, Kleyman, T.R., McLaughlin, M., Jackson, G.R. Jr., Lydon, J. and Cantiello, H.F. (1996). Renal epithelial protein (Apx) is an actin cytoskeleton-regulated Na^+ channel. *Journal of Biological Chemistry*. **271**: 18045-18053.

Preston, A.S., Muller, J. and Handler, J.S. (1988). Dexamethasone accelerates differentiation of A6 epithelia and increases responses to vasopressin. *American Journal of Physiology*. **255**: C661-C666.

Prince, L.S. and Welsh, M.J. (1998). Cell surface expression and biosynthesis of epithelial Na^+ channels. *Biochemical Journal*. **336**: 705-710.

Prince, L.S. and Welsh, M.J. (1999). Effect of subunit composition and Liddle's syndrome mutations on biosynthesis of ENaC. *American Journal of Physiology*. **276**: C1346-C1351.

Puoti, A., May, A., Canessa, C.M., Horisberger, J.-D., Schild, L. and Rossier, B.C. (1995). The highly selective, low conductance, epithelial sodium channel of *Xenopus laevis* A6 kidney cells. *American Journal of Physiology*. **269**: C188-C197.

Puoti, A., May, A., Rossier, B.C. and Horisberger, J.D. (1997). Novel isoforms of the beta and gamma subunits of the *Xenopus sp.* epithelial Na^+ channel provide information about the amiloride binding site and extracellular sodium sensing. *Proceedings of the National Academy of Sciences of the USA*. **94**: 5949-5954.

Quinton, P.M. (1981). Effects of some ion transport inhibitors on secretion and reabsorption in intact and perfused single human sweat glands. *Pflügers Archiv: European Journal of Physiology*. **391**: 309-313.

Rachamim, N., Latter, H., Asher, C., Wald, H. and Garty, H. (1995). Dexamethasone enhances expression of mitochondrial oxidative-phosphorylation genes in rat distal colon. *American Journal of Physiology*. **269**: C1305-C1310.

Reik, L., Petzold, G.L., Higgins, J.A., Greengard, P. and Barrnett, R.J. (1970). Hormone-sensitive adenylate cyclase: cytochemocal localization in rat liver. *Science*. 1970. **168**: 382-384.

Renard, S., Lingueglia, E., Voilley, N., Lazdunski, M. and Barbry, P. (1994). Biochemical analysis of the membrane topology of the amiloride-sensitive Na^+ channel. *Journal of Biological Chemistry*. **269**: 12981-12986.

Renard, S., Voillet, N., Bassilana, F., Lazdunski, M. and Barbry, P. (1995). Localization and regulation by steroids α, β and γ subunits of the amiloride-sensitive Na^+ channel in colon, lung and kidney. *Pflügers Archiv: European Journal of Physiology*. **430**: 299-307.

Richards, P.D.G. and Els, W.J. (1993). Cytochemical localization of adenylate cyclase in the sodium-transporting epithelium isolated from frog skin. *Histochemical Journal.* **26**: 495-503.

Rodriguez, J.A., Biglieri, E. and Schambelan, M. (1981). Pseudohyperaldosteronism with renal tubular resistance to mineralocorticoid hormones. *Transactions of the Association of American Physiologists.* **94**: 172-182.

Rodriguez-Commes, J., Isales, C., Kalghati, L, Gasalla-Herraiz, J. and Hayslett, J.P. (1994). Mechanism of insulin-stimulated electrogenic sodium transport. *Kidney International.* **46**: 666-674.

Rokaw, M.D., Sarac, E., Lechman, E., West, M., Johnson, J.P. and Zeidel, M.L. (1996a). Chronic regulation of transepithelial Na^+ transport by the rate of apical Na^+ entry. *American Journal of Physiology.* **270**: C600-C607.

Rokaw, M.D., West, M. and Johnson, J.P. (1996b). Rapamycin inhibits protein kinase C activity and stimulates Na^+ transport in A6 cells. *Journal of Biological Chemistry.* **271**: 32468–32473.

Rossier, B.C. and Palmer, L.G. (1992). Mechanisms of aldosterone action on sodium and potassium transport. In: *The Kidney: Physiology and Pathophysiology.* Volume 1. Seldin, D.W. and Giebisch, G. (eds). Raven, New York. pp. 1373-1409.

Rossier, B.C., Canessa, C.M., Schild, L. and Horisberger, J.-D. (1994). Epithelial sodium channels. *Current Opinion in Nephrology and Hypertension.* **3**: 487-496.

Salomon, Y. (1991). Cellular responsiveness to hormones and neurotransmitters: conversion of [^{3}H]adenine to [^{3}H]cAMP in cell monolayers, cell suspensions, and tissue slices. *Methods in Enzymology.* **195**: 22-28.

Santer, R.M., Partanen M. and Hervonen, A. (1980). Glyoxylic acid fluorescence and ultrastructural studies of neurones in the coeliac-superior mesenteric ganglion of the aged rat. *Cell and Tissue Research.* **211**: 475-485.

Sariban-Sohraby, S., Burg, M.B. and Turner, R.J. (1983). Apical sodium uptake in toad kidney epithelial cell line A_6. *American Journal of Physiology.* **245**: C167-C171.

Sariban-Sohraby, S., Sorscher, E.J., Brenner, B.M. and Benos, D.J. (1988). Phosphorylation of a single subunit of the epithelial Na^+ channel protein following vasopressin treatment of A6 cells. *Journal of Biological Chemistry.* **263**: 13875–13879.

Saumon, G. and Basset, G. (1993). Electrolyte and fluid transport across the mature alveolar epithelium. *Journal of Applied Physiology.* **74**: 1-15.

Saxena, S., Quick, M.W. and Warnock, D.G. (2000). Interaction of syntaxins with epithelial ion channels. *Current Opinion in Nephrology and Hypertension.* **9**: 523-527.

Schafer, J.A. and Hawk, C.T. (1992). Regulation of Na^+ channels in the cortical collecting duct by AVP and mineralocorticoids. *Kidney International.* **41**: 255-268.

Schiffman, S.S., Lockhead, E. and Maes, F.W. (1983). Amiloride reduces the taste intensity of Na^+ and Li^+ salts and sweeteners. *Proceedings of the National Academy of Sciences of the USA.* **80**: 6136-6140.

Schild, L., Scheeberger, E., Gautschi, I. and Firsov, D. (1997). Identification of amino acid residues in the α, β and γ subunits of the epithelial sodium channel (ENaC) involved in amiloride block and ion permeation. *Journal of General Physiology.* **109**: 15-26.

Schneeberger, E. E. and Lynch, R. D. (1992). Structure, function, and regulation of cellular tight junctions. *American Journal of Physiology.* **262**: L647-L661.

Schoen, H.F. and Erlij, D. (1987). Insulin action on electrophysiological properties of apical and basolateral membranes of frog skin. *American Journal of Physiology.* **252**: C411-C417.

Scott, W.N., Reich, I.M., Brown, J.A.J. and Young, C.-P.H. (1978). Comparison of toad bladder aldosterone-induced proteins and proteins synthesized *in vitro* using aldosterone-induced messenger RNA as a template. *Journal of Membrane Biology.* **40**: 213-220.

Shareghi, G.R. and Stoner, L.C. (1978). Calcium transport across segments of the rabbit nephron *in vitro*. *American Journal of Physiology.* **235**: F367-F375.

Shepard, C.J.R. (1993). Confocal microscopy – principles, practice and options. In: *Fluorescent and Luminescent Probes for Biological Activity. A Practical Guide to Technology for Quantitative Real-Time Analysis.* Mason, W.T. (ed.). In: *Biological Techniques. A series of Practical Guides to New Methods in Modern Biology.* Sattelle, D.B. (ed.). Academic Press, London. pp. 229-236.

Shimkets, R.A., Warnock, D.G., Bositis, C.M., Williams, C.N., Hansson, J.H., Schamelan, M. *et al.* (1994). Liddle's syndrome: heritable human hypertension caused by mutations in the β subunit of the epithelial sodium channel. *Cell.* **79**: 407-414.

Shimkets, R.A., Lifton, R. and Canessa, C.M. (1998). *In vivo* phosphorylation of the epithelial sodium channel. *Proceedings of the National Academy of Sciences of the USA.* **95**: 3301-3305.

Shimomura, O., Johnson, F. H. and Saiga, Y. (1962). Extraction, purification and properties of aequorin, a bioluminescent protein from the luminous hydromedusan, *Aequorea*. *Journal of Cellular and Comparative Physiology.* **59**: 223–227.

Sigworth, F.J. and Neher, E. (1980). Single Na-channel currents observed in cultured rat muscle cells. *Nature.* **287**: 447-449.

Silver, R.B., Frindt, G., Windhager, E.E. and Palmer, L.G. (1993). Feedback regulation of Na^+ channels in rat CCT. I. Effects of inhibition of Na^+ pump. *American Journal of Physiology.* **264**: F557-F564.

Smets, I., Zeiske, W., Steels, P. and Van Driessche, W. (1998). Na^+ dependence of single-channel current and channel density generate saturation of Na^+ uptake in A6 cells. *Pflügers Archiv: European Journal of Physiology.* **435**: 604: 609.

Smith,H.W. (1937). *The Physiology of the Kidney.* Oxford University Press. New York. p233

Snyder, P.M., McDonald, F.J., Stokes, J.B. and Welsh, M.J. (1994). Membrane topology of the amiloride-sensitive epithelial sodium channel. *Journal of Biological Chemistry.* **269**: 24379-24383.

Snyder, P.M., Price, M.P., McDonald, F.J., Adams, C.M., Volk, K.A., Zeiher, B.G. *et al.* (1995). Mechanism by which Liddle's syndrome mutations increase activity of a human epithelial Na^+ channel. *Cell.* **83**: 969-978.

Snyder, P.M., Cheng, C., Prince, L.S., Rogers, J.C. and Welsh, M.J. (1998). Electrophysiological and biochemical evidence that DEG/ENaC cation channels are composed of nine subunits. *Journal of Biological Chemistry.* **273**: 681-684.

Somsel Rodman, J. and Wandinger-Ness, A. (2000). Rab GTPases coordinate endocytosis. *Journal of Cell Science.* **113**: 183-192.

Stanton, B.A. (1989). Characterization of apical and basolateral membrane conductances of rat inner medullary collecting ducts. *American Journal of Physiology.* **256**: F862-F868.

Star, R.A., Nonoguchi, H., Balaban, R. and Knepper, M.A. (1988). Calcium and cyclic monophosphate as secondary messengers for vasopressin in the rat inner medullary collecting duct. *Journal of Clinical Investigation.* **81**: 1879-1888.

Starr, C. and Taggart, R. (1998). *Biology. The Unity and Diversity of Life.* 8th Edition. Wadsworth, Belmont, California. pp. 80-96.

Staub, O. and Rotin, D. (1997). WW domains. *Structure.* **4**: 495-499.

Staub, O., Dho, S., Henry, P.C., Correa, J., McGlade, J. and Rotin, D. (1996). WW domains of Nedd4 bind to proline-rich PY motifs in the epithelial Na^+ channel deleted in Liddle's syndrome. *EMBO Journal.* **15**: 2371-2380.

Staub, O., Yeger, H., Plant, P.J., Kim, H., Ernst, S.A. and Rotin, D. (1997a). Immunolocalization of the ubiquitin-protein ligase Nedd4 in tissues expressing the epithelial Na^+ channel (ENaC). *American Journal of Physiology.* **272**: C1871-C1880.

Staub, O., Gautschi, I., Ishikawa, T., Breitschopf, K., Ciechanover, A., Schild, L., and Rotin, D. (1997b). Regulation of stability and function of the epithelial Na^+ channel (ENaC) by ubiquitination. *EMBO Journal.* **16**: 6325–6336.

Staub, O., Abriel, H., Plant, P., Ishikawa, T., Kanelis, V., Saleki, R. and Horisberger, J.D. (2000). Regulation of the epithelial Na^+ channel by Nedd4 and ubiquitination. *Kidney International.* **57**: 809-815.

Steinman, R.M. and Cohn, Z.A. (1972). The interaction of soluble horseradish peroxidase with mouse peritoneal macrophages *in vitro*. *Journal of Cell Biology.* **55**: 186-204.

Stetson, D.L., Lewis, S.A., Alles, W. and Wade, J.B. (1982). Evaluation by capacitance measurements of antidiuretic hormone induced membrane area changes in toad bladder. *Biochimica et Biophysica Acta.* **689**: 267–274.

Stevenson, B.R., Silicano, J.D., Mooseker, M.S. and Goodenough, D.A. (1986). Identification of ZO-1: a high molecular weight polypeptide associated with the tight

junction (zona occludens) in a variety of epithelia. *Journal of Cell Biology.* **103**: 755-766.

Stevenson, B.R., Haskins, J., Hibbard, J., Tamber, M. and Weber, D. (1996). P130 is homologous to ZO-1 and ZO-2 and is a novel member of the MAGUK family of proteins. *Molecular Biology of the Cell, Supplement.* **7**: 605a.

Stryer, L. (1988). *Biochemistry.* 3rd edition. Freeman, New York. pp. 949-974.

Sudol, M. (1996). Structure and function of the WW domain. *Progress in Biophysical and Molecular Biology.* **65**: 113-132.

Sudol, M., Chen, H.I., Bougeret, C., Einbond, A. and Bork, P. (1995). Characterization of a novel protein-binding molecule – the WW domain. *FEBS Letters.* **369**: 67-71.

Sugimoto, T., Saito, M., Mochizuki, S., Watanabe, Y., Hashimoto, S. and Kawashima, H. (1994). Molecular cloning and functional expression of a cDNA encoding the human V1b receptor. *Journal of Biological Chemistry.* **269**: 27088-27092.

Szerlip, H.M. and Cox, M. (1989). Aldosterone-induced glycoproteins: further characterization. *Journal of Steroid Biochemistry.* **32**: 815-822.

Szerlip, H.M., Weisberg, L., Geering, K., Rossier, B.C. and Cox, M. (1988). Aldosterone-induced glycoproteins: electrophysiological-biochemical correlation. *Biochimica et Biophysica Acta.* **940**: 1-9.

Szerlip, H.M., Weisberg, L., Clayman, M., Neilson, E., Wade, J.B., and Cox, M. (1989). Aldosterone-induced proteins: purification and localization of GP65,70. *American Journal of Physiology.* **256**: C865-C872.

Szerlip, H., Palevsky, P., Cox, M. and Blazer-Yost, B. (1991). Relationship of the aldosterone-induced protein, GP70, to the conductive Na^+ channel. *Journal of the American Society of Nephrology.* **2**: 1108-1114.

Tamura, H., Schild, L., Enomoto, N., Matsui, N., Marumo, F., Rossier, B.C. and Sasaki, S. (1996). Liddle disease caused by a missense mutation of beta-subunit of the epithelial sodium channel gene. *Journal of Clinical Investigation.* **97**: 1780-1784.

Tarasova, N.I., Stauber, R.H., Choi, J.K., Hudson, E.A., Czerwinski, G., Miller, J.L., Pavlakis, G.N., Michejda, C.J. and Wank, S.A. (1997). Visualization of G protein-coupled receptor trafficking with the aid of the green fluorescent protein. Endocytosis and recycling of cholecystokinin receptor type A. *Journal of Biological Chemistry.* **272**: 14817-14824.

Taylor, A., Mamelak, M., Golbetz, H. and Maffly, R. (1978). Evidence for involvement of microtubules in the action of vasopressin in toad urinary bladder. *Journal of Membrane Biology.* **40**: 213–235.

Thilo, L. (1985). Quantification of endocytosis-derived membrane traffic. *Biochimica et Biophysica Acta.* **822**: 243-266.

Thilo, L., Stroud, E. and Haylett, T. (1995). Maturation of early endosomes and vesicular traffic to lysosomes in relation to membrane recycling. *Journal of Cell Science.* **108**: 1791-1803.

Thomas, S.R. and Mintz, E. (1987). Time-dependent apical membrane K^+ and Na^+ selectivity in cultured kidney cells. *American Journal of Physiology.* **253**: C1-C6.

Tousson, A., Fuller, C.M. and Benos, D.J. (1996). Apical recruitment of CFTR in T-84 cells is dependent on cAMP and microtubules but not Ca^{2+} or microfilaments. *Journal of Cell Science.* **109**: 1325–1334.

Truscello, A., Gaggeler, H.P. and Rossier, B.C. (1986). Thyroid hormone antagonizes an aldosterone-induced protein: a candidate mediator for the late mineralocorticoid response. *Journal of Membrane Biology.* **89**: 173-183.

Ussing, H.H. (1949). The active transport of sodium as the source of electric current in the light of tracer studies. *Acta Physiologica Scandinavica.* **17**: 1-37.

Ussing, H.H. and Zerahn, K. (1951). Active transport of sodium as the source of electric current in the short-circuited isolated frog skin. *Acta Physiologica Scandinavica.* **23**: 110-127.

Ussing, H.H., Erlij, D. and Lassen, V. (1974). Transport pathways in biological membranes. *Annual Review of Physiology.* **36**: 17-49.

Valentijn, J.A., Fyfe, G.K. and Canessa, C.M. (1998). Biosynthesis and processing of epithelial sodium channels in *Xenopus sp.* oocytes. *Journal of Biological Chemistry.* **273**: 30344-30351.

Vallet, V., Chraïbi, A., Gaeggeler, H.-P., Horisberger, J.-D. and Rossier, B.C. (1998). An epithelial serine protease activates the amiloride-sensitive sodium channel. *Nature.* **389**: 607-610.

Van Driessche, W. and Erlij, D. (1983). Noise analysis of inward and outward currents across the apical border of oubain-treated frog skin. *Journal of Physiology.* **398**: 179-188.

Van Driessche, W. and Gullentops, K. (1982). Conductance fluctuation analysis in epithelia. In: *Techniques in the life sciences. Techniques in Cellular Physiology.* Volume 2. Baker, P.F. (ed.). Elsevier/North-Holland Scientific Publishers, Amsterdam. pp. 1-13.

Van Driessche, W. and Lindemann, B. (1978). Low noise amplification of voltage and current fluctuations arising in epithelia. *Reviews of Scientific Instruments.* **49**: 52-57.

Van Driessche, W. and Lindemann, B. (1979). Concentration dependence of current through single sodium-selective pores in frog skin. *Nature.* **282**: 519-520.

Van Driessche, W. and Van Deynse, N. (1990). Analysis of transepithelial noise signals from ion channels: Advantages and limitations of the method. In: *Channels and Noise in Epithelial Tissues.* Helman, S.I. and Van Driessche, W. (eds.). In: *Current Topics in Membranes and Transport.* Volume 37. Bronner, F. (ed.). Academic Press, New York. pp. 37-60.

Van Driessche, W. and Zeiske, W. (1980). Ba^{2+}-induced conductance fluctuations of spontaneously fluctuating K^+ channels in apical membrane of frog skin (*Rana temporaria*). *Journal of Membrane Biology.* **56**: 31-42.

Van Driessche, W. and Zeiske, W. (1985). Ionic channels in epithelial cell membranes. *Physiological Reviews*. **65**(4): 833-903.

Van Itallie, C.M. and Anderson, J.M. (1997). Occludin confers adhesiveness when expressed in fibroblasts. *Journal of Cell Science*. **110**: 1113-1121.

Van Vliet, L.J., Sudar, D. and Young, I.T. (1998). Digital fluorescent imaging using cooled CCD array cameras. In: *Cell Biology*. 2nd Edition. Volume III. Academic Press, New York. pp.109-120.

Vega-Salas, D.E., Salas, P.J. and Rodriguez-Boulan, E. (1988). Exocytosis of vacuolar apical compartment (VAC): a cell-cell contact controlled mechanism for the establishment of the apical plasma membrane domain in epithelial cells. *Journal of Cell Biology*. **107**: 1717-1728.

Verrey, F. (1995). Transcriptional control of sodium transport in tight epithelia by adrenal steroids. *Journal of Membrane Biology*. **144**: 93-110.

Verrey, F., Schaerer, E., Zoerkler, P., Paccolat, M.P., Geering, K., Kraehenbuhl, J.P. and Rossier, B.C. (1987). Regulation by aldosterone of Na^+,K^+-ATPase mRNAs, protein synthesis, and sodium transport in cultured kidney cells. *Journal of Cell Biology*. **104**: 1231-1237.

Verrey, F., Digicaylioglu, M. and Bollinger, U. (1993). Polarised membrane movements in A6 kidney cells are regulated by aldosterone and vasopressin/vasotocin. *Journal of Membrane Biology*. **133**: 213-226.

Verrey, F., Groscurth, P. and Bolliger, U. (1995). Cytoskeletal disruption in A6 kidney cells: Impact on endo/exocytosis and NaCl transport regulation by antidiuretic hormone. *Journal of Membrane Biology*. **145**: 193-204.

Verrier, B., Champigny, G., Barby, P., Gerard, C., Mauchamp, J. and Lazdunski, M. (1989). Identification and properties of a novel type of Na^+-permeable amiloride-sensitive channel in thyroid cells. *European Journal of Biochemistry*. **183**: 499-505.

Vigne, P., Champigny, G., Marsault, R., Barby, P., Frelin, C and Lazdunski, M. (1989). A new type of amiloride-sensitive cationic channel in endothelial cells of brain microvessels. *Journal of Biological Chemistry*. **264**: 7663-7668.

Voet, D. and Voet, J.G. (1990). *Biochemistry*. Wiley, New York. pp. 484-503.

Voilley, N., Lingueglia, E., Champigny, G., Mattéi, M.-G., Waldmann, R., Lazdunski, M. and Barbry, P. (1994). The lung amiloride-sensitive Na^+ channel: Biophysical properties, pharmacology, ontogenesis, and molecular cloning. *Proceedings of the National Academy of Sciences of the USA*. **91**: 247-251.

Voilley, N.F., Bassilana, F., Mignon, C., Merscher, S., Mattei, M.G., Carle, G.F., Lazdunski, M. and Barbry, P. (1995). Cloning, chromosomal localization, and physical linkage of the beta and gamma subunits (SCNN1B and SCNN1G) of the human epithelial amiloride-sensitive sodium channel. *Genomics*. **28**: 560-565.

Volk, K.A., Husted, R.F., Snyder, P.M. and Stokes, J.B. (2000). Kinase regulation of hENaC mediated through a region in the COOH-terminal portion of the α-subunit. *American Journal of Physiology.* **278**: C1047-C1054.

Wachman, E.S., Niu, W. and Farkas, D. (1997). AOTF microscope for imaging with increased speed and spectral versatility. *Biophysical Journal.* **73**: 1215-1222.

Wagner, M., Rajaskaran, A.K., Hanzel, D.K., Mayor, S. and Rodriguez-Boulan, E. (1994). Brefeldin A causes structural and functional alterations of the trans-Golgi network of MDCK cells. *Journal of Cell Science.* **107**: 933-943.

Wang, C., Chan, T.K., Yeung, R.T.T., Coghlan, J.P., Scoggins, B.A. and Stockigt, J.R. (1981). The effect of triamterene and sodium intake on renin, aldosterone , and erythrocyte sodium transport in Liddle syndrome. *Journal of Clinical Endocrinology and Metabolism.* **52**: 1027-1032.

Wang, S. and Hazelrigg, T. (1994). Implications for bcd mRNA localization from spatial distribution of exu protein in *Drosophila* oogenesis. *Nature.* **369**: 400–403.

Wang, W., Sackin, H. and Giebisch, G. (1992). Renal potassium channels and their regulation. *Annual Review of Physiology.* **54**: 81-96.

Ward, W. W., Cody, C. W., Hart, R. C. and Cormier, M. J. (1980). Spectrophotometric identity of the energy transfer chromophores in *Renilla* and *Aequorea* green-fluorescent proteins. *Photochemistry and Photobiology.* **31**: 611–615.

Weisz, O.A., Wang, J.M., Edinger, R.S. and Johnson, J.P. (2000). Non-coordinate regulation of endogenous epithelial sodium channel (ENaC) subunit expression at the apical membrane of A6 cells in response to various transporting conditions. *Journal of Biological Chemistry.* **275**: 39886-39893.

Weng, K. and Wade, J.B. (1994). Effect of brefeldin A on ADH-induced transport responses of toad bladder. *American Journal of Physiology.* **266**: C1069-C1076.

White, J.G., Amos, W.B. and Fordham, M. (1987). An evaluation of confocal versus conventional imaging of biological structures by fluorescence light microscopy. *Journal of Cell Biology* **105**, 41-48 .

Will, P.C., Cortright, R.N., Delisle, R.C., Douglas, J.G. and Hopfer, U. (1985a). Regulation of amiloride-sensitive electrogenic sodium transport in the rat colon by steroid hormones. *American Journal of Physiology.* **248**: G124-G132.

Will, P.C., Cortright, R.N., Groseclose, R.G. and Hopfer, U. (1985b). Amiloride-sensitive salt and fluid absorption in small intestine of sodium-depleted rats. *American Journal of Physiology.* **248**: G133-G141.

Wills, N.K. and Millinoff, L.P. (1990). Amiloride-sensitive Na^+ transport across cultured renal (A6) epithelium: evidence for large currents and high Na:K selectivity. *Pflügers Archiv: European Journal of Physiology.* **416**: 481-492.

Wilson, P.D., and Horster, M.F. (1985). Histochemical localization of hormone sensitive adenylate cyclase in defined nephron epithelia in culture. *Histochemistry.* **82**: 539-545.

Yanase, M., and Handler, J.S. (1986a). Adenosine 3',5'-cyclic monophosphate stimulates chloride secretion in A6 epithelia. *American Journal of Physiology.* **251**: C810-C814.

Yanase, M., and Handler, J.S. (1986b). Activators of protein kinase C inhibit sodium transport in A6 epithelia. *American Journal of Physiology.* **250** (19): C517–C522.

Yang, T.T., Cheng, L. and Kain, S.R. (1996). Optimized codon usage and chromophore mutations provide enhanced sensitivity with the green fluorescent protein. *Nucleic Acids Research.* **24** (22): 4592–4593.

Yongkind, J.F., Verkerk, A., Visser, W.J. and Van Dongen, J.M. (1982). Isolation of autofluorescent "aged" human fibroblasts by flow sorting. Morphology, enzyme activity and proliferative capacity. *Experimental Cell Research.* **138**: 409-417.

Zeiske, W. and Van Driessche, W. (1984). The sensitivity of apical Na^+ permeability in frog skin to hypertonic stress. *Pflügers Archiv: European Journal of Physiology.* **400**: 130-139.

Zeiske, W., Atia, F. and Van Driessche, W. (1998). Apical Cl^- channels in A6 cells. *Journal of Membrane Biology.* **166**: 169-178.

Zuckerman, J.B., Chen, X., Jacobs, J.D., Hu, B., Kleyman, T.R. and Smith P.R. (1999). Association of the epithelial sodium channel with Apx and alpha-spectrin in A6 renal epithelial cells. *Journal of Biological Chemistry.* **274**: 23286-232895.